Towards the Total Synthesis of the Polyketide Natural Product DEM30355/A and Associated Crystallisation Studies

by

Ronnie Ragbirsingh

A thesis submitted in partial fulfilment of the requirements for the degree of

Doctor of Philosophy

February 2021

Acknowledgements

Thanks, must first go to my supervisor Dr. Michael Hall for his mentorship and support throughout this project. Thank you to all the members of the MJH group both past and present for their friendship and guidance throughout. Thanks, in particular to Lok whose superb skills as a chemist are beautifully juxtaposed against his dubious skills as a DJ (TUP TUP are you READYYYY!!!)

A special mention must go to Andrew for his early guidance in the lab and his continued friendship now. Thank you to Xin Wen for being a true friend and bringing even more life to the Johnston Lab whilst competing with Lok and myself for the loudest mouth on record….anywhere.

Thanks to Dr. Paul Waddell for all his help with X- Ray crystallography. Thank you to Dr. Corinne Wills and Professor William McFarlane for sharing their NMR expertise.

On a personal note, I must say thank you to Joe and Jenny for all their support over the years, without which, none of this would have been possible.

Thank you, Mom, for always being there for me.

Finally, thank you to my wife Faizy for putting up with me during this journey with Benjamin and Sophia in tow for good measure. Here's to the next chapter.

Abstract

Due to the continuing rise in drug resistant pathogenic bacteria, there is an urgent need for new Mode of Action antibiotics. We have identified the polyketide natural product DEM30355/A as a potential new Mode of Action antibiotic versus Methicillin-resistant *Staphylococcus aureus.* This project aims to develop a synthetic route to DEM30355/A and its synthetic analogues to support new antibiotic development.

We have shown that the ABC anthracene-like core of DEM30355/A can be constructed by employing a key tandem, Michael-Dieckmann reaction. The functionalised C-ring was synthesised via a stereoselective Michael-Wittig reaction introducing the desired C-4a/C-10a C=C double bond, C-2 methyl and C-3 ethyl ester, followed by a stereoselective Rubottom oxidation to introduce the required hydroxyl group at C-3. A Michael-Dieckmann reaction between the A-ring and C-ring precursors allowed access to the ABC fused ring carbon skeleton of our target DEM30355/A, with a significant number of the required functional groups in place. Future work will focus on lactone ring formation, oxidation of the C-ring and installation of the B-ring C=C double bond between C-10/C-10a (**Scheme 1.00**).

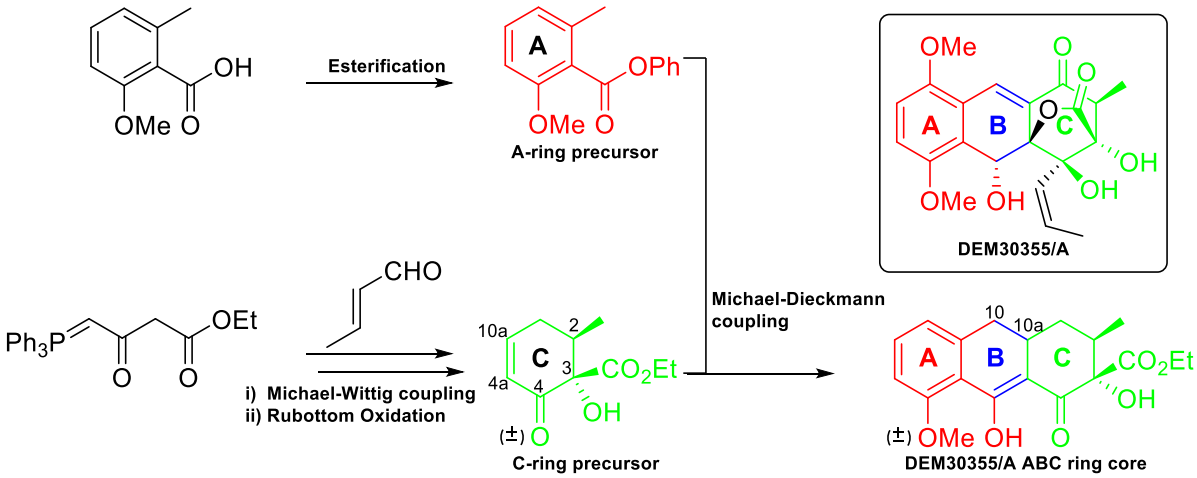

Scheme 1.00: Synthesis of the ABC fused ring core of DEM30355/A via a key Michael-Dieckmann cyclisation.

Our synthetic work was supported by crystallographic studies including an investigation into the propensity of shikimate esters to form high Z' structures and the crystallisation of biologically active small molecules. Our results serve to further confirm the tandem Michael-Dieckmann reaction as a robust method of coupling functionalised aromatic rings for the construction of natural product scaffolds.

List of Abbreviations

aq	Aqueous
Ac	Acetyl
Ar	Aromatic
Bn	Benzyl
Boc	*tert*-Butyloxycarbonyl
Bu	Butyl
Calcd	Calculated
Cat.	Catalyst
Cbz	Benzyloxybenzyl
CHP	Cumene Hydroperoxide
COSY	Correlation spectroscopy
DCC	Dicyclohexylcarbodiimide
DCM	Dichloromethane
DIPEA	*N,N*-Diisopropylethylamine
DMF	N,N-Dimethyl formamide
DMDO	Dimethyldioxirane
EDC	1-Ethyl-3-(3-dimethylaminopropyl)carbodiimide
DMSO	Dimethyl sulphoxide
Ee	Enantiomeric excess
eq	Equivalents
Et	Ethyl
Et_2O	Diethyl ether
Et_3N	Triethylamine
EtOAc	Ethyl Acetate
g	Grams
h	Hours

HATU	1-[Bis(dimethylamino)methylene]-1H-1,2,3-triazolo[4,5-b]pyridinium 3-oxid hexafluorophosphate
HMBC	Heteronuclear multiple bond correlation spectroscopy
HRMS	High Resolution Mass Spectrometry
HSQC	Heteronuclear single quantum correlation spectroscopy
IR	Infra-Red
KOH	Potassium hydroxide
lit.	Literature
M	Molar
mCPBA	3-Chloroperbenzoic acid
Me	Methyl
Mg	Milligram
MIC	Minimum Inhibitory Concentration
mL	Millilitre
MOA	Mode of Action
mol.	Molecular
MRSA	Methicillin-resistant *Staphylococcus aureus*
NBSH	2-Nitrobenzenesulfonylhydrazide
nm	nanometers
NMR	Nuclear Magnetic Resonance
O.N.	Over night
PMBO	2-(4-Methoxybenzyloxy)-4-methylquinoline
PPM	Parts per million
Rf	Retention factor
RT	Room temperature
SPE	Solid phase extraction

TAS-F	Tris(dimethylamino)sulfur trimethylsilyl difluoride
TBAF	Tetrabutylammonium fluoride
TFA	Trifluoroacetic acid
THF	Tetrahydrofuran
TLC	Thin layer chromatography
VCD	Vibrational Circular Dichrosim

Contents

Chapter 1 – Introduction

1.1 A Brief Modern History of Antibiotics

The use of antibiotics has changed the face of modern medicine. Across the spectrum of clinical medicine in areas such as child birth, surgical procedures and organ transplants, antibiotics have become instrumental in making these procedures safer[1]. By improving the outcome of bacterial infections in persons, antibiotics have increased life expectancy[2]. In the United States in 1920, before the advent of the widespread use of antibiotics to treat human ailments, the average life expectancy was 56.4 years whereas today, with the use of antibiotics, it stands at nearly 80 years[3]. Antibiotics continue to be our primary treatment response to potentially fatal bacterial diseases such as tuberculosis, syphilis and pneumonia. Any medicinal advances made via the beneficial use of antibiotics however, are in danger of being reversed by the looming spectre of antimicrobial resistance[4].

It was the American microbiologist Selman Waksman who in 1941, introduced the term 'antibiotic' to mean any small molecule, which inhibits the growth of a microbe[5]. Antibiotics, via their specific Mode-of-Action (MOA) can either be bactericidal whereby they kill the bacteria outright or bacteriostatic whereby they keep the bacteria in a stationary phase of growth.

Historically, natural products have played a major role in the identification and development of new antibacterial agents. Nature has proven to be an abundant source of bioactive molecules over the millennia with plants and fungi being particularly rich wellsprings. The serendipitous discovery of penicillin from a fungus by Alexander Fleming in 1929 drove drug discovery from microbial sources and ushered in a "Golden Age of Antibiotics" through the 1940s to 60s[6].

It was during this "Golden Age of Antibiotics" that most antibiotic classes we know today, were identified (**Figure 1.0**). It was widely believed at that time that due to the rate of discovery of new antibiotics, infectious disease would soon no longer be a public health concern[7].

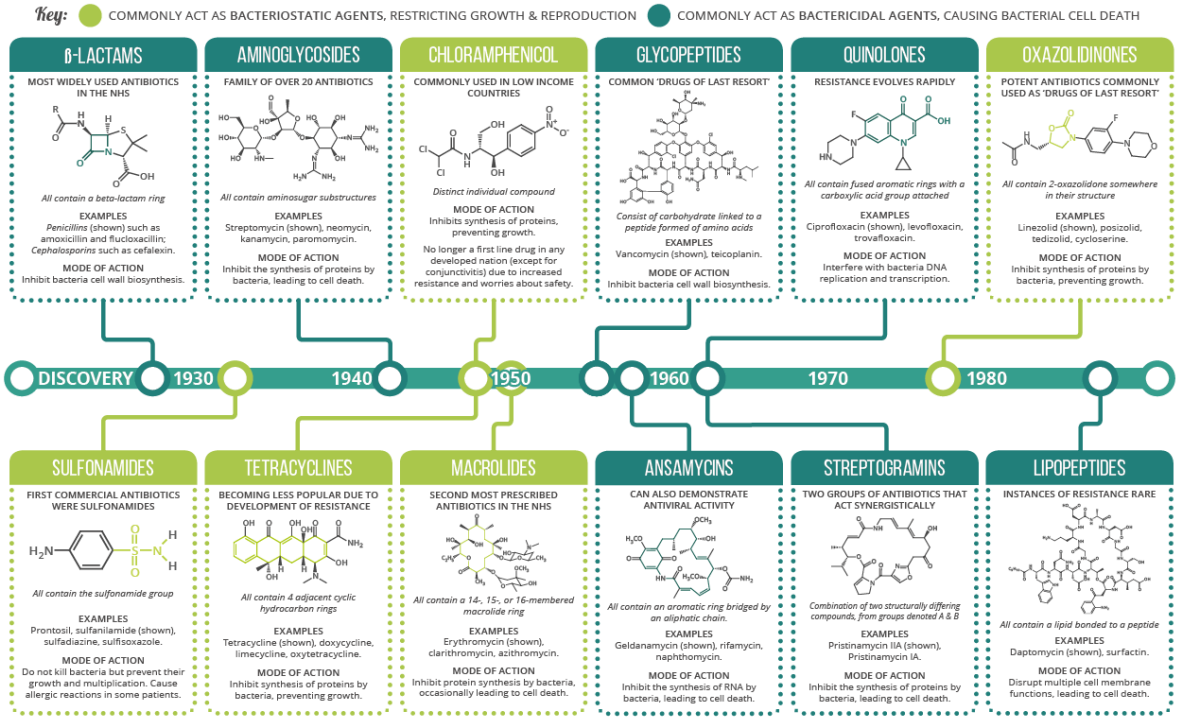

Figure 1.0: An illustrated timeline of discovery of the different classes of antibiotic and their mode of action[8]

1.2 Antibiotic Resistance

However, current global statistics by the WHO point to dangerously high antibiotic resistance levels in all parts of the world with new resistance mechanisms emerging and spreading globally. Treatments for a number of infections commonly treated with antibiotics including urinary tract infections (UTIs), tuberculosis (TB), sepsis and gonorrhoea are becoming increasingly less effective in large areas of the world due to resistance[9].

Presently, the U.S. Centers for Disease Control and Prevention (CDC) estimates that every year, over 2 million Americans acquire infections associated with antibiotic resistance with 23 000 deaths occurring as a result[10]. Current estimates put the annual number of global deaths attributable to antimicrobial resistance at 700 000. By 2050 this figure is projected to rise to a staggering 10 million deaths per year. The resulting cumulative cost to the global economy would be 100 trillion USD[4].

Of particular concern, are the ESKAPE pathogens (*Enterococcus faecium*, *Staphylococcus aureus*, *Klebsiella pneumoniae*, *Acinetobacter baumannii*, *Pseudomonas aeruginosa*, and *Enterobacter* species*)* as they represent some of the most common opportunistic pathogens observed in healthcare-related infections[11]. In 2017 the WHO, in an attempt to

direct research and development of new antibiotics, published a list of antibiotic-resistant "priority pathogens" that represent the greatest threat to human health. The three highest priority pathogens *Acinetobacter baumannii*, *Pseudomonas aeruginosa* and *Enterobacteriaceae* are all members of the ESKAPE group of pathogens[12].

A. baumannii is a Gram-negative, non-motile bacterium associated with nosocomial infections in critically ill patients. It has been known to cause urinary tract infections, skin and soft tissue infections, bloodstream infections, meningitis, ventilator-associated pneumonia and endocarditis with mortality rates for ventilator-associated pneumonia and bloodstream infections reaching up to 35 %[13,14]. The carbapenems, one of the last resort beta-lactam antibiotics, have been used as the drug of choice to treat serious infections caused by *A. baumannii*. Added to its penchant for multi-antibiotic resistance is the number of potential virulence factors *A. baumannii* possesses, including formation of biofilms and siderophore-mediated iron-acquisition systems, which detrimentally impact clinical outcomes[15,16].

The second highest priority opportunistic pathogen on the WHO list is the motile Gram-negative bacterium, *P. aeruginosa* which, globally is responsible for 6 million hospital admissions and over 4 million deaths per year[17,18]. In immunocompromised persons, *P. aeruginosa* can cause acute respiratory infection leading to septicemia and subsequent death and so is particularly dangerous for patients with chronic lung disease[19]. Certain types of multidrug-resistant *P. aeruginosa* have acquired resistance to a wide spectrum of antibiotics inclusive of carbapenems making clinical treatment a challenge[20].

The third critical pathogen on the WHO list of priority pathogens is *Enterobacteriaceae*, a family of Gram-negative bacilli including *Escherichia coli* and *Klebsiella pneumoniae* which cause infection in both community and healthcare settings. Extended-spectrum beta-lactamase (ESBL)-producing *Enterobacteriaceae* render commonly used antibiotics like penicillin and the cephalosporins inactive via hydrolysis. In the United States, in 2017 there were an estimated 197 400 cases of ESBL-producing *Enterobacteriaceae* infection in hospitalised patients with an estimated 9100 deaths and an estimated attributable healthcare cost of 1.2 billion USD. Increasingly, common infections such as urinary tract infections caused by ESBL-producing *Enterobacteriaceae* which were previously treated with oral antibiotics at home, now require hospitalization and the use of intravenous carbapenem antibiotics[20].

1.2.1 Strategies to Tackle Antibiotic Resistance

It is clear that the challenge of antibiotic resistance requires a comprehensive approach to maximise chances of success. As such, in January 2019, following on from a framework set out by the WHO's Global Action Plan on Antimicrobial resistance (GAP), the UK Government published their 5-year national action plan to tackle antimicrobial resistance. The plan includes three actionable areas:

1) Reducing the need for and unintentional exposure to antimicrobials by reducing the burden of human and animal infection through greater global access to clean water and sanitation and better food safety and production.

2) Optimising the use of antimicrobials in humans, animals and agriculture through the use of both therapeutic and diagnostic stewardship programmes informed by data mined from effective surveillance systems.

3) Investing in the research and development of and access to new and already known high quality antimicrobials by continuing to develop currently weak drug pipelines[21]. It is in this area that the MJH group have a vested interest with the aim being to achieve the total synthesis of a novel natural product small molecule antibiotic.

1.2.2 Recent Developments in Antibiotic Discovery

Since the "Golden Age of Antibiotics", there has been a steady decline in the output of the R&D programmes of the pharmaceutical industry. Over the last fifty years the continual need for new antibiotics has been mostly met by semi-synthetic tailoring of known natural product scaffolds[22]. Between 2017-2019, according to the WHO, 8 new small molecule antibiotics were approved for the treatment of bacterial infections. Of these, eravacycline and omadacycline are tetracycline derivatives with plazomicin being an aminoglycoside derivative. Half of these new agents target carbapenem resistant *Enterobacteriaceae*. None of the new approved antibiotics treat carbapenem-resistant *A. baumannii* or *P. aeruginosa* highlighting a clear disparity between this small number of approved drugs and the WHO list of priority pathogens[23].

This dramatic decline in antibiotic discovery over the last fifty years can be attributed to a number of factors including increased drug safety standards and a changing regulatory environment. There was also a cooling of interest in natural product chemistry by "big pharma" in favour of new techniques such as combinatorial chemistry to generate molecular libraries. These factors coupled with the failure of high throughput screening (HTS) as a modern drug discovery technique against the essential bacterial genome, to deliver vast numbers of novel targets in antibacterial space, combined to hasten the demise of antibiotic natural product research[24,25].

In recent times however, because of technological advances in fields such as bioinformatics and genome sequencing, there has been a resurgence in looking for novel antibiotics from bacterial sources e.g. *Streptomycetes, Actinomycetes*, cyanobacteria and 'unculturable' bacteria. This approach has uncovered several new antibiotics with distinctive scaffolds and/or new modes of action. The potential, therefore exists to exploit these bacterial targets with the aim of developing new antibiotic classes[26].

1.2.2.1 Teixobactin

A recent example includes an important new antibiotic compound called teixobactin (**Figure 1.1**), discovered in a soil sample screen of "unculturable" bacteria[27]. "Unculturable" bacteria account for approximately 99 % of all species in external environments and are so called because they do not grow under standard laboratory conditions[28]. A multichannel device called the iChip[29] was used to simultaneously isolate and grow "unculturable" bacteria. A sample of soil is diluted so that approximately one bacterial cell is delivered to a given channel. The device is then covered with two semi-permeable membranes and placed back in the soil. Diffusion of nutrients and growth factors through the chambers enables growth of "unculturable" bacteria in their natural environment thus enabling access to secondary metabolites from previously untapped species.

Teixobactin was found to inhibit cell wall synthesis by binding to lipid II (precursor of peptidoglycan) and also lipid III (precursor of cell wall teichoic acid). It also showed MIC activity against a wide spectrum of Gram-positive organisms, remained potent in blood serum and crucially showed low toxicity. Teixobactin was also shown to be active *in vivo* against *S. aureus* and *S. pneumonia* models[27].

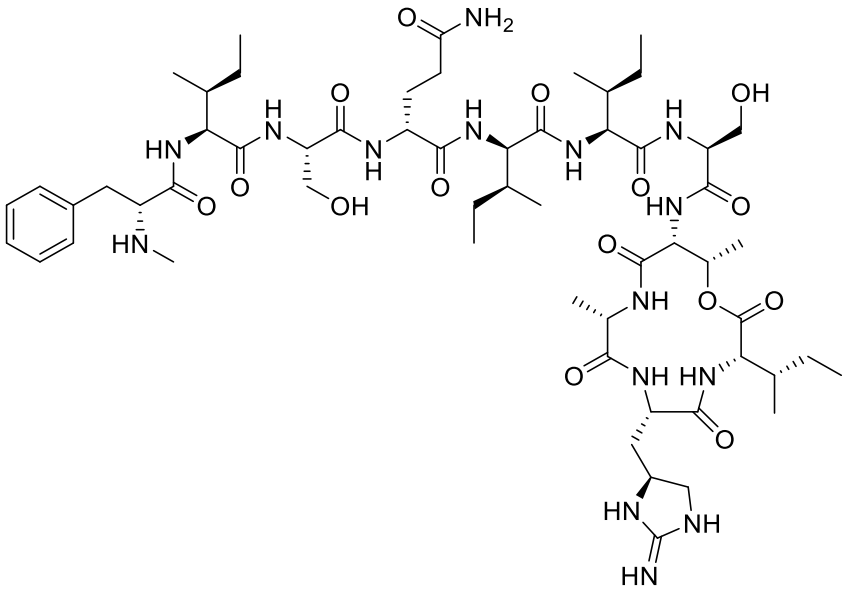

Figure 1.1: Structure of Teixobactin

1.2.2.2 Complestatin and Corbomycin

Even more recently in February 2020, Culp *et al.*[30] reported the discovery of two members of a new functional class of glycopeptide antibiotic - the known compound complestatin and a new compound dubbed corbomycin. Their novel mode of action inhibits peptidoglycan remodelling via binding to peptidoglycan and blocking its access to autolysins (essential peptidoglycan hydrolases). Blocking the breakdown of the bacterial cell wall renders the bacteria incapable of dividing and expanding essentially halting growth. Phylogenetic analysis of 71 complete biosynthetic gene clusters of the glycopeptide family combined with a strategy utilising the lack of known resistant genes led the researchers to the discovery of complestatin and corbomycin (**Figure 1.2**) which show vancomycin-comparable potency against Gram-positive bacteria including multi-drug resistant clinical isolates and promising activity in a mouse model of methicillin-resistant *Staphylococcus aureus* (MRSA) skin infections.

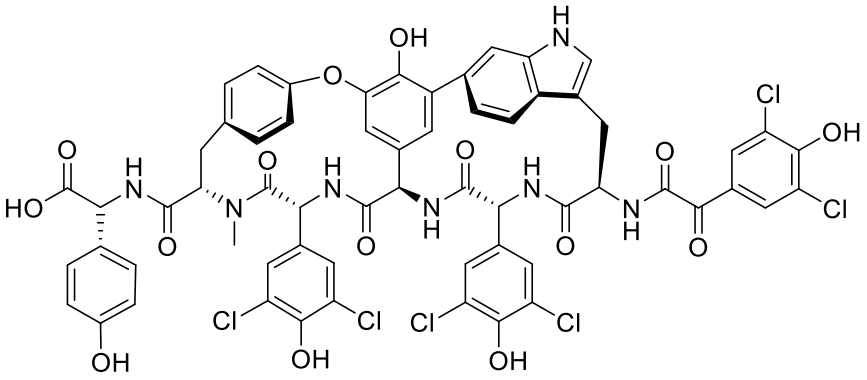

complestatin

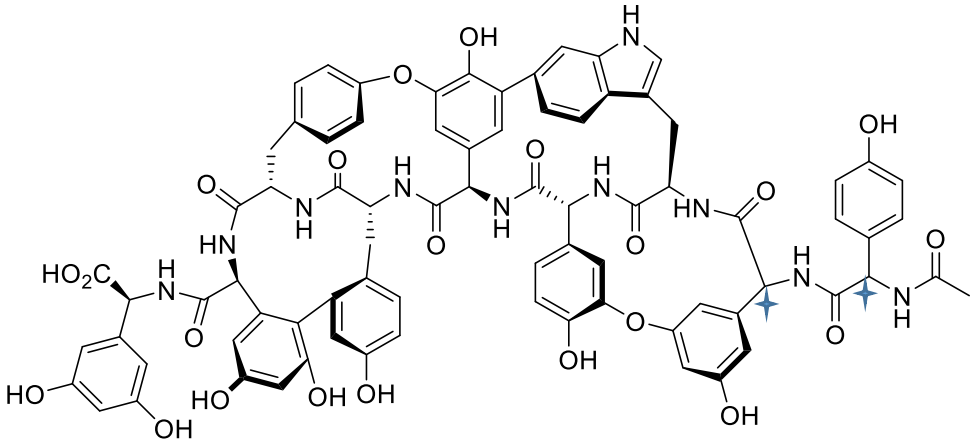

corbomycin

Figure 1.2: The chemical structures of complestatin and corbomycin (stereocentres not assigned ✦)

These examples of natural product-derived compounds with new chemical structures, high antibacterial activity and crucially, novel modes of action serve to illustrate the continuing importance of natural products as rich sources of antibiotics. The use of new methodologies for the cultivation of bacteria and the identification of novel natural products have opened up new avenues to drug discovery. Therefore, a renewed emphasis on natural product chemistry as a fast route to address the growing threat of antimicrobial resistance seems fully justified[22].

1.3 DEM30355/A – A Novel Polyketide Antibiotic

DEM30355/A (**1**), is a first in class polyketide natural product small molecule antibiotic. Working with our partners at the microbiology and antibiotic discovery company Demuris Ltd DEM30355/A (**1**) was isolated and identified utilizing a combined genomics and bioactivity approach, from the fermentation broth of the unusual extremophile *Amycolatopsis*

DEM30355. The absolute stereochemistry of DEM30355/A (**1**) has been determined via X-ray crystallography to be as shown in (**Figure1.3**)[31].

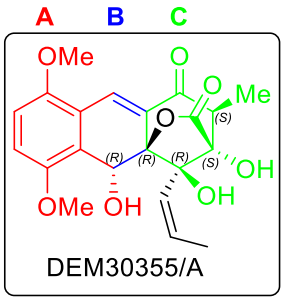

Figure 1.3: The molecular structure of DEM30355/A (**1**) indicating its 5 stereocentres.

DEM30355/A (**1**) consists of a highly oxygenated, linearly-fused tricyclic ABC anthracene-like core with multiple stereocentres (**Figure 1.3**). In addition to posing an interesting synthetic challenge, DEM30355/A (**1**) has been shown to have encouraging bioactivity vs several Gram-positive bacteria including *Bacillus subtilis*, *Enterococcus faecium*, *Listeria monocytogenes* and *Staphylococcus aureus* (MRSA). The mode of action of DEM30355/A (**1**) is as of yet unknown.

1.4 Project Aims

Our ultimate aim is to develop a synthetic route to the novel natural product DEM30355/A (**1**). In so doing we would also aim to synthesise analogues of DEM30355/A (**1**) for Structure-Activity Relationship (SAR) studies to probe its mode of action with the hope of identifying new antibiotic drug leads. For DEM30355/A (**1**) to reach the stage of clinical trials its efficacy has to be improved and its mode of action understood. Toxicity is also a leading cause of late stage attrition in drug development and therefore needs to be minimised. Developing a robust synthetic pathway to DEM30355/A (**1**) would therefore allow for these mitigating factors to be extensively investigated.

1.5 Total Synthesis of the Tetracyclines

To help to plan a total synthesis of our target molecule DEM30355/A (**1**) we revisited some of the seminal work done on similarly-structured fused ring polyketides with a view to employing some of these previously developed synthetic strategies in our own synthesis. The well-studied tetracycline class of natural products bears some structural similarity to DEM30355/A (**1**) being made up of four linearly fused six-membered carbon rings (**Figure 1.4**).

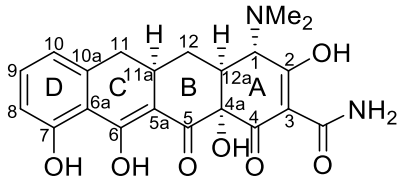

(±) sancycline (6-demethyl-6-deoxytetracycline) (1.01)

Figure 1.4: The ABCD fused ring structure of the tetracycline sancycline (**1.01**)

1.5.1 Total Synthesis of sancycline (1.01) by Woodward

In 1962, Woodward *et al.*[32] achieved the total synthesis of racemic sancycline (6-demethyl-6-deoxytetracycline) (**1.01**) (**Figure 1.4**). This route developed by Woodward starts with the construction of the D-ring, building sancycline in 25 steps.

Woodward begins his synthesis with a Claisen condensation of the methyl ester of the D-ring precursor, methyl 3-methoxy benzoate (**1.02**) (**Scheme 1.01**) (step a). The resulting keto-diester (**1.03)** was subsequently converted to the keto-triester (**1.04**) via a Michael addition (step b) to install the carbon framework for the CD fused ring system. A further 3 steps were required to afford the diacid (**1.05**): (step c) – a hydrolysis and decarboxylation to the corresponding β-keto-acid, (step d) – a catalytic hydrogenation to remove the benzylic ketone and (step e) – a chlorination at C-10 to protect the aromatic ring. The chlorination was required to block the more reactive C-10 position, and thus direct the subsequent intramolecular Friedel-Crafts acylation (step f) to the required but more sterically hindered C-6a position. Catalytic dehalogenation was used to later remove the directing chlorine. The acid (**1.05**) was then converted into the corresponding methyl ester (**1.06**) (step g). A cascade Claisen/Dieckmann condensation was then used to form the B-ring (step h). In the following 8 steps, Woodward set about constructing the framework for the installation of the final A-ring which was established through another Dieckmann condensation (step r). A global deprotection (step s) then yielded the dealkylated compound (**1.15**). The hydroxyl group at C-4a was then incorporated via oxygenation in the presence of cerium 3+ ions along with some competing oxidation at C-5a. A final equilibration of the stereocentre at C-1 under alkaline conditions afforded the thermodynamically stable product, racemic 6-demethyl-6-deoxytetracycline (**1.01**) (**Scheme 1.01**)[33,34]

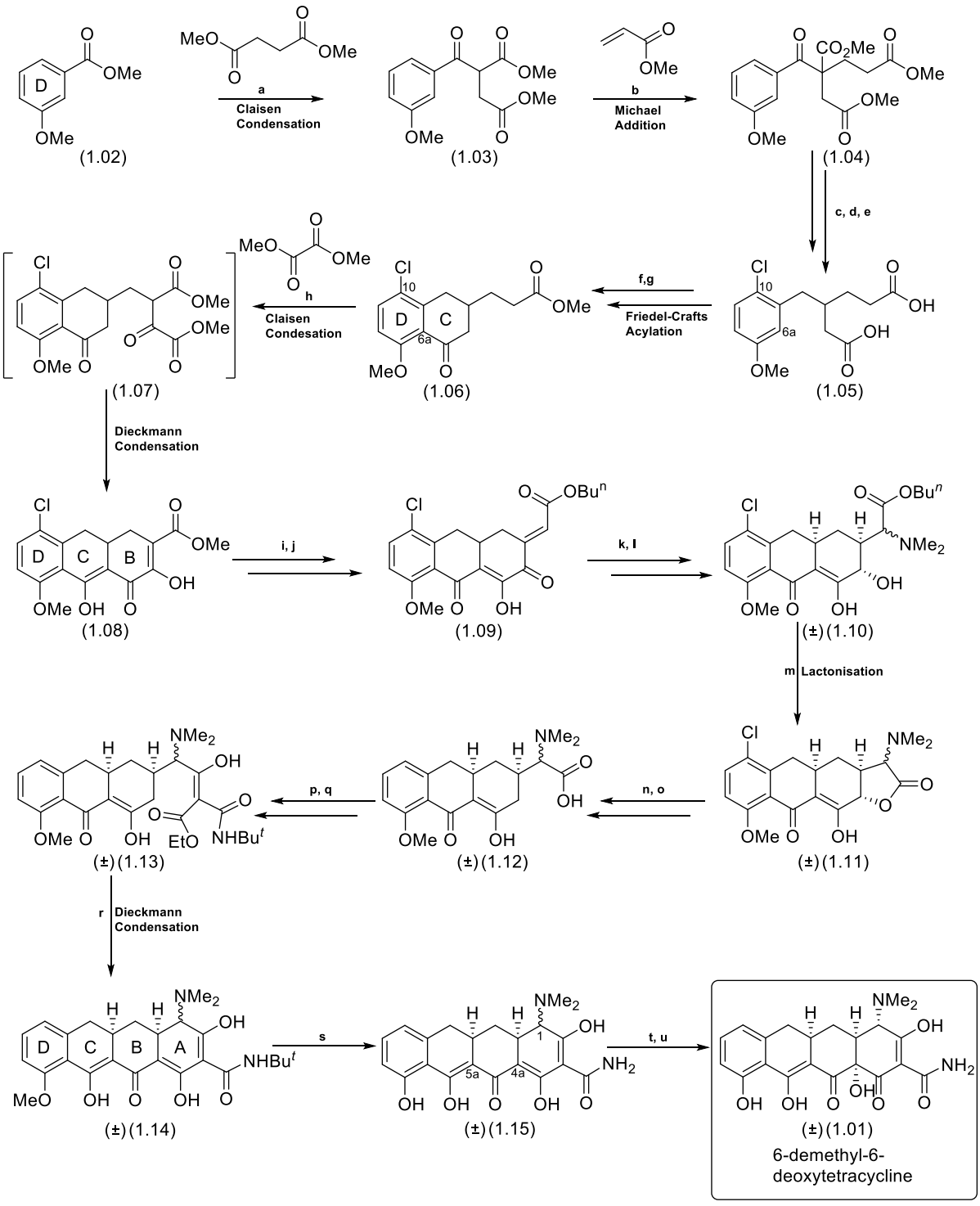

Scheme 1.01: Woodward's total synthesis of 6-demethyl-6-deoxytetracycline (**1.01**). Conditions: (a) NaH, DMF; (b) Triton B, MeOH; (c) AcOH, H_2SO_4, H_2O, 100 °C; (d) Pd/C : 1/10, AcOH, 200 p.s.i., 30 °C; (e) Cl_2, AcOH, 15 °C; (f) liquid HF, 15 °C; (g) MeOH, H_2SO_4; (h) NaH, DMF, MeOH, 80-120 °C; (i) H_2O, HCl, AcOH, 100 °C; (j) Butyl glyoxylate, $Mg(OMe)_2$, toluene; (k) liquid Me_2NH; (l) $NaBH_4$, 1,2-dimethoxyethane, H_2O, -70 °C; (m) TsOH, toluene; (n) Zn, formic acid, rt; (o) H_2, Pd/C 1 : 20, NEt_3, EtOH; (p) $ClCO_2Pr^i$, NEt_3, $CHCl_3$, 0 °C; (q) $EtOMg[CH(CO_2Et)CONHBu^t]$, MeCN, rt; (r) NaH, DMF, MeOH, 120 °C; (s) HBr, H_2O, 100 °C; (t) $CeCl_3$, MeOH, DMF, glycine, NaOH (pH 10), O_2; (u) $CaCl_2$, BuOH, H_2O, 2-aminoethan-1-ol (pH 8.5).

Woodward's seminal work inspired many subsequent efforts towards the total synthesis of the tetracyclines[35,36,37,38,39] with Woodward's Dieckmann condensation ring closure remaining a commonly used strategy.

1.5.2 Asymmetric Total Synthesis of (-)-Tetracycline (1.16) by Tatsuta

The first asymmetric total synthesis of a tetracycline was achieved in 2000 by Tatsuta and co-workers[40]. In a novel approach starting from a chiral carbohydrate A-ring precursor (**1.17**) and utilising a key ring-forming Diels-Alder reaction to form the AB ring system (**1.19**) and then a tandem Michael-Dieckmann reaction to couple the AB and CD ring systems (**1.20**), (-)-tetracycline (**1.16**) was linearly synthesised in 34 steps in 0.002 % overall yield (**Scheme 1.02**).

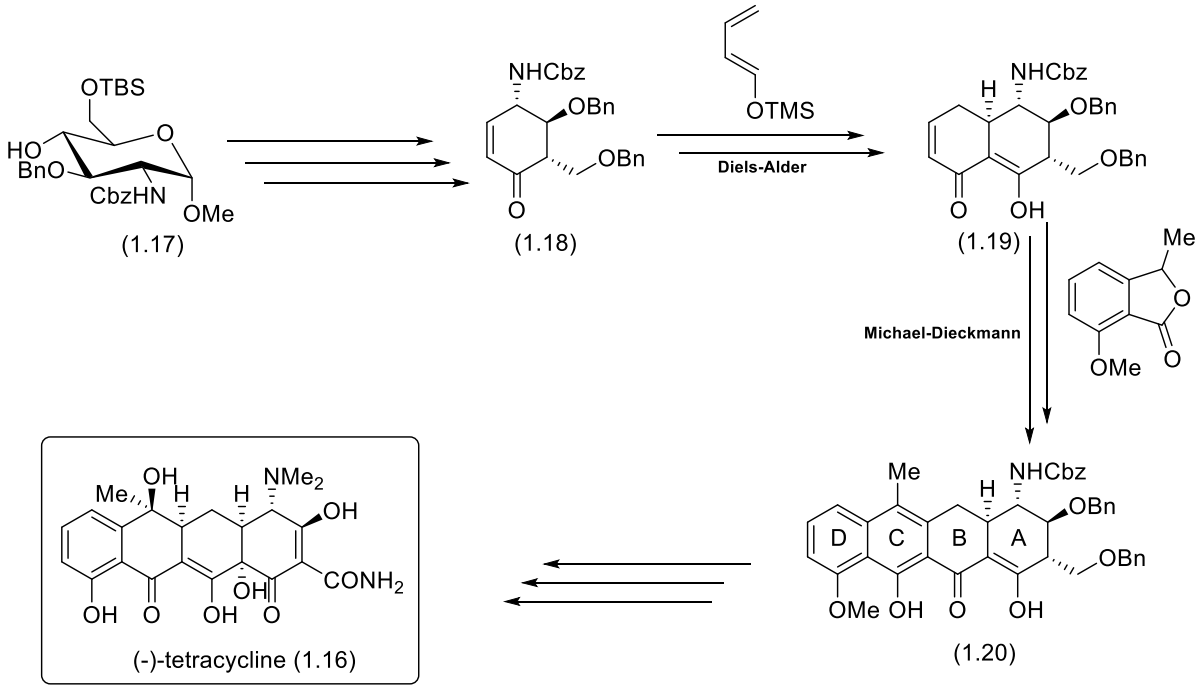

Scheme 1.02: Tatsuta's total synthesis of (-)-tetracycline (**1.16**) showing the chiral carbohydrate starting material and the key Diels-Alder and Michael-Dieckmann cyclisation steps. Conditions: Diels-Alder (i) 2,6-di-tert-butyl-4-methylphenol, 170 °C, 72 %, (ii) CrO_3, H_2SO_4, 0 °C, 10 min, 85 %; Michael-Dieckmann (i) LDA, -40 °C, 15 min, 85 %, (ii) $SOCl_2$, Et_3N, -30 °C, 10 min, 90 %.

1.5.3 Asymmetric Michael-Dieckmann Approach to the Tetracyclines by Myers

Later in 2005, Myers *et al.*[41] reported an asymmetric total synthesis of (-)-6-deoxytetracycline as well as another total synthesis of (-)-tetracycline in 17 steps in 1.1 % overall yield[42]. Myers' convergent synthetic strategy also involved key tandem Michael-Dieckmann cyclisation

reactions to construct the fused polycyclic ring structure of the tetracyclines which provided access to numerous tetracycline analogues. We will now examine Myers' synthesis of (-)-6-deoxytetracycline (**1.24**) with emphasis on his convergent approach utilising these key ring-forming reactions.

Building on knowledge gained from previous efforts at tetracycline synthesis, Myers' synthetic strategy involved installing the correct stereochemistry of the troublesome C-4a hydroxyl group early on and then building the molecule around this set stereocentre. With this in mind, he first constructed the AB-ring system (**1.22**) which he then coupled via a Michael-Dieckmann cyclisation reaction to the functionalised D-ring (**1.21**) to stereo-selectively generate the corresponding C-ring (**1.23**) (**Scheme 1.03**). This approach afforded rapid access to over fifty tetracyclines and analogues[41].

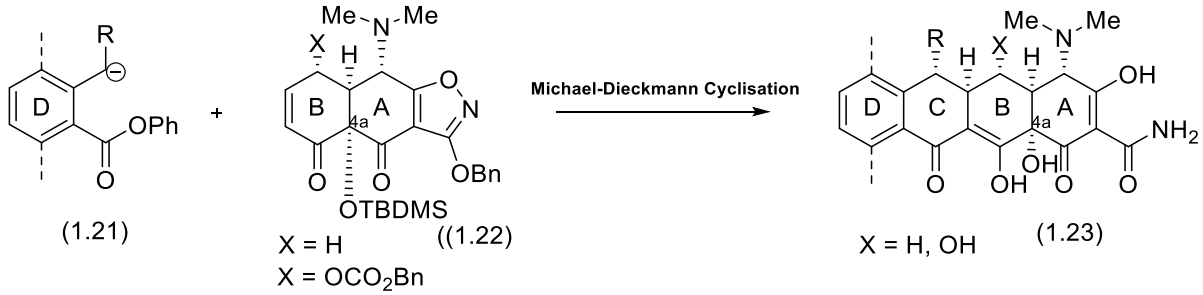

Scheme 1.03: Myers' approach to the tetracycline ABCD fused ring system via a key Michael-Dieckmann cyclisation to form the C-ring

1.5.4 Asymmetric Total Synthesis of (-)-6-deoxytetracycline (1.24) by Myers

As an example of Myers' rapid convergent approach to constructing fused polycyclic ring systems we will examine in detail his total synthesis of (-)-6-deoxytetracycline (**1.24**). Myers begins his synthesis with the enzymatic whole-cell microbial *syn*-dihydroxylation of benzoic acid (**1.25**) (step a) using *Alcaligenes eutrophus*, to generate the corresponding *cis*-diol (**1.26**). The *cis*-diol (**1.26**) was then subjected to a hydroxyl-directed epoxidation (step b) followed by a methyl esterification, isomerisation of the epoxide and bis-silyl protection (step c) to yield the methyl epoxy ester (**1.28**). Following a strategy established by Stork[39] the right side of the final A-ring i.e. the vinylogous carbamic acid moiety of the tetracyclines, was introduced as an isoxazole (step d) by addition of an organolithium reagent to the methyl epoxy ester (**1.28**) to provide ketone (**1.29**). The A-ring closure occurs through the reaction of the ketone (**1.29**) with lithium triflate and subsequent selective TBDMS deprotection (step e) yielding the

tricyclic AB-ring precursor (**1.30**). Myers postulates that this transformation to the AB-ring precursor (**1.30**) comes about via an initial S_N2 prime ring-opening of the allylic epoxide by the *N,N*-dimethylamino group, followed by ylide formation and a subsequent [2,3]-sigmatropic rearrangement. The conversion of the AB-ring precursor (**1.30**) to the desired enone (**1.31**) (step f) took place through a migration of the B-ring double bond with the hydroxyl group being concurrently reduced. Subsequent hydrolysis of the TBDMS ether protecting group (step g), oxidation of the resulting allylic alcohol (step h) and TBDMS protection of the stereo-specifically set tertiary alcohol at the future C-12a position (step i), yielded the α,β-unsaturated enone (**1.32**) (**Scheme 1.04**).

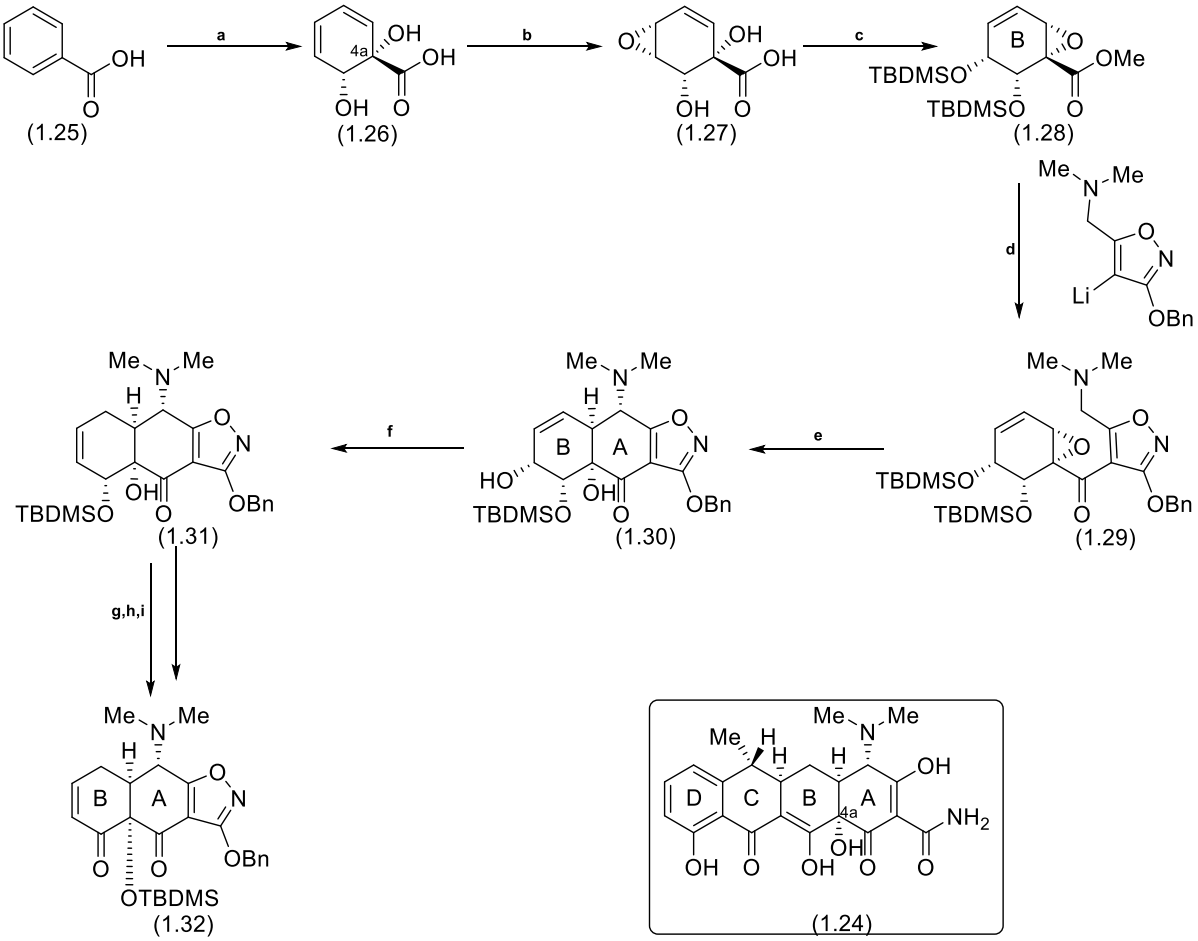

Scheme 1.04: Myers' synthesis of the AB-ring precursor (**1.32**) of (-)-6-deoxytetracycline (**1.24**). Conditions: (a) *A. eutrophus* B9, 79 %, >95 % ee; (b) *m*CPBA, EtOAc, 83 %; (c) i. $TMSCHN_2$, ii. TBDMSOTf, NEt_3, 70%; (d) *n*-BuLi, THF, -78 °C, 73 %; (e) i. LiOTf, toluene, 60 °C, ii. TFA, DCM, 62 %; (f) PPh_3, DEAD, toluene, NBSH, 74 %; (g) HCl, MeOH; (h) IBX, DMSO; (i) TBDMSOTf, 2,6-lutidine, 66 % (3 steps).

Myers now sought to couple this AB-ring precursor (**1.32**) with his D-ring precursor (**1.33**) (**Scheme 1.05**) (synthesised in 5 steps from anisic acid) to form the corresponding C-ring via

the tandem Michael-Dieckmann cyclisation reaction (step a) previously employed by Tatsutsa[40] in his total synthesis of (-)-tetracycline (**1.16**). Deprotonation *in situ* of the D-ring precursor at the benzylic position followed by addition of the AB-ring precursor did indeed form the desired ABCD fused ring structure (**1.34**). Subsequent cleavage of the TBDMS protection at C-4a (step b) and a final global deprotection of the Boc and the isoxazole groups via hydrogenolysis (step c) afforded the product (-)-6-deoxytetracycline (**1.24**) in 14 steps in an overall yield of 7.0 %.

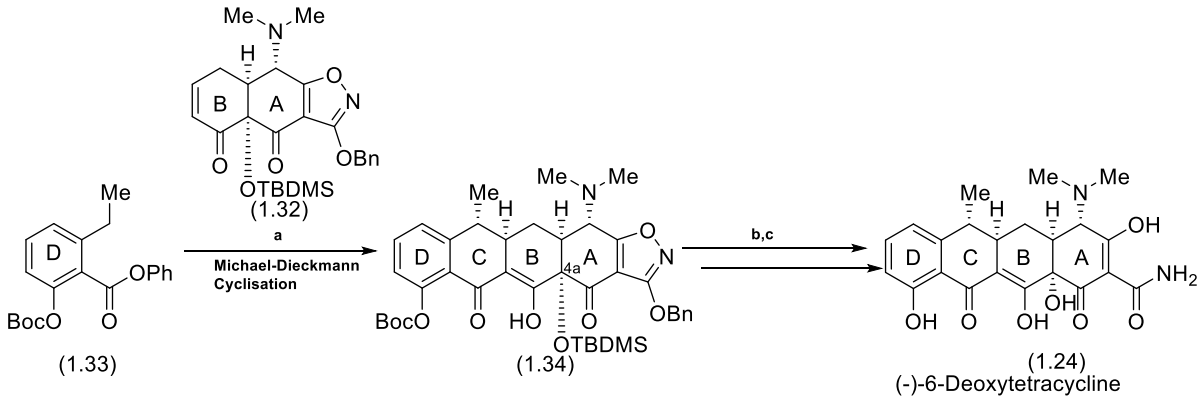

Scheme 1.05: Myers' rapid convergent total synthesis of (-)-6-deoxytetracycline (**1.24**). Conditions: (a) LDA, -78 °C – 0 °C, 81 %; (b) HF, MeCN; (c) H_2, Pd, 85 % (2 steps).

Myers was able to make several derivatives of (-)-6-deoxytetracycline (**1.24**) via this convergent approach utilising the key tandem Michael-Dieckmann coupling reaction. He was also successful in applying this approach to the synthesis of (-)-tetracycline (**1.16**). Tatsuta[40] as previously illustrated had achieved the first asymmetric total synthesis of (-)-tetracycline (**1.16**) in a linear synthesis also utilising this key Michael-Dieckmann cyclisation. Tatsuta and Myers in particular, thus clearly demonstrate the robust nature of the Michael-Dieckmann reaction as a key mechanistic pathway to constructing fused polycyclic ring-systems.

1.6 Reported Total Syntheses of Natural Products Bearing Close Structural Resemblance to DEM30355/A (1)

An examination of the literature revealed, our natural product of interest, DEM30355/A (**1**) bore a close structural resemblance to the natural products rishirilide A (**1.35**) and rishirilide B (**1.36**)[43] (**Figure 1.5**).

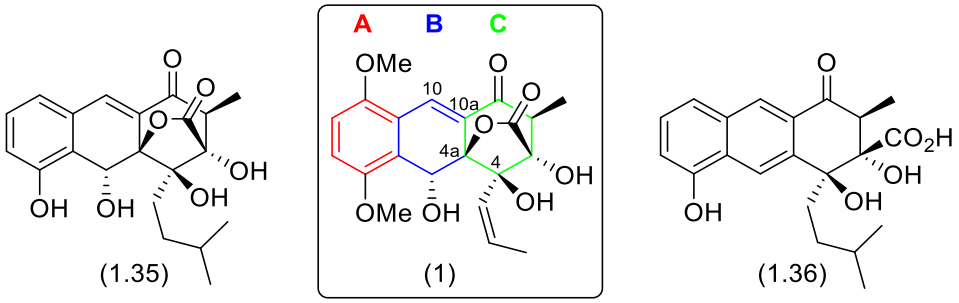

Figure 1.5: Comparison of DEM30355/A (**1**), rishirilide A (**1.35**) and rishirilide B (**1.36**)

The rishirilides A (**1.35**) and B (**1.36**) were originally isolated from *Streptomyces rishiriensis* in 1984 by Iwaki *et al.*[43] and subsequently reisolated from *Streptomyces bottropensis*[44]. Rishirilide A (**1.35**) and rishirilide B (**1.36**) were found to be inhibitors of α_2-macroglobulin with IC_{50} values of 100 µg/mL and 35 µg/mL respectively[45]. α_2-Macroglobulin (α2M), is a large (720 kDa) plasma protein primarily produced by the liver and found in the blood. α2M has antiprotease activity against several different proteases. In particular, α2M inhibits thrombin, a key enzyme responsible for the formation of blood clots. Hence the rishirilides could find use as anti-thrombotics for the treatment of clotting related diseases. Furthermore, rishirilide B (**1.36**) was subsequently found to be an inhibitor of glutathione *S*-transferase (GST) with an IC_{50} value of 26.9 µM[45]. The GSTs are a family of enzymes that can protect the cell against oxidative stress[46]. GSTs have been implicated in the development of resistance to chemotherapeutic agents and thus the development of GST inhibitors may be helpful in the fight against cancer[47].

1.6.1 Total Synthesis of Rishirilide B (1.36)

As a result of their bioactivity and the academic challenge they present on a synthetic level, the rishirilides have attracted considerable attention from many research groups. To date, there have been no reported total syntheses of rishirilide A (**1.35**). However, there have been a number of reported total syntheses of rishirilide B (**1.36**) and its close analogues. Due to the rishirilides' structural similarity to our target compound DEM30355/A (**1**), we will herein review the previously reported total syntheses of rishirilide B (**1.36**).

1.6.2 Total Synthesis of (±)-Methyl Rishirilide B (1.37) by Hauser

In 1999, Hauser's group[48] reported the first attempt at a total synthesis of racemic methyl rishirilide B (**1.37**) (**Scheme 7**). To construct the ABC ring core of methyl rishirilide B (**1.37**),

Hauser employed a convergent synthetic strategy whereby a phenylsulfonyl isobenzofuranone (**1.44**) acting as the A-ring precursor was condensed with a functionalised 2-cyclohexen-1-one (**1.43**) acting as the C-ring precursor. This condensation reaction between the A-ring and C-ring precursors produced the B-ring to give a regiospecifically constructed anthracenone intermediate (**1.45**).

Hauser began his synthesis by construction of the functionalised C-ring. A Diels-Alder reaction (step a) between piperylene (**138**) (diene) and (*E*)-6-methyl-2-heptenoic acid (dienophile) (**139**) produced the cyclic unsaturated carboxylic acid (**1.40**) as a 2:1 mixture of diastereomers (**1.40$_a$**) and (**1.40$_b$**), with the desired diastereomer (**1.40$_a$**) being predominant. Hauser then performed an iodo-lactonisation of the diastereomeric mixture of (**1.40$_a$**) and (**1.40$_b$**) (step b). Interestingly, only the major diastereomer (**1.40$_a$**) reacted to produce the corresponding bicyclic iodolactone (**1.41**), resulting in a kinetic resolution of (**1.40$_a$**) and (**1.40$_b$**).

The iodolactone (**1.41**) was then dehydrohalogenated (step c) to remove the iodine and install the carbon-carbon double bond to yield the lactone (**1.42**). A base-catalysed methanolysis (step d) followed by an oxidation with MnO_2 of the resulting allylic alcohol (step e) yielded the cyclohexenone (**1.43**) as the C-ring precursor (**Scheme 1.06**).

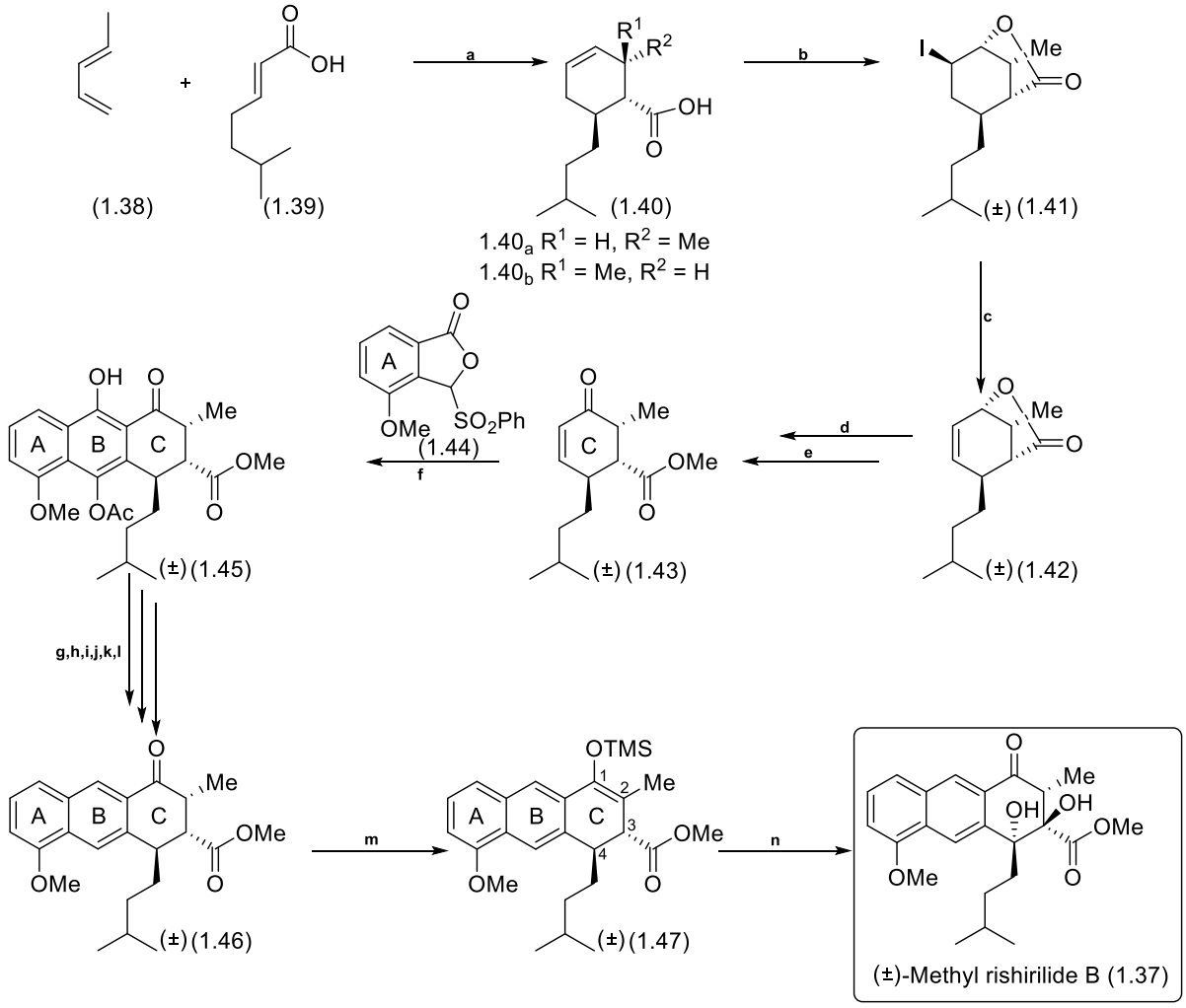

Scheme 1.06: Hauser's reported total synthesis of methyl rishirilide B (**1.37**) Conditions: (a) *tert*-butylcatechol, benzene, 180 ^{0}C, 45 %; (b) I_2, 2,4,6-trimethylpyridine, MeCN, 60 %; (c) DBU, benzene, 70 %; (d) K_2CO_3, MeOH, 87 %; (e) MnO_2, DCM, 80 %; (f) i *t*BuOLi, THF, ii Ac_2O, 81 %; (g) NaH, Tf_2O, 0 ^{0}C, 51 %; (h) H_2, Pd/C 75 %; (i) Claisen's alkali; (j) K_2CO_3, MeI, 73 %; (k) *t*BuOLi, Tf_2O, 0 ^{0}C, 77 %; (l) H_2, Pd/C, 84 %; (m) TMSOTf, NEt_3, benzene; (n) KHMDS, THF, 2-phenylsulfonyloxaziridine 66 %.

Having constructed the functionalised C-ring precursor (**1.43**), Hauser now sought to couple this C-ring precursor (**1.43**) to the A-ring precursor phenylsulfonyl isobenzofuranone (**1.44**). This key condensation reaction (step f) between the A-ring (**1.44**) and C-ring (**1.43**) precursors led to the formation of the ABC ring core of methyl rishirilide B (**1.45**). A series of triflations and catalytic hydrogenations was employed to remove the oxygen functionalities on the B-ring (step g-l) leading to the tricycle (**1.46**).

Hauser then protected the ketone functionality at C-1 of the tricycle (**1.47**) as a silyl enol ether (step m) to supress any competing keto-enolate reaction in the subsequent step. Hauser next employed the oxidant 2-phenylsulfonyloxaziridine (Davis' reagent-which is known to hydroxylate ketone and ester enolates at the α-position) (step n) to install the hydroxyl group

at the C-3 ester-enolate. Pleasingly, the benzylic hydroxyl at C-4 was simultaneously installed leading to the proposed formation of (±)-methyl rishirilide B (**1.37**) (**Scheme 1.06**).

In 2001, Danishefsky, achieved a racemic synthesis of (±)-rishirilide B (**1.36**), including a synthesis of (±)-methyl rishirilide B (**1.37**). The ^{1}H-NMR data for Danishefsky's (±)-methyl rishirilide B (**1.37**) was identical to Iwaki's (±)-methyl rishirilide B (**1.37**)[43] as derived from the natural product, thus confirming Danishefsky's structural assignment. However, Hauser's analytical data for (±)-methyl rishirilide B (**1.37**) did not match that of Iwaki's and Danishefsky's, suggesting a significant error in Hauser's structural assignment of his final product. Unfortunately, it is not known at which stage the Hauser synthesis of (±)-methyl rishirilide B (**1.37**) failed. We have however, included Hauser's synthetic route here for completeness.

1.6.3 Total Synthesis of (2*S*,3*S*,4*S*)-Rishirilide B (1.36) by Danishefsky

In 2001, Danishefsky[49] reported the first total synthesis of racemic rishirilide B, followed in 2003[50] by the first reported enantioselective total synthesis of (2*S*,3*S*,4*S*)-rishirilide B (**1.36**). Both syntheses employed a similar strategy whereby a functionalised dieneophilic C-ring precursor (**1.49**) was combined with an *o*-quinodimethide diene A-ring precursor (**1.48**) in a Diels-Alder cycloaddition to form the ABC ring core of rishirilide B (**1.50**) (**Scheme 1.07**).

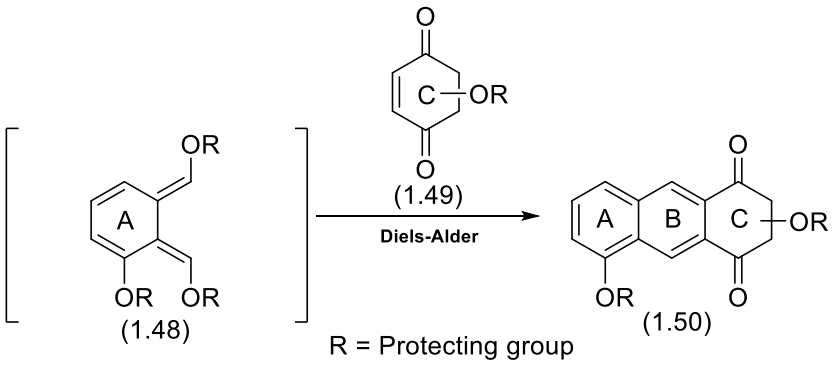

Scheme 1.07: Danishefsky's key ring-forming Diels-Alder step for both his racemic and asymmetric total synthesis of rishirilide B

In his enantioselective total synthesis of (2*S*,3*S*,4*S*)-rishirilide B (**1.36**), Danishefsky began by constructing the enantiomerically defined C-ring dienophile (**1.55**) (**Scheme 1.08**). Starting with (*R*)-methylcyclohexanone (**1.51**), he performed a dehydrogenation (step a) with the oxidant IBX to install the double bond between C-5 and C-6 and synthesise the enone (**1.52**). A subsequent Claisen condensation (step b) introduced the TSE-protected ester group at C-3

of the enone (**1.53**). A Rubottom-type oxidation (step c) then installed the desired OH functionality at C-3 with the Me group at C-2 sterically directing the addition of the incoming hydroxyl group of the enone (**1.54**). The desired ketone functionality was then installed at C-1 via a radical bromination (step d), followed by a substitution of the bromine with a hydroxyl group (step e) and a final oxidation of the resulting allylic alcohol (step f) to yield the enedione C-ring precursor (**1.55**) (**Scheme 1.08**).

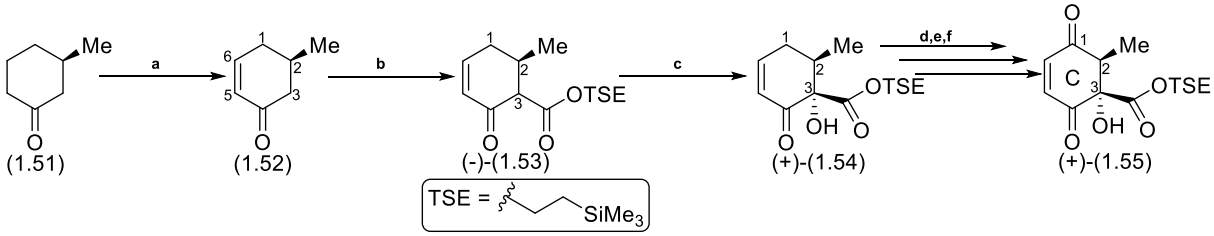

Scheme 1.08: Danishefsky's preparation of the enantioenriched enedione C-ring precursor (**1.55**). Conditions: (a) IBX, DMSO, toluene, 65 ^{0}C, 36 %; (b)LDA, 2-(trimethylsilyl)ethoxycarboxy cyanide, ether, 39 %; (c) i. NaH, TBDMSOTf, ii. DMDO, acetone, 28 % (2 steps); (d) NBS, AIBN, CCl_4; (e) Ag_2CO_3, acetone, water, 49 %; (f) DMP, DCM, 98 %.

With the functionalised dienophilic C-ring precursor (**1.55**) in hand, Danishefsky now sought to prepare the A-ring diene precursor (**1.59**) (**Scheme 1.09**). A Swern oxidation of the diol (**1.56**) (step a) yielded the benzocyclobutene 1,2-dione (**1.57**). The *peri*-methoxy group of the benzocyclobutene 1,2-dione (**1.57**) was de-methylated (step b) using 48 % HBr and the resultant phenol was subjected to silylation (step c). Reduction of the α-diketone (step d) afforded primarily the *trans*-diol which was then *bis*-silylated to yield the TBDMS-protected benzocyclobutene (**1.58**). The activated A-ring diene precursor (**1.59**) was generated *in situ* (step e) via a thermal conrotatory ring opening[51] of the TBDMS-protected benzocyclobutene (**1.58**) (**Scheme 1.09**).

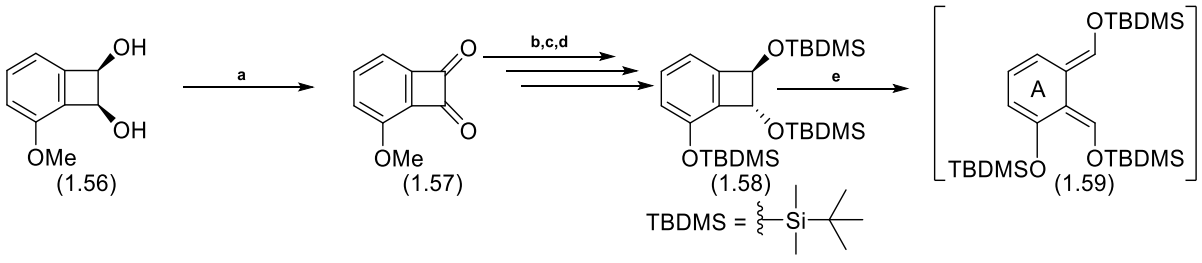

Scheme 1.09: Danishefsky's synthesis of the A-ring precursor (**1.59**). Conditions: (a) $(COCl)_2$, DMSO, NEt_3, 86 %; (b) 48 % HBr, 93 %; (c) TBDMSOTf, NEt_3, 91 %; (d) $NaBH_4$ then TBDMSOTf, NEt_3, 83 % (*cis*:*trans* = 1:6); (e) i toluene, 90 ^{0}C.

This activated A-ring diene precursor (**1.59**) and the C-ring dienophile (**1.55**) were then coupled together via a Diels-Alder reaction (step a) to yield the ABC ring core of rishirilide B

(**Scheme 1.10**). A subsequent acid catalysed β-elimination of both OTBDMS groups (step b) led to the aromatisation of the newly formed B-ring (**1.60**). Danishefsky then sought to regio and stereo direct the addition of the isopentyl group at C-4 (step c) via the vicinal hydroxyl group at C-3. By co-ordinating with the incoming Grignard reagent, the C-3 hydroxyl group directed the isopentyl group to the back face (*Re*) of the ketone (**1.61**) at C-4. A final fluoride-mediated global deprotection of the ester and phenol protecting groups (step d) yielded (2*S*,3*S*,4*S*)-rishirilide B (**1.36**) (**Scheme 1.10**).

The optical rotation reported by Danishefsky for his synthetic product (2*S*,3*S*,4*S*)-rishirilide B was = -13.6° (*c* = 0.320 in EtOH). At the time of Danishefsky's synthesis, only the relative stereochemistry of naturally occurring (+)-rishirilide B was known. The optical rotation of naturally occurring (+)-rishirilide B was reported in literature as (= +12.8° (*c* = 0.488 in EtOH))[43]. Because of the difference in sign, Danishefsky considered his asymmetrically synthesised (2*S*,3*S*,4*S*)-rishirilide B (**1.36a**) to be the enantiomer of the naturally occurring compound (+)-rishirilide B (**1.36**). Thus, leading him to conclude that the absolute configuration of the natural product (+)-rishirilide B (**1.36**) at the C2-C4 positions was (2*R*,3*R*,4*R*). It should be noted that, in 2017 Odagi and co-workers revised this assignment in a subsequent work. Further discussion of this reassignment follows later.

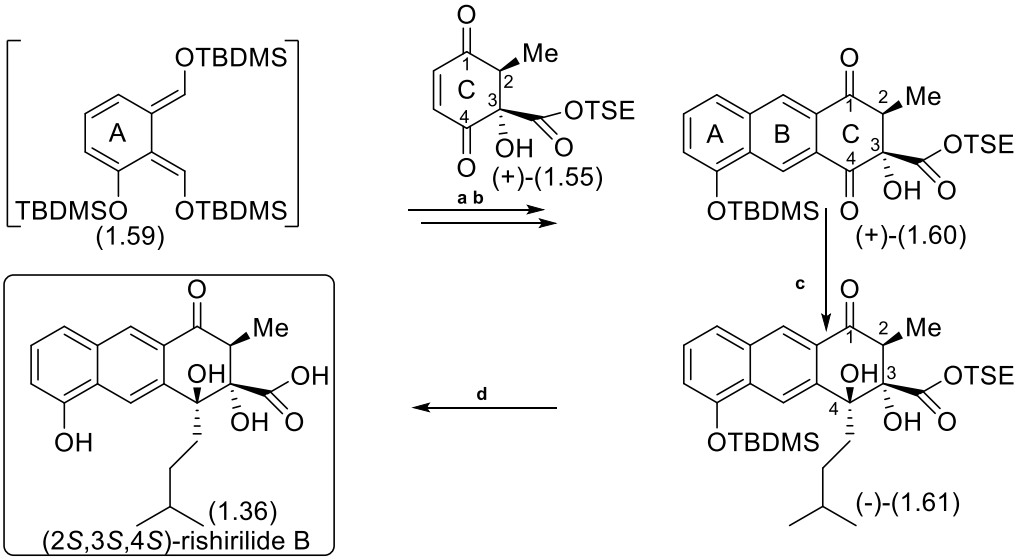

Scheme 1.10: Danishefsky's total synthesis of (2*S*,3*S*,4*S*)-rishirilide B (**1.36a**). Conditions: (a) C-ring precursor, toluene, 90 °C, 12 h; (b) CSA, pyridine, MeOH, 72 %, 2 steps; (c) iso-pentylmagnesium bromide, THF, 73 %; (d) TAS-F, THF, 43 %.

1.6.4 Total Synthesis of (2*R*,3*R*,4*R*)-Rishirilide B (1.36) by Pettus

In 2006, Pettus' group[52] followed Danishefsky's total synthesis of (2*S*,3*S*,4*S*)-rishirilide B (**1.36**) with the first reported total synthesis of (2*R*,3*R*,4*R*)-rishirilide B (**1.36**). Pettus employed a similar convergent synthetic strategy to Danishefsky, whereby a key Diels-Alder reaction formed the ABC ring core of the target compound (2*R*,3*R*,4*R*)-rishirilide B (**1.36**).

Pettus began by synthesising the densely functionalised C-ring dienophile (**Scheme 1.11**). The benzaldehyde (**1.62**) was converted in three steps (a,b,c) into the prochiral Boc-protected resorcinol (**1.63**). An amide chiral auxiliary was then introduced via a Mitsunobu reaction (step d) and a subsequent Boc-deprotection yielded the chiral resorcinol (**1.64**). The amide chiral auxiliary was incorporated in order to enantio-selectively affect the outcome of the ortho cyclisation step of the subsequent key oxidative dearomatisation (step e). Stereo-electronic considerations in the resulting transition states of the two dienophilic products favoured (**1.65$_a$**) as the major diastereomer (**Scheme 1.11**).

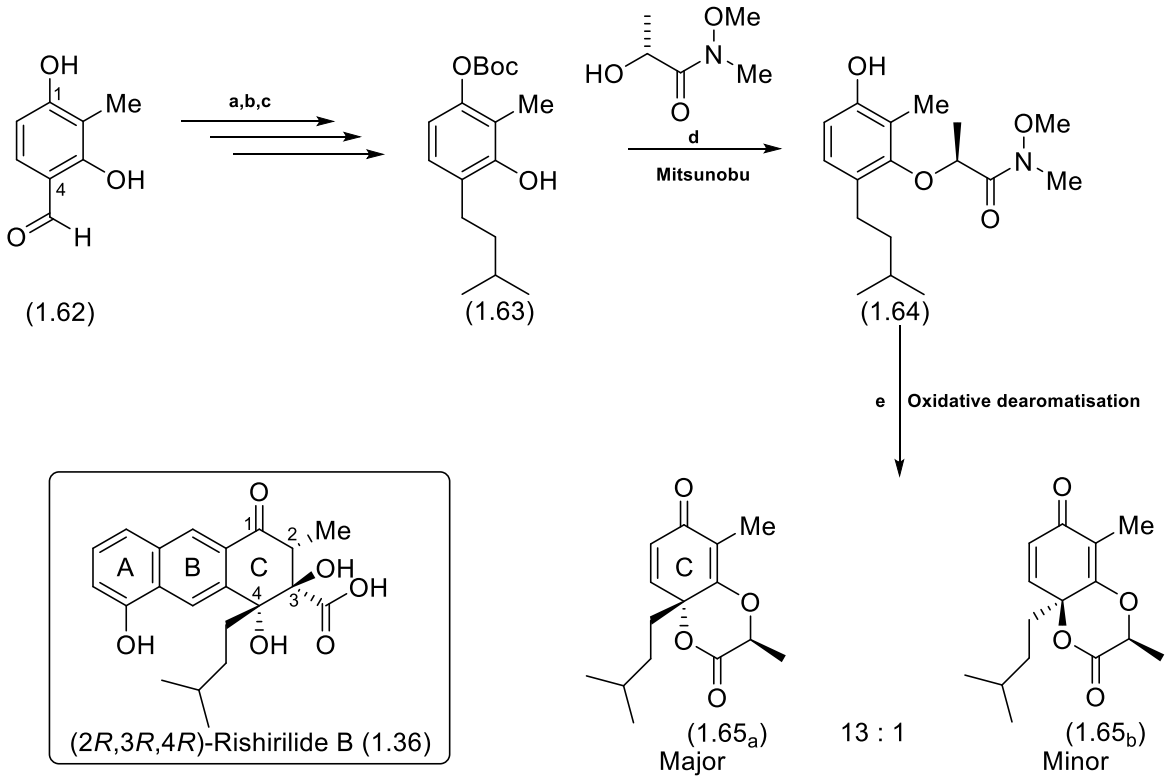

Scheme 1.11: Pettus' enantioselective synthesis of C-ring precursor (**1.65a**) with a comparison to target compound (**1.36**). Conditions: (a) Boc_2O, diethylisopropylamine, (b) $NaBH_4$, (c) excess pentylmagnesium bromide, (d) i PPh_3, DEAD, ii $ZnBr_2$, CH_3NO_2, 84 % (2 steps), (e) PhIO, TMSOTf, DCM, 73 %.

Pettus then looked to combine this optically active dienophilic C-ring precursor (**1.65a**) in a key Diels-Alder reaction with his own A-ring *ortho*-quinodimethane precursor (**1.66**) (step a) (**Scheme 1.12**) in order to construct the ABC tricyclic ring system of rishirilide B (**1.36**). A spontaneous β-elimination of the methoxy group followed by an oxidation of the resulting cyclohexenone intermediate yielded the ABC ring core (**1.67**) with the newly formed, aromatised B-ring. Cleavage of the chiral directing group on the C-ring was achieved via reaction with (2,2-dimethylhydrazineyl)dimethylaluminium amide (step b) to yield the tricycle (**1.68**). Protection of the C-1 ketone functionality with diethylcarbamyl chloride (step c) yielded the O-carbamyl product (**1.69**). Pettus next sought to install the required ester functionality at C-3 of the O-carbamyl product (**1.69**). By employing an excess of the lithiated ethyl vinyl ether (1-ethoxyvinyl)lithium and in a similar fashion to Danishefsky's hydroxyl-directed Grignard addition, Pettus used the hydroxyl group at C-4 of the O-carbamyl product (**1.69**) to regio and stereo-direct the organolithium addition at the C-3 vicinal ketone (step d) The carbonyl group of the vinyl carbamate at C-1 then slowly reacts with additional equivalents of (1-ethoxyvinyl)lithium to give the enolate (**1.70**). A subsequent oxidation (step e) gave the α, α'-dihydroxy ketone (**1.71**). The ketone functionality at C-3 was then reduced

to the 1,2-diol and cleaved with sodium periodate (step f) to yield the aldehyde (**1.72**). A subsequent oxidation to the required carboxylic acid and a final catalytic hydrogenolysis of the benzyl residue (step g) afforded (2*R*,3*R*,4*R*)-rishirilide B (**1.36**) (**Scheme 1.12**).

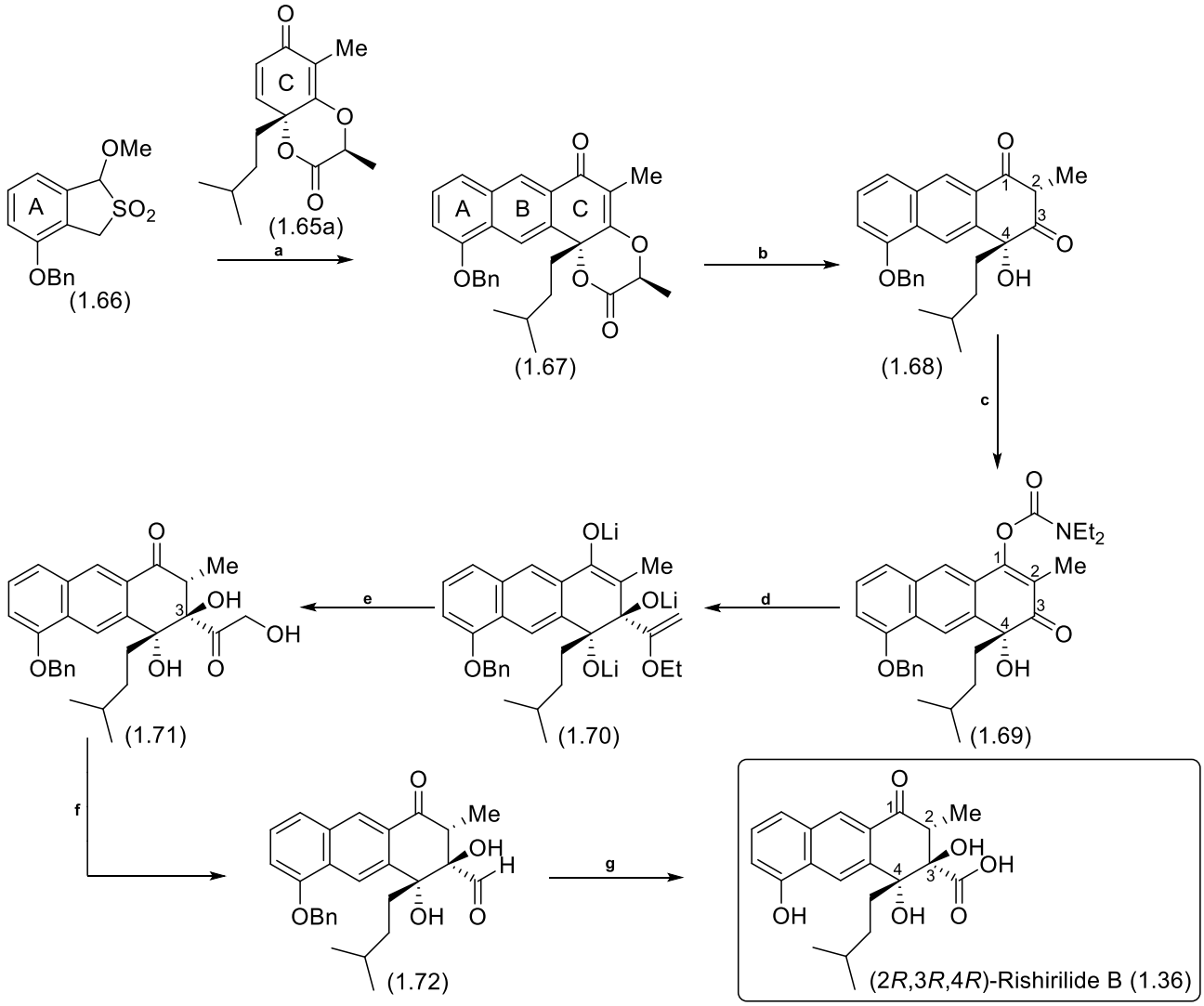

Scheme 1.12: Pettus' total synthesis of (2*R*,3*R*,4*R*)-rishirilide B (**1.36**). Conditions: (a) i. ZnO, 155 ^{0}C, 9 h ii. DDQ, 68 % (2 steps), (b) $Me_2AlNHNMe_2$, DCM, 69 %, (c) Di-ethyl carbamyl chloride, *N*,*N*-diisopropylethylamine, (d) (1-ethoxyvinyl)lithium (10 eq.), -78 ^{0}C , (e) DMDO, 1M HCl, 87 % (2 steps) (f) i. $Na(OAc)_3BH$, ii. $NaIO_4$ on silica, 75 % (2 steps), (g) i. NaOCl, ii. H_2, Pd/C, 68 % (2 steps).

Pettus reported the optical rotation of his synthetic (2*R*,3*R*,4*R*)-rishirilide B (**1.36**) to be +12.6^{o} (*c* = 0.5 in EtOH). The optical rotation originally reported for the natural product (2*R*,3*R*,4*R*)-rishirilide B (**1.36**) by Iwaki[43] was +12.8^{o} (c = 0.488 in EtOH) whilst the optical rotation reported by Danishefsky for his synthetic (2*S*,3*S*,4*S*)-rishirilide B (**1.36**) was -13.6^{o} (*c* = 0.320 in EtOH). Thus, Pettus concluded that the absolute stereochemistry of naturally occurring rishirilide B (**1.36**) was (2*R*,3*R*,4*R*). It should be noted that the absolute configuration of the natural product, rishirilide B (1.36) was later revised by Odagi.

1.6.5 Total Synthesis of (2*R*,3*R*,4*R*)-Rishirilide B (1.36) and (2*S*,3*S*,4*S*)-Rishirilide B (1.36) by Odagi

The most recently reported asymmetric total synthesis of both (2*R*,3*R*,4*R*)-rishirilide B and (2*S*,3*S*,4*S*)-rishirilide B was by Odagi and co-workers[53] in 2017. Odagi, like Pettus and Danishefsky before him, utilised a key Diels-Alder reaction to form the ABC ring core of rishirilide B (**1.36**). Unlike his predecessors however, Odagi constructed an enantioenriched dienophilic BC-ring precursor to couple with a diene to form the A-ring.

Odagi began his total synthesis of (2*R*,3*R*,4*R*)-rishirilide B (**1.36**) by construction of the enantio enriched dienophilic BC-ring precursor (**1.78**) (**Scheme 1.13**). The racemic tetralone (**1.73**) undergoes organocatalytic oxidative kinetic resolution (step a) (**1.74**-catalyst) to yield the desired (2*S*,3*R*)-hydroxy tetralone (**1.76**) in 99 % *ee* after recrystallisation. Reaction of the (2*S*,3*R*)-hydroxy tetralone (**1.76**) with the sterically-directed Grignard reagent, isopentyl magnesium bromide (step b), introduced the desired groups and stereochemistry at C-4 of the bicycle (**1.77**). Oxidative deprotection of the PMB protecting group (step c) yielded the phenolic hydroxyl group which was subsequently triflated (step d). The ketone at C-1 was then installed via a benzylic oxidation (step e) to yield the BC-ring precursor (**1.78**) (**Scheme 1.13**).

Odagi then looked to construct the A-ring via a Diels-Alder reaction with the BC-ring precursor (**1.78**) and furan. Thus, the benzyne intermediate (**1.79**) was generated *in situ* via a halogen-metal exchange and subsequent triflate elimination (step f). Reaction of this benzyne intermediate (**1.79**) with furan produced the ABC ring core (**1.80**). To introduce the required phenol group at C-6 on the A-ring, Odagi investigated regioselective isomerisation of the oxabenzonor-bornadiene moiety under acidic conditions (Bronsted and Lewis acids) eventually settling on BBr_3 (step g) which afforded a 6:1 mixture of regioisomers (**181_a: 181_b**). This regioselectivity arising as a direct result of the relative stability of the two considered transition states TS-1 and TS-2. TS-1 and thus **181_a** is favoured as it experiences less electronic repulsion as compared to TS-2. The synthesis concludes with hydrolysis of the *tert*-butyl ester group at C-3 of **181_a** via a Lewis-acid catalyst (step h) to afford (2*R*,3*R*,4*R*)-rishirilide B (**1.36**) (**Scheme 1.13**).

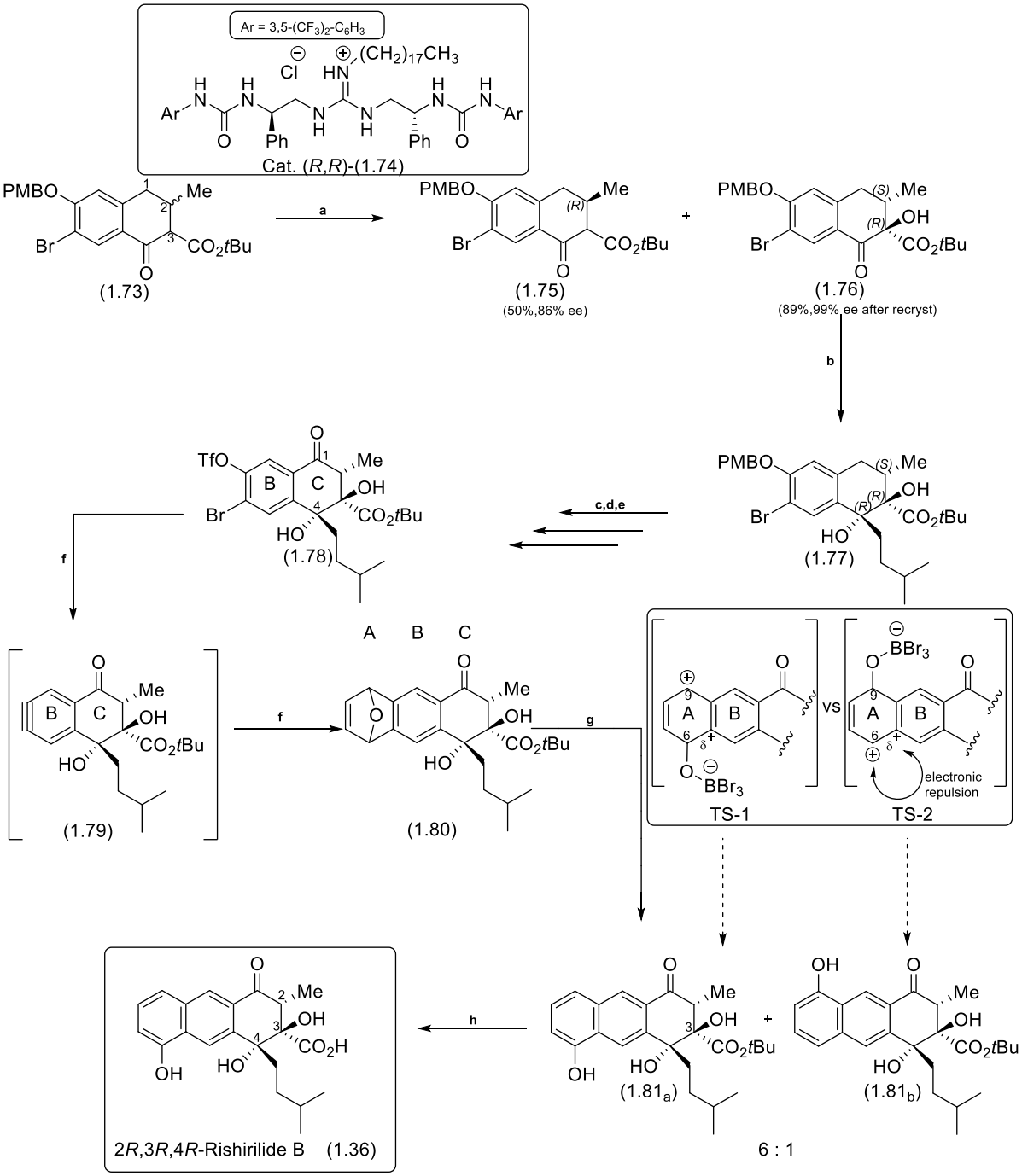

Scheme 1.13: Odagi's total synthesis of (-)-2*R*,3*R*,4*R*-rishirilide B (**1.36**). Conditions: (a) CHP, K_2CO_3, toluene, (b) isopentylmagnesium bromide, THF, 91%, (c) DDQ, DCM/H_2O, 76 %, (d) Tf_2O, NEt_3, DCM, 98 %, (e) $FeCl_3.6H_2O$, $KMnO_4$, acetone, 85 %, (f) *n*-BuLi, THF, furan, 81 %, (g) BBr_3, *i*Pr_2O, DCM, 1.81$_a$ 72 %, 1.81$_b$ 12 %, (h) $AlCl_3$, DCM, 95 %.

Interestingly, Odagi reported the optical rotation of his synthetic (2*R*,3*R*,4*R*)-rishirilide B (**1.36**) to be -14.8° (*c* = 0.27 in EtOH). The optical rotation of the natural product isolated by Iwaki was +12.8° (*c* = 0.488 in EtOH), whilst Danishefsky had reported -13.6° (*c* = 0.320 in EtOH) for his synthetic (2*S*,3*S*,4*S*)-rishirilide B (**1.36**) and Pettus had reported +12.6° (*c* = 0.5 in EtOH) for his synthetic (2*R*,3*R*,4*R*)-rishirilide B (**1.36**). The comparison of the values for the natural

product (+12.8°) and the three synthesised products (2*R*,3*R*,4*R*)-rishirilide B (Pettus = +12.6°) (Odagi = -14.8°) and (2*S*,3*S*,4*S*)-rishirilide B (Danishefsky = -13.6°), showed significant discrepancies in the reported numbers, casting doubt on the assignment of absolute configuration of the natural product. This prompted Odagi to synthesise (2*S*,3*S*,4*S*)-rishirilide B (**1.36**) for further comparison in an attempt to unambiguously assign the absolute stereochemistry of the natural product. Odagi utilised a similar synthetic route as before but starting from the corresponding (2*R*)-tetralone (**1.75**) to give (2*S*,3*S*,4*S*)-rishirilide B (**1.36**) in an 86 % *ee* (**Scheme 1.13**).

Odagi's synthetic (2*S*,3*S*,4*S*)-rishirilide B (**1.36**) showed an optical rotation of +13.8° (*c* = 0.26 in EtOH) which was consistent with that of the natural product (+12.8° (*c* = 0.488 in EtOH)), suggesting an absolute configuration of (2*S*,3*S*,4*S*). The absolute stereochemistry was confirmed by chiral HPLC of Odagi's synthetic (2*R*,3*R*,4*R*)-rishirilide B and (2*S*,3*S*,4*S*)-rishirilide B versus the natural product.

Good agreement was found between the retention time for Odagi's synthetic (2*S*,3*S*,4*S*)-rishirilide B (**1.36**) and for the natural product rishirilide B (**Figure 1.6**).

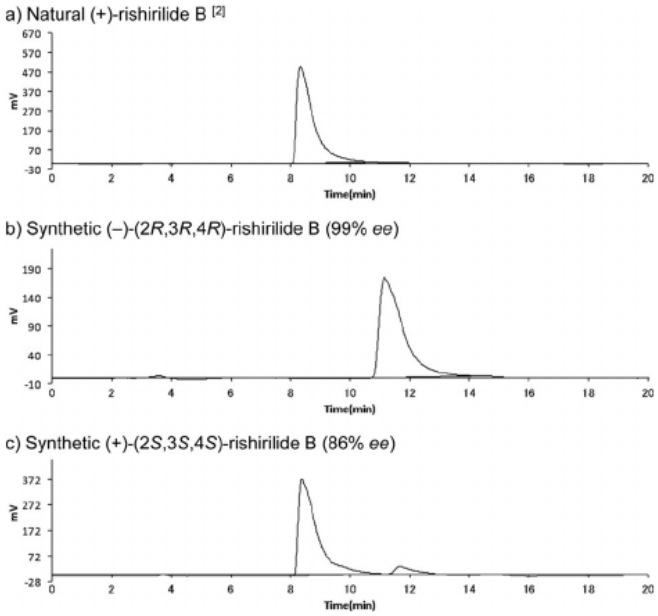

Figure 1.6: Comparison of retention times on chiral HPLC of Odagi's synthetic (2*S*,3*S*,4*S*) and (2*R*,3*R*,4*R*) rishirilide B versus the natural product[52].

These findings led Odagi to conclude that the absolute configuration of natural (+)-rishirilide B must therefore be (2*S*,3*S*,4*S*), overturning the previous assignments by Danishefsky and Pettus (**Figure 1.7**).

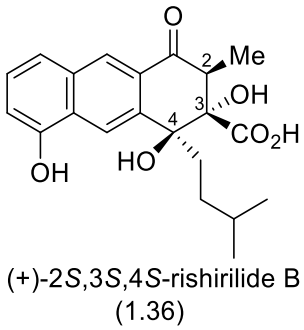

(+)-2*S*,3*S*,4*S*-rishirilide B
(1.36)

Figure 1.7: The reassigned absolute configurations of natural (+)-(2*S*,3*S*,4*S*)-rishirilide B (**1.36**)

Odagi's suggested that the previous misassignment of absolute stereochemistry by both Danishefsky and Pettus was likely due to the presence of impurities in the final products which may have resulted in errors in the observed optical rotations.

1.7 General Plan for the Total Synthesis of DEM30355/A (1)

Having reviewed both the seminal literature on constructing fused polycyclic rings and the literature on the total synthesis of structurally comparable natural products, we will now lay out our plan for the total synthesis of DEM30355/A (**1**). The key takeaway from the literature was the success of a convergent approach to the ABC fused carbon ring core via a naphthalene disconnection and the use of either Diels-Alder or Michael-Dieckmann reactions to couple both rings. In our case, for DEM30355/A (**1**), the construction of the quaternary centre at C-4a, whilst avoiding the competing aromatisation of the B-ring will be an additional challenge.

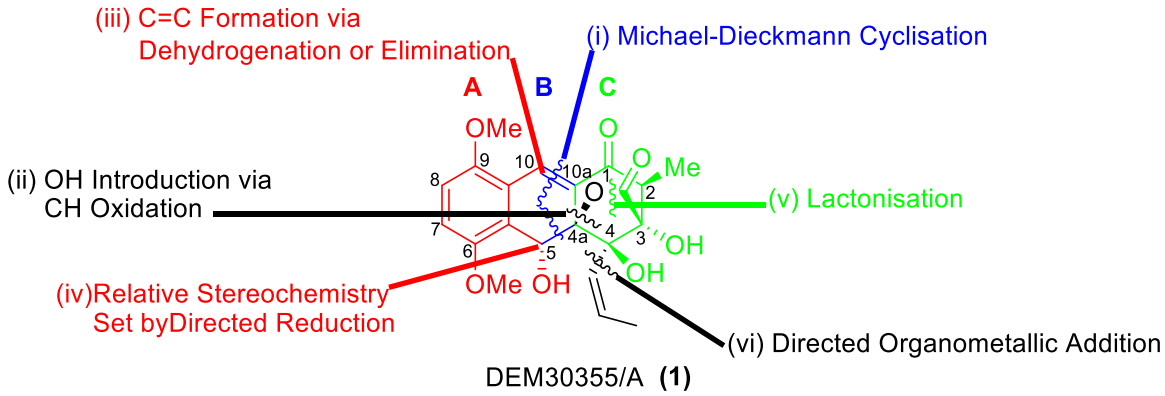

Figure:1.8: Overview of our plan to synthesise DEM30355/A (**1**).

Our synthetic plan towards DEM30355/A (**1**) (**Figure 1.8**) employs a key Michael-Dieckmann cyclisation reaction (i) to form the B-ring. After synthesis of our fused ABC tricyclic carbon ring skeleton, we would then aim to incorporate the hydroxyl group at the C-4a position (ii). The

carbon-carbon double bond between C-10/C-10a would be installed through a β-elimination or an oxidative dehydrogenation (iii). Our planned Michael-Dieckmann cyclisation would initially include a ketone at C-5. Thus, to install the required hydroxyl group at C-5, we envisioned that the hydroxyl group at C-4a could be used to stereoselectively direct a reduction of the ketone at C-5 (iv). A subsequent lactonization between the co-facial hydroxyl group at C-4a and the ester group at C-3 would install the required lactone (v). Our planned Michael-Dieckmann cyclisation would initially include a ketone at C-4. To install the required alkenyl group at C-4 we would direct an organometallic addition via the hydroxyl group at C-3 (vi).

In the subsequent chapter we will provide a more detailed discussion of our synthetic plans and our first synthetic steps towards DEM30355/A (**1**).

Chapter 1 - References

1) H. D. Marston, D. M. Dixon, J. M. Knisely, T. N. Palmore and A. S. Fauci, *JAMA.,* 2016, **316**, 1193-1204.
2) L. J. Piddock, *Lancet. Infect. Dis*., 2012, **12**, 249-253.
3) CDC. National Centre for Health Statistics. Life Expectancy. https://www.cdc.gov/nchs/fastats/life-expectancy.htm . (Accessed: June 2020).
4) J. O'Neill, Review on Antimicrobial Resistance: Tackling Drug-Resistant Infections Globally, Final Report and Recommendations, May, 2016.
5) J. Clardy, M.A. Fischbach and C. R. Currie, *Curr. Biol.* 2009, **19**, 437-441.
6) G. M. Cragg and D. J. Newman *Biochim. Biophys. Acta.*, 2013, **1830**, 3670–3695.
7) D. M. Livermore, *J. Antimicrob. Chemother.*, 2011, **66**, 1941-1944.
8) A Brief Overview of Classes of Antibiotics, https://www.compoundchem.com/2014/09/08/antibiotics/ (Accessed: June 2020).
9) WHO Report on Surveillance of Antibiotic Consumption 2016-2018 Early Implementation. https://apps.who.int/iris/bitstream/handle/10665/277359/9789241514880-eng.pdf (Accessed: June 2020).
10) Centres for Disease Control and Prevention, U.S. Department of Health and Human Services, Antibiotic resistance threats in the United States, Atlanta, GA 2013, http://www.cdc.gov/drugresistance/pdf/ar-threats-2013-508.pdf (Accessed: June 2020)
11) L. B. Rice, *J. Infect. Dis.*, 2008, **197**, 1079.
12) WHO publishes list of bacteria for which new antibiotics are urgently needed https://www.who.int/news-room/detail/27-02-2017-who-publishes-list-of-bacteria-for-which-new-antibiotics-are-urgently-needed (Accessed: June 2020).
13) A. Howard, M. O'Donoghue and A. Feeney, R.D. Sleator, *Virulence*, 2012, **3**, 243–250.
14) L. C. Antunes, P. Visca and K. J. Towner, *Pathog. Dis.*, 2014, **71**, 292–301.
15) L. S. Munoz-Price and R. A. Weinstein, *N. Engl. J. Med.*, 2008, **358**, 1271-1281.
16) I. Abbott, G. M. Cerqueira, S. Bhuiyan and A. Y. Peleg, *Expert. Rev. Anti. Infect. Ther.*, 2013, **11**, 395-409.

17) T. Ferkol, D. Schraufnagel, *Ann. Am. Thorac. Soc.*, 2014, **11**, 404-406.

18) W. Cookson, M. J. Cox and M. F. Moffatt, *Nat. Rev. Microbiol.*, 2018, **16**, 111-120.

19) S. L. Gellatly and R. E. Hancock, *Pathog. Dis.*, 2013, **67**, 159-173.

20) Antibiotic Resistance Threats in the United States, 2019 https://www.cdc.gov/drugresistance/pdf/threats-report/2019-ar-threats-report-508.pdf (Accessed: June 2020).

21) Tackling antimicrobial resistance 2019–2024. The UK's five-year national action plan https://assets.publishing.service.gov.uk/government/uploads/system/uploads/attachment_data/file/784894/UK_AMR_5_year_national_action_plan.pdf (Accessed: June 2020).

22) M. G. Moloney, *Trends. Pharmacol. Sci*., 2016, **37**, 689–701.

23) World Health Organization. 2019 Antibacterial Agents in Clinical Development: An Analysis of the Antibacterial Clinical Development Pipeline, https://apps.who.int/iris/bitstream/handle/ 10665/330420/9789240000193-eng.pdf (Accessed: June 2020).

24) D. J. Payne, M. N. Gwynn, D. J. Holmes and D. L. Pompliano, *Nat. Rev. Drug. Disc.*, 2007, **6**, 29.

25) M. N. Gwynn, A. Portnoy, S. F. Rittenhouse and D. J. Payne, *Ann. N. Y. Acad. Sci*., 2010, **5**, 1213.

26) J. Clardy, M. A. Fischbach and C. T. Walsh, *Nat. Biotechnol.*, 2006, **24**, 1541-1550.

27) L. L. Ling, T. Schneider and A. J. Peoples*, Nature*, 2015, **517**, 455-459.

28) K. Lewis, *Nature Rev. Drug Discov.,* 2013, **12**, 371–387.

29) D. Nichols *et al. Appl. Environ. Microbiol.*, 2010, **76**, 2445–2450.

30) E. J. Culp, N. Waglechner, W. Wang, *et al. Nature*, 2020, **578**, 582-587.

31) B. Kepplinger, PhD Thesis, Newcastle University, 2016.

32) L. H. Conover, K. Butler, J. D. Johnston, J. J. Korst and R. B. Woodward, *J. Am. Chem. Soc.*, 1962, **84**, 3222–3224.

33) R. B. Woodward, *Pure. Appl. Chem.*, 1963, **6**, 561-574.

34) J. J. Korst, J. D. Johnston, K. Butler, E. J. Bianco, L. H. Conover and R. B. Woodward, *J. Am. Chem. Soc.*, 1968, **90**, 439-457.

35) H. Muxfeldt and W. Rogalski, *J. Am. Chem. Soc.*, 1965, **87**, 933-934.

36) H. Muxfeldt, G. Hardtmann, F. Kathawala, E. Vedejs and J. B. Mooberry, *J. Am. Chem. Soc.*, 1968, **90**, 6534-6536.

37) H. Muxfeldt, G. Haas, G. Hardtmann, F. Kathawala, J. B. Mooberry and E. Vedejs, *J. Am. Chem. Soc.*, 1979, **101**, 689-701.

38) B. M. G. Gaveby, J. C. Huffmann and P. Magnus, *J. Org. Chem.*, 1982, **47**, 3779-3780.

39) G. Stork, J. J. La Clair, P. Spargo, R. P. Nargund and N. Totah, *J. Am. Chem. Soc*.,1996, **118**, 5304-5305.

40) K. Tatsuta, T. Yoshimoto, H. Gunji, Y. Okado and M. Takahashi, *Chem. Lett.* 2000, 646–647.

41) M. G. Charest, C. D. Lerner, J. D. Brubaker, D. R. Siegel and A. G. Myers, *Science.*, 2005, **308**, 395-398.

42) M. G. Charest, D. R. Siegel and A. G. Myers, *J. Am. Chem. Soc.*, 2005, **127**, 8292-8293.

43) H. Iwaki, Y. Nakayama, M. Takahashi, S. Uetsuki, M. Kido and Y. Fukuyama, *J. Antibiot.*, 1984, **37**, 1091.

44) X. Yan, K. Probst, A. Linnenbrink, M. Arnold, T. Paululat, A. Zeec and A. Bechtold, *ChemBioChem.*, 2012, **13**, 224-230.

45) D. Komagata, R. Sawa, N. Kinoshita, C. Imada, T. Sawa, H. Naganawa, M. Hamada, Y. Okami and T. Takeeuchi, *J. Antibiot*., 1992, **45**, 1681-1683.

46) D. Sheehan, G. Meade, V. M. Foley and C. A. Dowd, *Biochem J*., 2001, **360**, 1-16.

47) D. M. Townsend and K. D. Tew, *Oncogene*, 2003, **22**, 7369-7375.

48) F. M. Hauser and Y-J. Xu, *Org. Lett.*, 1999, **1**, 335-336.

49) J. G. Allen and S. J. Danishefsky, *J. Am. Chem*., 2001, **123**, 351-352.

50) K. Yamamoto, M. F. Hentemann, J. G. Allen and S. J. Danishefsky, *Chem. Eur. J.*, 2003, **22**, 7369-7375.

51) J. G. Allen, M. F. Hentemann and S. J. Danishefsky, *J. Am. Chem. Soc*., 2000, **122**, 571-575.

52) L. H. Mejorado and T. R. R. Pettus, *J. Am. Chem. Soc*., 2006, **128**, 15625-15631.

53) M. Odagi, K. Furukori, K. Takayama, K. Noguchi and K. Nagasawa, *Angew. Chem. Int. Ed*., 2017, **56**, 6609-6612.

Chapter 2 - Synthesis of the Left-Hand A-Ring of DEM30355/A

2.1 Introduction

In this chapter we will discuss our work towards the synthesis of the left-hand A-ring of our target molecule DEM30355/A (**1**). It should be noted that during the course of this work the absolute stereochemistry of DEM30355/A (**1**) was determined by both VCD and X-ray crystallography by our collaborators[1] (**Figure 2.0**).

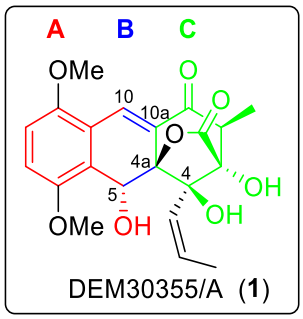

Figure 2.0: The absolute stereochemistry of our target molecule DEM30355/A (**1**).

2.1.1 Planned Synthetic Route to A-ring of DEM30355/A via a Benzyne Intermediate

Our plan to construct the fused ABC ring structure of DEM30355/A (**1**) was inspired by the previous syntheses of the structurally related rishirilide B (**1.36**) whereby the disconnection of the bonds at C-10/C-10a and C-4a/C5 would generate an A-ring precursor (**2.02**) and a C-ring precursor (**2.03**) (**Scheme 2.00**).

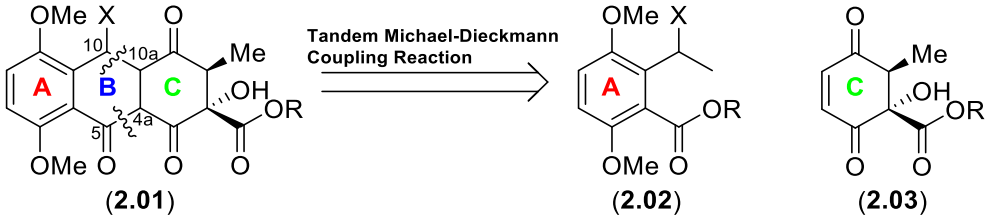

Scheme 2.00: The proposed route to the ABC fused ring core of DEM30355/A (**1**) with an illustration of its absolute stereochemistry. X = electron withdrawing group, R = alkyl group.

We would then look to couple the A-ring precursor (**2.05**) (**Scheme 2.01**) with the C-ring precursor (**2.06**) via a tandem Michael-Dieckmann cyclisation reaction whereby the A-ring precursor (**2.05**) would act as a suitably functionalised Michael-type donor and the C-ring precursor (**2.06**) would be our Michael-type acceptor. The initial 1,4-Michael addition and subsequent Dieckmann cyclisation would form the required B-ring to create our ABC fused ring skeleton (**Scheme 2.01**).

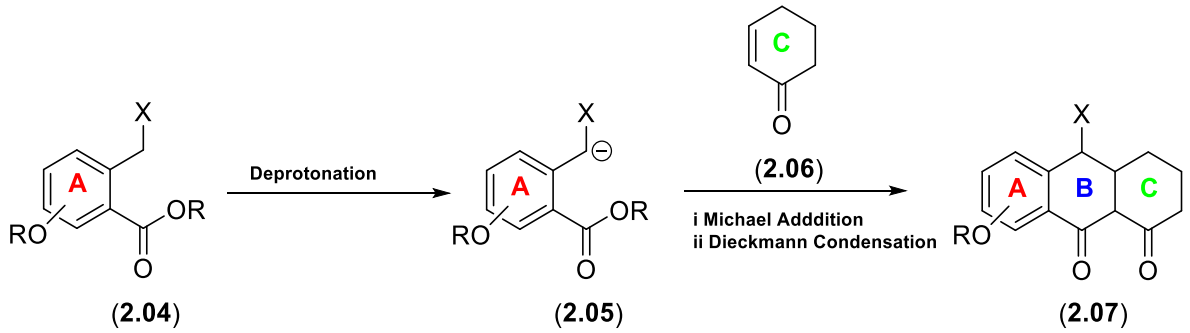

Scheme 2.01: Our plan to construct the fused ABC anthracene skeleton of DEM30355/A (**1**) via a key tandem Michael-Dieckmann cyclisation. R = alkyl group, X = electron withdrawing group.

2.2 Results and Discussion

2.2.1 Synthesis of the A-Ring Precursor

Our first synthetic target was therefore a suitable precursor for the A-ring of DEM30355/A (**1**), which would consist of a methyl or ethyl benzoate containing an *ortho*-(phenylsulfonyl) methyl group (**2.09**). We envisaged that our target A-ring precursor (**2.09**) could be prepared following the work of Huang[2] in which he demonstrated the insertion of arynes into an appropriately functionalised aryl sulfone (**2.08**) (**Scheme 2.02**).

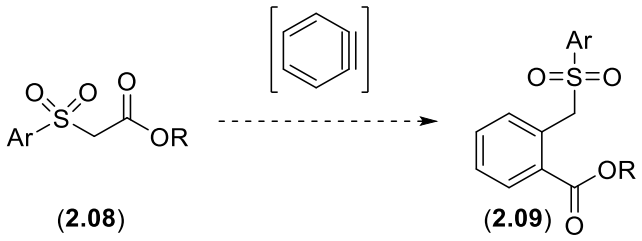

Scheme 2.02: Planned synthesis of A-ring precursor (**2.09**) following Huang's aryne insertion into an aryl sulfone (**2.08**)

We imagined this phenylsulfonyl benzoate system (**2.09**) would act as a good A-ring precursor with which to test our Michael-Dieckmann chemistry as it contains the electron withdrawing phenyl sulfonyl moiety which would stabilise the carbanion that initiates the Michael addition (Scheme **2.01**). The phenyl sulfonyl moiety has the added benefit of being a good leaving group. In addition, attached *ortho* to the phenyl sulfonyl moiety (**2.09**) is the electrophilic ester group required for the subsequent Dieckmann condensation.

Therefore, our first challenge was the synthesis of an appropriate aryl sulfone with which to test the aryne insertion chemistry. We chose methyl 2-(phenylsulfonyl) acetate (**2.13**) as our target molecule, which we envisaged synthesising via alkylation of thiophenol (**2.10**) with methyl-2-bromoacetate (**2.11**) to give methyl 2-(phenylthio) acetate (**2.12**) and subsequent oxidation (**Scheme 2.03**).

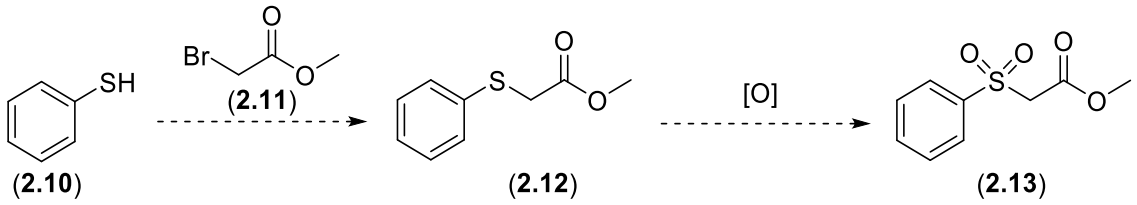

Scheme 2.03: Planned alkylation of thiophenol (**2.10**) and subsequent oxidation of methyl 2-(phenylthio) acetate (**2.12**) to give the aryl sulfone (**2.13**).

2.2.2 Synthesis of Methyl 2-(phenylthio) acetate (2.12)

Thus, thiophenol (**2.10**) was reacted with 1.2 eq of methyl bromoacetate (**2.11**) in refluxing acetonitrile in the presence of potassium carbonate[3] (**Scheme 2.04**). After 24 h, no further changes in the reaction composition could be observed by TLC. Following aqueous work-up and column chromatography methyl 2-(phenylthio) acetate (**2.12**) was isolated in a yield of 83 % from a 1 mmol scale reaction.

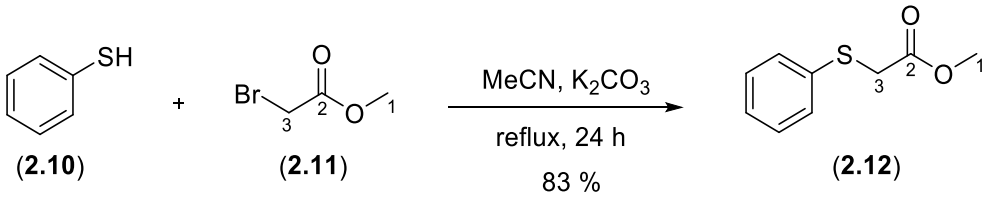

Scheme 2.04: Alkylation of thiophenol (**2.15**) with methyl bromoacetate (**2.16**) to give methyl 2-(phenylthio) acetate (**2.17**).

The structure of methyl 2-(phenylthio) acetate (**2.17**) was confirmed by ^{1}H NMR analysis in which the signal associated with the C-3 methylene group showed an upfield shift from 3.82 ppm in methyl bromoacetate (**2.11**) to 3.61 ppm in methyl 2-(phenylthio) acetate (**2.12**). Further synthetic work would require access to gram quantities of methyl 2-(phenylthio) acetate (**2.12**). Therefore, we repeated the alkylation of thiophenol (**2.10**) under these same conditions but on a larger 10 mmol scale, resulting in a promising isolated yield of 83 %. To test the reproducibility of these conditions, the alkylation reaction was performed a further three times, on a 10 mmol scale in each case, to give an average yield of 82 % over a total of four reactions (83, 83, 80 and 81 % SD = 1.3).

To further expand the alkylation chemistry available to us, we next examined an alternative alkylation of thiophenol (**2.10**) following the work of Hosomi[4]. Thus, thiophenol (**2.10**) was reacted with 1.2 eq of methyl bromoacetate (**2.11**) in toluene and Et_3N on a 1 mmol scale for 24 hours at room temperature. Following aqueous work-up and column chromatography methyl 2-(phenylthio) acetate (**2.12**) was isolated in a similar 84 % yield. As previously, the alkylation of thiophenol (**2.10**) was scaled up a to 10 mmol scale, with no loss of yield. Again, the alkylation was run on a 10 mmol scale a further three times to assess reproducibility giving an average yield of 83 % over a total of four reactions (84, 84, 80 and 82 % SD = 1.7) (**Scheme 2.05**).

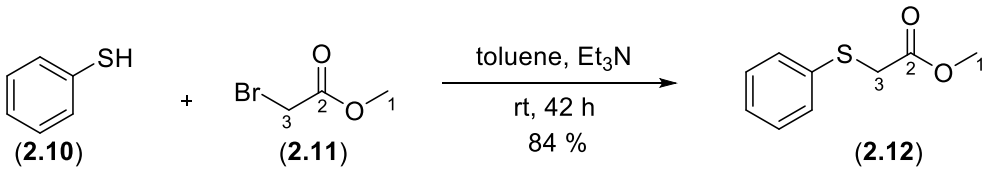

Scheme 2.05: Alternative alkylation of thiophenol (**2.10**) to methyl 2-(phenylthio) acetate (**2.12**).

The isolated yields obtained for both sets of alkylation conditions were very similar, including those obtained for the larger scale (10 mmol) reactions examined, thus either would be feasible for the synthesis of methyl 2-(phenylthio) acetate (**2.12**). In fact, during the course of our investigations we had produced multi-gram quantities of methyl 2-(phenylthio) acetate (**2.12**) allowing us to proceed to examine the subsequent oxidation of methyl 2-(phenylthio) acetate (**2.12**) to its corresponding sulfone.

2.2.3 Oxidation of Methyl 2-(phenylthio) acetate (2.12)

The next synthetic step we examined was the oxidation of methyl 2-(phenylthio) acetate (**2.12**) to the corresponding sulfone, methyl 2-(phenylsulfonyl) acetate (**2.13**) (**Scheme 2.06**).

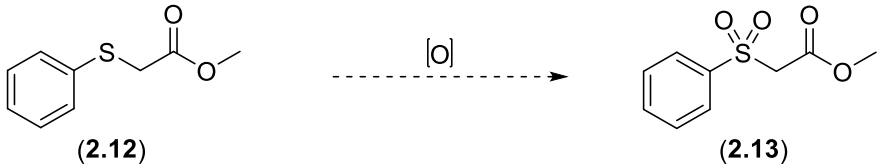

Scheme 2.06: Planned oxidation of methyl 2-(phenylthio) acetate (**2.12**) to methyl 2-(phenylsulfonyl) acetate (**2.13**).

Our first attempt at the oxidation of methyl 2-(phenylthio) acetate (**2.12**) was based on the work of Cowling *et al*.[5] employing *m*CPBA as the oxidant. Commercial *m*CPBA commonly contains trace quantities of *meta*-chlorobenzoic acid. Thus, *m*CPBA was purified by stirring the *m*CPBA with an $NaOH/NaH_2PO_4$ buffer solution (pH 7.5) for 6 h followed by recrystallisation at -20 °C from *n*-hexane/diethyl ether 3:1 and storage at -20 °C for up to 1 week prior to use. The oxidation of methyl 2-(phenylthio) acetate (**2.12**) was first carried out on a 1 mmol scale using 2.5 eq of *m*CPBA in dry DCM at 0 °C with warming to rt over 4 h. Following aqueous work-up, TLC analysis of the crude reaction mixture (UV 254 nm) showed the presence of starting material, methyl 2-(phenylthio) acetate (**2.12**), (R_f = 0.54), as well as two new compounds (R_f = 0.10 and 0.38).

Flash column chromatography of the crude material gave the desired product methyl 2-(phenylsulfonyl) acetate (**2.13**) in 18 % yield, alongside the starting material methyl 2-(phenylthio) acetate (**2.12**) in 70 % yield and another isolated compound at R_f = 0.38 in 9 % yield. ^{1}H NMR analysis showed that the most polar compound of the three isolates (R_f = 0.10) was our desired product methyl 2-(phenylsulfonyl) acetate (**2.13**). Structural assignment of methyl 2-(phenylsulfonyl) acetate (**2.13**) was supported by ^{1}H NMR analysis[6], which showed that the signal corresponding to the methylene

protons at C-3 had shifted downfield from 3.61 ppm (in methyl 2-(phenylthio) acetate (**2.12**)) to 4.13 ppm, which was consistent with the introduction of an electron withdrawing sulfonyl group (**Figure 2.1**).

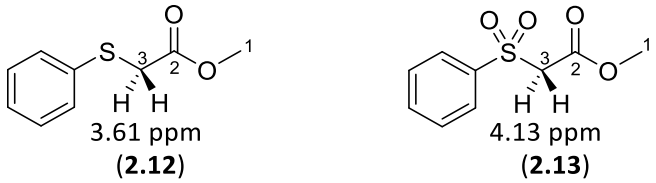

Figure 2.1: ^{1}H NMR chemical shift comparison of the C-3 methylene protons of starting material methyl 2-(phenylthio) acetate (**2.12**) and the oxidised product methyl 2-(phenylsulfonyl) acetate (**2.13**).

^{1}H NMR analysis of the second product of the oxidation of methyl 2-(phenylthio) acetate (**2.12**) (R_f = 0.38) indicated that it contained a diastereotopic methylene group, showing a clear geminal coupling (3.62 ppm, d, *J* = 13.7 Hz and 3.81 ppm, d, *J* = 13.7 Hz). Thus, we postulated that this compound was methyl 2-(phenylsulfinyl) acetate (**2.14**), which was formed via a single oxidation of the starting methyl 2-(phenylthio) acetate (**2.12**) (**Figure 2.2**).

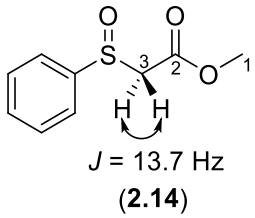

Figure 2.2: ^{1}H NMR analysis of methyl 2-(phenylsulfinyl) acetate (**2.14**) showing a key geminal coupling between the methylene protons at the C-3 position.

In light of the results of our first attempt at the oxidation of methyl 2-(phenylthio) acetate (**2.12**) (**Scheme 2.07**), we decided in our future efforts to increase the equivalents of the oxidant *m*CPBA to try to push the oxidation through to completion.

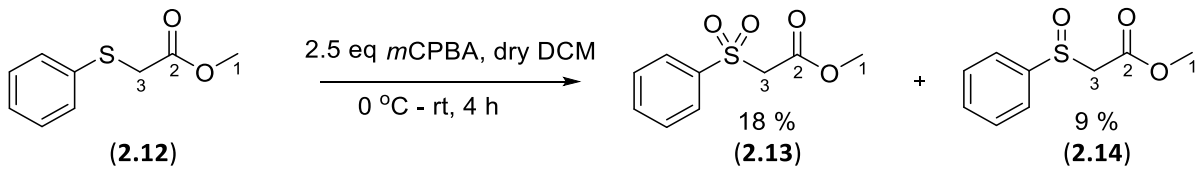

Scheme 2.07: Initial reaction conditions for the oxidation of methyl 2-(phenylthio) acetate (**2.12**) resulting in two products methyl 2-(phenylsulfonyl) acetate (**2.13**) and methyl 2-(phenylsulfinyl) acetate (**2.14**).

Subsequently, our next attempt at the oxidation of methyl 2-(phenylthio) acetate (**2.12**) was again done on a 1 mmol scale in dry DCM from 0 °C – rt but this time employing 4 eq of the oxidant *m*CPBA. After 4 h no further changes could be observed by TLC. Following work-up, methyl 2-(phenylsulfonyl) acetate (**2.13**) was isolated in a yield of 84 %. ^{1}H NMR analysis showed no signs of the diastereotopic protons with signals at 3.81 ppm and 3.62 ppm previously seen when the oxidation was attempted

with 2.5 eq of *m*CPBA and taken to be indicative of the single oxidation product methyl 2-(phenylsulfinyl) acetate (**2.14**). In order to access gram quantities of methyl 2-(phenylsulfonyl) acetate (**2.13**) for further synthesis the oxidation of methyl 2-(phenylthio) acetate (**2.12**) using 4 eq of *m*CPBA was repeated on a 5 mmol scale, pleasingly, with no loss in yield. We decided against testing a further scale-up to 10 mmol of the oxidation of methyl 2-(phenylthio) acetate (**2.12**) with 4 eq of *m*CPBA due to the potential hazards of working with multi-gram quantities of purified *m*CPBA. Instead, we decided to focus on reducing the equivalents of *m*CPBA required through reaction optimisation.

Having successfully completed the oxidation of methyl 2-(phenylthio) acetate (**2.12**) to methyl 2-(phenylsulfonyl) acetate (**2.13**) in good yield of 84 % using 4 eq of *m*CPBA and having postulated through using ^{1}H NMR and TLC data that the oxidation to the methyl 2-(phenylsulfonyl) acetate (**2.13**) when using 2.5 eq of *m*CPBA produced a mixture of the desired product, methyl 2-(phenylsulfonyl) acetate (**2.13**) as well as the single oxidation product methyl 2-(phenylsulfinyl) acetate (**2.14**) we imagined that using 3 eq of *m*CPBA might be the optimal conditionality between complete oxidation to our desired product methyl 2-(phenylsulfonyl) acetate (**2.13**) and efficient use of *m*CPBA. Thus, we again attempted the oxidation of methyl 2-(phenylthio) acetate (**2.12**) on a 1 mmol scale with 3 eq of *m*CPBA in dry DCM from 0 °C – rt. Pleasingly, the results bore out our reasoning and the product methyl 2-(phenylsulfonyl) acetate (**2.13**) was obtained after work-up again in 84 % isolated yield (**Scheme 2.08**).

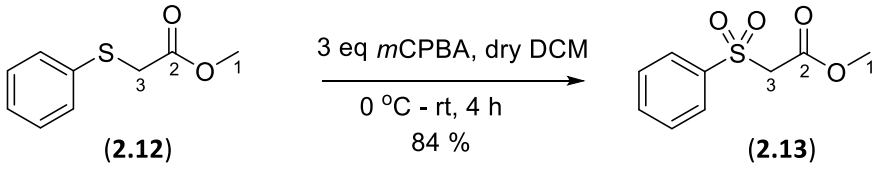

(**2.12**) (**2.13**)

Scheme 2.08: Optimal conditions for the oxidation of methyl 2-(phenylthio) acetate (**2.12**) to methyl 2-(phenylsulfonyl) acetate (**2.13**) using 3eq *m*CPBA.

Needing gram quantities for further synthetic work, we were able to scale the reaction to a 5 mmol scale using 3 equivalents of *m*CPBA with no resulting loss in yield. With gram quantities of methyl 2-(phenylsulfonyl) acetate (**2.13**) in hand we proceeded to examine the next synthetic step.

	Eq of *m*CPBA	Methyl 2-(phenylthio) acetate (**2.12**) /mmol	Isolated % yield of (**2.13**)
ENTRY 1	2.5	1	18
ENTRY 2	4.0	1	84
ENTRY 3	4.0	5	84
ENTRY 4	3.0	1	84
ENTRY 5	3.0	5	84

Table 2.0: Reaction conditions for the oxidation of methyl 2-(phenylthio) acetate (**2.12**) to methyl 2-(phenylsulfonyl) acetate (**2.13**) with mCPBA.

2.2.4 Synthesis of our A-ring precursor (2.17) via an aryne insertion into methyl 2-(phenylsulfonyl) acetate (2.13)

To complete the synthesis of our A-ring precursor (**2.17**) we wished to examine the insertion of arynes into our previously isolated methyl 2-(phenylsulfonyl) acetate (**2.13**). Thus, we planned to generate the required aryne *in situ* via a fluoride-initiated elimination of the triflate group of 2-(trimethylsilyl) phenyl triflate (**2.15**) as reported by Huang[2]. The *in situ* generated aryne (**2.16**) would then react with methyl 2-(phenylsulfonyl) acetate (**2.13**) to give our A-ring precursor, methyl 2-((phenylsulfonyl)methyl) benzoate (**2.17**) (**Scheme 2.09**).

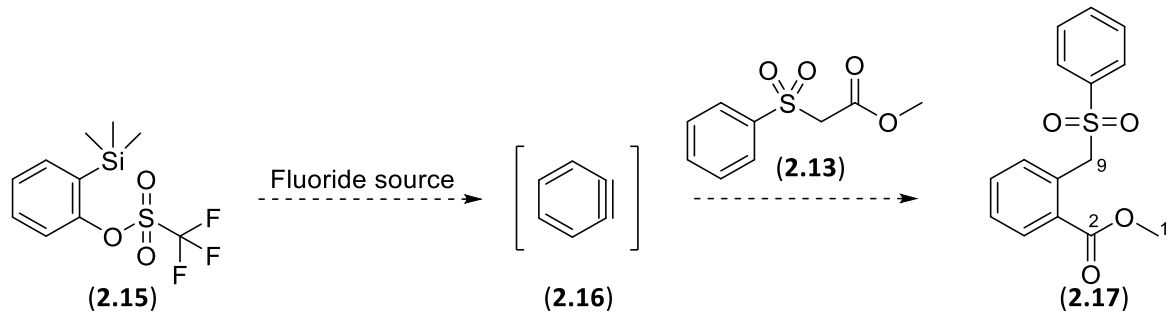

(**2.15**) (**2.16**) (**2.13**) (**2.17**)

Scheme 2.09: Planned route to our A-ring precursor methyl 2-((phenylsulfonyl)methyl) benzoate (**2.17**) via a fluoride-initiated *in situ* generation of aryne (**2.16**) from aryne precursor (**2.15**) and subsequent reaction with methyl 2-(phenylsulfonyl) acetate (**2.13**).

A number of reaction conditions and fluoride sources were screened to synthesise our A-ring precursor (**2.17**) starting with acetonitrile as solvent. The reaction was first attempted on a 0.5 mmol scale using CsF as the fluoride source with heating to 50 ^{o}C[7] yielding the desired A-ring precursor (**2.17**) after work-up and purification by column, in a modest yield of 21 % (**Table 2.1**: Entry 1).

In an attempt to improve yields, the reaction was repeated at rt using TBAF as the fluoride source[8]. TBAF was chosen as the new fluoride source for its more organo-soluble properties. After work-up and column chromatography, the A-ring precursor (**2.17**) was isolated in 60 % yield (**Table 2.1**: Entry 2). Our third reaction, utilised KF as the fluoride source[2] with methyl-2-(phenylsulfonyl) acetate (**2.13**)

used as the limiting reagent (**Table 2.1**: Entry 3). These conditions produced the best isolated yield of 81 % for our A-ring precursor (**2.17**) in just 4 h.

Requiring gram quantities of A-ring precursor (**2.17**) for further study, we scaled up our best reaction conditions from a 0.5 mmol scale to a 3 mmol scale giving the product (**2.17**) in high yield of 81 % (**Table 2.1**: Entry 4). This gave access to sufficient quantities of our β keto sulfone A-ring precursor (**2.17**) for further synthesis (**Scheme 2.10**).

Entry	(**2.13**) Mmol	(**2.13**) eq.	(**2.16**) eq.	Reaction conditions	Isolated % Yield (**2.17**)
1	0.5	2.0	1.0	1.5 eq CsF, MeCN, 50 ^{o}C, 96 h	21
2	0.5	2.0	1.0	1.5 eq TBAF, MeCN, rt, 21 h	60
3	0.5	1.0	1.3	2.6 eq KF, 2.6 eq 18-Crown-6, THF, rt, 4 h	81
4	3.0	1.0	1.3	2.6 eq KF, 2.6 eq 18-Crown-6, THF, rt, 4 h	81

Table 2.1: Reaction conditions to form A-ring precursor (**2.17**) from methyl 2-(phenylsulfonyl) acetate (**2.13**) and 2-(trimethylsilyl) phenyl triflate (**2.16**) in the presence of a fluoride source.

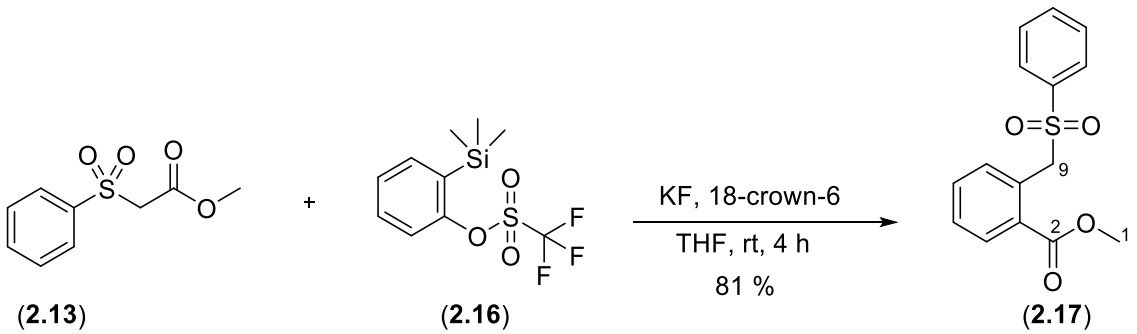

Scheme 2.10: Optimal conditions for the synthesis of A-ring precursor methyl 2-((phenylsulfonyl)methyl) benzoate (**2.17**) from aryne precursor 2-(trimethylsilyl) phenyl triflate (**2.16**) with methyl 2-(phenylsulfonyl) acetate (**2.13**) in the presence of KF as fluoride source.

To confirm the structure of our A-ring precursor, methyl 2-((phenylsulfonyl)methyl) benzoate (**2.17**) we examined the ^{1}H NMR data which confirmed the presence of the nine expected aromatic protons. The two benzylic protons at C-9 were also confirmed as a singlet at 5.06 ppm. Additionally, ^{13}C NMR data of A-ring precursor (**2.17**) confirmed 10 aromatic carbon signals, supporting the presence of two aromatic rings. Analysis by HRMS also showed a key molecular ion $[M+H]^{+}$ signal at m/z = 291.0687.

To further validate the authenticity of the structure of our A-ring precursor (**2.17**), we were able to grow crystals by slow solvent evaporation for X-ray analysis. The use of chloroform as solvent produced the desired high-quality single crystals of methyl 2-((phenylsulfonyl)methyl) benzoate

(**2.17**). The crystal structure also revealed the presence of an unusual intramolecular hydrogen bond between the benzylic hydrogen at C-9 and the carbonyl oxygen at C-2 with an intramolecular C-H···O hydrogen bond distance of 2.163 Å. Sureshan *et al.*[9] have reported on the presence of intramolecular C-H···O hydrogen bonds in sulfones and sulfoxides with C-H···O hydrogen bond distances between 2.35-2.45 Å. Thus, our observed intramolecular C-H···O hydrogen bond appears somewhat shorter than those reported.

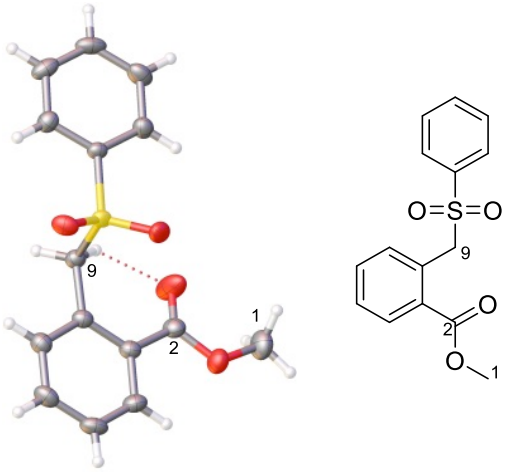

Figure 2.3: X-Ray crystal structure of our A-ring precursor methyl 2-((phenylsulfonyl)methyl) benzoate (**2.17**).

With our A-ring precursor (**2.17**) in hand we could now test our Michael-Dieckmann tandem reaction to form the ABC anthracene core of DEM30355/A (**1**). This chemistry is explored in detail in chapter three.

2.3 Synthesis of a Methoxy Containing A-ring Precursor

In an attempt to widen the synthetic scope afforded by our first A-ring precursor (**2.17**) we planned to examine a second A-ring precursor (**2.18**) that would allow us to form a more similarly functionalised analogue of the A-ring of DEM30355/A (**1**), i.e. with the inclusion of the required methoxy group at C-2 (**Figure 2.4**).

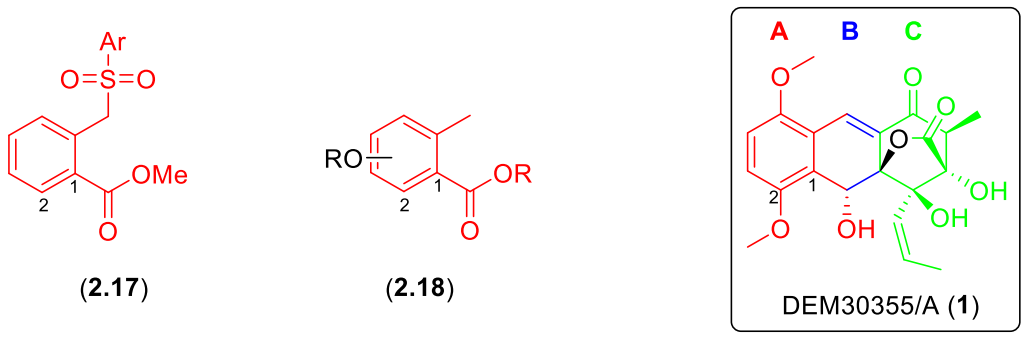

(**2.17**) (**2.18**)

Figure 2.4: The structures of our first A-ring precursor (**2.17**), our proposed second A-ring precursor (**2.18**) and our target DEM30355/A (**1**).

To access our second A-ring precursor, we envisioned starting with a functionalised benzoic acid, 2-methoxy-6-methylbenzoic acid (**2.19**) with the required methoxy group already installed at C-2. By converting the carboxylic acid functionality of 2-methoxy-6-methylbenzoic acid (**2.19**) to the corresponding ester (**2.20**) we could replicate the electrophilic C-1 ester group as contained in our first A-ring precursor (**2.17**) that is required for our subsequent Dieckmann chemistry. Subsequent utilisation of a strong base to deprotonate at the C-7 position of our ester (**2.20**) would create a nucleophilic site and set up the desired Michael addition chemistry (**Scheme 2.10**).

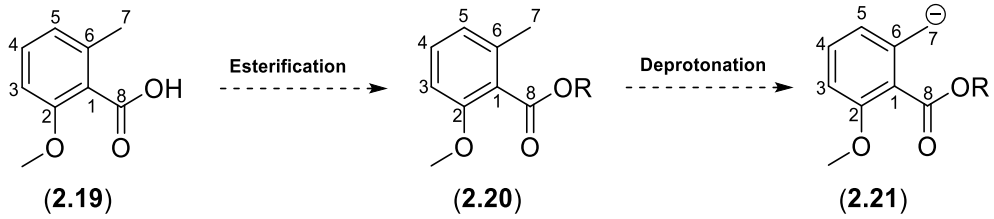

Scheme 2.10: Our planned second A-ring precursor via an esterification and subsequent deprotonation of 2-methoxy-6-methylbenzoic acid (**2.19**).

The coupling of our second A-ring precursor (**2.20**) containing the methoxy group at C-2 with our C-ring precursor would then allow us access to a functionalised ABC anthracene ring core more resembling of DEM30355/A (**1**). In addition, as suggested by Myers *et al.*[10, 11] the presence of a better anionic leaving group at the C-1 ester could more readily promote the Dieckmann cyclisation. Thus, we chose the phenoxy group as our test ester group.

Our synthesis began with 2-methoxy-6-methylbenzoic acid (**2.19**) which already contains the required methoxy group at the C-2 position. A Steglich esterification, done on a 2 mmol scale, of 2-methoxy-6-methylbenzoic acid (**2.19**) with 1.1 eq of phenol, in the presence of DMAP, and utilising 1.1 eq of EDC.HCl as a coupling agent yielded phenyl 2-methoxy-6-methylbenzoate (**2.22**) after work-up and column purification in an isolated yield of 58 % (**Scheme 2.11**).

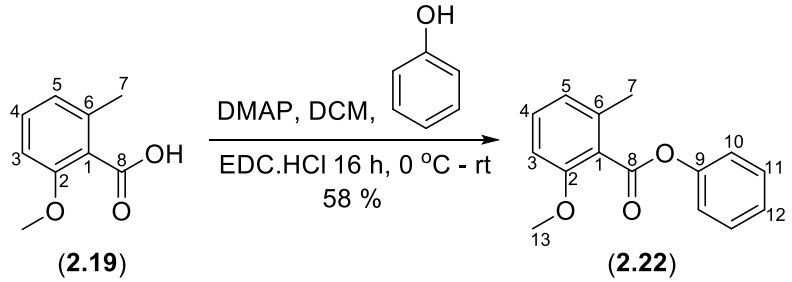

Scheme 2.11: Steglich esterification of 2-methoxy-6-methylbenzoic acid (**2.19**) with phenol and EDC.HCl as coupling reagent to synthesise our second A-ring precursor, phenyl 2-methoxy-6-methylbenzoate (**2.22**).

^{13}C NMR analysis of the spectra of **2.22** showed the presence of 10 aromatic carbon signals, indicative of the addition of a phenol to **2.19**. To confirm the structure of our second A-ring precursor (**2.22**) we

were also able to grow crystals by slow solvent evaporation for X-ray analysis. The use of DCM as solvent produced the desired high-quality crystals of phenyl 2-methoxy-6-methylbenzoate (**2.22**) (**Figure 2.5**).

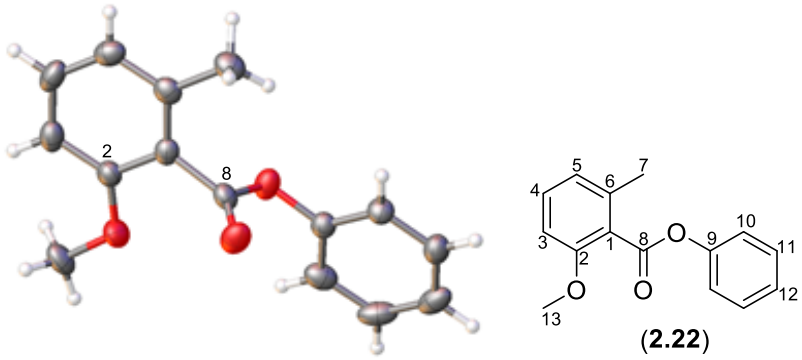

Figure 2.5: X-Ray crystal structure of our second A-ring precursor, phenyl 2-methoxy-6-methylbenzoate (**2.22**).

This esterification reaction was repeated in triplicate on the same scale giving an average isolated yield of 57 % (58, 57, 57 % SD = 0.5) and providing us with gram quantities of our second A-ring precursor **(2.22)**. With gram quantities of phenyl 2-methoxy-6-methylbenzoate (**2.22**) in hand, we could now attempt our Michael-Dieckmann chemistry to couple our A- ring to our C-ring to form the ABC anthracene core of DEM30355/A (**1**).

2.4 Conclusions and Future Work

For this project we aimed to develop a synthetic route to DEM30355/A (**1**) (**Figure 2.6**), a first in class polyketide isolated from a fermentation broth of the unusual extremophile *Amycolatopsis* DEM30355. The structure of DEM30355/A (**1**) consists of an anthracene-like ABC ring core. Our plan to construct this ABC ring core involved a retrosynthetic approach whereby we would synthesise an A-ring precursor, then the C-ring precursor and subsequently couple them via a tandem Michael-Dieckmann reaction. In this chapter we focused on the construction of two A-ring precursors of DEM30355/A (**1**).

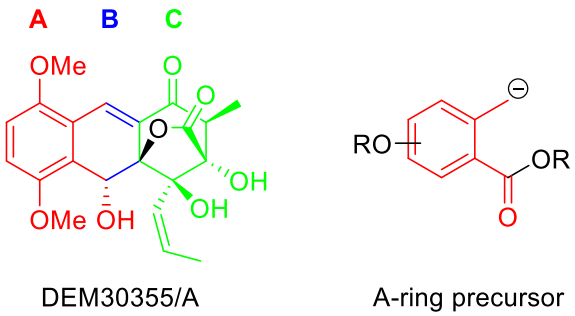

Figure 2.6: Structure of our target compound DEM30355/A and general structure of our A-ring precursor

Our first A-ring precursor (**2.17**) was synthesised through the insertion of an *in situ* generated aryne into an appropriately functionalised aryl sulfone (**2.13**). We chose methyl 2-(phenylsulfonyl) acetate

(**2.13**) as our aryl sulfone target, which we successfully synthesised via alkylation of thiophenol (**2.10**) and a subsequent oxidation using *m*CPBA. The aryne was generated *in situ* via the use of a fluoride source. To generate the aryne *in situ* a number of reaction conditions and fluoride sources were screened with the use of KF and 18-crown-6 proving the most successful method. We were able to validate the authenticity of the structure of our first A-ring precursor by X-ray crystallography (**Scheme 2.12**).

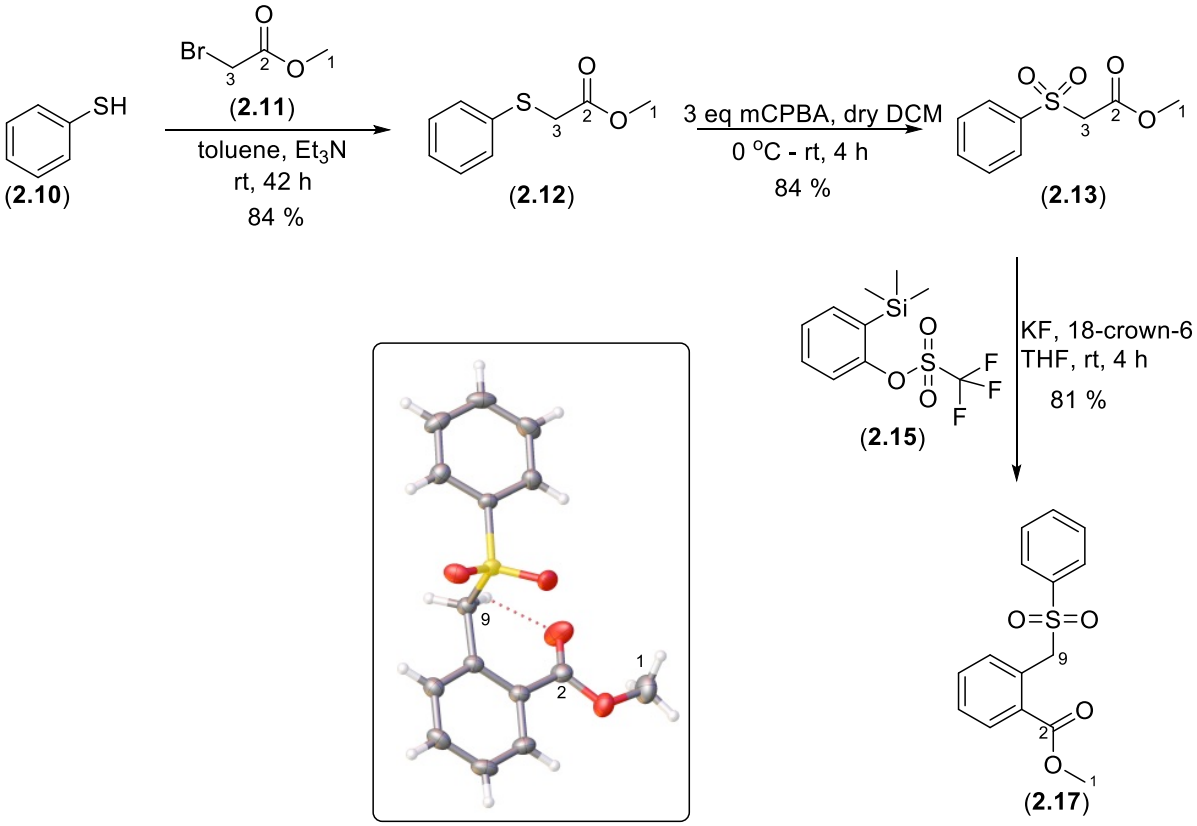

Scheme 2.12: Optimised route to our first A-ring precursor (**2.17**) showing its crystal structure.

To further expand our synthetic scope, we then looked at a second more functionalised A-ring precursor (**2.22**) containing the required methoxy group at C-2 and an improved ester leaving group at C-1. By starting with a functionalised benzoic acid, 2-methoxy-6-methylbenzoic acid (**2.19**) with the required methoxy group already installed at C-2 and then converting the carboxylic acid functionality of 2-methoxy-6-methylbenzoic acid (**2.19**) to the corresponding phenyl ester (**2.20**) we sought to replicate the electrophilic conditions established in our first A-ring precursor. Thus, a Steglich esterification starting with 2-methoxy-6-methylbenzoic acid (**2.19**) with phenol and EDC.HCl as a coupling agent yielded our second A-ring precursor, phenyl 2-methoxy-6-methylbenzoate (**2.22**). Again, we confirmed the structure of our second A-ring precursor via X-ray crystallography (**Scheme 2.13**).

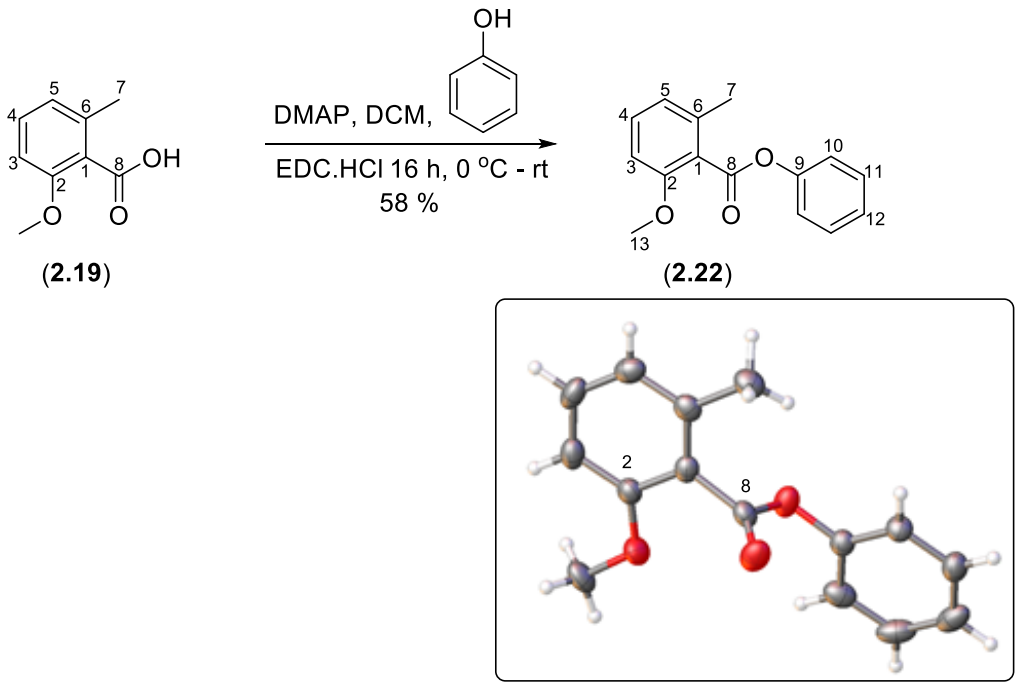

Scheme 2.13: Steglich esterification of 2-methoxy-6-methylbenzoic acid (**2.19**) to synthesise our second A-ring precursor (**2.22**) with its crystal structure shown.

Having synthesised two A-ring precursors in sufficient quantities we were now in a position to attempt to couple them with our C-ring precursor and test our Michael-Dieckmann chemistry. These investigations are explored in detail in the next chapter.

Chapter 2 – References

1) B. Kepplinger, PhD Thesis, Newcastle University, 2016.
2) X. Huang and J. Xue, *J. Org. Chem*., 2007, **72**, 3965-3968.
3) WO2014/16789, 2014, A1.
4) K.Miura, N. Fujisawa, H. Saito, D. Wang and A. Hosomi, *Org. Lett*., 2001, **3**, 2591-2594.
5) V. Aranapakam, G. T. Grosu, J. M. Davis, B. Hu, J. Ellingboe, J. L. Baker, J. S. Skotnicki, A. Zask, J. F. DiJoseph, A. Sung, M. A. Sharr, L. M. Killar, T. Walter, G. Jin and R. Cowling, *J. Med. Chem*., 2003, **46**, 2361-2375.
6) Z. Bo, S. Li, S. Yue, M. Cokoja, M-D. Zhou, S-L. Zang and F.E. Kuhn, *J. Organomet. Chem*.,2013, **744**, 108-112.
7) H. Y. Li, L. J. Xing, M. M. Lou, H. Wang, R. H. Liu and B. Wang, *Org. Lett.*, 2015, **17**, 1098-1101.
8) H. Yoshio, S. Takaaki and K. Hiroshi, *Chem. Lett.*, 1983, **12**, 1211-1214.
9) A. M. Vibhute, U. D. Priyakumar, A. Ravi and K. M. Sureshan, *Chem. Commun.*, 2018, **54**, 4629-4632.
10) M. G. Charest, C. D. Lerner, J. D. Brubaker, D. R. Siegel and A. G. Myers, *Science*, 2005, **308**, 395-398.
11) F. Liu, P. M. Wright and A. G. Myers, *Org. Lett*., 2017, **19**, 206-209.

Chapter 3 – Synthesis of Right-hand C-ring of DEM30355/A and Michael-Dieckmann Test Systems

3.1 Introduction

In chapter two we discussed our efforts towards the synthesis of the A-ring of DEM30355/A (**1**). In this chapter we focus on our efforts to test the planned Michael-Dieckmann cyclisation chemistry to form the ABC carbon ring core of DEM30355/A by building a suitably functionalised C-ring model of DEM30355/A, specifically targeting the oxygenation patterns at C-1, C-4a, and the quaternary centre at C-3 with both an ester and OH group present. An electron withdrawing ketone group installed at C-4 would also facilitate the planned Michael-Dieckmann cyclisation. Our convergent approach to DEM30355/A would then allow the formation of the B-ring through the coupling of the A-ring precursor (**3.01**) and functionalised C-ring precursor (**3.02**) via a tandem Michael-Dieckmann reaction to yield the ABC carbon ring skeleton of DEM30355/A (**3.03**) (**Scheme 3.00**).

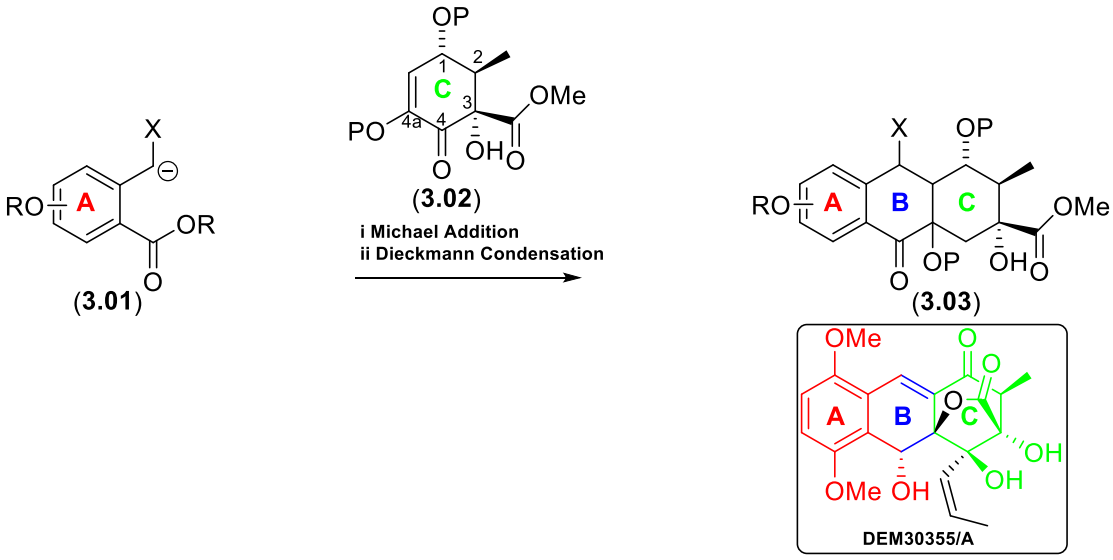

Scheme 3.00: Convergent approach to DEM30355/A via key Michael-Dieckmann reaction coupling of A-ring precursor (**3.01**) to a suitably functionalised C-ring precursor (**3.02**) to give the ABC ring core of DEM30355/A (**3.03**). X = electron withdrawing group, P = protecting group.

3.2 Michael-Dieckmann Cyclisation Chemistry using First generation A-ring precursor (2.17)

In order to test our key Michael-Dieckmann cyclisation step we planned to use our first-generation A-ring precursor (**2.17**) and cyclohex-2-en-1-one (**3.04**), as a C-ring precursor, to build the ABC fused ring skeleton of DEM30355/A (**1**) after which we could explore postfunctionalisation of the ABC ring core (**Scheme 3.01**).

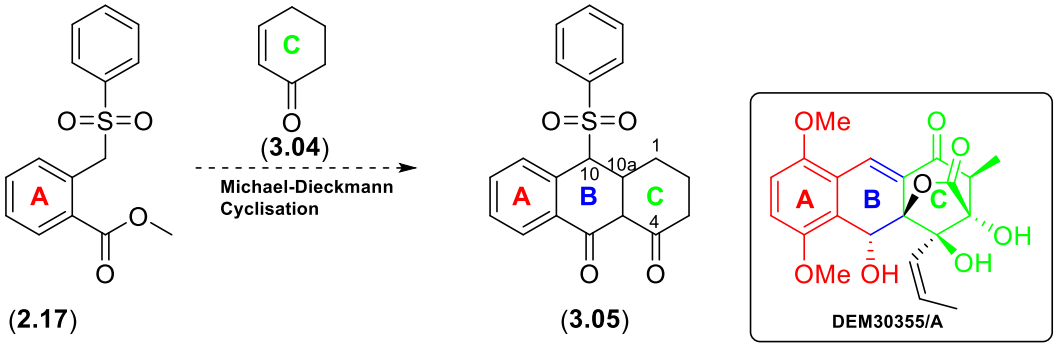

Scheme 3.01: Planned test reaction of our key Michael-Dieckmann cyclisation step using first generation A-ring precursor (**2.17**) and cyclohex-2-en-1-one (**3.04**) as C-ring precursor to build the ABC ring core of DEM30355/A (**3.05**) with a comparison to the target molecule.

Thus, our first-generation A-ring precursor (**2.17**) was refluxed in THF with cyclohex-2-en-1-one (**3.04**) and 2.5 eq NaH for 3 h[1]. Following aqueous work-up and purification by column chromatography, the desired ABC ring core (**3.05**) was isolated as a single diastereomer in 63 % yield along with a by-product (**3.06)** in 2 % yield. Repeating the reaction with extension to the reaction time (reflux for 4 h) gave very similar results, yielding 61 % of desired ABC ring core (**3.05**) and 3 % by-product (**3.06**).

To confirm the structure of our desired product (**3.05**) we conducted ^{1}H NMR spectral analysis of the ABC ring core (**3.05**) which showed a key doublet at 4.34 ppm (J = 4.9 Hz) corresponding to the benzylic proton at C-10 coupled to the proton at C-10a. The C-10a proton appeared at 3.36 ppm (1H, ddd, J = 12.1, 4.9, 1.5 Hz). The 12.1 Hz coupling of C-10a with one of the diastereotopic C-1 protons suggests an axial-axial orientation, thus the C-10/C-10a coupling of 4.9 Hz would suggest an axial-equatorial like arrangement. The C-10a proton also showed coupling to the other diastereotopic proton at C-1 (J = 1.5 Hz) suggesting an axial-equatorial like arrangement. Thus, we have assigned the relative stereochemistry between the C-10/C-10-a positions as *syn*. Furthermore, the observation of a signal at 15.61 ppm suggests an OH group involved in an intramolecular H-bond, suggesting that the ABC ring core (**3.05**) exists as the enol form.

^{1}H NMR of the isolated by-product (**3.06**) showed a loss of the sulfone group phenyl signal and the appearance of a key singlet signal at 7.03 ppm corresponding to a new aromatic proton and pointing to the aromatisation of the central B-ring. The aromatised by-product (**3.06**) may possibly have been formed via the elimination of the sulfone group at the C-10 position of the desired ABC ring core (**3.05**) (**Scheme: 3.02**).

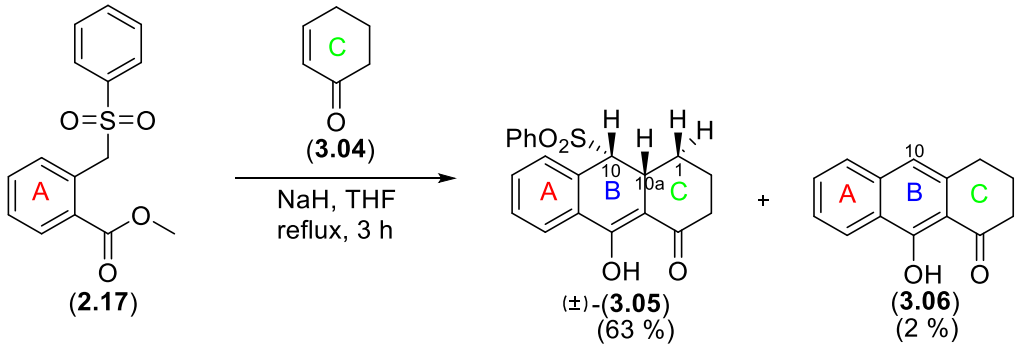

Scheme 3.02: Michael-Dieckmann cyclisation reaction between first generation A-ring precursor (**2.17**) and cyclohex-2-en-1-one (**3.04**) to give desired ABC ring core (**3.05**) and by-product (**3.06**).

Thus, we have successfully coupled our first-generation A-ring precursor (**2.17**) with cyclohex-2-en-1-one (**3.04**) as our model C-ring precursor via our Michael-Dieckmann cyclisation chemistry to form the ABC fused ring core of our target compound DEM30355/A (**1**). In so doing we have shown the viability of our chosen Michael-Dieckmann cyclisation chemistry. Our next step was a to build a more functionalised C-ring system with required methyl group at C-2 and the OH and ester groups at C-3 along with the C=C double bond between C-4a/C-10a required for our Michael-Dieckmann chemistry.

3.3 Synthesis of C-ring precursors

To synthesise a suitable C-ring precursor, we imagined constructing the required cyclohexenone C-ring from readily available aliphatic precursors. A retrosynthetic analysis of cyclohexenone points to two major disconnection approaches to access this compound. A "4 + 2" approach also known as the Robinson Annulation[2] and an alternative "3 + 3" approach (**Scheme 3.03**).

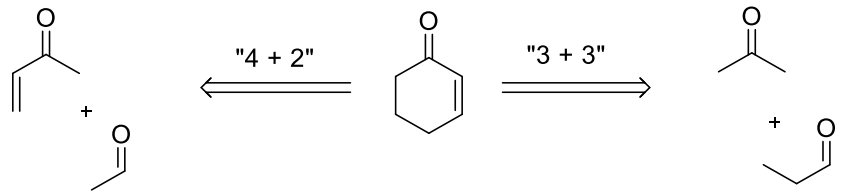

Scheme 3.03: The two major disconnection approaches to synthesise cyclohexenone C-ring.

Despite the considerable literature available for the Robinson Annulation, it is not a feasible approach for our system as it would require the use of acetaldehyde as a key reagent. An examination of the literature revealed an interesting protocol by Pietrusiewicz *et al.*[3] whereby a tandem Michael addition-Wittig reaction of triphenylphosphoranes (**3.07**) and α, β-unsaturated aldehydes (**3.08**) in the presence of base were coupled in a formal [3 + 3]

annulation reaction to form highly functionalized cyclohex-2-en-1-one ring systems. Pietrusiewicz *et al.* showed that enolates formed *in situ* could undergo Michael additions with α, β-unsaturated aldehydes, followed by a subsequent intramolecular Wittig reaction to give functionalised cyclohex-2-en-1-one systems. We therefore planned to use such a "3 + 3" approach for the synthesis of functionalised C-ring precursors (**Scheme 3.04**).

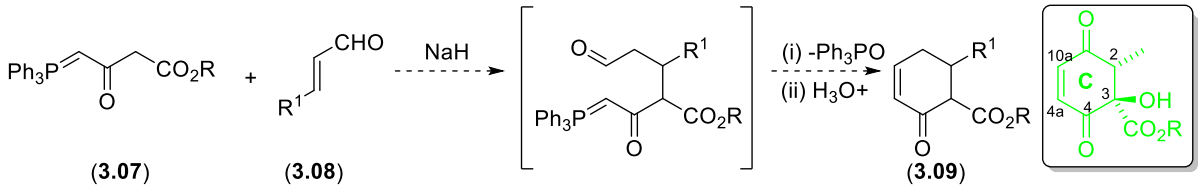

Scheme 3.04: Proposed annulation reaction to synthesise C-ring precursor where R and R^1 = alkyl groups.

3.3.1 Synthesis of Phosphonium Ylide (3.13)

The construction of our functionalised C-ring would therefore begin with the synthesis of an appropriate phosphonium ylide (**3.13**). We planned to brominate ethyl acetoacetate (**3.10**) at the terminal carbon to give ethyl bromoacetoacetate (**3.11**) which would then be reacted with triphenylphosphine to give phosphonium salt (**3.12**). Subsequent reaction of phosphonium salt (**3.12**) with base would provide access to the desired phosphonium ylide (**3.13**) (**Scheme 3.05**).

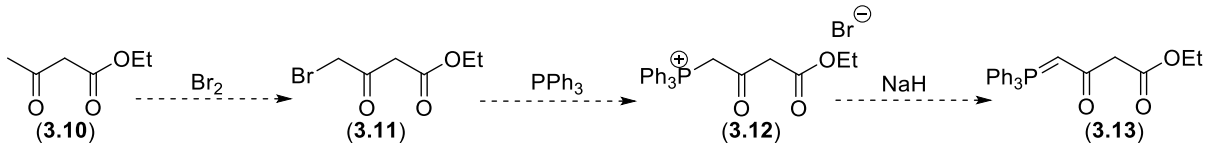

Scheme 3.05: Proposed synthetic route to phosphonium ylide (**3.13**) starting from ethylacetoacetate (**3.10**).

Thus, 5 mmol ethyl acetoacetate (**3.10**) was reacted with bromine in ethanoic acid for 3 h under a nitrogen atmosphere[4]. Following extraction with DCM and purification via a silica plug, the desired product ethyl 4-bromo-3-oxobutanoate (**3.11**) was isolated in 88 % yield in a keto-enol ratio of 1.0: 0.2. ^{1}H NMR analysis of ethyl 4-bromo-3-oxobutanoate (**3.11**) revealed a new signal at 4.05 ppm (2H, s) consistent with the methylene protons at C-6 and a signal at 5.27 ppm (1H, s) which we assigned as the corresponding C-4 C-H of the enol form. To access greater quantities of ethyl 4-bromo-3-oxobutanoate (**3.11**), we were able to scale the reaction to a 20 mmol scale with an average yield of 86 % over 6 reactions (**Scheme 3.06**).

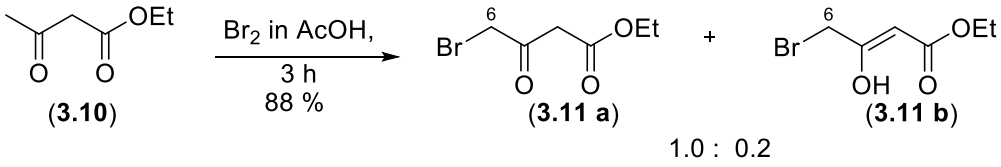

Scheme 3.06: Bromination of ethyl acetoacetate (**3.10**) to yield ethyl 4-bromo-3-oxobutanoate (**3.11**).

The next step in the preparation of our Wittig reagent was the addition of triphenylphosphine to bromoacetate (**3.11**) to form the phosphonium salt (4-ethoxy-2,4-dioxobutyl) triphenylphosphonium bromide (**3.12**). Thus, 5 mmol of the bromoacetate (**3.11**) was dissolved in anhydrous toluene and added dropwise to a solution of triphenylphosphine in anhydrous toluene[5]. After stirring overnight at rt, the precipitate was collected by filtration and then recrystallised from hot toluene to yield the light peach powder of (4-ethoxy-2,4-dioxobutyl) triphenylphosphonium bromide (**3.12**) (**Scheme 3.07**).

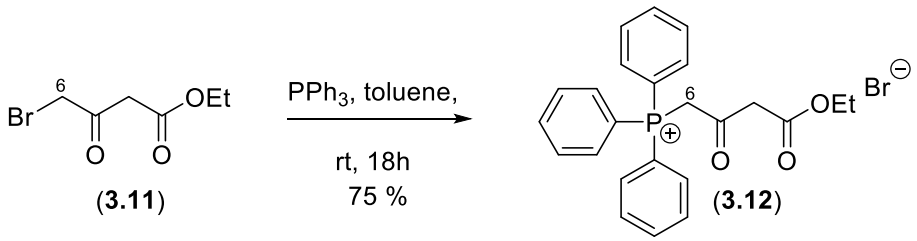

Scheme 3.07: Synthesis of (4-ethoxy-2,4-dioxobutyl) triphenylphosphonium bromide (**3.12**)

The ^{1}H NMR data of phosphonium salt (**3.12**) showed the presence of the 15 expected new aromatic protons with the change of the C-6 signal at 4.05 ppm (2H, s) of bromoacetate (**3.11**) to a signal at 6.25 ppm (2H, d, $^{2}J_{PH}$ = 11.5 Hz) corresponding to the C-6 methylene protons of phosphonium salt (**3.12**). Analysis by HRMS also showed the presence of the key molecular ion $[M]^{+}$ signal at m/z = 391.1453. Furthermore, we were also able to grow single crystals of our phosphonium salt (**3.12**) via slow solvent evaporation from $CDCl_3$ for analysis by X-ray diffraction (**Figure 3.0**).

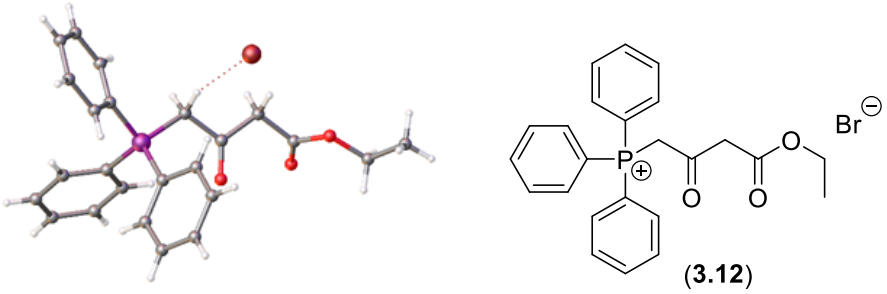

Figure 3.0: X-ray crystal structure of phosphonium salt (**3.12**).

Subsequently, we were able to scale the reaction to an 18 mmol scale with an average yield of 73 % over six reactions. With gram quantities of our phosphonium salt (**3.12**) in hand, we then looked to synthesise our phosphonium ylide (**3.13**) via the deprotonation of phosphonium salt (**3.12**).

Thus, to a solution of (4-ethoxy-2,4-dioxobutyl) triphenylphosphonium bromide (**3.12**) in dry THF, was added NaH (60 % in mineral oil) suspended in dry THF. After leaving the mixture stirring overnight at rt, the precipitated product was collected via vacuum filtration and washed with petrol to give ethyl 3-oxo-4-(triphenyl-phosphaneylidene) butanoate (**3.13**) as a yellow/orange powder in 80 % isolated yield.

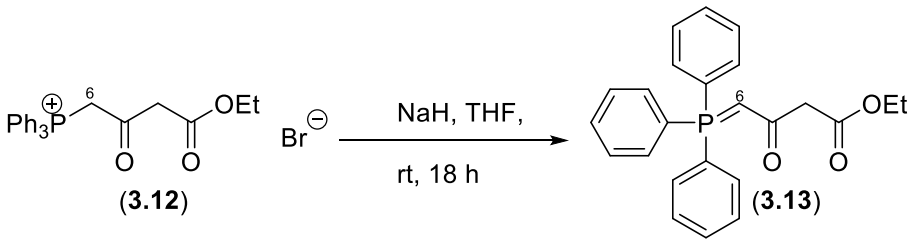

(**3.12**) (**3.13**)

Scheme 3.08: Synthesis of phosphonium ylide (**3.13**) from reaction of phosphonium salt (**3.12**) with NaH.

Analysis of the ^{1}H NMR and ^{13}C NMR data for phosphonium ylide (**3.13**) was a close match to the literature[6] data. In addition, we were also able to prove the structure of phosphonium ylide (**3.13**) by growing single crystals via slow solvent evaporation from $CDCl_3$ that were suitable for single crystal X-ray analysis (**Figure 3.1**).

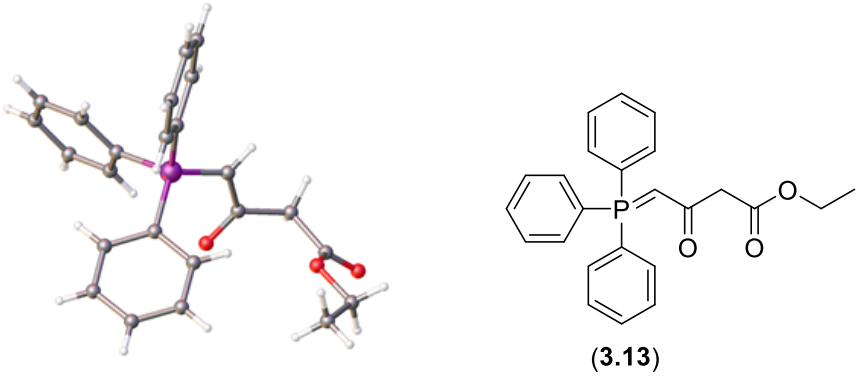

(**3.13**)

Figure 3.1: X-ray crystal structure of phosphonium ylide (**3.13**).

In order to access gram quantities of phosphonium ylide (**3.13**) for further synthetic use we were able to scale the reaction up to a 12 mmol scale with a pleasing increase in yield to 88 %. Repeating this reaction 4 times on a 12 mmol scale gave an average yield of 86 %. With

gram quantities of our phosphonium ylide (**3.13**) in hand, we could now proceed to the next synthetic step.

3.3.2 Formation of C-ring Precursor (3.15) via a Tandem Michael-Wittig Annulation between Phosphonium Ylide (3.13) and Crotonaldehyde (3.14)

Next, following a protocol established by Pietrusiewicz[3], we examined the formation of C-ring precursor enone (**3.15**). Phosphonium ylide (**3.13**) was combined with an equimolar amount of crotonaldehyde (**3.14**) in THF at 35 °C in the presence of an excess of NaH and an added trace of water. After 4 h the reaction was acidified by addition of 1M HCl and extracted with diethyl ether. The crude product was purified by column chromatography to give the enone, ethyl 6-methyl-2-oxocyclohex-3-ene-1-carboxylate (**3.15**), as a single diastereomer in 58 % isolated yield.

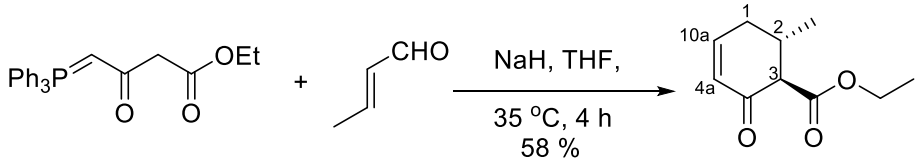

(**3.13**) (**3.14**) (±)-(**3.15**)

Scheme 3.09: Synthesis of ethyl 6-methyl-2-oxocyclohex-3-ene-1-carboxylate (**3.15**)

The overall structure of enone (**3.15**) was confirmed by analysis of the ^{1}H NMR spectra with the two diastereotopic protons at C-1 observed at 2.65-2.52 (1H, m) and 2.52 – 2.43 (1H, m) and the alkene C-4a and C-10a protons observed at 6.07 (1H, dd, *J* = 10.1, 2.7 Hz) and 7.01 – 6.94 (1H, m) respectively. ^{1}H – ^{1}H coupling analysis allowed the assignment of relative stereochemistry at the C-2/C-3 positions. The ^{1}H NMR signal at 3.11 ppm (1H, d) corresponding to the proton at C-3 showed a coupling constant of *J* = 11.7 Hz which would suggest an axial-axial arrangement of the C-2 and C-3 protons and thus that enone (**3.15**) is formed with an *anti*-configuration.

Attempts to scale-up this reaction to a 12 mmol scale resulted in a low yield of 20 %, therefore we carried out multiple 1 mmol scale reactions to access sufficient enone (**3.15**), with an average yield of 55 % over 12 reactions.

3.3.3 Incorporation of a C-3 hydroxyl group via Rubottom oxidation

Our next step involved establishing the key quaternary centre at the C-3 position of enone (**3.15**) through the incorporation of the required hydroxyl group. Furthermore, introducing an OH group at the C-3 position at this early stage, we envisioned, would help to promote our

Michael-Dieckmann cyclisation via an intramolecular hydrogen bond between the C-3 hydroxyl and the C-4 ketone[7] (**Figure 3.2**).

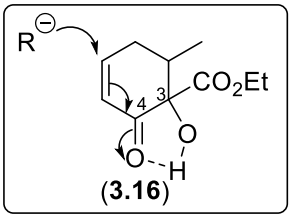

Figure 3.2: Postulated H-bond activation of enone (**3.16**) towards conjugate addition.

The literature revealed a protocol established by Nishiwaki *et al* [8] whereby a hydroxyl group was installed at the C-3 position of a similar cyclic keto-ester to the enone (**3.15**), via a Rubottom type oxidation with *m*-CPBA. Thus, we decided to attempt a Rubottom oxidation using *m*-CPBA[8] to introduce the required OH group at C-3 of enone (**3.15**) (**Scheme 3.10**).

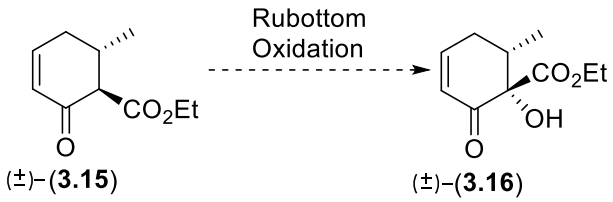

Scheme 3.10: Planned synthesis of hydroxylated enone (**3.16**) via Rubottom oxidation.

Thus, enone (**3.15**) was reacted with *m*-CPBA in DCM at -78 ^{o}C, warmed to rt and stirred for 4 h. Following aqueous work-up and purification by column chromatography, hydroxylated enone (**3.16**) was isolated in 47 % yield (**Scheme 3.11**).

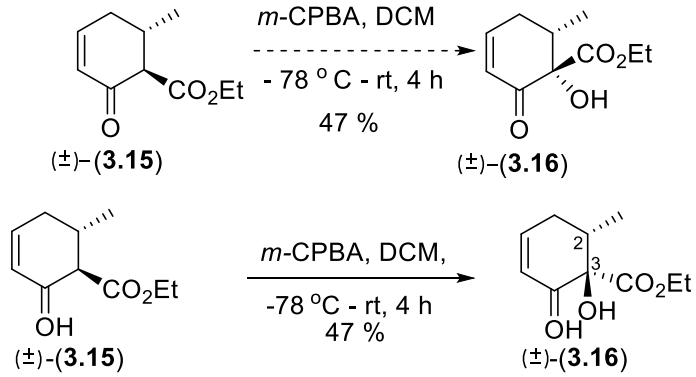

Scheme 3.11: Synthesis of enone (**3.15**) via Rubottom oxidation.

The structure of hydroxylated enone (**3.16**) was confirmed through analysis of the ^{1}H NMR data which showed the loss of the C-3 proton signal seen in enone (**3.15**). In addition, ^{13}C NMR analysis showed a downfield shift of the C-3 carbon signal from 64.3 ppm in enone (**3.15**) to

83.4 ppm in hydroxylated enone (**3.16**) reflecting the presence of the electron withdrawing hydroxyl group. To resolve the relative stereochemistry of hydroxylated enone (**3.16**) we attempted to grow single crystals via slow solvent evaporation (DCM), in a clear glass vial exposed to light. Interestingly, solution of the X-ray structure of the crystals recovered from the experiment, showed the presence of an unexpected "head-to-tail" dimer of hydroxylated enone (**3.16**) (**Figure: 3.3**).

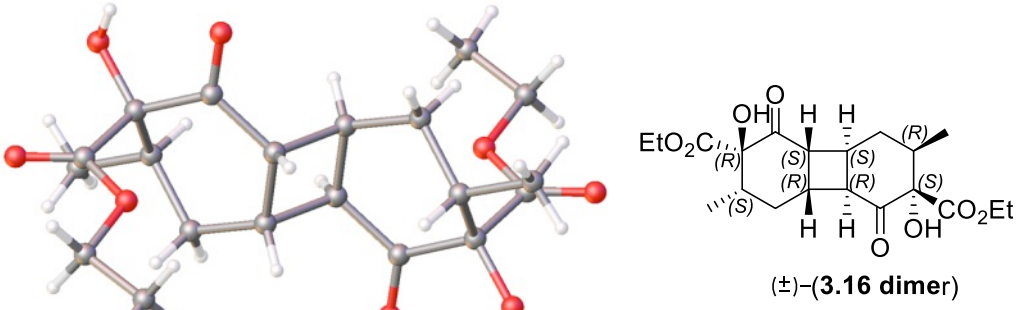

Figure 3.3: X-ray crystal structure of dimerised hydroxylated enone (**3.16 dimer**).

The observation of the dimer of hydroxylated enone (**3.16 dimer**) in our crystallisation experiment, suggested that a [2 + 2] photochemical cycloaddition had occurred between two molecules of the parent hydroxylated enone (**3.16**) during the course of the crystallisation[9]. Interestingly, correlation of the X-ray crystal structure of dimer of hydroxylated enone (**3.16 dimer**) to the parent hydroxylated enone (**3.16**) also revealed an inversion of the stereochemistry at C-3 in comparison to the starting material, enone (**3.15**), which must have occurred during the Rubottom oxidation step. We postulate that the Rubottom oxidation of enone (**3.15**) goes via the corresponding enol form, leading to a loss of stereochemistry at the C-3 position. The C-2 methyl group sterically blocks the *Si* face of the enol at C-3, therefore subsequent oxidation by *m*-CPBA occurs on the less hindered *Re* face to give a *syn*-arrangement between the ester and methyl groups in hydroxylated enone (**3.16**) (**Figure 3.4**).

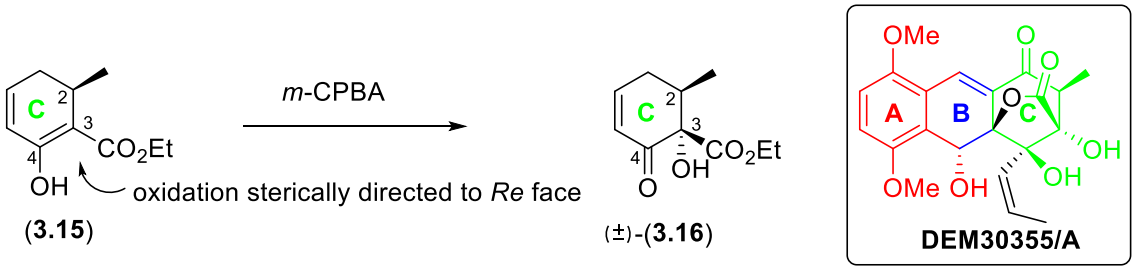

Figure 3.4: Sterically directed Rubottom oxidation to *Re* face of the enol of enone (**3.15**), with comparative stereochemistry for DEM30355/A shown.

This inversion of relative stereochemistry at C-3, results in hydroxylated enone (3.16) now matching the relative stereochemistry of our target molecule DEM30355/A (1) at both the C-2 and C-3 positions.

3.3.4 Synthesis of C-ring precursor analogue

It should be noted that in our target molecule DEM30355/A (**1**), the corresponding C-2 position contains a single methyl group adjacent to a ketone at C-1. The C-2 position in DEM30355/A (**1**) is therefore prone to epimerisation, and it is not known if there is a difference in bioactivity between the two epimers. Therefore, as part of our work we wished to make DEM30355/A (**1**) analogues to build up a structure activity relationship for the molecule. Thus, based on the positive results reported in this chapter, we decided to prepare a C-ring analogue containing a *gem*-dimethyl group at C-2 to shut-down the unwanted C-2 epimerisation.

Thus, following our previously developed tandem Michael-Wittig reaction chemistry, 3-methyl but-2-enal (**3.17**) was reacted with an equimolar amount of phosphonium ylide (**3.13**), trace of water and an excess of NaH in THF at 35 ^{o}C. After 3 h the reaction was acidified by addition of 1M HCl and extracted with diethyl ether. The crude product was purified by column chromatography to give *gem*-dimethyl enone, ethyl 6,6-dimethyl-2-oxocyclohex-3-ene-1-carboxylate (**3.18**), in a low 9 % isolated yield with the structure confirmed by ^{1}H NMR (**Scheme 3.12**).

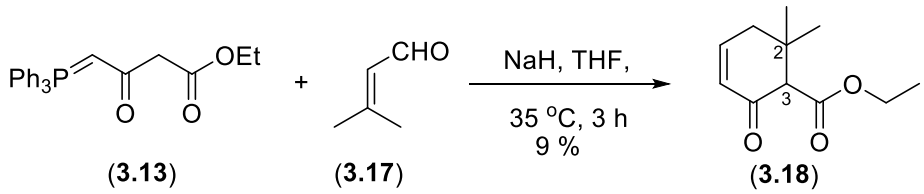

Scheme 3.12: Synthesis of C-ring analogue (**3.18**) via Michael-Wittig reaction.

The Michael-Wittig reaction to form *gem*-dimethyl enone (**3.18**) was scaled-up to 10 mmol to provide material for subsequent steps, however the yield did not improve, possibly due to

greater steric hindrance at the β-carbon of 3-methyl but-2-enal (**3.17**) as compared to crotonaldehyde (**3.14**)**,** with only 5 % of the desired product isolated.

We next attempted to install the hydroxyl group at C-2 of *gem*-dimethyl enone (**3.18**) via a Rubottom oxidation as previously. Thus, *gem*-dimethyl enone (**3.18**) was reacted with *m*-CPBA in DCM at -78 ^{o}C and allowed to warm to rt and stirred for 18 h. Following aqueous work-up and purification by column chromatography, hydroxylated *gem*-dimethyl enone (**3.19**) was isolated in low 13 % yield possibly attributable to the presence of the bulky *gem*-dimethyl group at C-2 .

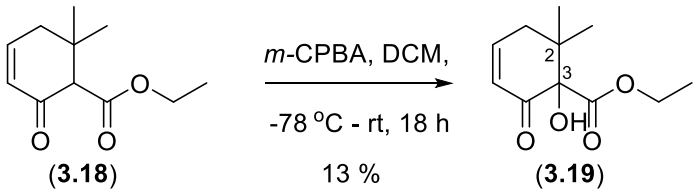

Scheme 3.13: Incorporation of hydroxyl group at C-3 of enone (**3.18**).

^{13}C NMR analysis allowed conformation of the structure of hydroxylated *gem*-dimethyl enone (**3.19**), showing a key downfield shift of the C-3 carbon signal from 65.2 ppm in *gem*-dimethyl enone (**3.18**) to 83.2 ppm in hydroxylated *gem*-dimethyl enone (**3.19**). In addition, a new, signal was observed at 4.09 ppm (1H, br, s) corresponding to the proton of the installed OH group.

3.4 Functionalised A-ring and C-ring coupling via Michael-Dieckmann Cyclisation

With the synthesis of hydroxylated *gem*-dimethyl enone (**3.19**) affording only low yields, we decided to focus on the Michael-Dieckmann reaction of C-ring precursor hydroxylated enone (**3.16**) with our second-generation A-ring precursor, phenyl 2-methoxy-6-methylbenzoate (**2.22**). The coupling of A-ring (**2.22**) and C-ring (**3.16**) precursors would then provide access to a highly functionalised fused tricyclic ring structure analogous to our target DEM30355/A (**1**). Thus, phenyl 2-methoxy-6-methylbenzoate (**2.22**) was deprotonated with LDA at -78 ^{o}C after which hydroxylated enone (**3.16**) was added and the reaction allowed to warm to rt overnight. Following aqueous work-up, the desired fused tricyclic compound (**3.20**) was isolated by column chromatography in 26 % yield with unreacted starting material not being recovered. (**Scheme 3.14**).

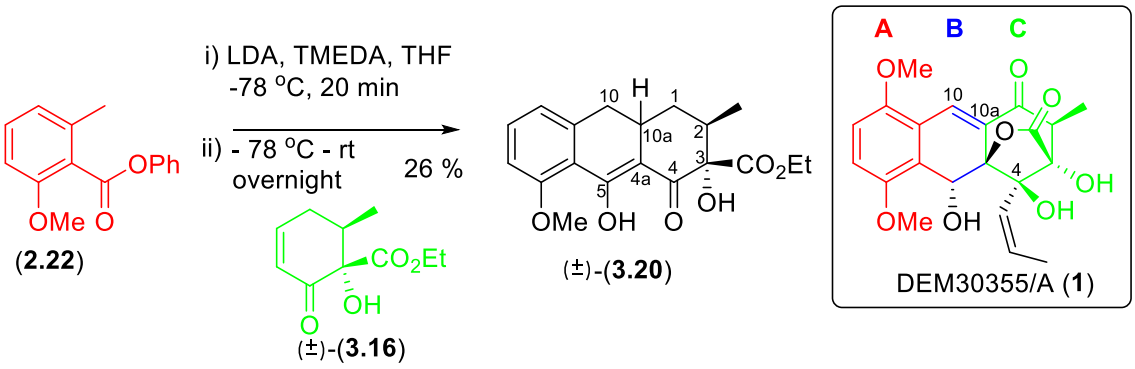

Scheme 3.14: Coupling of A-ring precursor (**2.22**) with C-ring precursor (**3.16**) via a Michael-Dieckmann cyclisation.

The structure of functionalised fused tricycle (**3.20**) was confirmed by analysis of the ^{1}H NMR spectra which showed a key signal at 2.91 - 2.71 ppm (3H, m) corresponding to the benzylic, diastereotopic protons at the C-10 position. This signal also contained another proton which we assigned as the C-10a proton. In addition, a signal observed at 15.81 ppm (1H, s, OH) suggests an OH group (C-5) involved in an intramolecular H-bond, suggesting that (as previously seen with ABC ring core (**3.05**)) fused tricycle (**3.20**) exists as the enol form.

We wished to assign relative stereochemistry by *J* value analysis of the proton at C-10a, but unfortunately, the key set of signals corresponding to the benzylic, diastereotopic protons at the C-10 position presented as a complex multiplet 2.91-2.71 ppm (m, 3H), overlapping with the C-10a proton signal.

3.5 Conclusion

In this chapter our aim was to investigate the Michael-Dieckmann cyclisation chemistry as a potential route to form the ABC carbon ring core of our target molecule DEM30355/A (**1**). This involved the construction and subsequent Michael-Dieckmann cyclisation of a number of suitably functionalised C-ring precursors, each containing a number of the functional groups ultimately present in the C-ring of DEM30355/A (**1**)

Our planned Michael-Dieckmann cyclisation chemistry was validated through the successful coupling of C-ring precursor cyclohex-2-en-1-one (**3.04**) with our first-generation A-ring precursor (**2.17**) (**Scheme 3.15**).

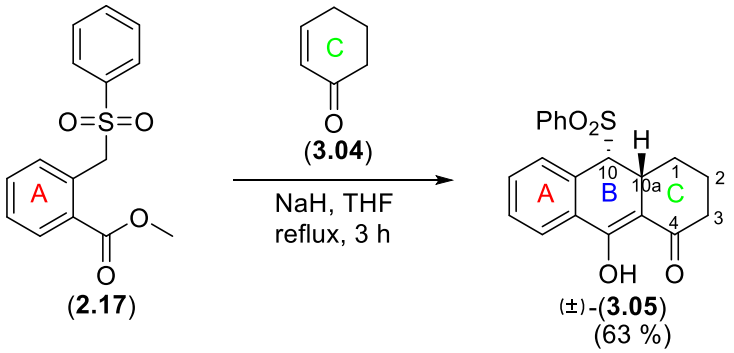

Scheme 3.15: Michael-Dieckmann Cyclisation Coupling of A-ring precursor (**2.17**) and C-ring precursor (**3.04**)

A more functionalised C-ring precursor was needed, with a quaternary centre at C-3 containing an ester and an OH group, a methyl group at C-2 and an oxygen atom at C-4 being our initial focus. In addition, the methyl group at C-2 and the ester group at C-3 were required to be *syn* to each other.as is the case in our target compound DEM30355/A (**1**).

Utilising a key Michael-Wittig reaction between phosphonium ylide (**3.13**) and crotonaldehyde (**3.14**) we successfully synthesised C-ring precursor (**3.15**) which contained the desired C-2 methyl group *anti* to the C-3 ester group and also incorporated the C-4 oxygen atom as a ketone functionality as well as the C=C double bond between C-4a/C-10a required to initiate the Michael-Dieckmann cyclisation.

A subsequent Rubottom oxidation supposedly sterically directed by the C-2 methyl group, successfully installed the OH group at the C-3 position, *syn* to the C-2 methyl group This *syn* arrangement of the C-2 methyl group and C-3 ester group was evidenced by analysis of the single crystals grown of hydroxylated enone (**3.16 dimer**) and matched the relative stereochemistry of our target compound DEM30355/A (**1**) at these positions. Interestingly, dimerization of hydroxylated enone (**3.16**) occurred with hydroxylated enone (**3.16 dimer**) showing stereochemical inversion of the C-3 quaternary centre. which, as postulated previously was as a result of the directing effect of the C-2 methyl group. This directing effect of the methyl group, could find use in further synthetic applications (**Scheme 3.16**).

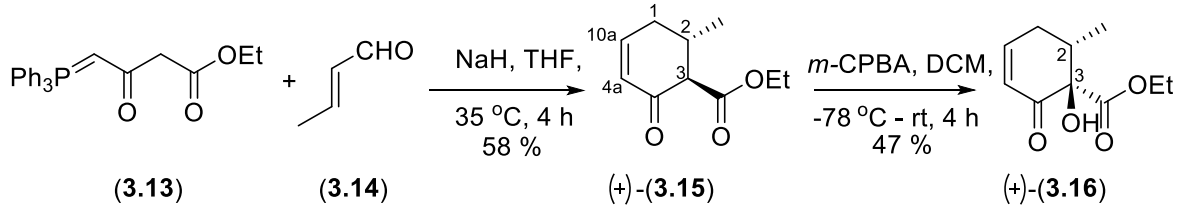

(**3.13**) (**3.14**) (+)-(**3.15**) (+)-(**3.16**)

Scheme 3.16: Synthesis of functionalised C-ring precursor (**3.16**).

To increase our understanding of the role of the methyl group at C-2 in the bioactive properties of our target compound DEM30355/A (**1**), we decided to prepare a C-ring analogue containing a *gem*-dimethyl group at C-2 for SAR studies. Thus, following our previously developed tandem Michael-Wittig chemistry we were able to synthesise *gem*-dimethyl enone (**3.18**) but only in very low yield of 9 %. We postulated that this low yield was as a result of increased steric hindrance at the β-carbon of starting material 3-methyl but-2-enal (**3.17**). Nevertheless, we were able to obtain sufficient quantities of *gem*-dimethyl enone (**3.18**) to perform the Rubottom oxidation to install the hydroxyl group at the C-3 position to obtain hydroxylated *gem*-dimethyl enone (**3.19**) in a disappointing yield of 13 %.

Because of the low yields obtained for *gem*-dimethyl enone (**3.18**) and hydroxylated *gem*-dimethyl enone (**3.19**), we decided to focus on the construction of the DEM30355/A (**1**) analogue coupling our C-ring precursor (**3.16**) with our second-generation A-ring precursor (**2.22**). This was achieved with the synthesis of our DEM30355/A analogue (**3.20**) which contained the required C-2 methyl group; the C-3 quaternary centre containing the ester group and OH group and the C-4 oxygen atom in the form of a ketone group. In addition, our DEM30355/A analogue (**3.20**) matched the relative stereochemistry of our target molecule DEM30355/A at the C-2 and C-3 positions. Our DEM30355/A analogue (**3.20**) also contained the required OMe group on the A-ring at the C-6 position and the required OH group on the B-ring at C-5 (**Figure 3.4**).

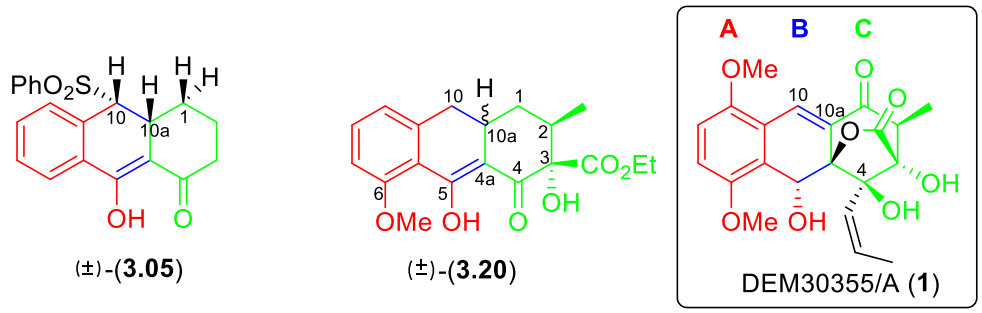

Figure 3.4: Comparison of ABC ring core analogues (**3.05**) and (**3.20**) to our target compound DEM30355/A (**1**).

With these promising results, we next looked to examine an approach whereby we would start with an enantiopure C-ring precursor and then add functionality at the C-3 position. We also needed to further functionalise our C-ring at the C-1 position with the incorporation of an oxygen atom. In the next chapter we discuss our efforts towards these goals.

Chapter 3 – References

1) X. Huang and J. Xue, *J. Org. Chem*., 2007, **72**, 3965-3968.
2) W. S. Rapson and R. Robinson, *J. Chem. Soc.,* 1935, 1285-1288.
3) K.M. Pietrusiewicz and J Monkiewicz, *J. Org. Chem.,* 1983, **48**, 788-790.
4) H. Y. Choi and D. Y. Chi, *Org. Lett.*, 2003, **5**, 411-414.
5) K. M. Sun, R. D. Dawe and B. Fraser-Reed, *Carbohydr. Res.*, 1987, **171**, 35-47.
6) H-S. Huang, R. Wang, W-J. Chen, J-Z. Chen, S-S. Gong and Q. Sun, *Tetrahedron. Lett.*, 2018, **59**, 3423-3427.
7) P. A. Evans, J. Cui, S. J. Gharpure, A. Polosukhin and H. R. Zhang, *J. Am. Chem. Soc*., 2003, **125**, 14702-14703.
8) H. Asahara and N. Nishiwaki, *J. Org. Chem*., 2014, **79**, 11735-11739.
9) S. Poplata, A. Troster, Y-Q. Zou and T. Bach, *Chem. Rev*., 2016, **17**, 9748-9815.

Chapter 4 – Enantioselective Synthesis of Right-hand C-ring of DEM30355/A

4.1 Introduction

In chapter three we showed the potential for the Michael-Dieckmann cyclisation chemistry to be used for the generation of racemic analogues of our target compound DEM30355/A (**1**). In this chapter, we will discuss our work towards an enantioselective synthesis of DEM30355/A (**1**).

The absolute stereochemistry of DEM30355/A (**1**) has been determined previously via both VCD and X-ray crystallography to be (2*S*, 3*S*, 4*R*, 4a*R*, 5*R*), therefore we will focus our efforts on the enantioselective synthesis of C-ring precursors containing the correct stereochemistry at the C-3 quaternary centre (**Figure 4.0**)[1].

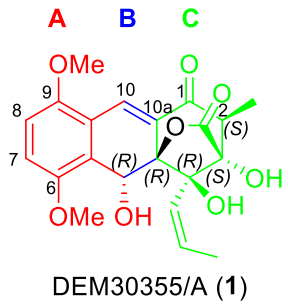

DEM30355/A (**1**)

Figure 4.0: Absolute stereochemistry of polyketide natural product antibiotic DEM30355/A (**1**)

4.1.1 Total Synthesis of 1st Generation Functionalised Enantiopure C-ring of DEM30355/A (1)

Since the four of the five stereocentres of DEM30355/A (**1**) are associated with the C-ring (2*S*, 3*S*, 4*R*, 4a*R*), we will focus on the enantioselective synthesis of a suitably functionalised C-ring precursor suitable for further Michael-Dieckmann cyclisation chemistry (**Scheme 4.01**).

We envisaged that enantiopure functionalised C-ring precursor (**4.05**), could be synthesised from commercially available (-)-shikimic acid (**4.01**) with the installation of the key C-3 chiral centre via a stereoselective dihydroxylation of the C-3/C-4 double bond. To achieve this, we would first need to selectively protect both the carboxylic acid and the multiple hydroxyl groups of (-)-shikimic acid (**4.01**). We imagined that the carboxylic acid functionality of (-)-shikimic acid (**4.01**) could be protected as the corresponding methyl ester (P^1), which would be used in a subsequent lactone formation later in the synthesis. Next, we planned to selectively protect the *trans*-vicinal diol at C-1/C-10a as a cyclic acetal (P^2).

Thermodynamically controlled cyclic acetal formation, should allow selective protection of the C-1/C-10a positions through the formation of a more stable *trans*-decalin ring system[2] Finally, for the remaining hydroxyl group at C-4a, we envisaged the use a bulky protecting group (e.g. Bn or TBDMS (P^3)) in order to sterically direct a subsequent *syn*-dihydroxylation at C-3/C-4. Following this a regioselective oxidation at C-4 would be used to install the desired ketone functionality, with a final E1cB elimination used to install the C=C double bond between C-4a/C-10a (**Scheme 4.01**).

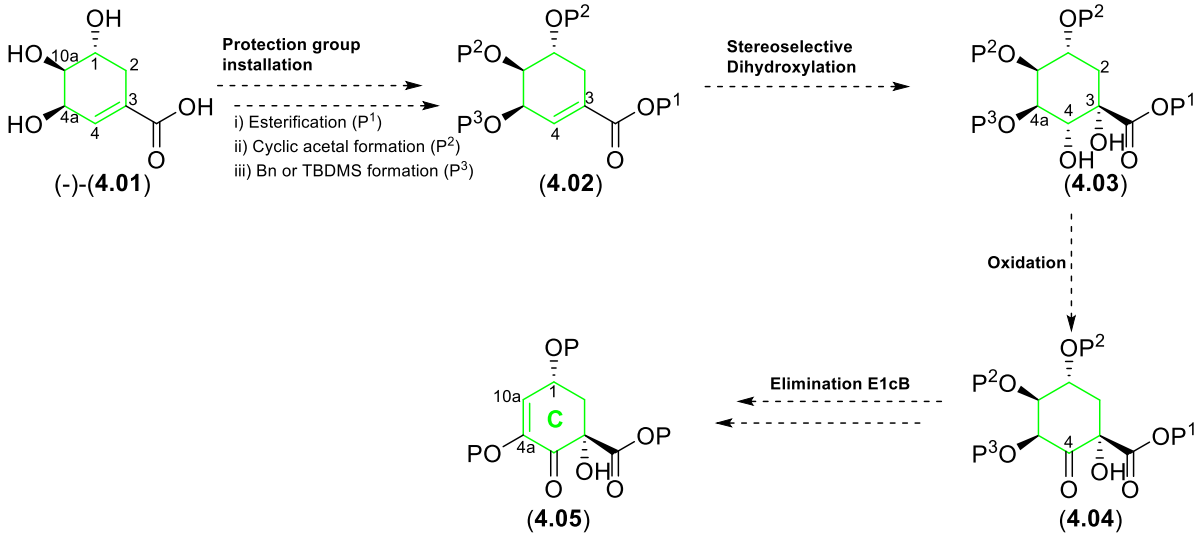

Scheme 4.01: Proposed enantioselective synthesis of C-ring precursor (**4.05**) from (-)-shikimic acid (**4.01**).

4.2 Results and Discussion

4.2.1 Synthesis of (-)-Methyl Shikimate (4.06)

Our synthesis commenced with the methylation of (-)-shikimic acid (**4.01**) via a Fischer esterification in order to protect the carboxylic acid functionality. Thus, the esterification of (-)-shikimic acid (**4.01**) was carried out over 48 h in refluxing methanol, using *p*-TSA-toluene as a catalyst, to give a 62 % isolated yield of (-)-methyl shikimate (**4.06**)[3]. Optimisation of the reaction, through extended reaction times (72 h), resulted in a maximum yield of 73 % even on scales of 28 mmol (**Table 4.0**). Hot-to-cold recrystallisation of (-)-methyl shikimate (**4.06**) from minimal EtOAc allowed access to multiple grams without the need for chromatography.

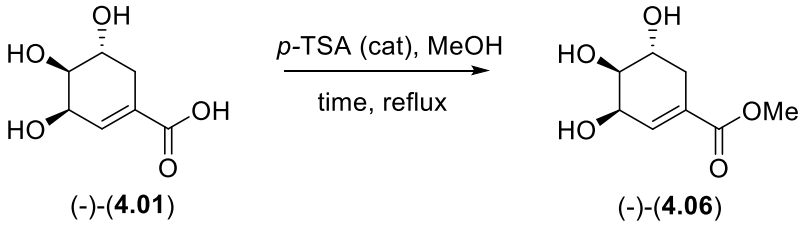

ENTRY	TIME/h	mmol of **4.01**	ISOLATED % YIELD (**4.06**)
1	48	5.7	62
2	48	28.7	69
3	48	28.7	70
4	72	28.7	73

Table 4.0: Fischer esterification of (-)-shikimic acid (**4.01**) to the corresponding (-)-methyl shikimate (**4.06**).

To confirm the structure of our (-)-methyl shikimate (**4.06**) we were able to grow single crystals by slow solvent evaporation (MeOH) for X-ray analysis (**Figure 4.1**). Interestingly, these (-)-methyl shikimate crystals gave an observed Z' (number of molecules in the asymmetric unit) value of 12. Crystal structures with high values of Z' are very rare. This unexpected discovery led to further investigations into the crystallography of (-)-methyl shikimate (**4.06**) and related analogues as discussed in chapter five.

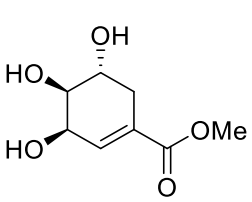

(-)-(**4.06**)

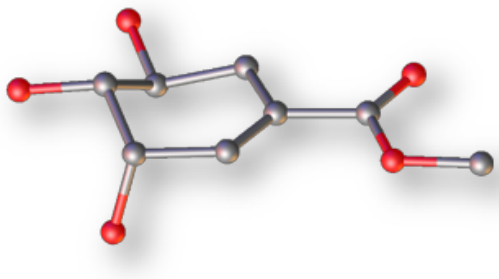

Figure 4.1: Single crystal X-ray crystal structure of (-)-methyl shikimate (**4.06**).

4.2.2 Regioselective Protection of the *trans*-vicinal diol of (-)-Methyl Shikimate (4.06)

The next protection step involved the regioselective C-1/C-10a protection of the *trans*-vicinal diol of (-)-methyl shikimate (**4.06**) as a cyclic diacetal under thermodynamic conditions. Thus, 5 mmol (-)-methyl shikimate (**4.06**), was reacted with 2,3-butanedione and trimethyl orthoformate, in the presence of a Brønsted acid catalyst, in refluxing methanol[3] After 48 hours, TLC analysis suggested that two compounds with similar retention times had been formed in the reaction. Two closely related products were subsequently isolated by column chromatography, the desired C-1/C-10a *trans*-vicinal diol protected product (**4.07**) and the C-4a/C-10a *cis*-vicinal diol protected product (**4.08**) in a 3.6 : 1 ratio and total isolated yield of 91 % (71 % (**4.07**), 20 % (**4.08**)) (**Scheme 4.02**).

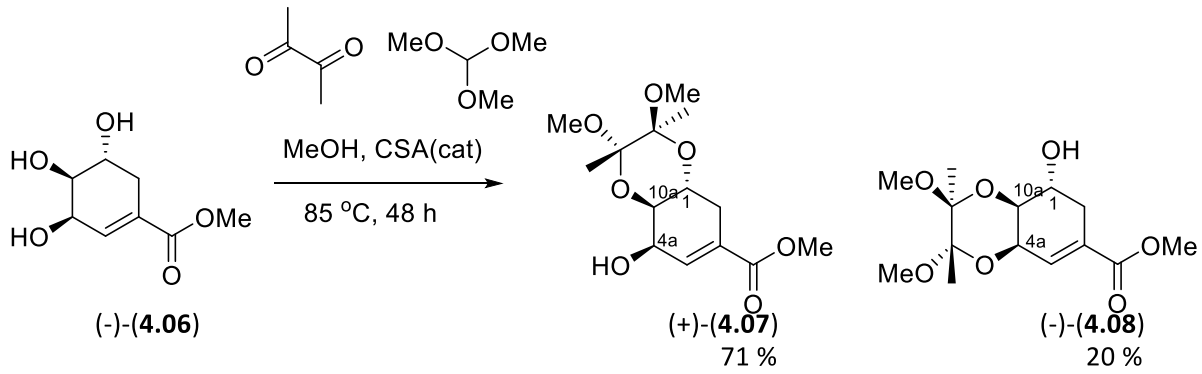

Scheme 4.02: Cyclic acetal protection of (-)-methyl shikimate (**4.06**).

Structural assignment of both the C-1/C-10a *trans*-vicinal diol protected product (**4.07**) and C-4a/C-10a *cis*-vicinal diol protected product (**4.08**) was initially performed by ^{1}H NMR analysis of the ring protons at the respective C-1/C-10a and C-4a/C-10a positions. For the C-1/C-10a *trans*-vicinal diol protected product (**4.07**), the H-1 and H-10a protons showed a ^{1}H-^{1}H coupling constant of 10.9 Hz, consistent with an axial-axial configuration and thus an overall *trans*-decalin structure. Whilst for C-4a/C-10a *cis*-vicinal diol protected product (**4.08**), the H-4a and H-10a protons showed a ^{1}H-^{1}H coupling constant of 1.2 Hz, consistent with an axial-equatorial configuration and thus an overall *cis*-decalin structure.[3,4]

To further confirm the structures of both regioisomers, C-1/C-10a *trans*-vicinal diol protected product (**4.07**) and C-4a/C-10a *cis*-vicinal diol protected product (**4.08**), crystals of both were grown for subsequent X-ray crystallographic analysis by slow solvent evaporation from petrol/acetone (5:1). The X-ray crystal structure of the major *trans*-vicinal diol protected product (**4.07**) confirmed that the cyclic diacetal had been formed at the C-1/C-10a positions. Importantly in the major *trans*-vicinal diol protected product (**4.07**), the diacetal and the shikimate core form a thermodynamically favoured *trans*-decalin like structure, explaining the preferential protection of the C-1/C-10a positions. Similarly, the X-ray crystal structure of C-4a/C-10a *cis*-vicinal diol protected product (**4.08**) confirmed the formation of a thermodynamically less favourable *cis*-decalin like arrangement of the diacetal and shikimate rings.

Interestingly, a clear example of the anomeric effect is seen in both crystal structures with the two methoxy groups of the cyclic diacetal ring system orientated axially in both cases to maximise anomeric stabilisation, with the methyl groups orientated in the equatorial positions (**Figure 4.2 and 4.3**).

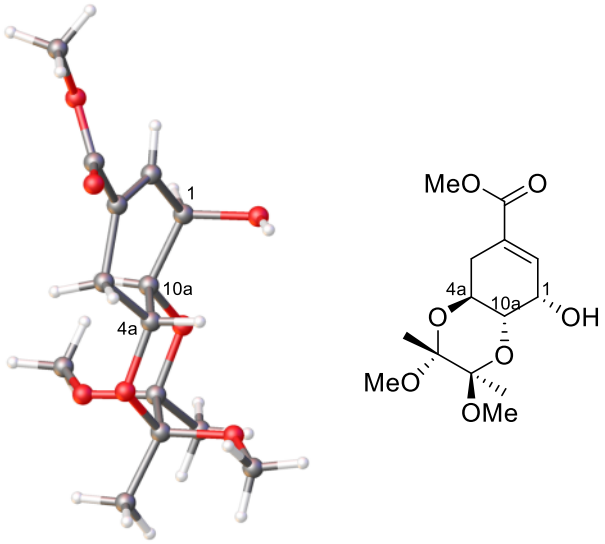

Figure 4.2: Single crystal X-ray crystal structure of the major *trans*-vicinal diol protected product (+)-(**4.07**).

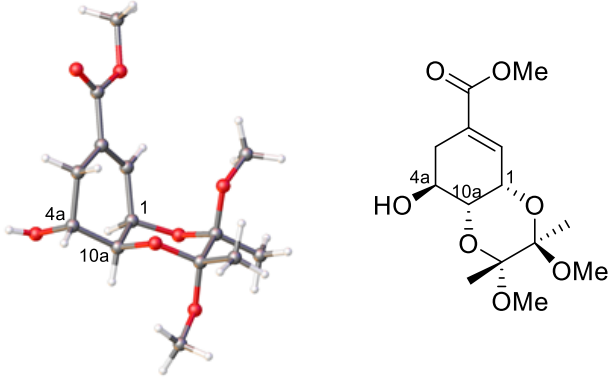

Figure 4.3: Single crystal X-ray crystal structure of the minor *cis*-vicinal diol protected product (-)-(**4.08**).

In order to access more material for the next steps, the acetal protection was scaled-up to first a 8 mmol scale and then a 15 mmol scale, with extension of the reaction times to 72 h. In both cases the *trans*- (+)-(**4.07**) and *cis*-vicinal protected products (-)-(**4.08**) were formed in a 3.5 : 1 ratio, by ^{1}H NMR analysis of the crude reaction material. Unfortunately, in these reactions the isolated yields of the major *trans*-vicinal protected products (+)-(**4.07**) decreased to 33 and 35 % respectively, likely due to isolation difficulties.

In a further attempt to rapidly access *trans*-vicinal protected product (+)-(**4.07**), we also examined a one-pot reaction in which the both the esterification and acetal protection of the shikimic acid (-)-(**4.01**) could take place in a single step. Such an approach would have the potential advantage of reducing the number of synthetic steps needed to make the *trans*-vicinal protected product (+)-(**4.07**)[5] (**Scheme 4.03**).

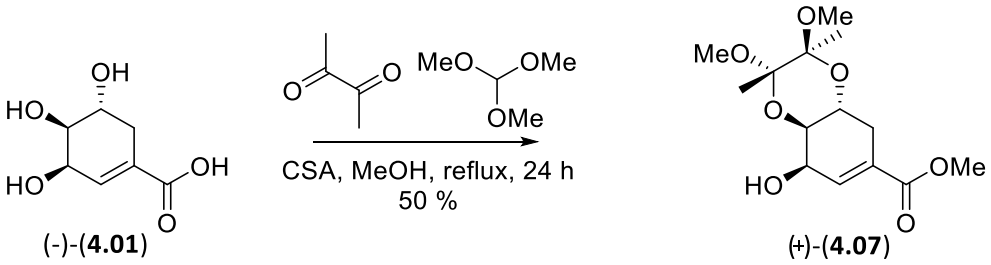

Scheme 4.03: One-pot esterification/acetal protection of shikimic acid (**4.01**) to give *trans*-vicinal diol protected product (**4.07**)

Therefore, 18 mmol of shikimic acid (-)-(**4.01**) was reacted in refluxing methanol for 24 h, with a mixture of 2 eq. 2,3-butanedione, 5 eq. trimethyl orthoformate, in the presence of catalytic camphorsulfonic acid. Unfortunately, analysis of the crude reaction mixture by ^{1}H NMR revealed a complex mixture of products, requiring multiple chromatography steps and resulting in a moderate 50 % isolated yield of *trans*-vicinal protected product (+)-(**4.07**). Scale-up of the reaction to 28 mmol gave very similar results, with again a 50 % isolated yield of *trans*-vicinal protected product (+)-(**4.07**).

Due to the difficult separations required for the one-pot protocol examined, we concluded that future synthesis of *trans*-vicinal protected product (+)-(**4.07**) would still be better carried out using our initial two-step method. It was considerded whether to resubmit the various *cis*-vicinal collected products (-)-(**4.08**) to the reaction conditions to observe whether they would equilibriate but in the end it was decided to collect all the isolated (-)-(**4.08**) to attempt to grow a single crystal structure of (-)-(**4.08**), which was achieved. Through combination of material from the various attempts, we had multigram quantities of the *trans*-vicinal diol protected product (+)-(**4.07**) in hand, allowing us to proceed to the next synthetic step.

4.2.3 Protection of the C-4a OH group of the *Trans*-Vicinal Diol Protected Methyl Shikimate (+)-(4.07)

In order to facilitate our planned sterically directed a *syn*-dihydroxylation step later in the synthesis, we need to incorporate a bulky protecting group on the remaining unprotected secondary alcohol at C-4a of *trans*-vicinal diol protected product (+)-(**4.07**).

Therefore, a benzyl group was chosen as the preferred protecting group for the alcohol at C-4a, with the protection step first attempted under standard benzylation conditions. Thus, *trans*-vicinal diol protected product (**4.07**) was deprotonated using NaH (60% in mineral oil) at 0 ^{o}C for 30 min in THF, followed by addition of 2 eq. of benzyl bromide and warming to r.t.

overnight[6]. However, following work-up, ^{1}H NMR analysis of the crude reaction material showed only starting material (**Table 4.1: Entry 1**).

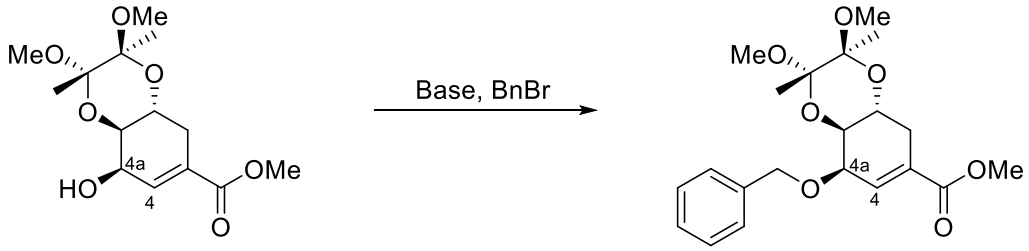

(-)-(**4.07**) (**4.09**)

Entry	BnBr eq.	Base	Base eq.	Reaction conditions	Reaction outcome
1	2	NaH[b]	1.3	THF, 0 °C, 30 min, then warm to rt over 18 h	No reaction observed, (**4.07**) and BnBr unchanged[a]
2	2	NaH[b]	1.3	DMF, 0 °C, 30 min, then warm to rt, 18 h	No reaction observed, (**4.07**) and BnBr unchanged[a]
3	2	NaH[b]	1.5	DMF, $KI_{(cat)}$, rt, 10 min, then 80 °C, 48 h	No reaction observed, (**4.07**) and BnBr unchanged[a]
4	1.3	NaHMDS	5	THF, $TBAI_{(cat)}$, reflux, 24 h	No reaction observed, (**4.07**) and BnBr unchanged[a]
5	2	NaH[b]	1.5	MeCN, $KI_{(cat)}$, reflux, 24 h	(**4.07**) : (**4.09**) in 4 : 1 ratio;[a] 19% isolated yield (**4.09**)
6	2	NaH[b]	2.5	MeCN, $KI_{(cat)}$, reflux, 24 h	(**4.07**) : (**4.09**) in 4 : 1 ratio;[a] 20% isolated yield (**4.09**)

Table 4.1: Protection of the secondary alcohol group at C-4a of *trans*-vicinal diol protected methyl shikimate (**4.07**) with BnBr. [a]Determined using the ^{1}H-NMR spectrum of the crude reaction material, [b]NaH used was in 60 % mineral oil

Due to the poor solubility of NaH in THF, we repeated the reaction in DMF, however again none of the desired product was observed by ^{1}H NMR of the crude reaction mixture (**Table 4.1: Entry 2**). Next, we included a nucleophilic catalyst (KI) to increase the reactivity of BnBr, and ran the reaction at an elevated temperature, but again none of the desired product could be identified (**Table 4.1: Entry 3**). The use of NaHMDS[7] as a more organosoluble strong base (5 eq) in THF, in the presence of catalytic TBAI, also did not result in the formation of benzyl protected shkimate (**4.09**) (**Table 4.1: Entry 4**). Finally, returning to the use of NaH (1.5 eq.) in conjugation with KI and BnBr (2 eq.) but in the more polar solvent MeCN, resulted in the observation of the desired benzyl protected shkimate (**4.09**) after 24 hours at reflux[8] Following work up and column chromatography, benzyl protected shikimate (**4.09**) was

isolated in a 19 % yield, with the structure confirmed by the observation of new signals in the ^{1}H NMR at 5.04 (1H, d, *J* = 11.2 Hz) and 4.67 (1H, d, *J* = 11.3 Hz) corresponding to newly formed benzylic methylene (CH_2) protons[9] (**Table 4.1: Entry 5**). Repeating the benzylation reaction with 2.5 equivalents of NaH did not however produce a significant increase in isolated yield, 20% (**Table 4.1: Entry 6**).

Due to the poor yields observed in our previous based-mediated benzylation reactions, an alternative acid catalysed benzylation was examined using benzyl 2,2,2-trichloroacetimidate (**4.10**)[10] . Thus, we reacted the *trans*-vicinal diol protected product (**4.07**) with the benzylating reagent benzyl 2,2,2-trichloroacetimidate (**4.10**) in the presence of triflic acid, in cyclohexane/DCM for 24 h at rt. Unfortunately, none of the desired product was observed, with 90 % starting material (**4.07**) being recovered by column chromatography (**Scheme 4.04**).

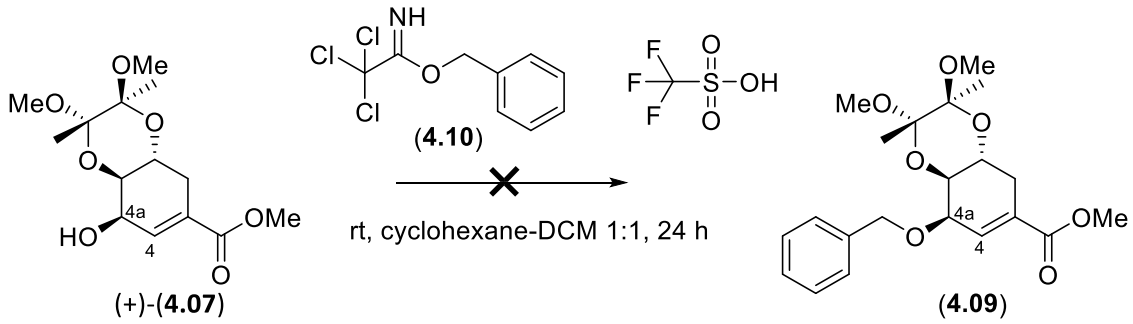

Scheme 4.04: Attempted benzylation of diacetal-protected methyl shikimate (**4.07**) under acidic conditions using benzylating agent (**4.10**).

Due to the difficulties in achieving a high yielding benzylation of *trans*-vicinal diol protected product (**4.07**), under both basic and acidic conditions, we decided to examine an alternative protecting group strategy.

We decided to use a silyl ether protecting group (TBDMS) that would be both sterically bulky, to aid in the planned *syn*-dihydroxylation later in the synthesis, and to have the potential for later orthogonal deprotection.

Thus, 0.5 mmol of *trans*-vicinal diol protected product (+)-(**4.07**) was reacted with TBDMSCl (2.5 eq.) and imidazole (2.5 eq.) in DCM at rt, for 4 days. Following work-up and column chromatography silyl ether (**4.11**) was isolated in 51 % yield. ^{1}H NMR analysis revealed two new signals at 0.10 ppm and 0.12 ppm, each integrating to 3 protons, consistent with the two methyl groups of TBDMS, as well as a new signal at 0.89 ppm, integrating to 9 protons, corresponding to the *tert*-butyl group (**Scheme 4.05**)[3]

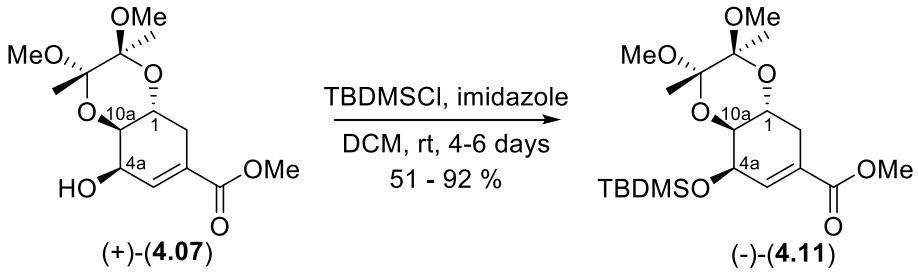

Scheme 4.05: TBDMS protection of the C-4a OH group of trans-vicinal diol protected product (**4.07**) to give silyl ether (**4.11**)

To access the gram quantities of silyl ether (-)-(**4.11**) required for later steps, the silyl protection reaction was first scaled-up to 5 mmol, with an extended reaction time of 5 days, giving an improved 65 % isolated yield. A further scale-up to 10 mmol, with a further extension of the reaction time to 6 days, pleasing gave a further increase in yield to 92 %. The long reaction time required due to the steric encumbrance around the C-4a hydroxyl group making any reaction at this position slow. This may also explain the difficulties in the previous benzylation chemistry, in which only low yields of benzyl protected shikimate (**4.09**) were ever observed.

Despite these long reaction times, accessing large quantities of silyl ether (**4.11**) proved feasible, allowing us to move on to examine the planned stereoselective dihydroxylation of the C-3/C-4 double bond.

4.2.4 Stereoselective Dihydroxylation of Silyl Ether (-)-(4.11)

Having successfully protected the OH functionalities of (-)-shikimic acid (**4.01**) to yield silyl ether (**4.11**), we were now in a position to examine a stereoselective dihydroxylation of the C-3/C-4 double bond. We envisaged that the steric bulk of the TBDMS group at C-4a would direct the dihydroxylation to the opposite face, setting the required (*S*)-stereochemistry at the quaternary C-3 position.

Thus, an Upjohn dihydroxylation of silyl ether (**4.11**) was attempted on a 1 mmol scale, using catalytic osmium tetroxide along with stoichiometric amounts of *N*-methyl morpholine-*N*-oxide as a co-oxidant in acetone/water at rt. After 7 days, the reaction was quenched with sodium thiosulphate and the resulting dihydroxylated product (**4.12**) isolated by column chromatography in 73% yield.

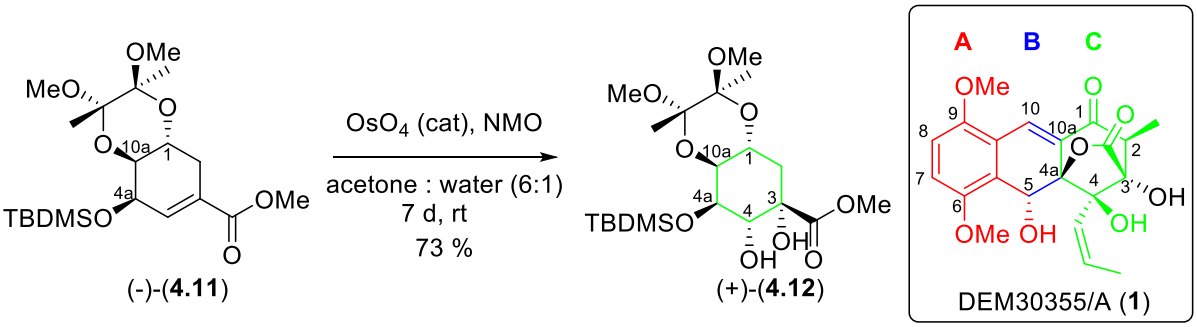

Scheme 4.06: Synthesis of diol (**4.12**) via a *syn*-dihydroxylation of our silyl ether (**4.11**) to set the stereocentre at C-3 with a comparison to our target compound DEM30355/A **(1)**.

In order to determine the stereochemistry of dihydroxylated product (+)-(**4.12**), we grew single crystals by slow evaporation of a $CDCl_3$ solution for analysis by X-ray crystallography. The crystal structure of the dihydroxylated product (+)-(**4.12**) allowed the *de novo* assignment of the absolute stereochemistry (Flack parameter = -0.029(13)). Examination of the C-3, C-4 and C-4a positions, showed that the dihydroxylation had been directed to the opposite face by the bulky TBDMS group as predicted, forming the required (*S*)-configuration at the quaternary centre (**Figure: 4.4**).

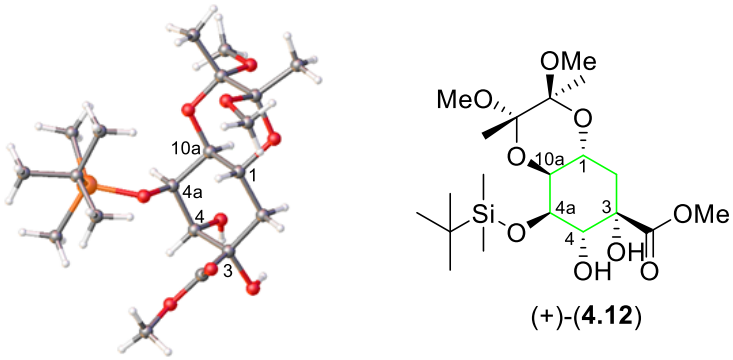

Figure 4.4: X-Ray crystal structure of dihydroxylated product (**4.12**) confirming the predicted stereoselectivity of the dihydroxylation.

In an attempt to optimise the reaction conditions, we repeated the dihydroxylation reaction in the presence of catalytic pyridine. After 4 days, dihydroxylated product (+)-(**4.12**) was isolated in a 60% yield, however complexities in the purification steps, in comparison to our original reaction, meant that we chose not to continue with these reaction conditions.

Therefore, to access more material, we repeated the dihydroxylation reaction three more times at the same 1 mmol scale, using our initial Upjohn conditions. An average isolated yield of 71 % was obtained, allowing access to sufficient dihydroxylated product (+)-(**4.12**) for the next step.

4.2.5 Regioselective Synthesis of Ketone (4.13)

The next synthetic step involved the selective oxidation of the secondary alcohol at C-4 of the dihydroxylated product (+)-(**4.12**) to the corresponding ketone, to assist with the subsequently planned E1cB reaction in the formation of the C-4a/C-10a double bond (**Scheme 4.07**).

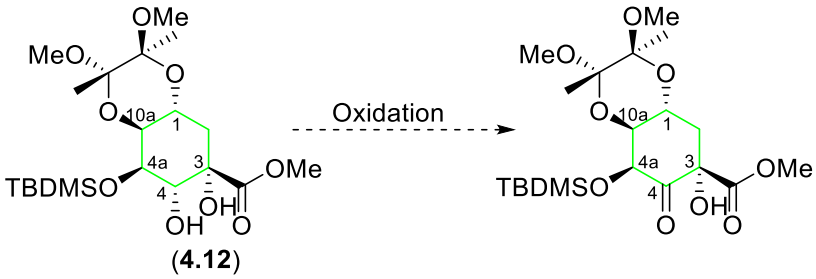

Scheme 4.07: Proposed selective oxidation of dihydroxylated product (**4.12**).

The oxidation of the secondary alcohol at C-4 was examined under Swern conditions. 5 eq. of DMSO was added to 2 eq. oxalyl chloride in DCM at -78 °C, after 30 min a solution of dihydroxylated product (+)-(**4.12**) in DCM was added and the reaction stirred at -78 °C for a further 30 min. Finally, 5 eq. of triethylamine was added, the reaction mixture stirred at -78 °C for 2 h and then allowed to warm to rt over 30 min. The reaction mixture was then quenched with saturated NH_4Cl. Following aqueous work-up, the crude material was purified by flash chromatography to yield the desired ketone (**4.13**) in 44 % isolated yield (**Scheme 4.08**).

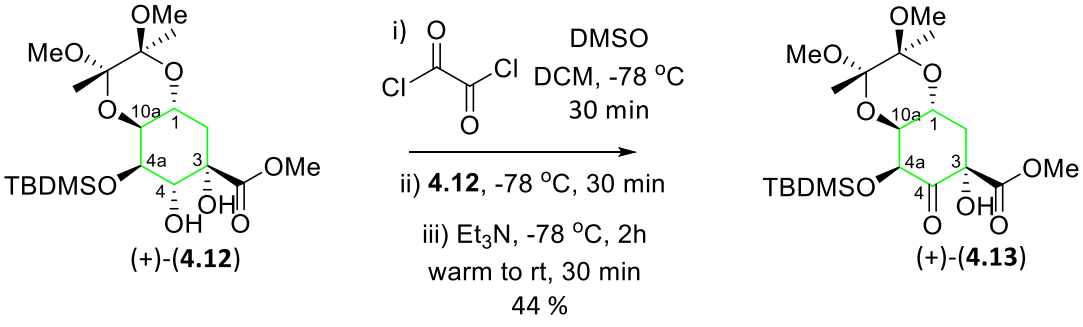

Scheme 4.08: Selective Swern oxidation of hydroxylated product (+)-(**4.12**)at C-4 to give ketone (+)-(**4.13**).

Analysis of the ^{13}C NMR spectrum of ketone (+)-(**4.13**) showed a new signal at 201.8 ppm, characteristic of the carbonyl carbon of the newly formed ketone. Additionally, analysis of ketone (+)-(**4.13**) by HRMS also showed a key molecular ion $[M+NH_4]^+$ signal at m/z = 466.2458 matching the expected mass for the desired product.

In an attempt to improve the yield of the Swern oxidation of dihydroxylated product (+)-(**4.12**), the reaction was repeated. In this case, following the addition of triethylamine, the reaction was stirred at -78 °C for 2 h as before, and then allowed to warm to rt over an extended period of 45 min. On this occasion, TLC analysis showed the presence of both the expected ketone (+)-(**4.13**) along with a new by-product (**4.14**). Separation of the two products by column chromatography resulted in an isolated yield of 93 % for the by-product (**4.14**), whilst the desired ketone (+)-(**4.13**) could only be observed in trace amounts.

Analysis of by-product (**4.14**) by ^{13}C NMR data showed a new carbonyl signal at 198.4 ppm, corresponding to a ketone group, further supported by a peak in the IR spectrum at 1736 (C=O). Analysis of the ^{1}H NMR data showed new signals at 4.75 ppm (1H, d, *J* = 11.5 Hz) and 4.66 ppm (1H, d, *J* = 11.5 Hz) corresponding to two geminally coupled methylene protons (CH_2) along with signals corresponding to a methyl group at 2.18 ppm (3H, s). The methyl group (^{1}H NMR: 2.18 ppm, CH_3) could be correlated via HMBC to the methylene group (^{13}C NMR: 70.9 ppm, CH_2), suggesting these two groups were linked by a heteroatom. This allowed us to conclude that by-product (**4.14**) contained a new thioacetal group at the C-3 positon (**4.13**) (**Figure 4.5**).

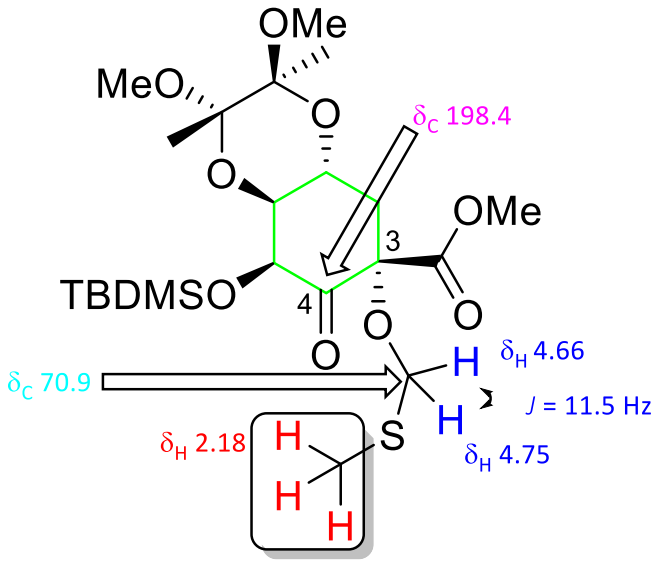

Figure 4.5: Structure of thioacetal (**4.14**).

The formation of thioacetals as a by-product in the Swern reaction has been observed previously, when the reactions are performed at higher temperatures. We propose that the formation of thioacetal (+)-(**4.14**) occurs when the chlorodimethylsulfonium, formed *in situ*, reacts with triethylamine to undergo an E2 elimination, to give a highly reactive sulfonium

carbocation ($H_2C=S(+)CH_3$) that subsequently reacts with the tertiary alcohol at C-3 (+)-(**4.14**). We postulated that the thioacetal formation had occurred in this case, due to the longer time over which the reaction was allowed to warm to room temperature (45 min verses 30 min) in the final step of the reaction (**Scheme 4.09**).

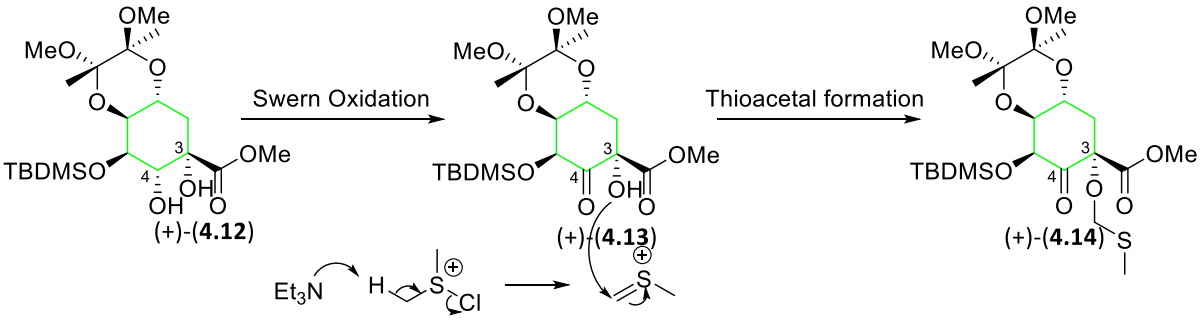

Scheme 4.09: Mechanism of formation of thioacetal (**4.14**) from excess chlorodimethylsulfonium

Having obtained the thioacetal (+)-(**4.14**) in such an excellent 93 % yield, and with the knowledge that the C-3 hydroxyl group would likely require protection later in the synthesis, we decided to continue to utilise the serendipitously discovered thioacetal (+)-(**4.14**) in further chemistry. Therefore, we repeated the Swern oxidation of dihydroxylated product (+)-(**4.12**) a further two times at the same scale, giving an average isolated yield of 91 % over all three reactions (93, 90 and 90 %) and affording us access to sufficient quantities of thioacetal (+)-(**4.14**) for use in the next synthetic step (**Scheme 4.10**).

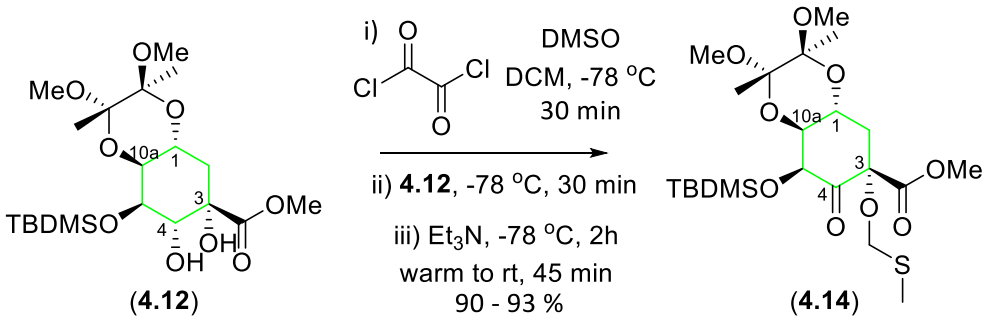

Scheme 4.10: Formation of thioacetal (+)-(**4.14**) under Swern conditions

4.2.6 Attempted E1cB Reaction of Thioacetal (4.14) under Basic Conditions

The next step in our planned synthetic route was to use an E1cB reaction to introduce a new carbon-carbon double bond at the C-4a/C10a positions. With the hydroxyl proton at C-3 now protected as a thioacetal, we anticipated that the proton at C-4 would now be the most acidic. Thus, the reaction of thioacetal (+)-(**4.14**) with base would lead to the formation of the

corresponding enolate, followed by an E1cB elimination to give enone (**4.15**), ready for a subsequent Michael-Dieckmann reaction (**Scheme 4.11**).

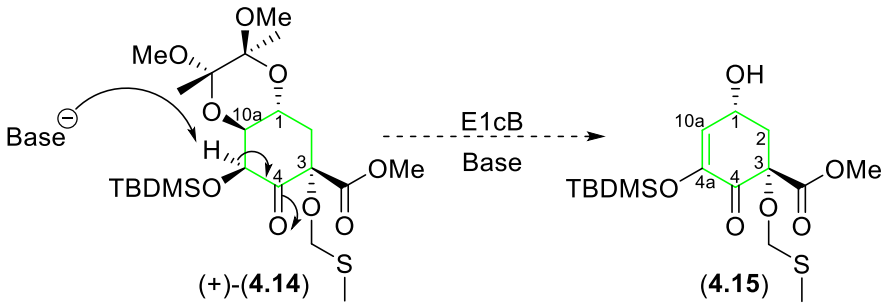

Scheme 4.11: Proposed E1cB reaction leading to enone (**4.15**).

Next, we examined the proposed base mediated E1cB elimination reactions of thioacetal (+)-(**4.14**) to generate enone (**4.15**). Initially thioacetal (+)-(**4.14**) was dissolved in pyridine, as the solvent, and the reaction was stirred at rt. However, after 11 days ^{1}H NMR analysis of the crude reaction mixture showed only unreacted starting material (**Table 4.2: Entry 1**). Similarly, reaction of thioacetal (+)-(**4.14**) with 2 eq. of DIPEA in refluxing THF gave only unreacted starting material, even after 4 days (**Table 4.2: Entry 2**).

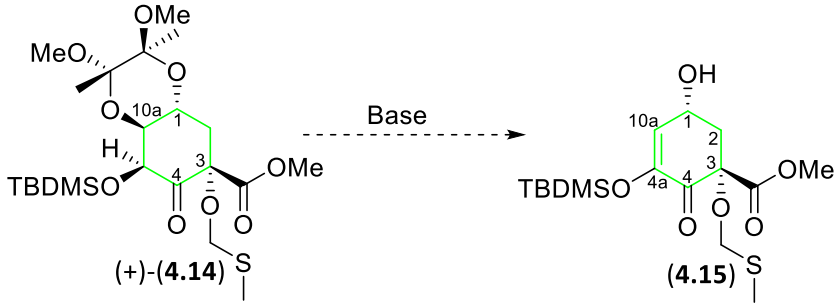

Entry	**4.14** eq.	Base	Base eq.	Reaction conditions	Reaction outcome[a]
1	1	Pyridine	as solvent	rt, 11 days	No reaction, unreacted (**4.14**)
2	1	DIPEA	2.0	THF, rt, reflux, 4 days	No reaction, unreacted (**4.14**)
3	1	NaHMDS	2.5	THF, -78 ^{0}C to rt, 24 h	Aromatic by-products observed
4	1	LDA	2.0	THF, -78 ^{0}C to rt, 24 h	Aromatic by-products observed

Table 4.2: Attempted E1cB eliminations of thioacetal (+)-(**4.14**) under basic conditions to synthesise enone (**4.15**). [a]Determined from analysis of the ^{1}H NMR spectrum of the crude reaction material

When NaHMDS and LDA (**Table 4.2 Entries 3 and 4**) were employed as strong, organo-soluble bases, no signals characteristic of the desired enone were observed in the ^{1}H-NMR of the crude reaction mixture, however new signals were observed that suggested the formation of aromatic by-products. This suggests that under forcing conditions the enone (**4.15**) maybe unstable towards aromatisation. Therefore, we decided at this point examine an alternative route to an enantiopure C-ring precursor to try to circumvent any possible ring aromatisation.

4.3 Synthesis of Cyclic Thiocarbonate (4.23)

In our second-generation synthesis of an enantiopure C-ring precursor we again imagined starting from enantiopure (-)-methyl shikimate (**4.06**), but this time we would attempt introduce the key C-4a/C-10a alkene early in the synthesis.

Therefore, we planned to use a Corey-Winter olefination to form the C-4a/C-10a alkene, via the selective conversion of the C-4a/C-10a *cis*-vicinal diol into the corresponding cyclic thiocarbonate, using 1,1'-thiocarbonydiimidazole (**4.22**) (**Scheme 4.12**). Following suitable protection of the other functional groups, subsequent elimination of the cyclic thiocarbonate would install the C-4a/C-10a double bond required for our later Michael-Dieckmann chemistry.

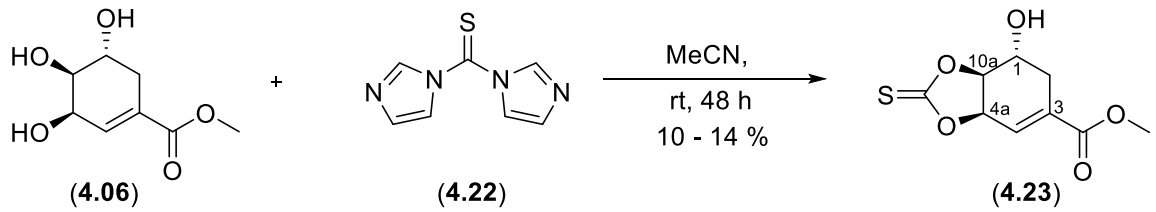

Scheme 4.12: Stereospecific protection of *cis*-vicinal diols of methyl shikimate (**4.06**).

Thus, 1 mmol of (-)-methyl shikimate (**4.06**) in MeCN was reacted with 2 eq of 1,1'-thiocarbonyldiimidazole (**4.22**) at rt for 48 h[11]. After purification by column chromatography, the desired cyclic thiocarbonate (**4.23**) was isolated in a low 10 % yield. ^{13}C NMR analysis showed a new signal at 188.4 ppm consistent with the C=S carbon, whilst the HRMS showed a key molecular ion $[M+H]^{+}$ at m/z = 231.0322, giving us confidence that we had synthesised the desired cyclic thiocarbonate (**4.23**) (**Scheme 4.12**).

We next examined the HMBC data in an attempt to prove the regiochemistry of the cyclic thiocarbonate formation, unfortunately the only HMBC correlation observed to the

thiocarbonyl carbon was from the proton at C10a, which does not allow for differentiation between the possible regioisomers.

In an attempt to access more material for study, the reaction was scaled up to 5 mmol resulting in a small increase in yield to 14 %. Increasing the number of equivalents of 1,1'-thiocarbonyldiimidazole to 2.5, on a similar 5 mmol scale, gave a very similar isolated yield of 11 %. However, at this point we had synthesised enough of cyclic thiocarbonate (**4.23**) to examine the next synthetic step, with a view to resolving the low yields of this protection step at a later date.

4.3.1 TBDMS Protection of C-1 OH group of Cyclic Thiocarbonate (4.23)

Next, we sought to protect the remaining hydroxyl functionality of cyclic thiocarbonate (**4.23**) with the silyl ether TBDMS. Thus, cyclic thiocarbonate (**4.23**) was reacted with imidazole (2.5 eq) and TBDMSCl (2.5 eq) in DCM at rt for 44 h. Following aqueous work-up and column chromatography, the desired TBDMS protected cyclic thiocarbonate (**4.24**) was isolated in 56 % yield (Scheme 4.13).

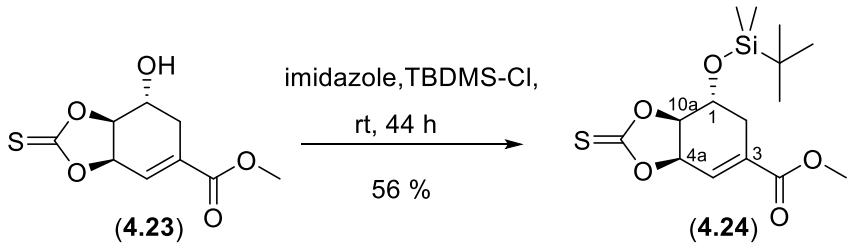

Scheme 4.13: TBDMS protection of cyclic thiocarbonate (**4.23**).

To confirm the formation of the desired TBDMS protected cyclic thiocarbonate (**4.24**) we analysed the ^{1}H NMR data, which revealed new signals at 0.88 ppm (9H, s), 0.13 ppm (3H, s) and 0.10 ppm (3H, s) corresponding to the *tert*-butyl and methyl groups of the TBDMS. Further examination of the HMBC data for TBDMS protected cyclic thiocarbonate (**4.24**) revealed correlations between the protons at both the C4a and the C10a and the thiocarbonyl carbon, helping to assign the regiochemistry of the cyclic thiocarbonate formed in the previous step.

4.3.2 Dihydroxylation of TBDMS protected carboxylate (4.24)

Finally, we decided to test the dihydroxylation of previously synthesised TBDMS protected cyclic thiocarbonate (**4.24**). Thus, employing a similar Upjohn dihydroxylation protocol as previously in this chapter, TBDMS protected cyclic thiocarbonate (**4.24**) in acetone: water (6:

1) was reacted with NMO and OsO_4 at rt for 44 h. The reaction was quenched with $Na_2S_2O_3$, and following aqueous work-up and column chromatography the desired dihydroxylated cyclic thiocarbonate (**4.25**) was isolated in 29 % yield as a single diastereomer (**Scheme 4.14**).

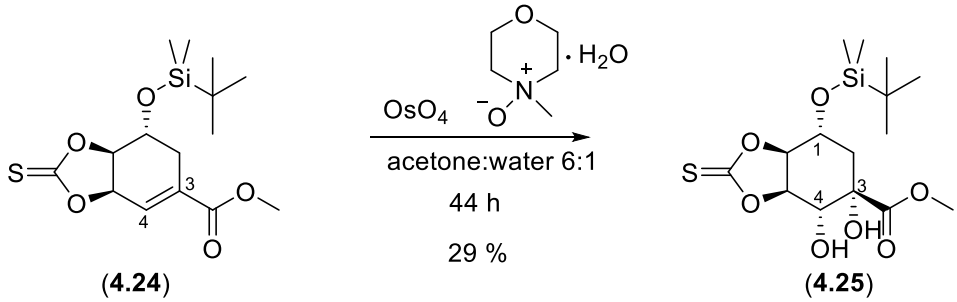

Scheme 4.14: Upjohn dihydroxylation of TBDMS protected cyclic thiocarbonate (**4.24**).

Structural assignment was supported by ^{13}C NMR analysis which showed a significant shift in the C-3 and C-4 signals from 134.1 ppm and 128.1 ppm respectively in TBDMS protected cyclic thiocarbonate (**4.24**), to 84.1 ppm and 66.3 ppm in dihydroxylated cyclic thiocarbonate (**4.25**). Unfortunately, at this point time constraints prevented further work on this series and the assignment of relative stereochemistry of dihydroxylated cyclic thiocarbonate (**4.25**) remains to be completed.

4.4 Conclusions

In this chapter our aim was to synthesise an enantiopure C-ring precursor, containing much of the required oxygenation pattern and with a specific focus on setting the correct stereochemistry at the C-3 quaternary centre. We imagined this could be achieved by starting with commercially available enantiopure (-)-shikimic acid (**4.01**) which already contains a key oxygen atom at the C-1 position and the required carboxylic acid at C-3. Whilst installation of the key C-3 chiral centre would be achieved through a dihydroxylation at C-3/C-4, sterically directed by a suitably protected C-4a hydroxyl group.

Thus, our synthesis began with the protection of methylation of the carboxylic acid of (-)-shikimic acid (**4.01**), via a high yielding (73 %) Fischer esterification. Next, we selectively protected the *trans*-vicinal diol at C-1/C10a through a thermodynamically controlled cyclic acetal formation. Benzyl protection of the C-4a hydroxyl group proved problematic, with only low yields (20 %) obtained even with extended reaction times. Protection as the silyl ether (TBDMS) was however successful, again with long reaction times (6 days) being required to obtain high yields (92 %) of the desired silyl ether (**4.11**). The difficulties in the protection of

the C-4a hydroxyl group being attributed to the steric encumbrance around the alcohol (**Scheme 4.15**).

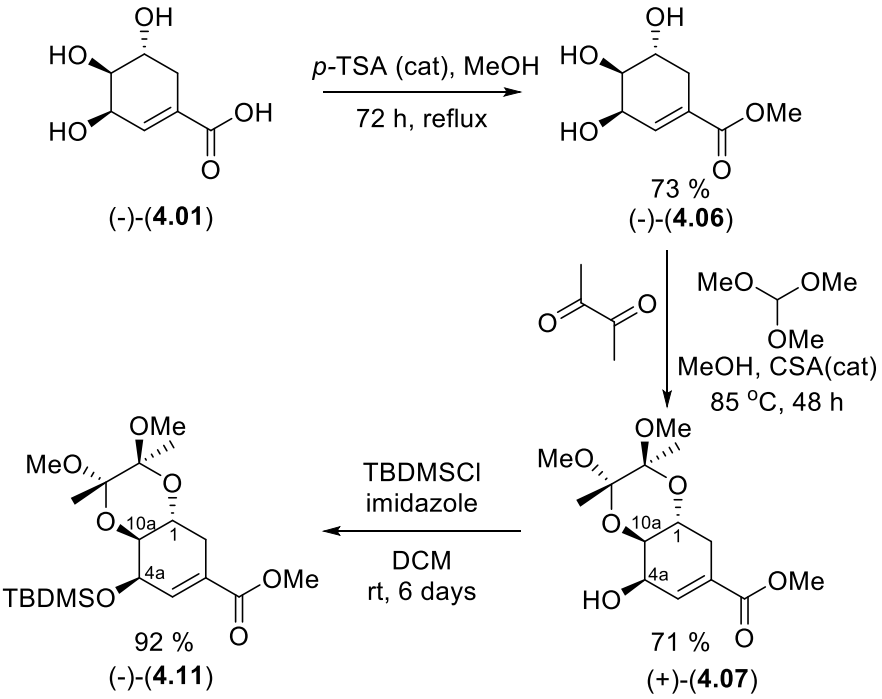

Scheme 4.15: Selective protection of the carboxylic acid and three hydroxyl groups of (-)-shikimic acid (**4.01**).

Following our protecting group manipulations, we examined an Upjohn *syn*-dihydroxylation of the C-3/C-4 alkene. We were pleased to see that the TBDMS protected hydroxyl group at C-4a had directed the dihydroxylation to the opposite face of the C-3/C-4 alkene, forming the dihydroxylated product (**4.12**) in 73 % yield with the required (*S*)-configuration at the C-3 quaternary centre. Next, we employed a serendipitously discovered one-pot Swern oxidation/thioacetal protection to introduce the required ketone at C-4 (**4.13**) whilst simultaneously protecting the C-3 hydroxyl group to thioacetal (**4.14**) in high yields of 93 %. Unfortunately, attempted E1cB elimination chemistry to install the C=C double bond at C4a/C10a failed, prompting us to examine an alternative synthetic approach (**Scheme 4.16**).

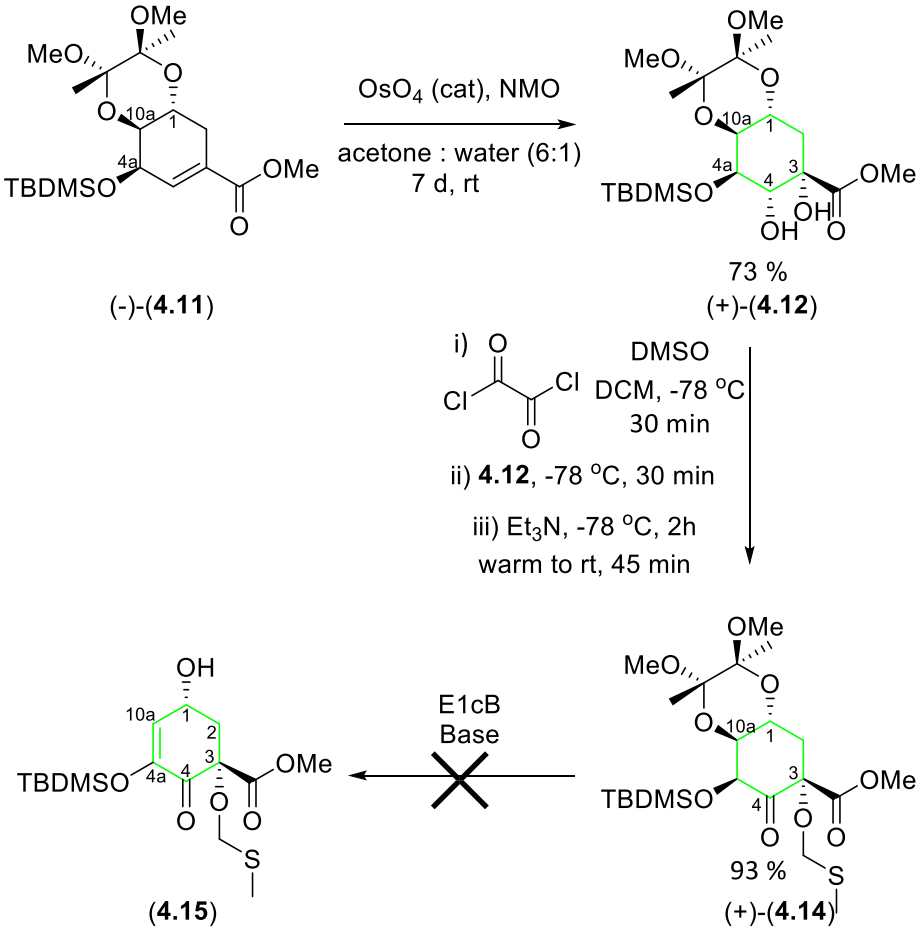

Scheme 4.16: Upjohn dihydroxylation of silyl ether (-)-(**4.11**) at C-3/C-4 with subsequent oxidation at C-4 and simultaneous thioacetal protection at C-3 to give thioacetal (+)-(**4.14**) and unsuccessful E1cB elimination.

In our second-generation synthesis we focussed on the use of Corey-Winter chemistry to introduce the key C=C double bond at C4a/C10a. Thus, starting with (-)-methyl shikimate (**4.06**) we attempted to selectively convert the C-4a/C-10a *cis*-vicinal diol into a cyclic thiocarbonate, using 1,1'-thiocarbonyldiimidazole (**4.22**). Subsequently, the C-1 hydroxyl group of cyclic thiocarbonate (**4.23**) was protected as the silyl ether (TBDMS) followed by a stereoselective Upjohn *syn*-dihydroxylation of the C-3/C-4 alkene (**Scheme 4.17**).

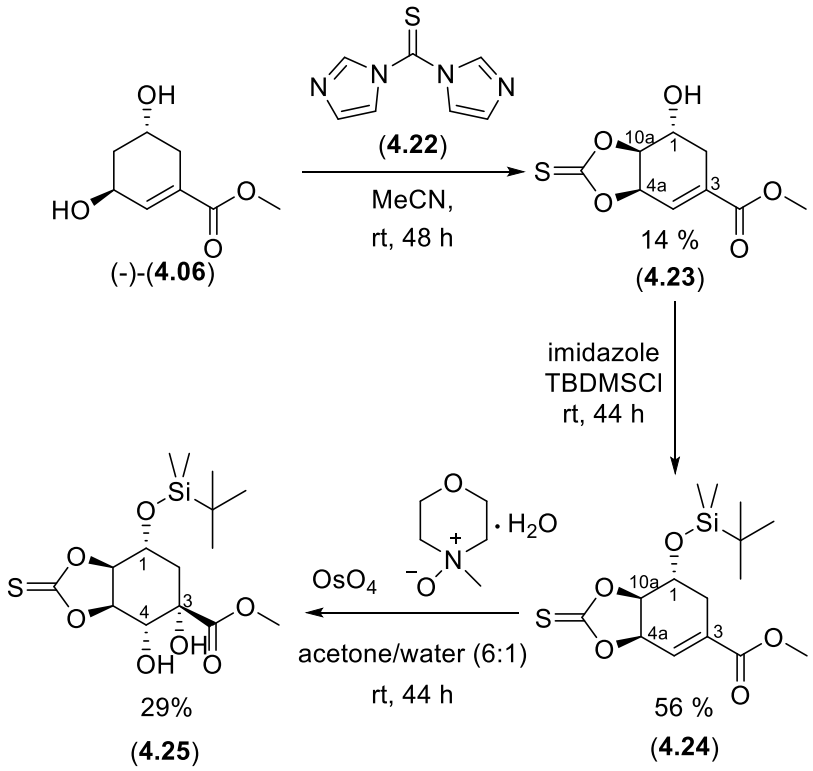

Scheme 4.17: Synthesis of cyclic thiocarbonate (**4.23**) with subsequent TBDMS protection of the C-1 hydroxyl group and Upjohn *syn*-dihydroxylation at C-3/C-4 to yield dihydroxylated cyclic thiocarbonate (**4.25**)

4.5 Future work

Despite making significant progress in the synthesis of DEM30355/A (**1**) a number of key challenges still remain, thus the future work in this section of the project would focus on completing an enantioselective route to DEM30355/A (**1**), and analogues.

To progress our promising Corey-Winter chemistry from the dihydroxylated cyclic thiocarbonate (**4.25**) we would first look to optimise the currently low yielding formation of our initial cyclic thiocarbonate (**4.23**) (e.g. via nucleophilic catalysis), and to validate the regiochemistry of the product through single crystal X-ray diffraction. Following the subsequent synthesis of dihydroxylated cyclic thiocarbonate (**4.25**), with improved yields, we will examine the trimethylphosphite mediated *syn*-elimination at C-4a/C-10a and the Swern oxidation of the C-4 hydroxyl group to give the enone (**4.26**) required for our subsequent Michael-Dieckmann chemistry with our suitably functionalised A-ring precursor (**4.27**) (**Scheme 4.18**).

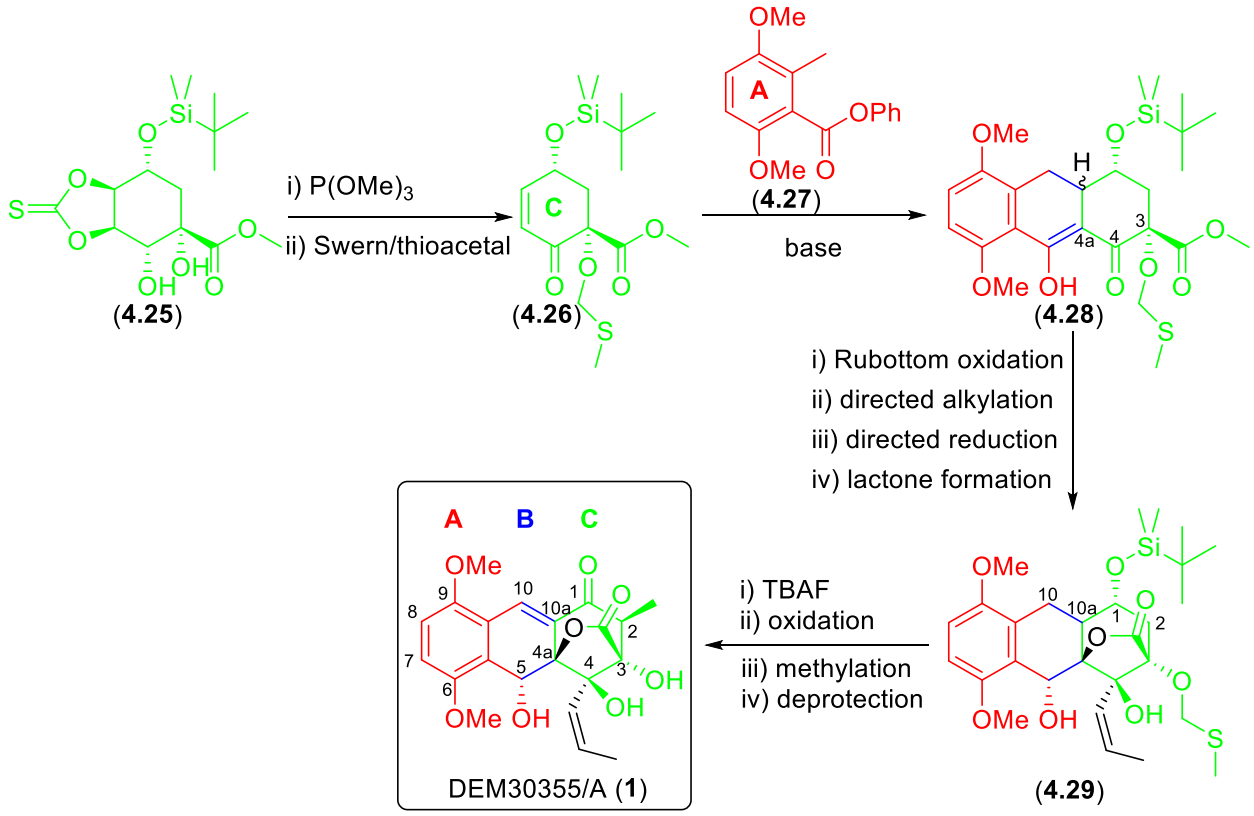

Scheme 4.18: Planned synthetic route to complete the total synthesis of DEM30355/A (**1**).

Completion of our planned synthesis of DEM30355/A (**1**) would involve a Rubottom oxidation at C-4a, followed by a directed organometallic addition to the ketone at C-4, directed reduction of the C-5 ketone to the corresponding alcohol and a lactonization between the C-4a OH and C-3 ester to form the lactone ring attached to the C-ring of DEM30355/A (**1**). Following TBMDS deprotection, we would set the C=C double bond at C-10/C-10a either through a dehydrogenation or elimination reaction. A late stage methylation would then be used to install the C-2 methyl group to complete the total synthesis of target compound DEM30355/A (**1**)(**Scheme 4.18**).

Our ultimate goal is to achieve a total synthesis of DEM30355/A (**1**) and its analogues to probe its mode of action. We will look to examine analogues of DEM30355/A (**1**) at the C-2 position where a methyl group present in the original compound can be replaced by a number of different groups (R^1 = ethyl, propyl, benzyl) or R^1 may be replaced by a gem-dimethyl group or removed altogether.

Another position for possible manipulation on the C-ring is at C-4 (R^2) where the original alkenyl substituent could be replaced by a methyl, ethyl or propyl substituent.

On the B-ring of DEM30355/A (**1**) there exists the possibility at C-5 (R^3) of forming either the top facing or back facing hydroxyl group from the reduction of the C-5 ketone, directed by the C-4a hydroxyl group.

Finally, by manipulation of the starting material A-ring precursor we can change the number and position of the OMe (OR^4) functional groups around the A-ring.

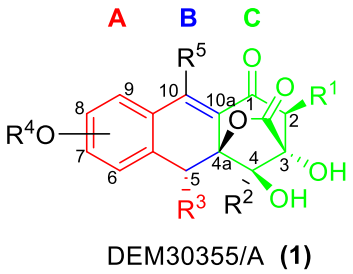

DEM30355/A **(1)**

Figure 4.6: Plan for future work to synthesise DEM30355/A (**1**) analogues**.**

Chapter 4 – References

1) B. Kepplinger, PhD Thesis, Newcastle University, 2016.
2) S. V. Ley, D. K. Baeschlin, D. J. Dixon, A. C. Foster, S. J. Ince, H. W. M. Priepke and D. J. Reynolds, *Chem. Rev*., 2001, **101**, 53-80.
3) A. Liu, Z. Z. Liu, Z. M. Zou, S. Z. Chen, L.Z. Xu and S. L. Yang, *Tetrahedron*, 2004, **60**, 3689-3694.
4) Y. Zhang, A. Liu, Z. G. Ye, J. Lin, L. Z. Xu and S. L. Yang *Chem. Pharm. Bull.*, 2006, **54** 1459—1461.
5) N. Armesto, M. Ferrero, S. Fernandez and V. Gotor, *Tetrahedron Lett*., 2000, **41**, 8759-8762.
6) S. Czernecki, C. Georgoulis and C. Provelenghiou, *Tetrahedron Lett.*, 1976, **17**, 3535-3536.
7) S. J. Danishefsky, J. J. Masters, W. B. Young, J. T. Link, L. B. Snyder, T.V. Magee, D. K. Jung, R. C. A. Isaacs, W. G. Bornmann, C. A. Alaimo, C. A. Coburn, and M. J. Di Grandi, *J. Am. Chem. Soc.*, 1996, **118**, 2843-2859.
8) D. Lee, C. L. Williamson, L. Chan and M. S. Taylor, *J. Am. Chem. Soc.*, 2012, **134**, 8260-8267.
9) M. Psotka, M. Martinkovka and J. Gonda, *Chem. Pap.,* 2017, **71**, 709-719.
10) G. E. Veitch, E. Beckmann, B. J. Burke, A. Boyer, S. L. Maslen and S. V. Ley, *Angew. Chem. Int. Ed*., 2007, **46**, 7629 –7632.
11) S. Matsumura, Y. Matsui, M. Nagatomo and M. Inoue, *Tetrahedron*, 2016, **72**, 4859-4866.

Chapter 5 – Synthesis of Shikimate Derivatives to Probe Z' Character

5.1 Introduction

In chapter four we briefly touched on our discovery, by single crystal X-ray crystallography analysis, of a compound, (-)-methyl shikimate (**4.06**) that crystallises with an unusually high Z' value (Z' = 12). In this chapter we will discuss our efforts to synthesise and crystallise a library of shikimate analogues with a view to probing their propensity to exhibit high Z' values.

5.1.1 High Z' in Crystallography

In crystallography, the parameter Z represents the number of formula units (e.g. molecules) in the unit cell of a crystal structure, whilst the parameter Z' is commonly used to denote the number of formula units (e.g. molecules) in the asymmetric unit. More specifically, Z' is defined as the number of formula units in the unit cell (Z) divided by the number of independent general positions (*m*), and is given by Z' = Z/*m*. A crystal structure is said to have a high Z' when Z' > 1, with approximately 10 % of all crystal structures found in the CSD having a Z' > 1[1,2].

Currently, there are only 58 known crystal structures with a Z' $\geq$ 12, from over one million crystal structures in the Cambridge Structural Database (CSD). There is considerable interest in the phenomena of high Z' crystal structures, due to the impact on the understanding and prediction of crystal forms, especially in the case of active pharmaceutical ingredients[3]. Therefore, we felt that the uniqueness of our serendipitous finding of a new crystal structure with Z' = 12 warranted further investigation.

The formation of crystal structures with high Z' has been linked to a number of key molecular properties such as the presence of single enantiomers, of multiple accessible low energy conformers, and of strong directional intermolecular interactions (e.g. hydrogen bonding) often in competition with other strong intermolecular interactions[4-11].

Despite the considerable interest in high Z' crystal structures, there have been few systematic attempts to probe the impact of the molecular structure on Z'. Consequently, we planned to synthesise and then crystallise a series of shikimate esters and amides, with variations of the R group of the esters and amides, whilst retaining the key hydrogen-bonding motif of the

1,2,3-triol. We would then examine the obtained crystal structures of this series with a view to probing the origins of the high Z' phenomenon.

5.2 Results and Discussion

5.2.1 Synthesis of Shikimate Esters

In chapter four, we synthesised methyl shikimate (**4.06**) in a 73 % isolated yield via a Fischer esterification in refluxing methanol (72 h) with *p*-TSA, starting from enantiopure (-)-shikimic acid (**4.01**)[12] (**Scheme 5.01**).

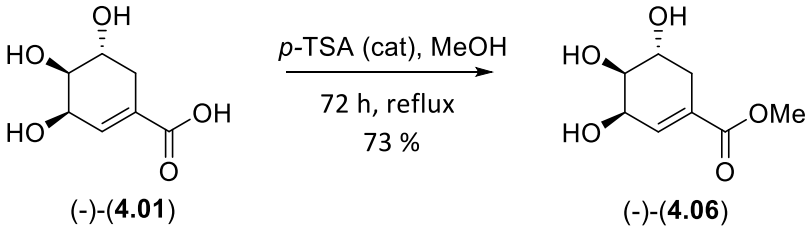

Scheme 5.01: Fischer esterification of (-)-shikimic acid (**4.01**) to give (-)-methyl shikimate (**4.06**)

In order to synthesise our planned shikimate ester series we decided to use similar Fischer esterification chemistry to esterify (-)-shikimic acid (**4.01**) using a range of alcohols (**Table 5.1**)

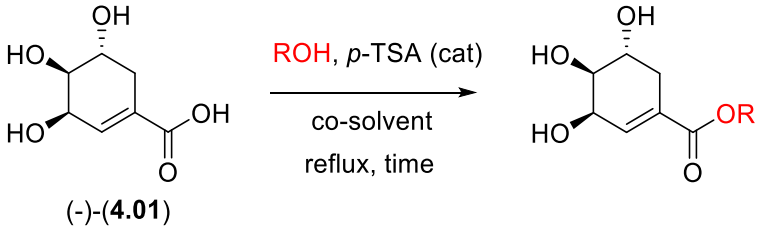

ENTRY	TIME/h	mmol of **4.01**	REACTION CONDITIONS	ISOLATED % YIELD
1	72	28	MeOH	73 % (**4.06**)[a]
2	72	28	EtOH	75 % (**5.01**)
3	72	12	Propan-1-ol	61 % (**5.02**)
4	72	28	Propan-2-ol	74 % (**5.03**)
5	4	6	BnOH/toluene (1:4)	37 % (**5.04**)

Table 5.1: Reaction conditions for synthesis of shikimate ester series. [a] Previously discussed in chapter 4.

Ethyl shikimate (**5.01**) was synthesised via a Fischer esterification in refluxing ethanol over 72 h, giving an isolated yield of 75 % following hot-to-cold recrystallisation from minimal EtOAc. *n*-Propyl shikimate (**5.02**) was synthesised in a similar manner over 72 h. On cooling the reaction to rt, *n*-propyl shikimate (**5.02**) precipitated from solution and was collected by filtration. Purification by column chromatography (DCM/MeOH, 9:1) yielded *n*-propyl shikimate (**5.02**) in 61 % yield. We then looked to synthesise *i*-propyl shikimate (**5.03**) under similar conditions. Again, after 72 h the reaction was cooled to rt and *i*-propyl shikimate (**5.03**) was collected by filtration and purified by column chromatography (DCM/MeOH, 9: 1) to give a 74 % isolated yield. Finally, to include an aryl group at the ester, we chose to make benzyl shikimate (**5.04**) on a 6 mmol scale under similar Fischer esterification conditions. Due to the high boiling point of benzyl alcohol (b.p. = 205.3 °C), we decided in this case to use 5 mL of benzyl alcohol in 20 mL toluene as a co-solvent. After 4 h the reaction was cooled to rt and benzyl shikimate (**5.04**) precipitated from the reaction and was collected by filtration and purified by chromatography (DCM/MeOH, 9: 1) to give a 37 % isolated yield. With a set of five shikimate esters in hand we next decided to examine the related shikimic amides.

5.2.2 Synthesis of Shikimic Amides

Next, we decided to synthesise and crystallise a number of related shikimic amides to study their potential to form crystal structures with high Z', due to the introduction of additional directional intermolecular interactions via the amide group. We planned to examine the use of amide coupling reagents to activate (-)-shikimic acid (**4.01**) to undergo amide bond formation with a range of amines to give the corresponding amides (**Scheme 5.02**).

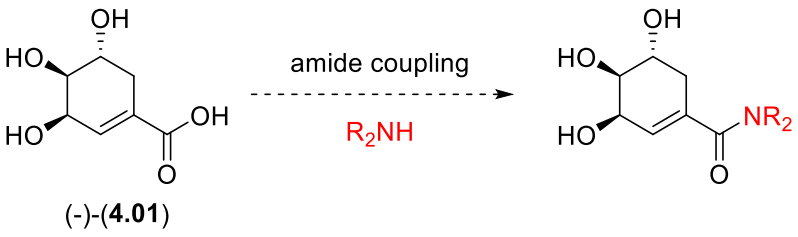

(-)-(**4.01**)

Scheme 5.02: Planned synthetic route to amide series starting from (-)-shikimic acid (**4.01**).

Firstly, we decided to focus on the synthesis of tertiary shikimic amides, shikimic dimethyl amide (**5.05**) and shikimic diethyl amide (**5.06**) via an EDCI coupling. Thus, in two concurrent

reactions, (-)-shikimic acid (**4.01**) (1eq) was reacted with EDCI (1.5 eq) in DCM for 20 min at rt, followed by the addition of either dimethyl or ethyl amine (1.3 eq) and DIPEA (1.5 eq), and the reaction mixtures were stirred at rt for 48 h. Following work-up of the two reactions, ^{1}H NMR analysis of both crude reaction mixtures showed no evidence of any reaction occurring with only starting material observed (**Table 5.2**).

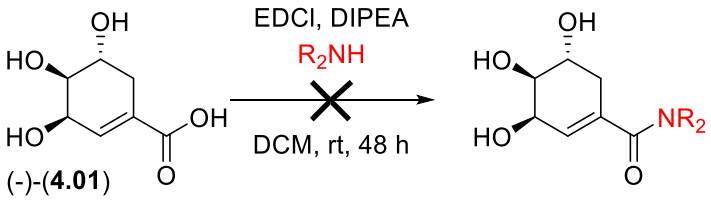

ENTRY	TIME/h	R_2NH	REACTION OUTCOME[a]
1	48	Me_2NH	No reaction. Starting material observed (**5.05**)
2	48	Et_2NH	No reaction. Starting material observed (**5.06**)

Table 5.2: Attempted synthesis of shikimic amides (**5.05** and **5.06**) via EDCI coupling.

[a] As observed by ^{1}H NMR analysis of the crude reaction mixture.

Due to the poor results from initial EDCI coupling attempts, we next examined the use of HATU as an improved amide coupling reagent to synthesise both shikimic dimethyl amide (**5.05**) and shikimic diethyl amide (**5.06**). Thus, in two concurrent reactions, (-)-shikimic acid (**4.01**) (1eq) was reacted with HATU (1.2 eq) in DMF for 20 min at 0 ^{o}C, followed by the addition of either dimethyl or ethyl amine (1.5 eq) and DIPEA (1.5 eq), and the reactions were stirred at rt for 72 h. Following work up and purification by column chromatography (DCM/MeOH, 4: 1) shikimic dimethyl amide (**5.05**) and shikimic diethyl amide (**5.06**) were isolated in 34 % and 53 % yield from their respective reactions (**Table 5.3**).

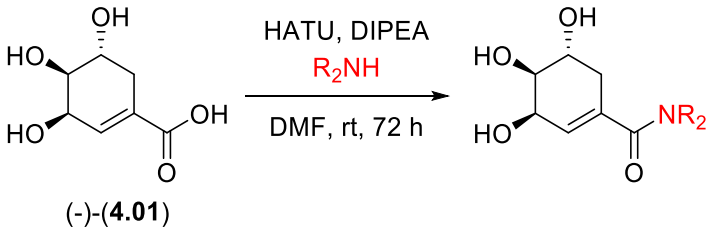

ENTRY	TIME/h	R_2NH	ISOLATED % YIELD
1	72	Me_2NH	34 % (**5.05**)
2	72	Et_2NH	53 % (**5.06**)

Table 5.3: Reaction conditions for the synthesis of shikimic amides (**5.05** and **5.06**) via HATU coupling.

Finally, we attempted to synthesise the primary shikimic amide (**5.07**) using HATU as a coupling reagent. Therefore, to a stirred solution of (-)-shikimic acid (**4.01**) (6 mmol) in DMF at 0 ^{o}C, was added with DIPEA (2 eq). After 20 min HATU (2 eq) and ammonia solution in water (29 %) (6 eq) were added and the reaction allowed to warm to rt over 5 h. Unfortunately, following work up ^{1}H NMR of the crude reaction mixture showed only starting material. Due to time constraints, we did not investigate this reaction further (**Scheme 5.03**).

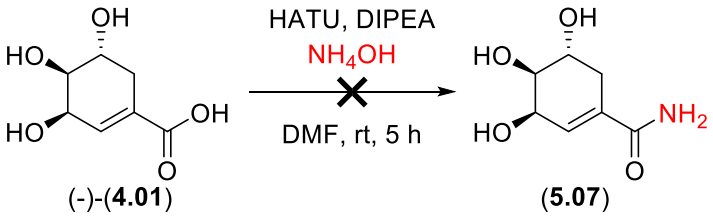

Scheme 5.03: Attempted synthesis of primary shikimic amide (**5.07**).

5.2.3 Crystallisation of Shikimate Esters and Shikimic Amides

Following the successful synthesis of five shikimate esters (**4.06**, **5.01** - **5.04**) and two shikimic amides (**5.05** and **5.06**), we next focussed on evaluating their solid-state properties. Thus, our next challenge was to grow high quality single crystals suitable for X-ray analysis for each of the shikimate esters and shikimic amides synthesised.

As previously discussed in Chapter 4, single crystals of (-)-methyl shikimate (**4.06**) were grown from slow evaporation of a DCM solution. Whilst, a crystal structure of the parent (-)-shikimic acid (**4.01**) has not been previously published, with only sodium (-)-shikimate being reported in the CCDC as the dihydrate (Z' = 2, VUXROV)[13]. In parallel to our work Dr. Paul Waddell (Newcastle) showed that single crystals of (-)-shikimic acid (**4.01**) could be grown via slow evaporation of a MeOH solution.

Based on these preliminary results, we examined the crystallisation of our shikimate esters (**4.06**, **5.01** - **5.04**) and shikimic amides (**5.05** and **5.06**) through slow evaporation of MeOH, DCM, $CHCl_3$, toluene, hexane and DMF solutions. No crystals were obtained for *n*-propyl shikimate (**5.02**), benzyl shikimate (**5.04**) and diethyl amide (**5.06**), whilst suitable crystals were obtained for ethyl shikimate (**5.01**), *i*-propyl shikimate (**5.03**) and dimethyl amide (**5.05**). Interestingly, early attempts to crystallise *i*-propyl shikimate (**5.03**) from the reaction mixture resulted in a 2:1 co-crystal of (-)-shikimic acid (**4.01**) and *i*-propyl shikimate (**5.03**). MeOH as solvent (**Table 5.4**).

COMPOUND	CRYSTALLISATION SOLVENT
Shikimic acid **4.01**	MeOH
Methyl shikimate **4.06**	DCM
Ethyl shikimate **5.01**	$CHCl_3$
i-Propyl shikimate **5.03**	$CHCl_3$
Shikimic dimethyl amide **5.05**	$CHCl_3$
Shikimic acid **4.01**/*i*-Propyl shikimate **5.03** (2:1 co-crystal)	MeOH

Table 5.4: Successful crystallisation conditions for shikimate esters and shikimic amides.

5.3 Crystallography Results

For all successful crystallisation experiments, single crystals were subjected to X-ray analysis. The crystal structures reported below were all solved by Dr. Paul Waddell (Newcastle). In this section we will use graph-set assignments to define the morphology of the intermolecular hydrogen-bonding motifs found in the structures studied[14].

Thus, intermolecular hydrogen-bonds will be described as either C (chain), R (ring), and D (dimer), with intramolecular hydrogen-bonds described as S. The number of hydrogen-bond donors are given as subscripts, and the number of acceptors as superscripts, whilst the number of atoms in the ring (R) will be given in brackets.

5.3.1 Crystal Structure of (-)-Shikimic acid (4.01)

Crystals of the parent molecule (-)-shikimic acid (**4.01**) were grown and analysed by Dr. Paul Waddell (Newcastle) and are discussed here for comparison to later structures. (-)-Shikimic acid (**4.01**) formed crystals in the monoclinic space group $P2_1$, with Z' = 1. Examination of the crystal structure of (-)-shikimic acid (**4.01**), shows that the molecules form a chain held together by hydrogen-bonds between the carboxylic acid of one molecule and the C-4/C-5 hydroxyl groups of a second neighbouring molecule, forming a $R^2_2(9)$ ring. This strongly directional hydrogen-bonding network appears to dominate the crystal structure and likely explains the low Z' observed. The main chain structure is both stabilised and cross-linked by additional $R^3_3(9)$ hydrogen-bonded rings involving three adjacent molecules, two from one chain and one from the neighbouring chain (**Figure 5.1**).

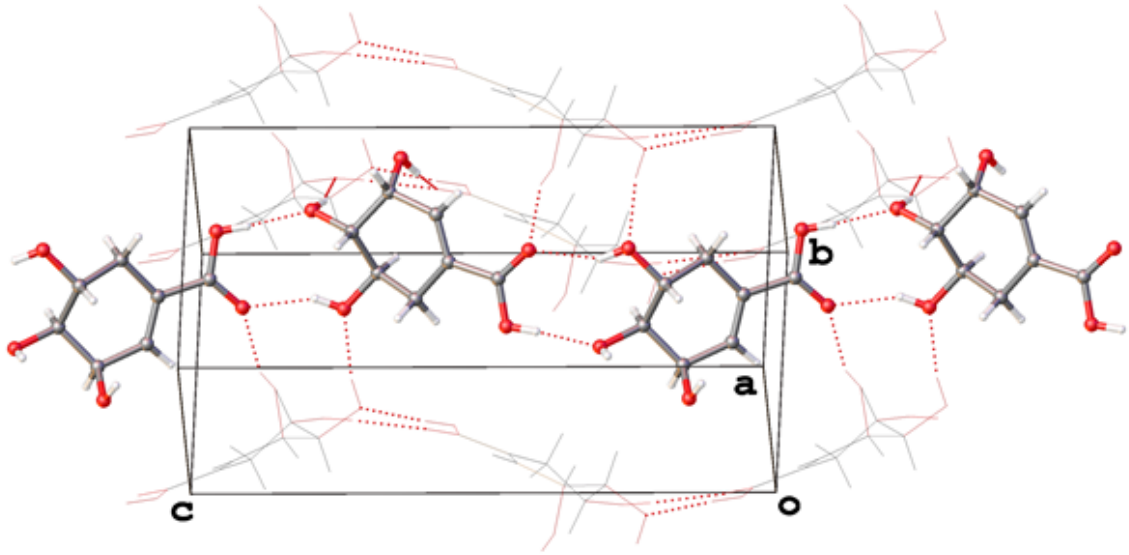

Figure 5.1: Unit cell of (-)-shikimic acid (**4.01**), showing the main chain of hydrogen-bonded molecules, hydrogen atoms omitted for clarity (Figure prepared by Dr. Paul Waddell).

5.3.2 Crystal Structure of Shikimic Dimethyl Amide (5.05)

Shikimic dimethyl amide (**5.05**) crystallised in the triclinic space group P1 with Z' = 2, as a one-to-one chloroform solvate. Each molecule of chloroform is held in place through a weak C-H--O hydrogen-bond to the carbonyl oxygen atom of the amide group. The asymmetric unit contains two molecules of shikimic dimethyl amide (**5.05**), forming a hydrogen-bonded dimer ($R^2_2(10)$) between the C-4/C-5 hydroxyl groups of one molecule and the C-3'/C-4' hydroxyl

groups of the other. The observation of Z' = 2 arises from the lack of symmetry in the hydrogen bonding between the two molecules in the asymmetric unit (**Figure 5.2**).

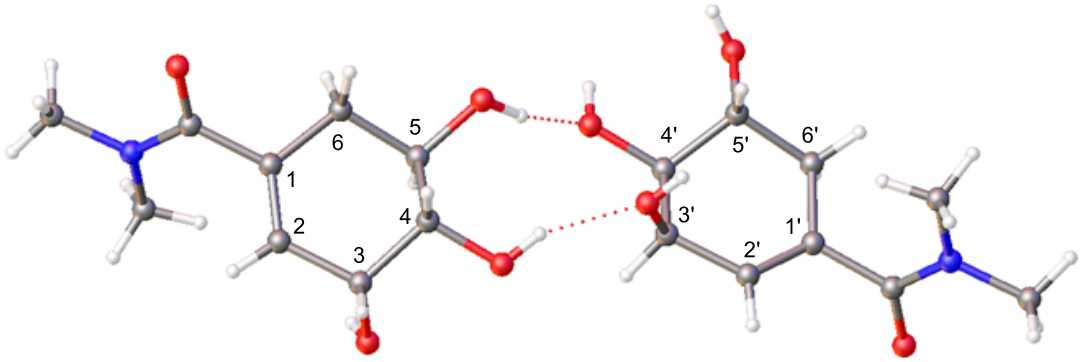

Figure 5.2: Dimer of dimethyl amide (**5.05**)

5.3.3 Crystal Structure of Isopropyl Shikimate (5.03)

Isopropyl shikimate (**5.03**) crystallised in the monoclinic space group $P2_1$. The asymmetric unit comprises of just one molecule resulting in a Z' = 1. In a similar fashion to the dimethyl amide (**5.05**), in the crystal structure of isopropyl shikimate (**5.03**) a $R^2_2(10)$ hydrogen bonding motif is present between the C-4/C-5 hydroxyl groups of one molecule and the C-3'/C-4' hydroxyl groups of its neighbour. However, in the case of isopropyl shikimate (**5.03**), all three of the hydroxyl groups in each molecule are involved in $R^2_2(10)$ hydrogen bonding. This creates a highly symmetrical chain of isopropyl shikimate (**5.03**) molecules resulting in low Z' (**Figure 5.3**).

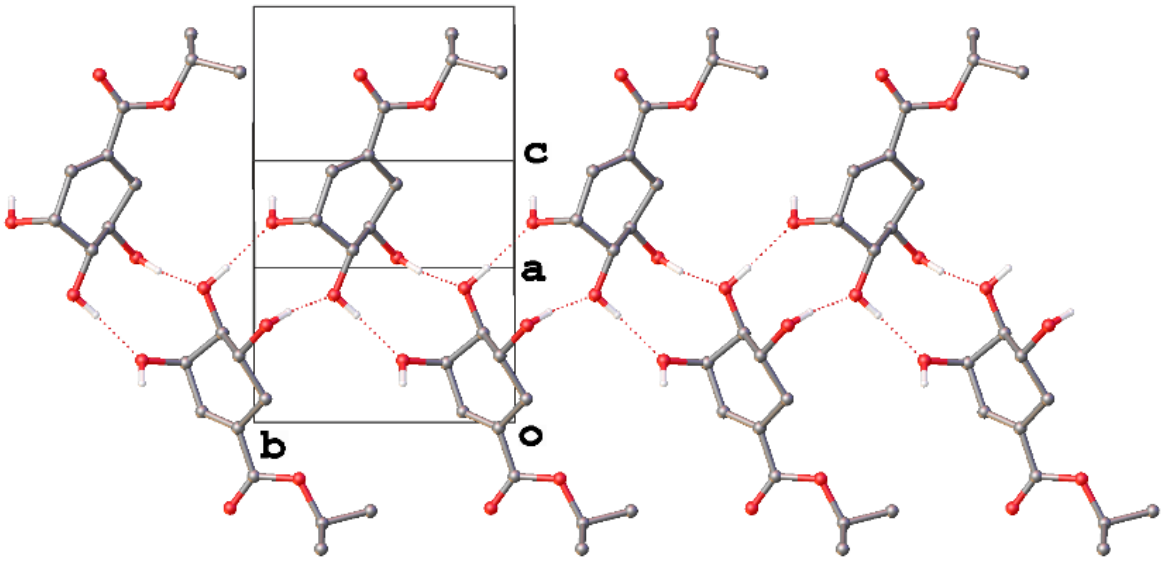

Figure 5.3: Crystal structure of isopropyl shikimate (**5.03**), showing the chain formed via a hydrogen-bonded $R^2_2(10)$ motif. Hydrogen atoms not directly involved in hydrogen bonding have been omitted for clarity (Figure prepared by Dr. Paul Waddell).

5.3.4 Crystal Structure of 2:1 co-crystal of (-)-Shikimic acid (4.01) and Isopropyl shikimate (5.03)

The serendipitous co-crystallisation of (-)-shikimic acid (**4.01**) and isopropyl shikimate (**5.03**) allowed us to probe a related structure to our planned series. Thus (-)-shikimic acid (**4.01**) and isopropyl shikimate (**5.03**) formed a 2:1 co-crystal with the monoclinic space group $P2_1$. Due to the classification of the 2:1 co-crystal as a single formula unit, the crystal structure has a Z' = 1 (or Z'' = 3, where Z'' represents the number of independent molecules in the asymmetric unit).

Through analogy with the crystal structure of (-)-shikimic acid (**4.01**), in the asymmetric unit of the 2:1 co-crystal the two molecules of (-)-shikimic acid (**4.01**) form a $R^2_2(9)$ hydrogen bonding motif between the carboxylic acid of the first molecule and the C-4/C-5 hydroxyl groups of the second molecule. The second (-)-shikimic acid (**4.01**) molecule then forms another $R^2_2(9)$ hydrogen bonding motif between its carboxylic acid and the C-4/C-5 hydroxyl groups of the isopropyl shikimate (**5.03**). This trimeric structure is then capped by the isopropyl ester, preventing further chain extension (**Figure 5.5**).

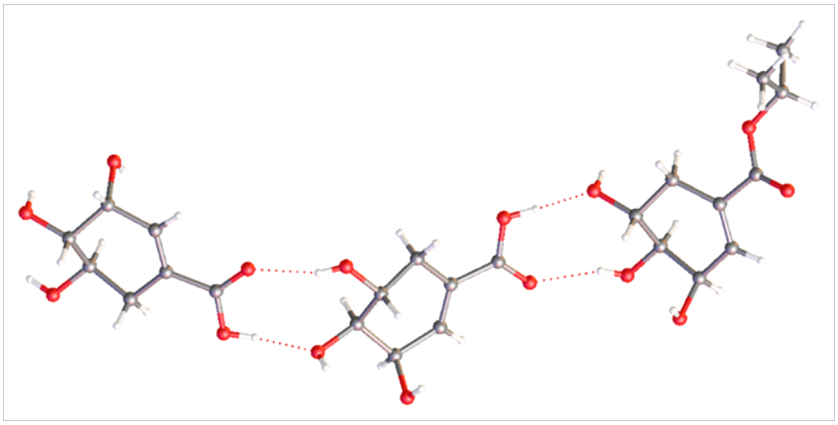

Figure 5.5: The asymmetric unit of the 2:1 co-crystal of (-)-shikimic acid (**4.01**) and isopropyl shikimate (**5.03**), showing the trimer formed by two $R^2_2(9)$ hydrogen bonding systems.

As in the crystal structure of (-)-shikimic acid (**4.01**), the trimeric 2:1 units are also cross-linked via hydrogen-bonding to adjacent units. The previously discussed $R^2_2(9)$ hydrogen-bonding system, between the carboxylic acid of the central (-)-shikimic acid (**4.01**) and the C-4/C-5 hydroxyl groups of isopropyl shikimate (**5.03**) molecule, is also involved in a series of bridging hydrogen bonds with a further molecule of (-)-shikimic acid (**4.01**). The C-3/C-4 hydroxyl groups of isopropyl shikimate (**5.03**) form a $R^2_2(10)$ hydrogen bonding motif with the C-4/C-5 hydroxyl groups of the adjacent (-)-shikimic acid (**4.01**), whilst the C-3/C-4 hydroxyl groups of the adjacent (-)-shikimic acid (**4.01**) participate in a further $R^3_3(9)$ system bridging the C-4 hydroxyl of isopropyl shikimate (**5.03**) and the carboxylic acid of the other (-)-shikimic acid (**4.01**) molecule. A related $R^3_3(9)$ bridge can also be observed in the (-)-shikimic acid (**4.01**) crystal structure (**Figure 5.6**).

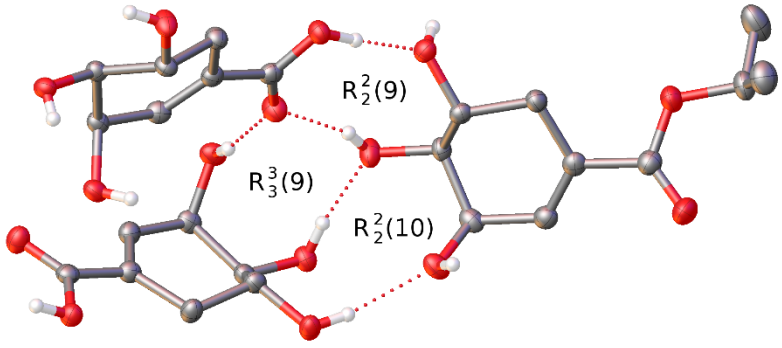

Figure 5.6: The asymmetric unit of 2:1 co-crystal of (-)-shikimic acid (**4.01**) and isopropyl shikimate (**5.03**) showing the fused hydrogen-bonded ring system. Hydrogen atoms bound to carbon have been omitted for clarity. (Figure prepared by Dr. Paul Waddell).

We postulate that the dominance of these strongly directional hydrogen-bond networks in the 2:1 co-crystal of (-)-shikimic acid (**4.01**) and isopropyl shikimate (**5.03**) is the likely reason for Z' = 1 in this structure.

5.3.5 Crystal Structure of Ethyl Shikimate (5.01)

The ethyl shikimate (**5.01**) crystallised in the monoclinic space group C2, with Z' = 2. It should also be noted that the ethyl ester groups show a level of disorder in the structure. The asymmetric unit of ethyl shikimate (**5.01**) contains a pseudosymmetrical dimer held together by a $R^2_2(10)$ hydrogen bonding motif with the C-4/C-5 hydroxyls of one ethyl shikimate molecule hydrogen-bonded to the C-4'/C-5' of another. The symmetry between the two molecules is however broken by the positions of the hydrogen atoms of the hydroxyl groups within the $R^2_2(10)$ bonding system, resulting in a Z' = 2 (**Figure 5.7**).

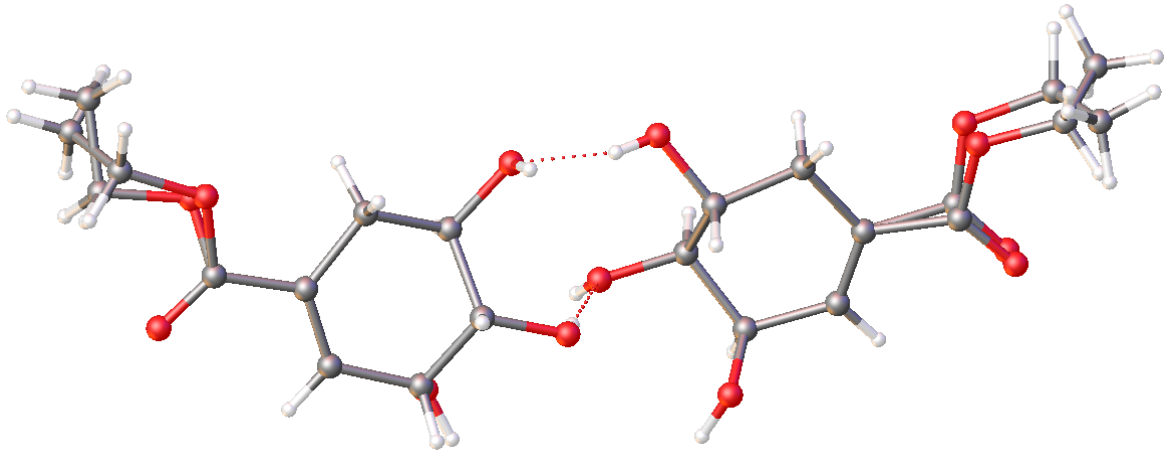

Figure 5.7: The asymmetric unit of ethyl shikimate (**5.01**), showing disorder in the ethyl groups.

5.3.6 Crystal structure of (-)-Methyl Shikimate (4.01)

Finally, (-)-methyl shikimate (**4.01**) crystallised in the monoclinic $P2_1$ space group, with an unusually high Z' = 12, with twelve crystallographically independent molecules in the asymmetric unit. This high Z' appears to arise from a number of different factors, including the presence of different conformers and a mixture of different intermolecular bonding interactions.

Firstly, within the crystal structure the cyclohexene rings of (-)-methyl shikimate (**4.01**) adopt the energetically-favourable half-chair conformation with little conformational variation of this ring between the molecules of the various structures. However, two conformers of the ester group are present, which we have defined as the s-*cis*- and the s-*trans*-conformers based on analogy to butadiene. The s-*cis*-ester is favoured in the crystal structure with an overall 3 : 1 ratio, or 9 s-*cis*- and 3 s-*trans*-esters being present within the asymmetric unit. The presence of two conformers already contributes to high Z', whilst the 3 : 1 ratio of the 9 s-*cis*- and 3 s-*trans*-conformers reduces the possible symmetry within the asymmetric unit further contributing to the high Z' value. Indeed, in order to accommodate the two conformers in a 3 : 1 ratio the asymmetric unit must necessarily have a Z' $\geq$ 4 (**Figure 5.8**).

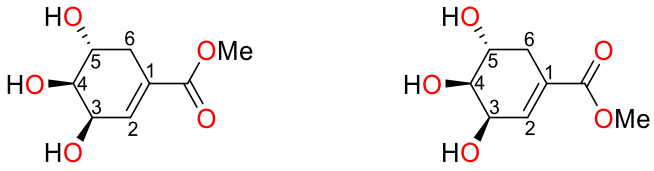

Figure 5.8: The s-*cis*- and s-*trans*- conformations (3 :1) of the (-)-methyl shikimate (**4.01**)

The impact of the presence of both s-*cis*- and s-*trans* conformers on Z' can be shown by viewing the asymmetric unit down the crystallographic [010] direction. This shows that the asymmetric unit comprises two very similar sets of six molecules each, however symmetry is broken due to a one s-*cis*- and one s-*trans* conformer occupying the otherwise symmetry related iii and ix positions (**Figure 5.9**).

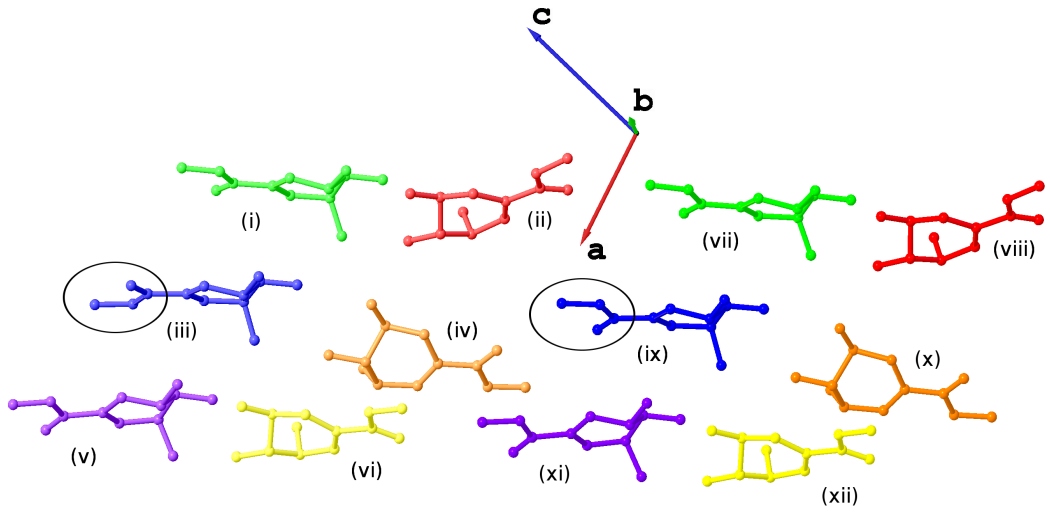

Figure 5.9: The asymmetric unit of (-)-methyl shikimate (**4.01**) viewed along the [010] direction. Each independent molecule has been assigned a label i-xii. i-vi (left) and vii-xii (right) comprising the two sets of six molecules related by an approximate translation. Pairs of atoms related by this approximate translation have been rendered in similar colours and the conformational variation between iii and ix has been highlighted. Hydrogen atoms have been omitted for the sake of clarity. (Figure prepared by Dr. Paul Waddell).

Secondly, there are multiple hydrogen bonding patterns present between the molecules of (-)-methyl shikimate (**4.01**). Within each of the two related sets of six molecules of (-)-methyl shikimate (**4.01**), we observe two pairs of dimers bonded together via a $R^2_2(10)$ hydrogen bonding motif through interactions between the C-4/C-5 hydroxyl groups of one molecule with the C4'/C5' hydroxyl groups of the neighbouring molecule as observed in previous structures in this series. These dimers are then linked together by another pair of molecules, which are themselves connected by a single hydrogen bond to form a $R^6_6(24)$ $[R^4_4(14)R^4_4(14)]$ motif across the whole set of six molecules (**Figure 5.10**).

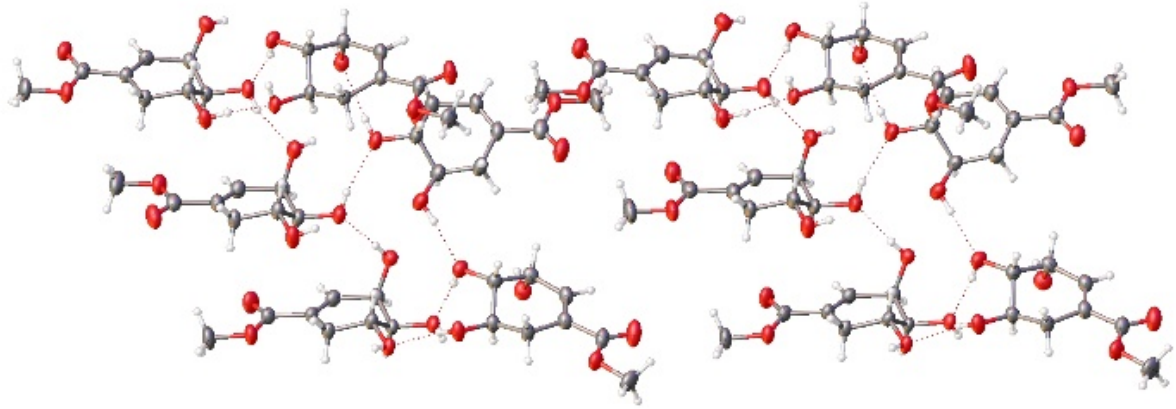

Figure 5.10: The 12 crystallographically independent molecules of (-)-methyl shikimate (**4.01**) that comprise the asymmetric unit Z'=12 showing the hydrogen-bonding ring motifs.

It is likely that the high Z' observed for the (-)-methyl shikimate (**4.01**) structure arises from a combination of a number of factors including, the homochiral nature of the molecule reducing possible symmetry in the system, the accessibility of different ester conformers and the complexity of the directional hydrogen bonding network.

5.4 Conclusion

Our aim in this chapter was to synthesise and crystallise a library of shikimate analogues in order to examine their Z' values and attempt a rationale for these values. Starting from (-)-shikimic acid (**4.01**) we were able to synthesise a series of shikimate esters: (-)-methyl shikimate (**4.06**), ethyl shikimate (**5.01**), *n*-propyl shikimate (**5.02**), isopropyl shikimate (**5.03**) and benzyl shikimate (**5.04**). From these synthesised shikimate esters, we were able to grow high quality single crystals for X-Ray analysis of the methyl, ethyl and isopropyl variants. A serendipitously obtained 2:1 co-crystal of (-)-shikimic acid (**4.01**) and isopropyl shikimate (**5.03**) was also examined as part of the series.

We also attempted to synthesise and crystallise a series of related shikimic amides, again starting from (-)-shikimic acid (**4.01**). We were able to successfully synthesise shikimic dimethyl amide (**5.05**) and shikimic diethyl amide (**5.06**). We were then able to obtain high quality single crystals of shikimic dimethyl amide (**5.05**) before time constraints prevented further work being completed on this series.

In all cases, networks of directional hydrogen bonding are present with a particular $R^2_2(10)$ dimer motif being particularly prevalent. In the case of methyl shikimate (**4.01**), the structure contains a number of structural features commonly associated with high Z', including: homochirality, multiple directional molecular interactions in the form of complex hydrogen bonding networks and two accessible s-*cis* and *s*-trans conformers [Brock[15]]. Through examination of a small set of molecules, it seems that for the shikimate esters, the steric bulk of the ester is important in accessing high Z' structures, with

a trend shown of the greater the steric bulk of the ester, the lower the Z' value (methyl Z' = 12, ethyl Z' = 2, iso propyl Z' = 1). In the particular case of the (-)-methyl shikimate (**4.01**), the unusually high Z' value of 12 seems to be due to the resulting presence of two accessible ester conformers and the relatively close packing of the (-)-methyl shikimate (**4.01**) molecules assisting in greater hydrogen bonding.

Future work would focus on expanding our data set, through the synthesis and crystallisation of a greater range of related shikimic acid based esters and amides to provide greater insights into the formation of high Z' crystal structures It may be possible to engineer molecules of specific steric bulk (at the ester or amide) to maintain the conformational flexibility and intermolecular hydrogen bonding chain motifs present in (-)-methyl shikimate (**4.01**), that favour the formation of crystal structures with high Z' values.

Chapter 5 – References

1) J. W. Steed, *CrystEngComm*, 2003, **5**, 169.
2) G. R. Desiraju, *CrystEngComm*, 2007, **9**, 91.
3) K. M. Steed and J. W. Steed, *Chem. Rev.*,2015, **115**, 2895-2933.
4) B. Braun, I. Kalf and U. Englert, *Chem. Commun.*, 2011, **47**, 3846-3848.
5) C. H. Görbitz, K. W. Törnroos and G. M. Day, *Acta Cryst.*, 2012, B**68**, 549-557.
6) M. Krasnopolski, R. W. Seidel, R. Goddard, J. Breidung, M. V. Winter, A. Devi and R. A. Fischer, *J. Mol. Struct.*, 2013, **1031**, 239-245.
7) P. Bombicz, *Cryst. Rev*., 2017, **23**, 118–151.
8) L. N. Kuleshova, M. Y. Antipin and I. V. Komkov, *J. Mol. Struct.*, 2003, **647**, 41.
9) X. Hao, A. Siegler, S. Parkin and C. P. Brock, *Cryst. Growth Des.*, 2005, **5**(, 2225-2232.
10) A. Lemmerer and C. Esterhuysen, *CrystEngComm*, 2011, **13**, 5773-5782.
11) R. Taylor, J. C. Cole and C. R. Groom, *Cryst. Growth Des.*, 2016, **16**, 2988-3001.
12) A. Liu, Z. Z. Liu, Z. M. Zou, S. Z. Chen, L.Z. Xu and S. L. Yang, *Tetrahedron*, 2004, **60**, 3689-3694.
13) C. Abell, F. H. Allen, T. D. H. Bugg, M. J. Doyle and P. R. Raithby, *Acta Crystallographica,Section C: Crystal Structure Communications*, 1988, **44**, 1204.
14) M. C. Etter, *Acc. Chem. Res.*, 1990, **23**, 120-126.
15) C. P. Brock, *Acta Cryst.*, 2016, B**72**, 807.
16) Y. Yamashita, K. Hanaya, T. Sugai, T. Mizushima and M. Shoji, *Tetrahedron*., 2013, **69**, 6527-6532.

Chapter 6 - Experimental

6.1 General Experimental Information

6.1.1 Analysis

Melting points (MP) were obtained via Stuart SMP3 melting point apparatus. Thin layer chromatography (TLC) was carried out on silica gel 60 F254 plates and visualised via ultraviolet light unless staining technique was stated. ^{1}H NMR and $^{13}C\{^{1}H\}$ NMR spectra were recorded on a Bruker Avance III 300 MHz, Jeol ECS-400 MHz, Jeol Lambda 500 MHz or Bruker Avance III HD 700 MHz spectrometers. Infrared (IR) spectra were obtained on a Varian 800 FT-IR Scimitar Series spectrometer. High resolution mass (HRMS) spectra were provided by the National Mass Spectrometry Service (Swansea University) and SAgE Mass Spectrometry Facility (Newcastle University) performed by Dr Rachael Dack and Dr Alex Charlton. Schlenk techniques were performed for all chemical reactions involving air-sensitive reagents, under an atmosphere of nitrogen. Anhydrous solvents were distilled under an atmosphere of nitrogen and used directly, THF and ether weredistilled from sodium/ benzophenone, toluene was distilled from sodium and DCM was distilled from calcium hydride. Manual flash column chromatography was carried out using Geduran silicagel 60 (40-63 µm). Optical rotation measurements were obtained with a POLAAR 2001 polarimeter at λ = 589 nm using a 0.5 dm cell path length at 20 ^{o}C in spectrophotometric grade methanol, ethanol and chloroform.

6.1.2 Experimental Procedures and Structural Characterisation

6.2 Experimental – Chapter 2

Methyl 2-(phenylthio) acetate (2.12)

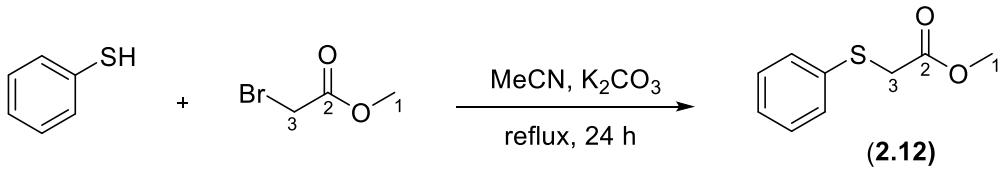

Method A[3]

To a round bottomed flask (250 mL) was added K_2CO_3 (2.76 g, 20.0 mmol). The round bottomed flask was then fitted with a reflux condenser and placed under a nitrogen atmosphere after which dry acetonitrile (50 mL) was added. To this was added via syringe thiophenol (1.0 mL, 10 mmol), followed by methyl 2-bromoacetate (1.14 mL, 10.2 mmol). The resulting mixture was then heated to reflux on an oil bath and monitored by TLC. After 24 h, the organic layer of the reaction mixture was extracted with ethyl acetate (3 x 20 mL) and washed with water (20 mL) and then brine (10 mL). The combined organic extracts were dried with $MgSO_{4(s)}$, filtered and the solvent removed under reduced pressure. The crude product was purified by column chromatography (petroleum ether: ethyl acetate, 4:1, column diameter = 2 cm, silica = 18 cm) to give methyl 2-(phenylthio) acetate as a clear oil (1.52 g, 8.34 mmol, 83 %).

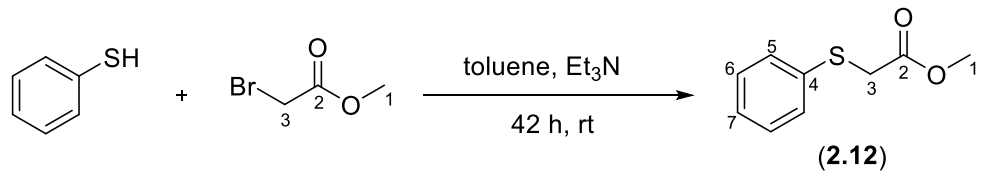

Method B[4]

To a round bottomed flask (250 mL) under a nitrogen atmosphere was added dry toluene (50 mL) via syringe. To this was added via syringe thiophenol (1.0 mL, 10 mmol), followed by Et_3N (1.39 mL, 10.0 mmol) and then methyl 2-bromoacetate (0.96 mL, 10.1 mmol). The reaction mixture was stirred at rt and monitored by TLC. After 24 h, the organic layer of the reaction mixture was extracted with ethyl acetate (3 x 20 mL) and washed with water (20 mL) and then brine (10 mL). The combined organic extracts were dried with $MgSO_{4(s)}$, filtered and the solvent removed under reduced pressure. The crude product was purified by column

chromatography (petroleum ether: ethyl acetate, 4:1, column diameter = 2 cm, silica = 18 cm) to give methyl 2-(phenylthio) acetate (**2.12**) as a clear oil (1.55 g, 8.35 mmol, 84 %).

R_f = 0.54 (petroleum ether:ethyl acetate, 4:1; UV light);

^{1}H NMR (300 MHz, Chloroform-*d*) δ_H 7.40 – 7.32 (2H, m, H^5), 7.29 – 7.23 (2H, m, H^6), 7.22 – 7.17 (1H, m, H^7), 3.66 (3H, s, H^1), 3.61 (2H, s, H^3);

^{13}C NMR (75 MHz, Chloroform-*d*) δ_C 170.1 (C^2), 134.9 (C^4), 129.9 (C^5), 129.0 (C^6), 127.0 (C^7), 52.5 (C^1), 36.5 (C^3);

IR (neat): ν_{max}cm^{-1} 3050-2700 (CH, w), 1730 (CO, s).

MS (pEI): calcd for $C_9H_{10}O_2S$ $[M]^+$: 182.0 observed 182.0.

Methyl 2-(phenylsulfonyl) acetate (2.13)[5]

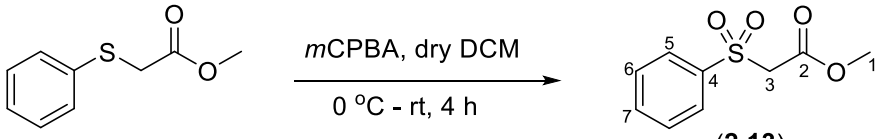

(**2.13**)

To a stirred round bottomed flask (100 mL) was added methyl 2-(phenylthio) acetate (182 mg, 5.00 mmol) and *m*CPBA (2.59 g, 15.0 mmol). The reaction vessel was placed under a nitrogen atmosphere and dry DCM (25 mL) was added via syringe. The reaction mixture was stirred at 0 °C and allowed to warm to rt. The reaction was monitored by TLC. After 4 hours the reaction was quenched with $Na_2S_2O_3$ (20 mL) and placed in an ice bath. Na_2CO_3 (20 mL) and water (20 mL) was added followed by extraction with DCM (3 x 15 mL). The combined organic layers were washed with brine (20 mL), dried with $MgSO_{4(s)}$, filtered and the solvent removed under reduced pressure to give the product methyl 2-(phenylsulfonyl) acetate as a clear oil (897 mg, 4.20 mmol, 84 %).

R_f = 0.10 (petroleum ether:ethyl acetate, 4:1; UV light);

^{1}H NMR (300 MHz, Chloroform-*d*) δ_H 7.98 – 7.93 (2H, m, H^5), 7.74 – 7.66 (1H, m, H^7), 7.63 – 7.55 (2H, m, H^6), 4.13 (2H, s, H^3), 3.71 (3H, s, H^1);

^{13}C NMR (75 MHz, Chloroform-*d*) δ_C 163.0(C^2), 138.8(C^4), 134.5(C^7), 129.4(C^6), 128.7(C^5), 60.9(C^3), 53.2(C^1);

IR (neat): ν_{max}cm^{-1} 3020-2850 (CH, w), 1735 (CO, s).

Observed data (^{1}H, ^{13}C, IR) are consistent with that previously reported by Kuhn *et al*[6]

Methyl 2-((phenylsulfonyl)methyl) benzoate (2.17)

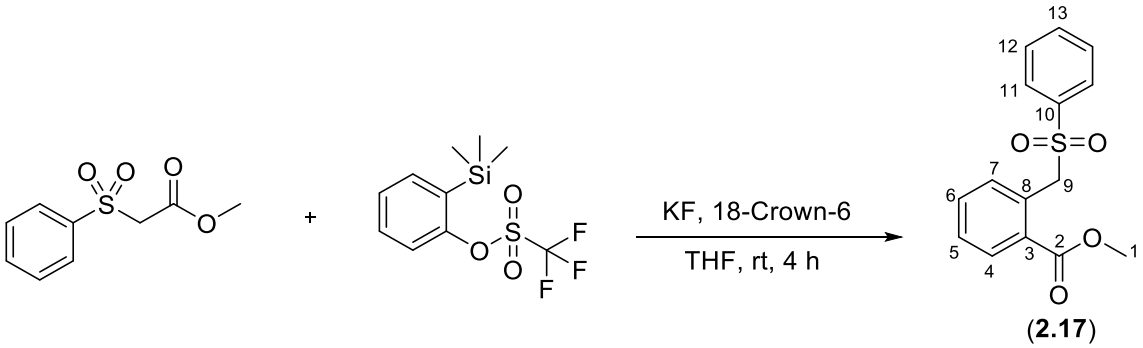

(**2.17**)

To a stirred Schlenk flask was added KF (482 mg, 8.29 mmol) and 18-Crown-6 (2.19 g, 8.29 mmol). The reaction vessel was then put under nitrogen atmosphere. Dry THF (10 mL) was added by syringe followed by 2-(trimethylsilyl) phenyl triflate (0.76 mL, 3.12 mmol). The reaction mixture was left to stir for 5 min. Methyl 2-(phenylsulfonyl) acetate (0.67 mL, 4.05 mmol) was then added by syringe to the reaction mixture. The reaction was left to stir for 4 h (monitored by TLC) after which time water (10 mL) was added to the mixture. Extraction was done with ethyl acetate (3 x 15 mL). The combined organic extracts were dried with $MgSO_{4(s)}$, filtered and the solvent removed under reduced pressure to give a yellow/orange oil. The crude product was purified by column chromatography (petroleum ether:ethyl acetate, 4:1, column diameter = 2 cm, silica = 18 cm) to give methyl 2-((phenylsulfonyl)methyl)benzoate as a white crystalline solid (701 mg, 2.53 mmol, 81 %).

Mp = 102.5 – 102.8 ^{o}C;

R_f = 0.20 (petroleum ether:ethyl acetate, 4:1; UV light);

^{1}H NMR (300 MHz, Chloroform-*d*) δ_H 7.87 (1H, dd, *J* = 7.7, 1.5, Hz, Ar), 7.62 (2H, dd, *J* = 8.4, 1.2 Hz, Ar), 7.60 – 7.55 (1H, m, Ar), 7.50 – 7.37 (4H, m, Ar), 7.32 (1H, dd, *J* = 7.5, 1.5 Hz, Ar), 5.06 (2H, s, H^9), 3.74 (3H, s, H^1).

^{13}C NMR (75 MHz, Chloroform-*d*) δ_C 167.2(C^2), 138.5, 133.7, 133.6, 132.2, 131.1, 130.9, 129.3, 129.0, 128.9, 128.8, 59.4(C^9), 52.3(C^1).

IR (neat): ν_{max}cm^{-1} 3135 - 2935 (CH, w), 1707 (CO, s), 1385 (S=O);

HRMS (pNSI): calcd for $C_{15}H_{14}O_4S$ $[M+H]^+$ 291.0686; observed 291.0687.

Phenyl 2-methoxy-6-methylbenzoate (2.22)

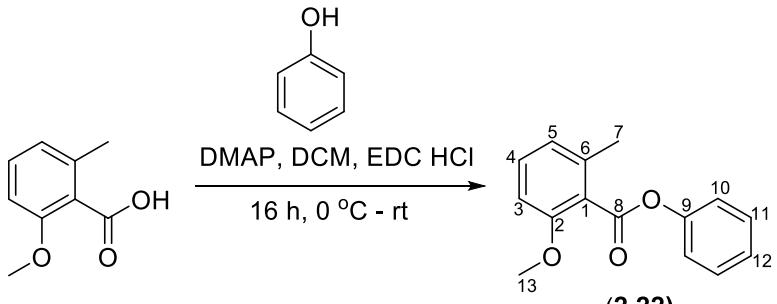

(**2.22**)

To a stirred round bottomed flask (50 mL) was added 2-methoxy-6-methylbenzoic acid (332 mg, 2.00 mmol) and phenol (207 mg, 2.20 mmol) followed by DMAP (134 mg, 1.10 mmol). The reaction vessel was then put under nitrogen atmosphere and placed in an ice bath. Dry DCM (1 mL) was then added by syringe. In a separate stirred round bottomed flask (25 mL) was added EDC.HCl (422 mg, 2.20 mmol). The reaction vessel was then put under nitrogen atmosphere and dry DCM (1 mL) was added by syringe. The EDC.HCl solution was then transferred by syringe to the 50 mL round bottomed flask by syringe. The reaction vessel was left to stir at 0 °C and left to come to rt overnight. After 16 h the contents of the reaction vessel were poured into an extraction funnel containing 10 mL of water. Extraction was done with DCM (3 x 10 mL). The combined organic extracts were dried with $MgSO_{4(s)}$, filtered and the solvent removed under reduced pressure to give a yellow oil. The crude product was purified by column chromatography (petroleum ether: ethyl acetate, 10: 1, column diameter = 2 cm, silica = 18 cm) to give phenyl 2-methoxy-6-methylbenzoate as a white crystalline solid (283 mg, 1.17 mmol, 58 %).

Mp = 60.0 – 60.5 °C;

R_f = 0.30 (petroleum ether:ethyl acetate, 10:1; UV light);

^{1}H NMR (400 MHz, Chloroform-*d*) δ_H 7.37 (2H, d, *J* = 7.8 Hz, H^{10}), 7.23 (1H, t, *J* = 7.7 Hz, H^4), 7.21 – 7.18 (3H, m, $H^{11and12}$), 6.80 (1H, d, *J* = 7.6 Hz, H^5), 6.76 (1H, d, *J* = 8.4 Hz, H^3), 3.83 (3H, s, H^{13}), 2.39 (3H, s, H^7);

^{13}C NMR (101 MHz, Chloroform-*d*) δ_C 167.0(C^8), 157.0(C^2), 151.1(C^9), 136.9(C^6), 130.9(C^4), 129.6(C^{10}), 126.1(C^{12}), 123.2(C^1), 122.6(C^5), 121.9(C^{11}), 108.8(C^3), 56.2(C^{13}), 19.5(C^7);

IR (neat): ν_{max}cm^{-1} 3140 - 2945 (CH, w), 1742 (CO, s);

HRMS (pNSI) calcd: for $C_{15}H_{15}O_3$ $[M+H]^+$: 243.1016; observed 243.1014.

6.3 Experimental - Chapter 3

(±)-9-hydroxy-10-(phenylsulfonyl)-3,4,4a,10-tetrahydroanthracen-1(2H)-one (**3.05**) and 9-hydroxy-3,4-dihydroanthracen-1(2H)-one (**3.06**)[1]

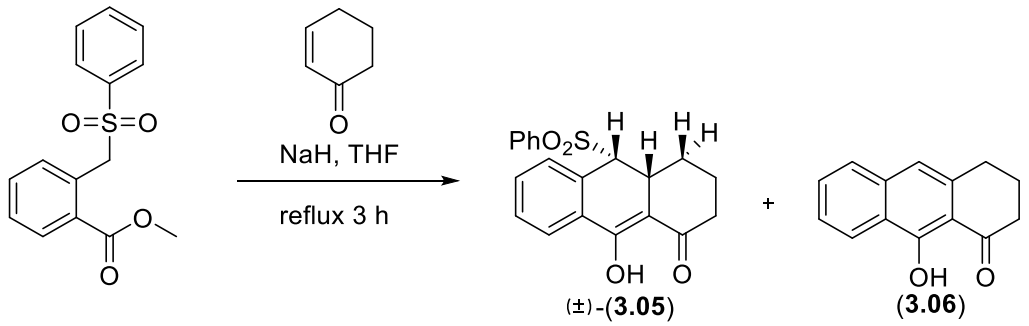

To a stirred Schlenk flask was added NaH 60 % dispersion in mineral oil (52 mg, 1.25 mmol) and methyl 2-((phenylsulfonyl)methyl) benzoate (150 mg, 0.517 mmol). The Schlenk flask was then placed under a nitrogen atmosphere. Dry THF (5 mL) was then added via syringe, followed by the addition of cyclohex-2-en-1-one (0.05 ml, 0.517 mmol) via syringe. The reaction mixture was then placed under reflux. After 3 h, the reaction was taken off of reflux and allowed to cool to rt after which it was quenched with water (25 mL), extracted with DCM (3 x 20 mL) and washed with brine (25 mL). The combined organic extracts were dried over $MgSO_{4(s)}$, filtered and the solvent removed under reduced pressure. The crude product was purified by column chromatography (petroleum ether: ethyl acetate, 3:1, column diameter = 2 cm, silica = 15 cm) to give (±)-9-hydroxy-10-(phenylsulfonyl)-3,4,4a,10-tetrahydroanthracen-1(2H)-one (**3.05**) (0.115 g, 0.32 mmol, 63 %) as a white solid and 9-hydroxy-3,4-dihydroanthracen-1(2H)-one (**3.06**) (2.2 mg, 0.010 mmol, 2 %) as a yellow solid.

(±)-9-hydroxy-10-(phenylsulfonyl)-3,4,4a,10-tetrahydroanthracen-1(2H)-one (**3.05**)[1]

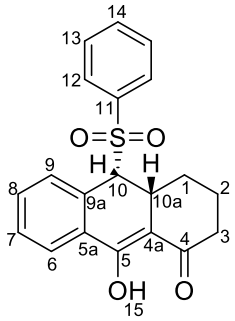

(±)-(**3.05**)

Mp = 166.5 – 167.3 °C

R_f = 0.26 (petroleum ether:ethyl acetate, 3:1; UV light);

^{1}H NMR (300 MHz, Chloroform-*d*) δ_H 15.61 (1H (OH), s, H^{15}), 7.81 (1H, dd, *J* = 7.6, 1.5 Hz, H^6), 7.51 (1H, ddt, *J* = 8.5, 7.1, 1.5 Hz, H^{14}), 7.45 (1H, td, *J* = 7.6, 1.5 Hz H^7), 7.40 (1H, td, *J* = 7.6, 1.5 Hz, H^8), 7.33 - 7.22 (4H, m, $H^{12,13}$), 7.14 (1H, d, *J* = 7.5 Hz, H^9), 4.34 (1H, d, *J* = 4.9 Hz, H^{10}), 3.36 (1H, ddd, *J* = 12.1, 4.9, 1.5 Hz, H^{10a}), 2.85 – 2.65 (1H, m, H^1), 2.50 (1H, dddd, *J* = 18.2, 12.0, 5.9, 1.6 Hz H^3), 2.45 – 2.36 (1H, m, H^3), 2.28 - 2.20 (1H, m, H^1), 2.15 – 2.05 (1H, m, H^1), 1.65 – 1.53 (2H, m, H^2);

^{13}C NMR (75 MHz, Chloroform-*d*) δ_C 186.5(C^4), 182.4(C^5), 137.6(C^{11}), 134.1(C^{14}), 133.8, 133.0, 132.2(C^8), 131.1(C^9), 129.9(C^7), 129.5, 128.7, 126.7(C^6), 104.5(C^{4a}), 69.1(C^{10}), 36.5(C^{10a}), 32.3(C^3), 26.4(C^1), 21.5(C^2);

IR (neat): ν_{max}cm^{-1} 3430 (OH), 3000-2850 (CH), 1735 (C=O);

MS (pNSI): 729.2 $[M-2H+Na]^-$ (40%), 353.1 $[M-H]^-$ (100%).

HRMS (pNSI) calcd for $C_{20}H_{17}O_4S$ $[M-H]^-$: 353.0853, found 353.0851.

9-hydroxy-3,4-dihydroanthracen-1(2H)-one (**3.06**)[1]

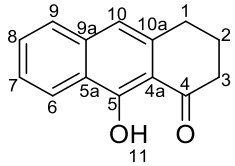

(**3.06**)

Mp = 91.5 – 92.1 °C [lit. 92 - 93 °C][1]

R_f = 0.65 (petroleum ether:ethyl acetate, 4:1; UV light);

^{1}H NMR (300 MHz, Chloroform-*d*) δ_H 14.25 (1H (OH), s, H^{11}), 8.41 (1H, d, *J* = 8.5 Hz,), 7.65 (1H, d, *J* = 8.0 Hz), 7.65 -7.55 (1H, m), 7.45 (1H, ddd, *J* = 8.0, 6.5, 1.5 Hz), 7.03 (1H, s, H^{10}), 3.06 – 2.99 (2H, m, H^1), 2.80 – 2.70 (2H, m, H^3), 2.22 – 2.08 (2H, m, H^2);

^{13}C NMR (75 MHz, Chloroform-*d*) δ_C 205.5(C^4), 163.5(C^5), 138.5, 137.6, 130.5, 127.0, 125.1, 124.6, 124.0, 116.5, 111.7, 39.4(C^3), 30.5(C^1), 23.3(C^2);

IR (neat): $v_{max}cm^{-1}$ 3360 (OH),3080-2850 (CH), 1625 (C=O);

Observed data (^{1}H, ^{13}C, IR) are consistent with that previously reported by Huang *et al*[1]

Ethyl 4-bromo-3-oxobutanoate (**3.11**)[4]

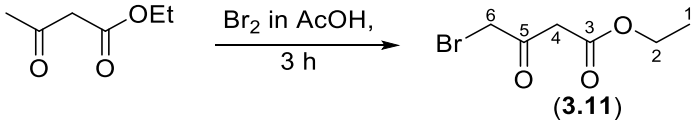

(**3.11**)

To a stirred round bottom flask (20 mL) was added acetic acid (8 mL) and Br_2 (1.05 mL, 20.4 mmol) via syringe. The reaction vessel was then placed under a nitrogen atmosphere and left to stir for 10 minutes. To another stirred round bottom flask (50 mL) was added acetic acid (8 mL) and ethyl acetoacetate (2.55 mL, 20 mmol). The reaction vessel was then placed under a nitrogen atmosphere and left to stir for 10 minutes. The contents of the round bottom flask containing the Br_2 dissolved in acetic acid was then added via syringe to the round bottom flask containing the ethyl acetoacetate, dissolved in acetic acid. The reaction vessel was left stirring at room temperature for 3 h after which the organic layer was extracted with DCM (3 x 15 mL). The combined organic extracts were dried over $MgSO_{4(s)}$, filtered and the solvent removed under reduced pressure. The residue was passed through a short silica column (3 cm) under house vacuum with DCM as solvent after which the solvent was removed under reduced pressure to give ethyl 4-bromo-3-oxobutanoate as a light reddish-brown oil (3.67 g, 17.5 mmol, 88 %). (keto form: enol form = 1.0: 0.20)

R_f = 0.60 (DCM);

(Keto form) ^{1}H NMR (300 MHz, $CDCl_3$) δ_H 4.19 (2H, q, *J* = 7.2 Hz, H^2), 4.05 (2H, s, H^6), 3.70 (2H, s, H^4), 1.27 (3H, t, *J* = 7.2 Hz, H^1);

^{13}C NMR (75 MHz, $CDCl_3$) δ_C 194.7 (C^5), 166.7 (C^3), 61.6 (C^2), 45.9 (C^4), 33.7 (C^6), 14.2 (C^1);

(Enol form) ^{1}H NMR (300 MHz, $CDCl_3$) δ_H 12.00 (1H, s, $OH^{3\ or\ 5}$(br)), 5.27 (1H, s, H^4), 4.21 (2H, q, *J* = 7.2 Hz, H^2) 3.85 (2H, s, H^6), 1.30 (3H, t, *J* = 7.2 Hz, H^1).

IR (neat): $v_{max}cm^{-1}$ 1746 (C=O), 1725 (C=O);

Observed data (^{1}H, ^{13}C) are consistent with that previously reported by Choi and Chi[4].

(4-ethoxy-2,4-dioxobutyl) triphenylphosphonium bromide (**3.12**)[5]

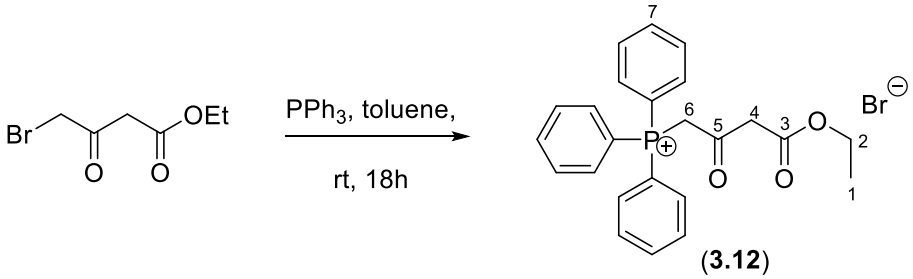

(**3.12**)

To a stirred round bottom flask (50 mL) was added tri-phenylphosphine (3.83 g, 14.6 mmol). The flask was put under a nitrogen atmosphere and anhydrous toluene (5 mL) was added via syringe and the mixture left stirring at room temperature for 10 minutes. To another stirred round bottom flask (50 mL) was added ethyl 4-bromo-3-oxobutanoate (3.67 g, 17.5 mmol). The flask was put under a nitrogen atmosphere and anhydrous toluene (5 mL) was added via syringe and the mixture left stirring for 10 minutes. The contents of the round bottom flask containing the ethyl 4-bromo-3-oxobutanoate dissolved in anhydrous toluene were then added dropwise via syringe to the round bottom flask containing the tri-phenylphosphine dissolved in anhydrous toluene. The reaction mixture was then left stirring for 18 h at room temperature. After 18 h, the precipitate was collected by Buchner filtration and washed with toluene (50 mL). The precipitate was then recrystallised from hot toluene to yield (4-ethoxy-2,4-dioxobutyl)triphenylphosphonium bromide (**3.12**) as a peach coloured powder (5.15 g, 10.92 mmol, 75 %).

^{1}H NMR (300 MHz, $CDCl_3$) δ_H 7.71-7.61 (6H, m, ArH),7.59-7.51 (3H, m, ArH), 7.49-7.42 (6H, m, ArH) 6.23 (2H, d, J_{PH} = 11.5 Hz H^6), 4.19-4.10 (4H, m, $H^{2 \text{ and } 4}$), 1.24 (3H, t, *J* = 7.2 Hz, H^1);

^{13}C NMR (75 MHz, $CDCl_3$) δ_C 196.8 (C^5), 166.3 (C^3), 135.0, 130.4, 129.5, 118.1, 60.1 (C^2), 20.9 (C^6), 14.1 (C^1);

HRMS (pNSI): calcd for $C_{24}H_{24}O_3P^+$ $[M\text{-}Br]^+$: 391.1453; observed: 391.1458.

Ethyl 3-oxo-4-(triphenyl-phosphaneylidene) butanoate (**3.13**)[6]

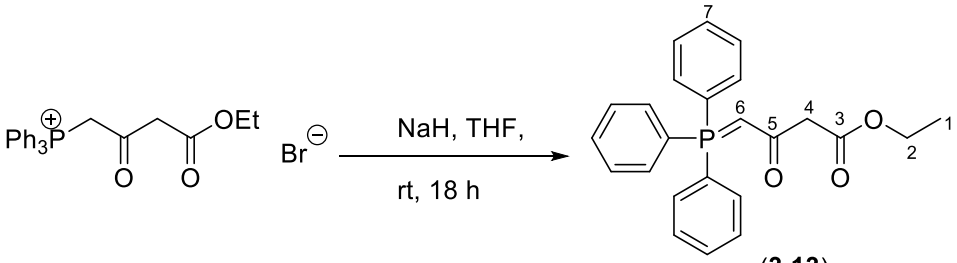

(**3.13**)

To a stirred Schlenk tube was added (4-ethoxy-2,4-dioxobutyl) triphenylphosphonium bromide (6 g, 12.73 mmol). The reaction vessel was put under a nitrogen atmosphere. Anhydrous THF (20 mL) was then added via syringe to the Schlenk tube and the mixture left stirring at room temperature for 15 min. To a stirred round bottom flask (50 mL) was added NaH (60 % in mineral oil) (1.02 g, 25.46 mmol). The reaction vessel was put under a nitrogen atmosphere. Anhydrous THF (10 mL) was then added via syringe to the round bottom flask and the mixture left stirring at room temperature for 15 minutes. The NaH dissolved in the anhydrous THF was then added via syringe to the Schlenk tube containing the (4-ethoxy-2,4-dioxobutyl) triphenylphosphonium bromide dissolved in anyhydrous THF. The mixture was left stirring at room temperature for 20 h. The residue was then removed by sintered vacuum filtration to give the filtrate ethyl 3-oxo-4-(triphenyl-phosphaneylidene) butanoate (3.13) as a yellow orange powder (4.38 g, 1.12 mmol, 88 %).

Mp = 102.5 – 104.7 ^{o}C (lit. Mp = 102 – 103 ^{o}C)[6]

^{1}H NMR (300 MHz, $CDCl_3$) δ_H 7.71-7.60 (6H, m, ArH), 7.59-7.51 (3H, m, ArH), 7.49-7.40 (6H, m, ArH), 4.18 (2H, q, *J* = 7.1 Hz, H^2), 3.75 (1H, br, H^6) 3.35 (2H, d, *J* = 1.5 Hz, H^4), 1.27 (3H, t, *J* = 7.1 Hz, H^1).

^{13}C NMR (75 MHz, $CDCl_3$) δ_C 184.0 (C^5), 170.7 (C^3), 133.4, 132.3, 128.9, 126.7, 60.3 (C^2), 14.1 (C^1)

IR (neat): $v_{max}cm^{-1}$ 3055 (CH), 1730 (C=O), 1715 (C=O).

(±)-Ethyl 6-methyl-2-oxocyclohex-3-ene-1-carboxylate (**3.15**)[3]

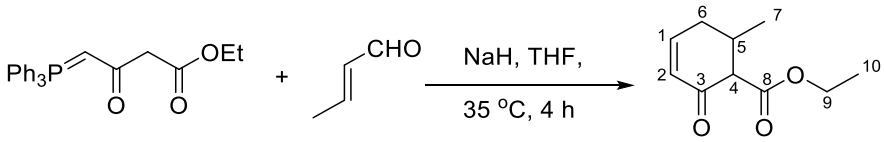

(**3.15**)

To a stirred round bottom flask (50 mL) was added ethyl 3-oxo-4-(triphenyl-phosphaneylidene) butanoate (1.6 g, 4.1 mmol) and anhydrous THF (10 mL). Crotonaldehyde (0.34 mL, 4.1 mmol) was then added via syringe and the reaction vessel warmed to 35 °C in an oil bath. NaH (60 % in mineral oil) (0.33 g, 8.2 mmol) was then added to the reaction vessel followed by careful addition of 3 drops of water. The reaction was left stirring at 35 °C and monitored by TLC. After 4 h the reaction was acidified by addition of 1M HCl (10 mL) via syringe and extracted with diethyl ether (3 x 20 mL). The combined organic extracts were washed with brine (20 mL), dried over $MgSO_{4(s)}$, filtered and the solvent removed under reduced pressure. The crude product was purified by column chromatography (chloroform: petroleum ether 5:1, column diameter = 1 cm, silica = 15 cm) to give ethyl 6-methyl-2-oxocyclohex-3-ene-1-carboxylate as a yellow oil (433 mg, 2.4 mmol, 58 %).

R_f = 0.64 (chloroform:petroleum ether, 5:1; UV light);

^{1}H NMR (300 MHz, $CDCl_3$) δ_H 7.01 – 6.94 (1H, m, H^1), 6.07 (1H, dd, *J* = 10.1, 2.7 Hz, H^2), 4.25 (2H, q, *J* = 7.1 Hz, H^9), 3.11 (1H, d, *J* = 11.7 Hz, H^4), 2.65-2.52 (1H, m, H^6) 2.52 – 2.43 (1H, m, H^6), 2.18 – 2.07 (1H, m, H^5), 1.30 (3H, t, *J* = 7.1 Hz, H^{10}), 1.08 (3H, d, *J* = 6.4 Hz, H^7).

^{13}C NMR (75 MHz, $CDCl_3$) δ 194.3 (C^3), 171.3 (C^8), 149.0 (C^1), 131.2 (C^2), 64.3 (C^4), 61.2 (C^9), 33.3 (C^6), 32.4 (C^5), 18.3 (C^7), 12.2 (C^{10})

IR (neat): $v_{max}cm^{-1}$ 3475 (OH), 2981 (CH), 1736 (C=O), 1679 (C=O).

(±)-Ethyl (1*S*,6*R*)-1-hydroxy-6-methyl-2-oxocyclohex-3-ene-1-carboxylate **(±)-(3.16)**

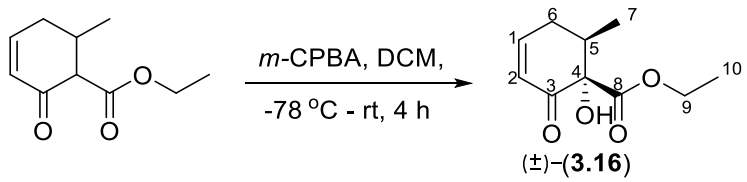

(±)-(**3.16**)

To a stirred round bottom flask (50 mL) was added ethyl 6-methyl-2-oxocyclohex-3-ene-1-carboxylate (0.127 g, 0.68 mmol). The reaction vessel was then placed under a nitrogen atmosphere. Anhydrous DCM (3 mL) was then added via syringe. The reaction vessel was then placed in an acetone/dry ice bath and its contents cooled to -78 °C. To another stirred round bottom flask (50 mL) was added purified *m*CPBA (0.19 g, 1.10 mmol). The reaction vessel was then placed under a nitrogen atmosphere. Anhydrous DCM (5 mL) was then added via syringe. The contents of the round bottom flask containing the *m*CPBA solution were then transferred dropwise via syringe to the round bottom flask containing the ethyl 6-methyl-2-oxocyclohex-3-ene-1-carboxylate solution. The reaction was left stirring at -78 °C and allowed to warm to room temperature. After 4 h the reaction was quenched with Na_2SO_3 (5 mL) and the extracted with diethyl ether (3 x 5 mL). The combined organic extracts were dried over $MgSO_{4(s)}$, filtered and the solvent removed under reduced pressure. The crude product was purified by column chromatography (petroleum ether:ethyl acetate 4:1, column diameter = 1 cm, silica = 10 cm) to give ethyl 1-hydroxy-6-methyl-2-oxocyclohex-3-ene-1-carboxylate as a pale yellow oil (63 mg, 0.32 mmol, 47 %).

R_f = 0.30 (petroleum ether:ethyl acetate, 4:1; UV light);

^{1}H NMR (300 MHz, $CDCl_3$) δ_H 7.14 – 7.06 (1H, m, H^1), 6.15 (1H, dd, *J* = 10.1, 2.9 Hz, H^2), 4.27 – 4.17 (2H, m, H^9), 4.17 (1H, s, br, OH^4), 2.64 (1H, ddt, *J* = 19.5, 10.9, 2.6 Hz, H^6), 2.54 – 2.41 (1H, m, H^6), 2.40 – 2.29 (1H, m, H^5), 1.26 (3H, t, *J* = 7.1 Hz, H^{10}), 1.16 (3H, d, *J* = 6.7 Hz, H^7).

^{13}C NMR (75 MHz, $CDCl_3$) δ_C 194.6 (C^3), 171.6 (C^8), 153.9 (C^1), 126.70 (C^2), 83.4 (C^4), 64.5 (C^9), 37.9 (C^6), 29.2 (C^5), 15.0 (C^7), 11.3 (C^{10}).

IR (neat): ν_{max}cm^{-1} 3476 (OH), 2981 (CH), 2935 (CH), 1737 (C=O), 1679 (C=O), 1459 (OH).

MS(ES+):199.0$[M+H]^+$(100%), 221.0 $[M+Na]^+$(72%).

(±)-Ethyl-6,6-dimethyl-2-oxocyclohex-3-ene-1-carboxylate (**3.18**)

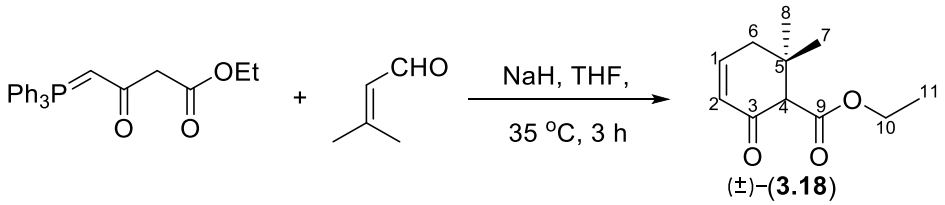

(±)–(**3.18**)

To a stirred round bottom flask (50 mL) was added ethyl 3-oxo-4-(triphenyl-phosphaneylidene) butanoate (1.0 g, 2.56 mmol) and anhydrous THF ((10 mL). 3-methylbut-2-enal (0.24 mL, 2.56 mmol) was then added via syringe and the reaction vessel warmed to 35 °C in an oil bath. NaH (60 % in mineral oil) (0.21 g, 5.12 mmol) was then added to the reaction vessel followed by careful addition of 3 drops of water. The reaction was left stirring at 35 °C and monitored by TLC. After 3 h the reaction was quenched by addition via syringe of 1M HCl (10 mL), extracted with diethyl ether (3 x 20 mL). The combined organic extracts were washed with brine (10 mL), dried over $MgSO_{4(s)}$, filtered and the solvent removed under reduced pressure. The crude product was purified by column chromatography (petroleum ether:ethyl acetate 4:1, column diameter = 1 cm, silica = 10 cm) to give (±)-ethyl 6,6-dimethyl-2-oxocyclohex-3-ene-1-carboxylate as a yellow oil (45 mg, 0.23 mmol, 9 %).

R_f = 0.42 (petroleum ether:ethyl acetate, 4:1; UV light);

^{1}H NMR (300 MHz, $CDCl_3$) δ_H 6.93 (1H, ddd, *J* = 10.2, 4.5, 3.7 Hz, H^1), 6.08 (1H, dt, *J* = 10.2, 2.1 Hz, H^2), 4.18 (2H, q, *J* = 7.1 Hz, H^{10}), 3.21 (1H, s, H^4), 2.56 (1H, ddt, *J* = 19.0, 3.8, 2.3 Hz, H^6), 2.24 – 2.20 (1H, m, H^6), 1.27 (3H, t, *J* = 7.1 Hz, H^{11}), 1.15 (3H, s, $H^{7 \text{ or } 8}$), 1.10 (3H, s, $H^{7 \text{ or } 8}$);

^{13}C NMR (75 MHz, $CDCl_3$) δ_C 194.6 (C^3), 168.4 (C^9), 149.3 (C^1), 126.1 (C^2), 65.2 (C^4), 60.2 (C^{10}), 39.2 (C^6), 36.5 (C^5), 28.4 ($C^{7 \text{ or } 8}$), 23.9 ($C^{7 \text{ or } 8}$) 14.3 (C^{11});

IR (neat): ν_{max}cm^{-1} 2965 (CH), 1728 (C=O), 1675 (C=O), 1465 (CH);

MS(ES+):219.1$[M+Na]^+$(100%), 151.1$[M\text{-}OEt]^+$(5%);

HRMS (TOF ES+): calcd for $C_{11}H_{16}O_3Na[M+Na]^+$219.0997, found 219.0919.

(±)-Ethyl (S)-1-hydroxy-6,6-dimethyl-2-oxocyclohex-3-ene-1-carboxylate (**3.19**)

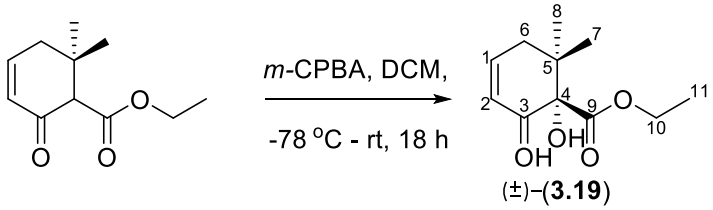

(±)–(**3.19**)

To a stirred round bottom flask (50 mL) was added ethyl 6,6-dimethyl-2-oxocyclohex-3-ene-1-carboxylate (0.263 g, 1.34 mmol). The reaction vessel was then placed under a nitrogen atmosphere. Anhydrous DCM (5 mL) was then added via syringe. The reaction vessel was then placed in an acetone/dry ice bath and its contents cooled to -78 °C. To another stirred round bottom flask (50 mL) was added purified *m*-CPBA (0.463 g, 2.68 mmol). The reaction vessel was then placed under a nitrogen atmosphere. Anhydrous DCM (5 mL) was then added via syringe. The contents of the round bottom flask containing the *m*-CPBA solution were then transferred dropwise via syringe to the round bottom flask containing the ethyl 6-methyl-2-oxocyclohex-3-ene-1-carboxylate solution. The reaction was left stirring at -78 °C and allowed to warm to room temperature overnight. After 18 h the reaction was quenched with Na_2SO_3 (5 mL) and the extracted with diethyl ether (3 x 10 mL). The combined organic extracts were dried over $MgSO_{4(s)}$, filtered and the solvent removed under reduced pressure. The crude product was purified by column chromatography (petroleum ether: ethyl acetate 4:1, column diameter = 1 cm, silica = 10 cm) to give (±)-ethyl 1-hydroxy-6-methyl-2-oxocyclohex-3-ene-1-carboxylate as a pale-yellow oil (3.7 mg, 0.017 mmol, 13 %).

R_f = 0.42 (petroleum ether:ethyl acetate, 4:1; UV light);

^{1}H NMR (300 MHz, $CDCl_3$) δ_H 6.99 (1H, ddd, *J* = 10.2, 5.6, 2.6 Hz, H^1), 6.16 (1H, ddd, *J* = 10.2, 3.0, 1.1 Hz, H^2), 4.20 (2H, q, *J* = 7.1 Hz, H^{10}), 4.09 (1H, br s, OH^4) 2.92 – 2.83 (1H, m, H^6), 2.27 (1H, ddd, *J* = 19.5, 5.7, 1.2 Hz, H^6), 1.26 (3H, t, *J* = 7.1 Hz, H^{11}), 1.15 (1H, s, $H^{7 \text{ or } 8}$), 1.03 (1H, s, $H^{7 \text{ or } 8}$).

^{13}C NMR (75 MHz, $CDCl_3$) δ_C 194.6 (C^3), 170.4 (C^9), 149.3 (C^1), 126.1 (C^2), 83.2 (C^4), 60.2 (C^{10}), 39.2 (C^6), 36.5 (C^5), 28.4 ($C^{7 \text{ or } 8}$), 24.0 ($C^{7 \text{ or } 8}$) 14.1 (C^{11});

IR (neat): ν_{max}cm^{-1} 2965 (CH), 1728 (C=O), 1675 (C=O), 1465 (CH), 1428 (OH).

(±)-Ethyl-2,9-dihydroxy-8-methoxy-1-oxo-1,2,3,4,4a,10-hexahydroanthracene-2-carboxylate (**3.20**)

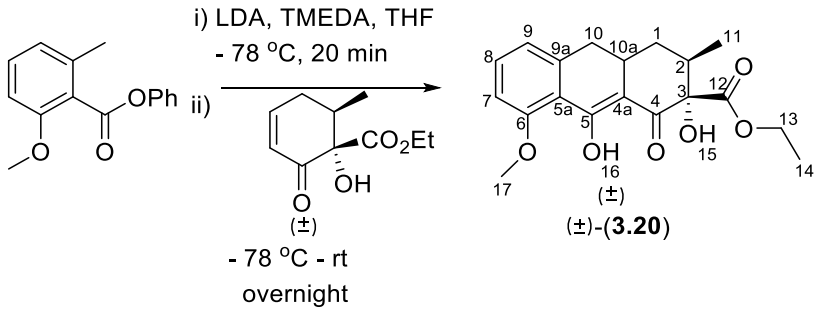

To a Schlenk flask under nitrogen atmosphere was added 5 mL dry THF, di-isopropylamine (1.31 mL, 9.4 mmol), and *n*-BuLi 1.6 M in hexane (5.8 mL, 9.4 mmol). The reaction mixture was stirred at -78 °C for 30 min after which TMEDA (1.28 mL, 8.6 mmol) was added via syringe. Phenyl-2-methoxy-6-methylbenzoate (0.65 g, 2.7 mmol) was dissolved in 2 mL of dry THF and then added to the LDA solution after which the reaction mixture was left to stir at -78 °C for 20 min. Ethyl 1-hydroxy-6-methyl-2-oxocyclohex-3-ene-1-carboxylate (0.53 g, 2.7 mmol) was dissolved in 2 mL of dry THF and added to the reaction mixture via syringe. The mixture was stirred at -78 °C for a further 3h and then allowed to warm to rt overnight with stirring. The rection mixture was quenched with saturated $NH_4Cl_{(aq)}$ (10 mL) and extracted with ethyl acetate (3 x 20 mL). The combined organic extracts were dried over $MgSO_{4(s)}$, filtered and the solvent removed under reduced pressure. The crude product was purified by column chromatography (petroleum ether:ethyl acetate 2:1, column diameter = 1 cm, silica = 10 cm) to give (±)-ethyl-2,9-dihydroxy-8-methoxy-1-oxo-1,2,3,4,4a,10-hexahydroanthracene-2-carboxylate as a pale yellow oil (238 mg, 0.68 mmol, 26 %).

R_f = 0.28 (petroleum ether:ethyl acetate, 2:1; UV light);

^{1}H NMR (300 MHz, $CDCl_3$) δ_H 15.81 (1H, s, OH^{16}), 7.40 (1H, dd, *J* = 8.5, 7.5 Hz, H^8), 6.89 (1H, d, *J* = 8.5 Hz, H^9), 6.83 (1H, d, *J* = 7.5 Hz, H^7), 4.30 (2H, q, *J* = 7.1 Hz, H^{13}), 3.95 (3H, s, H^{17}), 3.93 (1H, s, OH^{15}) 2.91 – 2.71 (3H, m, $H^{10, 10a}$), 2.23 – 2.13 (1H, m, H^2), 1.91 – 1.79 (2H, m, H^1), 1.30 (3H, t, *J* = 7.1 Hz, H^{14}), 1.03 (3H, d, *J* = 7.1 Hz, H^{11});

^{13}C NMR (75 MHz, $CDCl_3$) δ_C 188.4 (C^4), 175.3 (C^{12}), 173.7 (C^6), 163.2 (C^5), 145.8 (C^{9a}), 133.4 (C^8), 120.7 (C^9), 118.9 (C^{5a}), 110.7 (C^7), 109.4 (C^{4a}), 77.8 (C^3), 62.5 (C^{13}), 55.6 (C^{17}), 37.5 (C^{10}), 36.5 (C^2), 32.3 (C^1), 29.6 (C^{10a}),15.7 (C^{11}), 14.3 (C^{14});

IR (neat): ν_{max}cm^{-1} 3585-3245 (OH), 3165-2750 (CH), 1733 (C=O), 1594 (C=O);

MS (ES+): 715.3 $[2M+Na]^+$ (15%), 369.1 $[M+Na]^+$ (100%);

HRMS (TOF MS ES+) calcd $C_{19}H_{22}O_6Si_2Na$ $[M+Na]^+$: 369.3790, found 369.1345.

6.4 Experimental – Chapter 4

Methyl (3*R*,4*S*,5*R*)-3,4,5-trihydroxycyclohex-1-ene-1-carboxylate (-)-(**4.06**)[3]

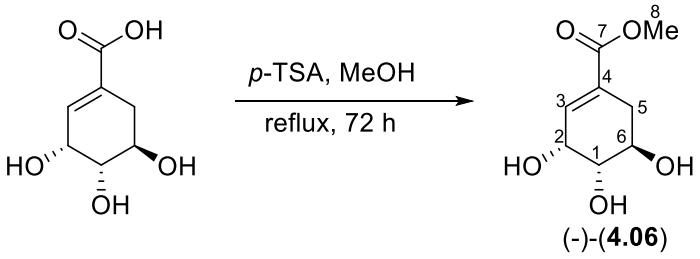

(-)-(**4.06**)

To a stirred round bottom flask (250 mL) was added shikimic acid (5.00 g, 28.7 mmol), MeOH (125 mL) and *p*-toluenesulfonic acid monohydrate (0.50 g, 2.6 mmol). The resulting solution was put under a nitrogen atmosphere and heated at reflux. The reaction was monitored by TLC. After 72 h the reaction mixture was then cooled to rt, filtered to remove insoluble impurities, and the solvent removed under reduced pressure. The crude product was recrystallized from hot EtOAc (15 mL) to afford methyl (3*R*,4*S*,5*R*)-3,4,5-trihydroxycyclohex-1-ene-1-carboxylate as an off-white solid (3.97 g, 21 mmol, 73 %).

Mp = 114.5 - 115.7 ^{o}C (lit. Mp = 112 – 113 ^{o}C);

$[\alpha]_D^{20}$ = -127.6 (*c* = 1.8, EtOH) (lit. $[\alpha]_D^{20}$ = -125.0 (*c* = 1.8, EtOH);

^{1}H NMR (300 MHz, MeOD-d_4) δ_H 6.79 (1H, dtd, *J* = 3.7, 1.9, 0.7 Hz, H^3), 4.40 – 4.34 (1H, m, H^6), 4.01 (1H, dddd, *J* = 7.1, 5.4, 4.9, 0.6 Hz, H^1), 3.74 (3H, s, H^8), 3.69 (1H, dd, *J* = 7.2, 4.1 Hz, H^2), 2.76 – 2.62 (1H, m, H^5), 2.20 (1H, ddt, *J* = 18.2, 5.4, 1.7 Hz, H^5);

^{13}C NMR (75 MHz, MeOD-*d*4) δ_C 167.3 (C^7), 137.7 (C^3), 128.8 (C^4), 71.1 (C^2), 67.0 (C^1), 65.8 (C^6), 50.9 (C^8), 30.1 (C^5);

IR (neat): v_{max}cm^{-1} 3311 (br, OH), 2901 (CH), 1717 (s, C=O).

Trans-vicinal protected diol (+)-(**4.07**) and *cis*-vicinal protected diol (-)-(**4.08**)[3].

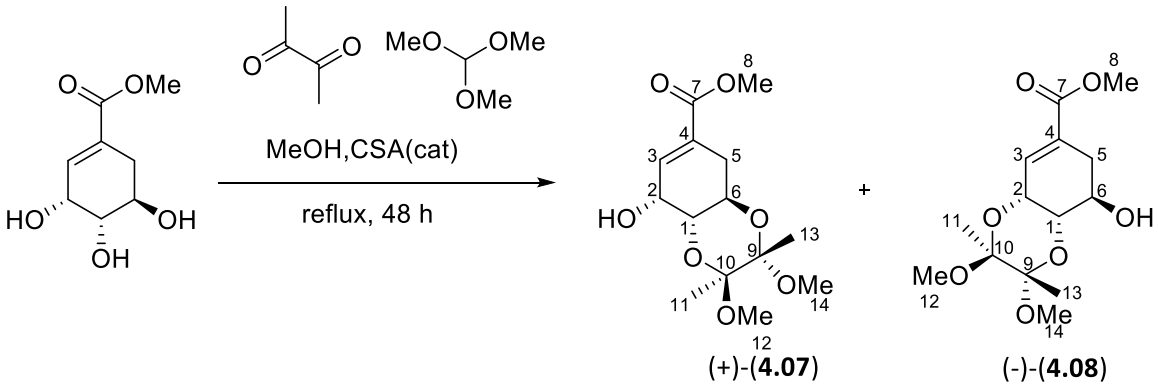

To a stirred round bottom flask was added methyl (3*R*,4*S*,5*R*)-3,4,5-trihydroxycyclohex-1-ene-1-carboxylate (1.00 g, 5.31 mmol), followed by MeOH (20 mL), 2,3-butanedione (1.1 mL, 12.75 mmol) and then camphor sulfonic acid (123 mg, 0.53 mmol). The reaction mixture was put under a nitrogen atmosphere. Trimethyl orthoformate (3.48 mL, 31.88 mmol) was added, after which the reaction mixture was heated to reflux and monitored by TLC. After 48 h the reaction mixture was cooled to rt and quenched by the addition of solid $NaHCO_3$ (1.1 g, 13.0 mmol). The reaction mixture stirred for a further 10 min and was then filtered to remove insoluble inorganics. The solvent was then removed under reduced pressure and the crude product was purified by flash column chromatography (petroleum ether:acetone, 5:1, column diameter 3cm, silica = 20 cm) to give methyl(2*R*,3*R*,4a*R*,8*R*,8a*R*)-8-hydroxy-2,3-dimethoxy-2,3-dimethyl-2,3,4a,5,8,8a-hexahydrobenzo[*b*][1,4]dioxine-6-carboxylate (**4.07**) as a pale yellow oil (1.15 g, 3.80 mmol, 71 %) and methyl (2S,3S,4aR,8R,8aS)-8-hydroxy-2,3-dimethoxy-2,3-dimethyl-2,3,4a,7,8,8a-hexahydrobenzo[b][1,4]dioxine-6-carboxylate (**4.08**) as a pale yellow solid (0.32g, 1.07 mmol, 20 %).

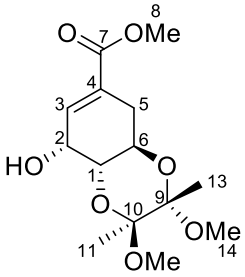

(**4.07**)

R_f = 0.22 (petroleum ether: acetone, 5:1; UV light);

$[\alpha]_D^{20}$ = +18.6 (*c* = 1, $CHCl_3$) (lit. $[\alpha]_D^{20}$ = +23.1 (*c* = 0.89, $CHCl_3$)[3]

^{1}H NMR (300 MHz, $CDCl_3$) δ_H 6.91 (1H, dd, *J* = 5.4, 2.8 Hz, H^3), 4.39 (1H, t, *J* = 4.8 Hz, H^2), 4.10 (1H, td, *J* = 10.7, 5.8 Hz, H^6), 3.75 (s, 3H^8), 3.62 (1H, dd, *J* = 10.9, 4.3 Hz, H^1), 3.28 (3H, s, $H^{12 \text{ or } 14}$), 3.26 (3H, s, $H^{12 \text{ or } 14}$), 2.83 (1H, dd, *J* = 17.6, 5.8 Hz, H^5), 2.31 – 2.19 (1H, m, H^5), 1.34 (3H, s, $H^{11 \text{ or } 13}$), 1.30 (3H, s, $H^{11 \text{ or } 13}$);

^{13}C NMR (75 MHz, $CDCl_3$) δ_C 165.5 (C^7), 135.5 (C^3), 131.6 (C^4), 100.0 ($C^{9 \text{ or } 10}$), 99.2 ($C^{9 \text{ or } 10}$), 70.6 (C^1), 65.0 (C^2), 62.5 (C^6), 52.1 (C^8), 48.0 ($C^{12 \text{ or } 14}$), 47.9 ($C^{12 \text{ or } 14}$), 30.1 (C^5), 17.9 ($C^{11 \text{ or } 13}$), 17.7 ($C^{11 \text{ or } 13}$);

IR (neat): v_{max}cm^{-1}3560 (OH), 2991 – 2836 (CH), 1720 (C=O).

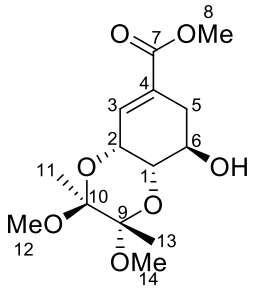

(**4.08**)

Mp = 136 - 137 °C (lit. Mp = 137 – 138 °C)

R_f = 0.10 (petroleum ether:acetone, 5:1; UV light);

$[\alpha]_D^{20}$ = -135.1 (*c* = 1, $CHCl_3$) (lit. $[\alpha]_D^{20}$ = -144.2 (*c* = 0.26, $CHCl_3$)[3];

^{1}H NMR (300 MHz, $CDCl_3$) δ_H 6.95 (1H, s, H^3), 4.39 (1H, d, *J* = 1.2 Hz, H^2), 4.20 (1H, s, H^6), 4.12 (1H, s, H^1) 3.75 (3H, s, H^8), 3.27 (3H, s, $H^{12 \text{ or } 14}$), 3.25 (3H, s, $H^{12 \text{ or } 14}$), 2.65 (1H, ddd, *J* = 18.2, 6.3, 3.1 Hz, H^5), 2.40 (1H, d, *J* = 18.3 Hz, H^5), 1.29 (3H, s, $H^{11 \text{ or } 13}$), 1.25 (3H, s, $H^{11 \text{ or } 13}$);

^{13}C NMR (75 MHz, $CDCl_3$) δ_C 166.6 (C^7), 135.2 (C^3), 131.6 (C^4), 100.0 ($C^{9 \text{ or } 10}$), 99.2 ($C^{9 \text{ or } 10}$), 70.6 (C^1), 65.0 (C^2), 62.4 (C^6), 52.1 (C^8), 48.0 ($C^{12 \text{ or } 14}$), 47.9 ($C^{12 \text{ or } 14}$), 30.1 (C^5), 17.9 ($C^{11 \text{ or } 13}$), 17.7 ($C^{11 \text{ or } 13}$);

IR (neat): v_{max} cm^{-1}3562 (OH), 2985 – 2836 (CH), 1720 (C=O).

Methyl (2*S*,3*S*,4a*R*,8*R*,8a*S*)-8-(benzyloxy)-2,3-dimethoxy-2,3-dimethyl-2,3,4a,5,8,8a-hexahydrobenzo[b][1,4]dioxine-6-carboxylate (**4.09**)[9]

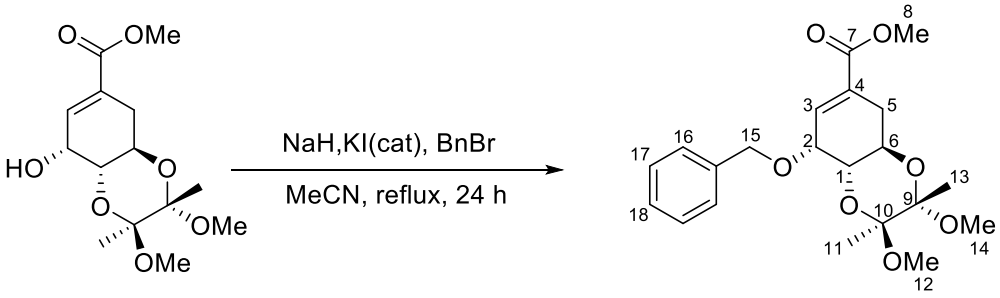

(**4.09**)

To a stirred round bottomed flask (25 mL) was added methyl (2*S*,3*S*,4a*R*,8*R*,8a*R*)-8-hydroxy-2,3-dimethoxy-2,3-dimethyl-2,3,4a,5,8,8a-hexahydrobenzo[*b*][1,4]dioxine-6-carboxylate (100 mg, 0.33 mmol) and NaH (60 % in mineral oil) (12 mg, 0.495 mmol).The reaction vessel was then put under a nitrogen atmosphere and dry MeCN (10 mL) was added via syringe. To another stirred round bottomed flask (25 mL) was added KI (5 mg,0.033 mmol) and then BnBr (0.078 mL, 0.66 mmol).The KI and BnBr mixture was stirred for 10 min and then added via syringe to the first round bottom flask and stirred at rt for 10 min. The mixture was then placed under reflux and monitored by TLC. After 24 h the reaction mixture was taken off reflux and allowed to cool after which saturated $NaHCO_3$ solution (5 mL) was added to the reaction mixture, extracted with EtOAc (3 x 10 mL) and the combined organic extracts were washed with brine (20 mL). The combined organic extracts were dried over $MgSO_{4(s)}$, filtered and the solvent removed under reduced pressure. The crude product was purified by column chromatography (petroleum ether:acetone, 5:1, column diameter = 1 cm, silica = 10 cm) to give methyl (2*S*,3*S*,4a*R*,8*R*,8a*S*)-8-(benzyloxy)-2,3-dimethoxy-2,3-dimethyl-2,3,4a,5,8,8a-hexahydrobenzo[b][1,4]dioxine-6-carboxylateas a pale yellow oil (25 mg, 0.06 mmol, 19 %).

R_f = 0.30 (petroleum ether: acetone, 5:1; UV light);

$[\alpha]_D^{20}$ = -18.6 (c = 0.20, $CHCl_3$);^{1}H NMR (300 MHz, $CDCl_3$) δ_H 7.51 – 7.41 (2H, m, H^{16}), 7.41 – 7.29 (2H, m, H^{17}), 7.34 – 7.21 (1H, m, H^{18}), 6.82 (1H, dd, *J* = 5.6, 2.8 Hz, H^3), 5.04 (1H, d, *J* = 11.2 Hz, H^{15}), 4.67 (1H, d, *J* = 11.3 Hz, H^{15}), 4.28 (1H, dd, *J* = 10.5, 6.1 Hz, H^2), 4.17 (1H, dd, *J* = 5.6, 3.9 Hz H^6), 3.72 (3H, s, H^8), 3.78 – 3.65 (1H, m, H^1), 3.30 (3H, s, $H^{12 \text{ or } 14}$), 3.28 (3H, s, $H^{12 \text{ or } 14}$) 2.83 (1H, dd, *J* = 17.7, 6.1, H^5), 2.24 (1H, ddd, *J* = 17.8, 10.3, 2.9 Hz, H^5), 1.37(1H, s, $H^{12 \text{ or } 14}$), 1.32 (1H, s, $H^{12 \text{ or } 14}$).

^{13}C NMR (75 MHz, $CDCl_3$) δ_C 166.4 (C^7), 138.7, 134.4 (C^3), 130.9 (C^4), 128.2 ($C^{16 \text{ and } 18}$) 127.5 (C^{17}) 100.0 ($C^{9 \text{ or } 10}$), 99.2 ($C^{9 \text{ or } 10}$), 72.0 (C^1), 71.3 (C^2), 62.8 (C^6), 52.1 (C^8), 48.0 ($C^{12 \text{ or } 14}$), 47.9 ($C^{12 \text{ or } 14}$), 30.1 (C^5), 17.9 ($C^{11 \text{ or } 13}$), 17.7 ($C^{11 \text{ or } 13}$);

IR (neat): $v_{max}cm^{-1}$ 2991 – 2835 (CH), 1722 (C=O).

Methyl (2*S*,3*S*,4a*R*,8*R*,8a*S*)-8-((*tert*-butyldimethylsilyl)oxy)-2,3-dimethoxy-2,3-dimethyl-2,3,4a,5,8,8a-hexahydrobenzo[*b*][1,4]dioxine-6-carboxylate (-)-(**4.11**)[3]

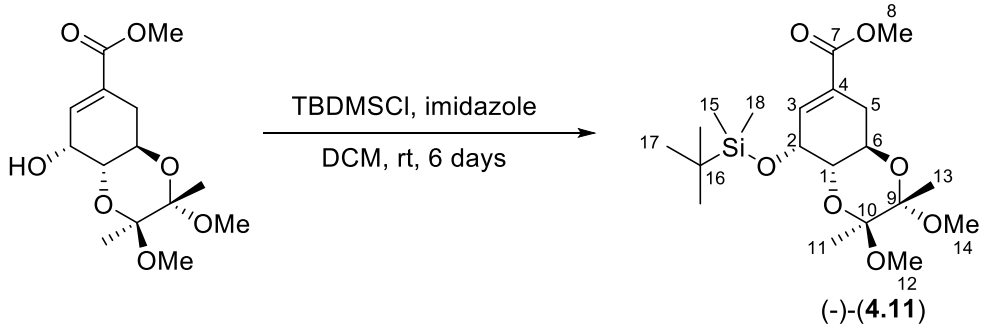

(-)-(**4.11**)

To a stirred round bottomed flask (100 mL) was added methyl (2*S*,3*S*,4a*R*,8*R*,8a*R*)-8-hydroxy-2,3-dimethoxy-2,3-dimethyl-2,3,4a,5,8,8a-hexahydrobenzo[*b*][1,4]dioxine-6-carboxylate (2910 mg, 9.63 mmol) and imidazole (1638 mg, 24 mmol).The reaction vessel was then put under a nitrogen atmosphere. Dry DCM (10 mL) was added via syringe. To another stirred round bottomed flask (50 mL) was added *tert*-butyldimethylsilyl chloride (3627 mg, 24 mmol). The 50 mL RBF was placed under a nitrogen atmosphere and then dry DCM (10 mL) was added via syringe. Once the *tert*-butyldimethylsilyl chloride had dissolved, it was then added via syringe to the 100 mL RBF containing and imidazole. The reaction mixture was stirred at rt and monitored by TLC. After 6 days no starting material was apparent on TLC. The reaction mixture was then quenched with saturated aqueous NH_4Cl (5 mL), extracted with DCM (3 x 30 mL) and the combined organic extracts were washed with brine (20 mL). The combined organic extracts were dried over $MgSO_{4(s)}$, filtered and the solvent removed under reduced pressure. The crude product was purified by column chromatography (petroleum ether:acetone, 10:1, column diameter = 4 cm, silica = 20 cm) to give methyl (2*S*,3*S*,4a*R*,8*R*,8a*S*)-8-((*tert*-butyldimethylsilyl)oxy)-2,3-dimethoxy-2,3-dimethyl-2,3,4a,5,8,8a-hexahydrobenzo[*b*][1,4]dioxine-6-carboxylate as a white solid (3690 mg, 8.86 mmol, 92 %).

Mp = 72.1 – 73.3 °C;

R_f = 0.46 (petroleum ether:acetone, 10:1);

$[\alpha]_D^{20}$ = -16.7 (*c* = 0.18, $CHCl_3$);

^{1}H NMR (300 MHz, Chloroform-*d*) δ_H 6.77 (1H, dd, *J* = 5.6, 2.8 Hz, H^3), 4.31 (1H, t, *J* = 4.5 Hz, H^2), 4.12 (1H, td, *J* = 10.6, 6.0 Hz, H^6), 3.75 (3H, s, H^8), 3.48 (1H, dd, *J* = 10.8, 3.9 Hz, H^1), 3.24 (3H, s, $H^{12 \text{ or } 14}$), 3.23 (3H, s, $H^{12 \text{ or } 14}$), 2.81 (1H, dd, *J* = 17.6, 6.1 Hz, H^5), 2.22 (1H, ddd, *J* = 17.5,

10.2, 2.6 Hz, H^5), 1.29 (3H, s, $H^{11 \text{ or } 13}$), 1.28 (3H, s, $H^{11 \text{ or } 13}$), 0.89 (9H, s, H^{17}), 0.12 (3H, s, $H^{15 \text{ or } 18}$), 0.10 (3H, s, $H^{15 \text{ or } 18}$);

^{13}C NMR (75 MHz, Chloroform-*d*) δ_C 167.1 (C^7), 136.8 (C^3), 129.8 (C^4), 99.5 ($C^{9 \text{ or } 10}$), 98.7 ($C^{9 \text{ or } 10}$), 70.8 (C^1), 65.9 (C^2), 62.4 (C^6), 52.0 (C^8), 47.8 ($C^{12 \text{ or } 14}$), 47.6 ($C^{12 \text{ or } 14}$), 30.4 (C^5), 25.8 (C^{17}), 18.4 (C^{16}), 17.9 ($C^{11 \text{ or } 13}$), 17.7 ($C^{11 \text{ or } 13}$), -4.7 ($C^{15 \text{ or } 18}$), -4.8 ($C^{15 \text{ or } 18}$);

IR (neat): $v_{max}cm^{-1}$ 2999- 2852 (CH), 1705 (C=O)

MS (pNSI): 434.3 $[M+NH_4]^+$ (100%), 385.2 $[M\text{-}OMe]^+$ (46 %)

HRMS (pNSI): calcd for $C_{20}H_{36}O_7Si$ $[M+NH_4]^+$: 434.2569; observed: 434.2562.

Methyl (2*S*,3*S*,4a*R*,6*S*,7*R*,8*R*,8a*S*)-8-((*tert*-butyldimethylsilyl)oxy)-6,7-dihydroxy-2,3-dimethoxy-2,3-dimethyloctahydrobenzo[*b*][1,4]dioxine-6-carboxylate (+)-(**4.12**)

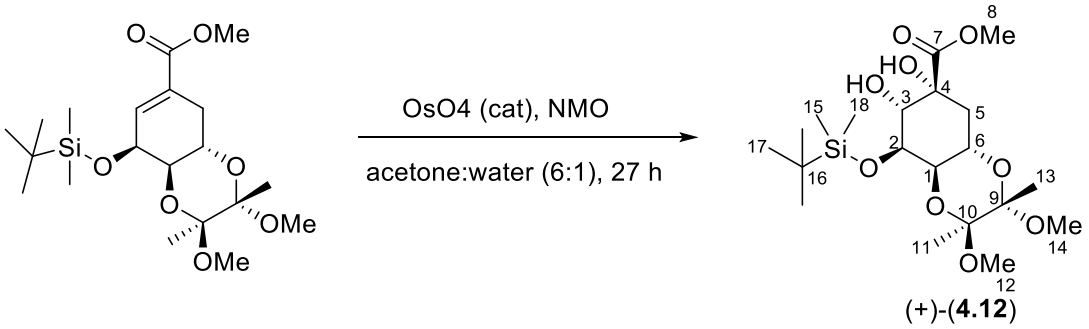

To a stirred Schlenk flask was added methyl (2*S*,3*S*,4a*R*,8*R*,8a*S*)-8-((*tert*-butyldimethylsilyl)oxy)-2,3-dimethoxy-2,3-dimethyl-2,3,4a,5,8,8a-hexahydrobenzo[*b*][1,4]dioxine-6-carboxylate (416 mg, 1 mmol)) and 4-methylmorpholine-*N*-oxide (200 mg, 2 mmol). The reaction vessel was placed under a nitrogen atmosphere. Acetone:water (6:1 v/v, 2 mL) was then added via syringe to the reaction vessel. To the resultant stirred solution was added osmium tetroxide (0.1 mL 4 % aqueous solution, 0.016 mmol). The reaction mixture was stirred at rt and monitored by TLC. After 7 days the reaction was quenched with saturated aqueous Na_2SO_3 solution (4 mL), diluted with water (10 mL) and the organic layer extracted with ethyl acetate (3 x 10 mL). The combined organic extracts were washed with brine (10 mL), dried with $MgSO_{4(s)}$, filtered and the solvent removed under reduced pressure. The crude product was purified by column chromatography (petroleum ether:acetone 2:1, column diameter = 3 cm, silica = 20 cm) to give methyl (2*S*,3*S*,4a*R*,6*S*,7*R*,8*R*,8a*S*)-8-((*tert*-butyldimethylsilyl)oxy)-6,7-dihydroxy-2,3-dimethoxy-2,3-dimethyloctahydrobenzo[*b*][1,4]dioxine-6-carboxylate as a clear oil (3300 mg, 2.22 mmol, 73 %).

R_f = 0.22 (petroleum ether:acetone, 2:1);

$[\alpha]_D^{20}$ = +63 (*c* = 0.64, $CHCl_3$);

^{1}H NMR (300 MHz, Chloroform-*d*) δ_H 4.22 (1H, ddd, *J* = 12.3, 10.3, 4.4 Hz, H^6), 4.07 (1H, dd, *J* = 3.7, 2.6 Hz H^2), 4.02 (1H, dd, *J* = 3.7, 1.3 Hz, H^3), 3.77 (1H, d, *J* = 2.6 Hz, H^1), 3.74 (3H, s, H^8), 3.20 (6H, s, H$^{12 \text{ and } 14}$), 2.21 (1H, ddd, *J* = 12.3, 4.5, 1.4 Hz, H^5), 1.77 (1H, t, *J* = 12.3 Hz, H^5), 1.24

(3H, s, $H^{11 \text{ or } 13}$), 1.23 (3H, s, $H^{11 \text{ or } 13}$), 0.82 (9H, s, H^{17}), 0.06 (3H, s, $H^{15 \text{ or } 18}$), 0.02 (3H, s, $H^{15 \text{ or } 18}$);

^{13}C NMR (75 MHz, Chloroform-*d*) δ_C 173.17 (C^7), 99.8 ($C^{9 \text{ or } 10}$), 99.1 ($C^{9 \text{ or } 10)}$, 75.9 (C^4), 74.6 (C^3), 71.9 (C^2), 69.2 (C^1), 62.6 (C^6), 52.7 (C^8), 47.8 ($C^{12 \text{ or } 14}$), 47.3 ($C^{12 \text{ or } 14}$), 32.9 (C^5), 25.9 (C^{17}), 18.4 (C^{16}), 17.9 ($C^{11 \text{ or } 13}$), 17.7 ($C^{11 \text{ or } 13}$), -4.8 ($C^{15 \text{ or } 18}$), -5.0 ($C^{15 \text{ or } 18}$);

IR (neat): $v_{max}cm^{-1}$ 3451 (OH), 2952 (CH), 1734 (C=O);

HRMS (pNSI): calcd for $C_{20}H_{37}O_9Si$ $[M-H]^-$: 449.2213; observed: 449.2212.

Methyl (2*S*,3*S*,4a*R*,6*S*,8*S*,8a*S*)-8-((*tert*-butyldimethylsilyl)oxy)-6-hydroxy-2,3-dimethoxy-2,3-dimethyl-7-oxooctahydrobenzo[*b*][1,4]dioxine-6-carboxylate (+)-(**4.13**).

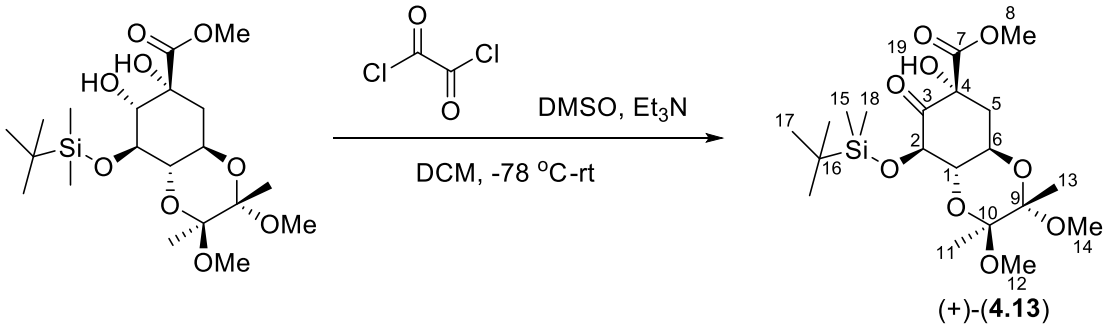

To a stirred Schlenk flask under a nitrogen atmosphere was added dry DCM (2 mL) and oxalyl chloride (0.12 mL, 1.41 mmol). The resultant solution was cooled to -78 °C after which dry DMSO (0.25 mL, 3.53 mmol) was added dropwise via syringe. After 30 min at -78 °C, a solution of methyl (2*S*,3*S*,4a*R*,6*S*,7*R*,8*R*,8a*S*)-8-((*tert*-butyldimethylsilyl)oxy)-6,7-dihydroxy-2,3-dimethoxy-2,3-dimethyloctahydrobenzo[*b*][1,4]dioxine-6-carboxylate (318 mg, 0.705 mmol) in dry DCM (3 mL) was slowly added to the reaction mixture via syringe while it stirred at -78 °C for 30 min. Triethylamine (0.49 mL, 3.50 mmol) was then added and the reaction mixture was stirred at -78 °C for 2 h after which it was allowed to warm up in atmospheric temperature for 30 min. The reaction was then quenched with saturated NH_4Cl solution (5 mL) and extracted with DCM (3 x 10 mL). The combined organic extracts were washed with water (20 mL) and brine (20 mL), then dried with $MgSO_{4(s)}$, filtered and the solvent removed under reduced pressure. The crude product was purified by column chromatography (petroleum ether:ethyl acetate, 5:1, column diameter = 2 cm, silica = 18 cm) to give methyl (2*S*,3*S*,4a*R*,6*S*,8*S*,8a*S*)-8-((*tert*-butyldimethylsilyl)oxy)-6-hydroxy-2,3-dimethoxy-2,3-dimethyl-7-oxooctahydrobenzo[*b*][1,4]dioxine-6-carboxylate as a clear oil (138 mg, 0.31 mmol, 44 %).

R_f = 0.26 (petroleum ether:ethyl acetate, 5:1); $[\alpha]_D^{20}$ = +58 (*c* = 0.64, $CHCl_3$);

^{1}H NMR (300 MHz, Chloroform-*d*) δ_H 4.49 (1H, ddd, *J* = 12.3, 10.2, 4.7 Hz, 1H^6), 4.35 (1H, d, *J* = 2.5 Hz, H^2), 4.18 (1H, s, H^{19}), 3.73 (3H, s, H^8), 3.43 (1H, dd, *J* = 10.2, 2.5 Hz, H^1), 3.29 (3H, s, H$^{12 \text{ or } 14}$), 3.21 (3H, s, H$^{12 \text{ or } 14}$), 2.85 (1H, dd, *J* = 12.8, 4.7 Hz, H^5), 1.56 (1H, t, *J* = 12.6 Hz, H^5), 1.28 (3H, s, H$^{11 \text{ or } 13}$), 1.27 (3H, s, H$^{11 \text{ or } 13}$), 0.88 (9H, s, H^{17}), 0.14 (3H, s, H$^{15 \text{ or } 18}$), 0.02 (3H, s, H$^{15 \text{ or } 18}$);

^{13}C NMR (75 MHz, Chloroform-*d*) δ_C 201.8(C^3), 167.9(C^7), 99.5($C^{9 \text{ or } 10}$), 99.1($C^{9 \text{ or } 10}$), 78.7(C^4), 76.1(C^2), 72.5(C^1), 61.8(C^6), 52.9(C^8), 47.9($C^{12 \text{ or } 14}$), 47.6($C^{12 \text{ or } 14}$), 35.9(C^5), 25.6(C^{17}), 18.3(C^{16}), 17.7($C^{11 \text{ or } 13}$), 17.4($C^{11 \text{ or } 13}$), -4.7($C^{15 \text{ or } 18}$), -5.2($C^{15 \text{ or } 18}$);

IR (neat): $v_{max}cm^{-1}$ 3478 (OH), 2953 – 2851 (CH), 1754 (C=O), 1735 (C=O);

HRMS (pNSI): calcd for $C_{20}H_{37}O_9Si[M+H]^+$ 449.2201 observed 449.2201; calcd for $C_{20}H_{40}O_9SiN[M+NH_4]^+$ 466.2467 observed 466.2458.

Methyl (2*S*,3*S*,4a*R*,6*S*,8*S*,8a*S*)-8-((*tert*-butyldimethylsilyl)oxy)-2,3-dimethoxy-2,3-dimethyl-6-((methylthio)methoxy)-7-oxooctahydrobenzo[*b*][1,4]dioxine-6-carboxylate (+)-(**4.14**)

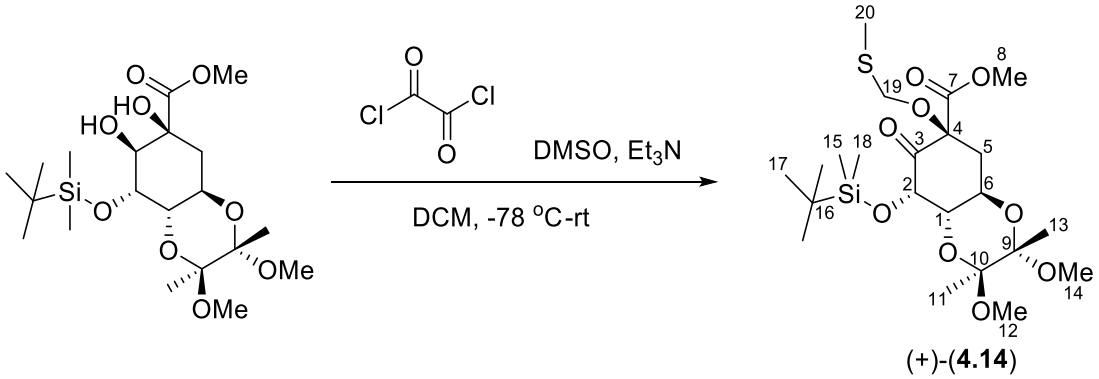

(+)-(**4.14**)

To a stirred Schlenk flask under nitrogen atmosphere was added dry DCM (5 mL) and oxalyl chloride (0.076 mL, 0.887 mmol). The resultant solution was cooled to -78 °C and DMSO (0.16 mL, 2.21 mmol) was added dropwise. After 30 min at -78 °C, a solution of methyl (2*S*,3*S*,4a*R*,6*S*,7*R*,8*R*,8a*S*)-8-((*tert*-butyldimethylsilyl)oxy)-6,7-dihydroxy-2,3-dimethoxy-2,3-dimethyloctahydrobenzo[*b*][1,4]dioxine-6-carboxylate (200 mg, 0.44 mmol) in dry DCM (3 mL) was slowly added to the reaction mixture and stirred at -78 °C for 30 min. Triethylamine (0.31 mL, 2.2 mmol) was then added and the reaction mixture stirred at -78 °C for 2 h after which it was allowed to warm up in atmospheric temperature for 45 min. The reaction was then quenched with saturated NH_4Cl solution (5 mL) and extracted with DCM (3 x 10 mL). The combined organic extracts were washed with water (20 mL) and brine (20 mL), then dried with $MgSO_{4(s)}$, filtered and the solvent removed under reduced pressure. The crude product was purified by column chromatography (petroleum ether:ethyl acetate, 5:1, column diameter = 2cm, silica = 18 cm) to give methyl (2*S*,3*S*,4a*R*,6*S*,8*S*,8a*S*)-8-((*tert*-butyldimethylsilyl)oxy)-2,3-dimethoxy-2,3-dimethyl-6-((methylthio)methoxy)-7-oxooctahydrobenzo[*b*][1,4]dioxine-6-carboxylate as a clear oil (185 mg, 0.36 mmol, 93 %).

R_f = 0.45 (petroleum ether:ethyl acetate, 5:1);

$[\alpha]_D^{20}$ = +33 (*c* = 1, $CHCl_3$);

^{1}H NMR (300 MHz, Chloroform-*d*) δ_H 4.75 (1H, d, *J* = 11.5 Hz, H^{19}), 4.66 (1H, d, *J* = 11.5 Hz, H^{19}), 4.40 (1H, ddd, H^6), 4.20 (1H, d, *J* = 2.5 Hz, H^2), 3.72 (3H, s, H^8), 3.44 (1H, dd, *J* = 10.2, 2.4 Hz, H^1), 3.23 (3H, s, $H^{12 \text{ or } 14}$), 3.15 (3H, s, $H^{12 \text{ or } 14}$), 2.84 (1H, dd, *J* = 12.4, 4.7 Hz, H^5), 2.13 (3H, s,

H^{20}), 1.62 (1H, t, *J* = 12.3 Hz, H^{5}), 1.23 (3H, s, $H^{11\ or\ 13}$), 1.22 (3H, s, $H^{11\ or\ 13}$), 0.83 (9H, s, H^{17}), 0.07 (3H, s, $H^{15\ or\ 18}$), -0.03 (3H, s, $H^{15\ or\ 18}$);

^{13}C NMR (75 MHz, Chloroform-*d*) δ_C 198.4 (C^{3}), 166.6 (C^{7}), 99.4 ($C^{9\ or\ 10}$), 99.1 ($C^{9\ or\ 10}$), 83.6 (C^{4}), 77.5 (C^{2}), 72.2 (C^{1}), 70.5 (C^{19}), 61.8 (C^{6}), 53.1 (C^{8}), 47.9 ($C^{12\ or\ 14}$), 47.6 ($C^{12\ or\ 14}$), 33.8 (C^{5}), 25.7 (C^{17}), 18.3 (C^{16}), 17.7 ($C^{11\ or\ 13}$), 17.4 ($C^{11\ or\ 13}$), 14.6 (C^{20}), -4.5 ($C^{15\ or\ 18}$), -5.2 ($C^{15\ or\ 18}$);

IR (neat): $\nu_{max}cm^{-1}$ 2951 – 2857 (CH), 1736 (C=O), 1717 (C=O);

HRMS (pNSI): calcd for $C_{22}H_{41}O_9SSi$ $[M+H]^+$ 509.2235 observed 509.2232.

Methyl (3aS,7S,7aR)-7-hydroxy-2-thioxo-3a,6,7,7a-tetrahydrobenzo[d][1,3]dioxole-5-carboxylate (**4.23**)

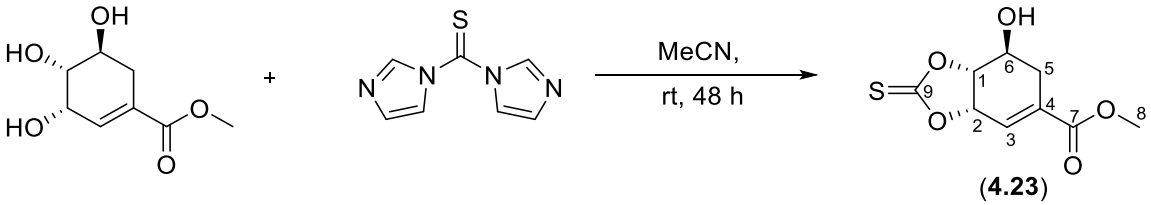

(**4.23**)

To a stirred round bottom flask (100 mL) was added methyl shikimate (0.95 g, 5 mmol), 1,1'-thiocarbonyldiimidazole (1.78 g, 10 mmol) after which the contents of the round bottom flask were placed under a nitrogen atmosphere. Anhydrous MeCN (50 mL) was then added via syringe and the resulting solution left to stir at rt. The reaction was monitored by TLC. After 48 h the stirrer bar was removed and the solvent removed under reduced pressure. The crude product was purified by flash column chromatography (ethyl acetate:chloroform, 2:3, column diameter 1cm, silica = 15 cm) to give methyl (3aS,7S,7aR)-7-hydroxy-2-thioxo-3a,6,7,7a-tetrahydrobenzo[d][1,3]dioxole-5-carboxylate as a clear oil (0.16 g, 0.70 mmol, 14 %).

R_f = 0.32 (ethyl acetate:chloroform, 2:3; UV light);

$[\alpha]_D^{20}$ = +22 (*c* = 1, $CHCl_3$),

^{1}H NMR (300 MHz, $CDCl_3$) δ_H 6.86 (1H, ddd, *J* = 3.7, 2.2, 1.4 Hz, H^3), 5.42 (1H, dd, *J* = 7.7, 3.8 Hz, H^2), 4.85 (1H, t, *J* = 7.5 Hz, H^1), 4.13 (1H, td, *J* = 7.6, 4.8 Hz, H^6), 3.75 (3H, s, H^8), 2.86 (1H, dd, *J* = 18.0, 4.8 Hz, H^5), 2.35 (1H, ddt, *J* = 18.0, 7.9, 1.8 Hz, H^5).

^{13}C NMR (75 MHz, $CDCl_3$) δ_C 188.4 (C^9), 165.6 (C^7), 135.4 (C^4), 128.9 (C^3), 82.6 (C^1), 78.0 (C^2), 66.2 (C^6), 53.4 (C^8), 28.6 (C^5);

IR (neat): v_{max}cm^{-1} 3443 (OH), 2921 (CH) 2851 (CH), 1799 (C=O), 1715 (C=O), 1260 (C=S), 1057 (C-O 2^o alcohol), 734 (C=C);

HRMS (pNSI): calcd for $C_9H_{11}O_5S$ $[M+H]^+$: 231.0323; observed: 231.0322.

Methyl (3aS,7S,7aS)-7-((tert-butyldimethylsilyl)oxy)-2-thioxo-3a,6,7,7a-tetrahydrobenzo[d][1,3]dioxole-5-carboxylate (**4.24**)

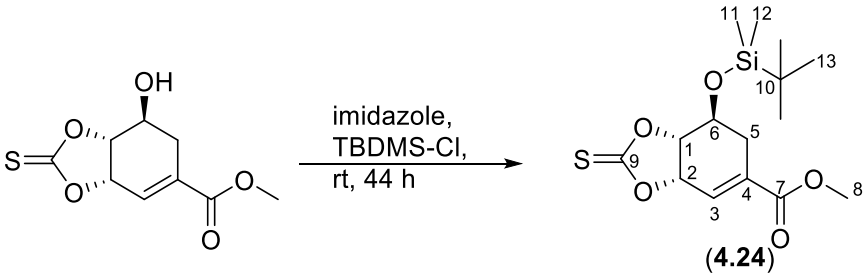

(**4.24**)

To a stirred round bottom flask (25 mL) was added methyl (3aS,7S,7aR)-7-hydroxy-2-thioxo-3a,6,7,7a-tetrahydrobenzo[d][1,3]dioxole-5-carboxylate (0.16 g, 0.70 mmol), imidazole (0.12 g, 1.75 mmol) and TBDMS-Cl (0.26 g, 1.74 mmol) after which the contents of the round bottom flask were placed under a nitrogen atmosphere. Anhydrous DCM (5 mL) was added via syringe and the resulting solution left to stir at rt. The reaction was monitored by TLC. After 44 h the reaction was quenched by addition via syringe of saturated aqueous NH_4Cl, extracted with DCM (3 x 5 mL) and the combined organic extracts were washed with brine. The combined organic extracts were dried over $MgSO_{4(s)}$, filtered and the solvent removed under reduced pressure. The crude product was purified by column chromatography (petroleum ether:ethyl acetate, 5:1, column diameter = 1 cm, silica = 15 cm) to give methyl (3aS,7S,7aS)-7-((tert-butyldimethylsilyl)oxy)-2-thioxo-3a,6,7,7a-tetrahydrobenzo[d][1,3]dioxole-5-carboxylate as light brown oil (133 mg , 0.39 mmol, 56 %). R_f = 0.36 (petroleum ether:ethyl acetate, 5:1; UV light);

$[\alpha]_D^{20}$ = +20 (*c* = 1, $CHCl_3$),^{1}H NMR (300 MHz, $CDCl_3$) δ_H 6.88 (1H, dt, *J* = 3.6, 1.7 Hz, H^3), 5.43 (1H, dd, *J* = 7.5, 3.8 Hz, H^2), 4.80 (1H, t, *J* = 7.1 Hz, H^1), 4.16 (1H, td, *J* = 6.8, 4.3 Hz, H^6), 3.81 (3H, s, H^8), 2.74 (1H, dd, *J* = 17.9, 4.4 Hz, H^5), 2.40 (1H, ddt, *J* = 17.9, 6.8, 1.5 Hz, H^5), 0.88 (9H, s, H^{13}), 0.14 (3H, s, $H^{11 \text{ or } 12}$)), 0.11 (3H, s, $H^{11 \text{ or } 12}$);

^{13}C NMR (75 MHz, $CDCl_3$) δ_C 190.4 (C^9), 165.7 (C^7), 134.1 (C^3), 128.1 (C^4), 82.9 (C^1), 78.2 (C^2), 65.0 (C^6), 54.8 (C^8), 29.5 (C^{10}), 24.8 (C^{13}), 17.9 (C^5) -4.7 ($C^{11 \text{ or } 12}$), -4.8 ($C^{11 \text{ or } 12}$);
IR (neat): ν_{max}cm^{-1} 2929 (CH), 2857 (CH),1715 (C=O), 1252 (C=S).HRMS (pNSI): calcd for $C_{15}H_{25}O_5SSi$ $[M+H]^+$: 345.1186; observed: 345.1191.

Methyl (3a*S*,4*S*,5*R*,7*S*,7a*S*)-7-((*tert*-butyldimethylsilyl)oxy)-4,5-dihydroxy-2-thioxohexahydrobenzo[*d*][1,3]dioxole-5-carboxylate (**4.25**)

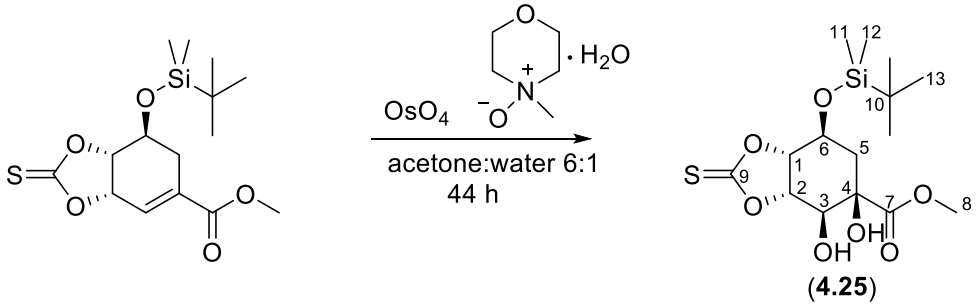

To a stirred Schlenk tube was added methyl (3aS,7S,7aS)-7-((tert-butyldimethylsilyl)oxy)-2-thioxo-3a,6,7,7a-tetrahydrobenzo[d][1,3]dioxole-5-carboxylate (133 mg, 0.386 mmol), acetone:water 6:1 (2 mL), 4-Methylmorpholine N-oxide monohydrate (104 mg, 0.772 mmol) and osmium tetroxide solution (4 wt % in H_2O) (100 µL) via syringe. The reaction was stirred at rt and monitored by TLC. After 44 h, the reaction was quenched with $Na_2S_2O_3$ (5 mL) and extracted with EtOAc (3 x 20 mL) and the combined organic extracts were washed with brine (10 mL) The combined organic extracts were then dried over $MgSO_{4(s)}$, filtered and the solvent removed under reduced pressure. The crude product was purified by column chromatography (petroleum ether:acetone, 5:2, column diameter = 1 cm, silica = 15 cm) to give methyl (3a*S*,4*S*,5*R*,7*S*,7a*S*)-7-((*tert*-butyldimethylsilyl)oxy)-4,5-dihydroxy-2-thioxohexahydrobenzo[*d*][1,3]dioxole-5-carboxylate as a clear oil (42 mg, 0.11 mmol, 29 %).
$[\alpha]_D^{20}$ = -45 (*c* = 1, $CHCl_3$);^{1}H NMR (300 MHz, $CDCl_3$) δ_H 5.14 (d1H, d, *J* = 7.6, 4.7 Hz, H^2), 4.82 (1H, dd, *J* = 7.5, 6.1 Hz, H^1), 4.33 (d, *J* = 4.7 Hz, H^6), 4.28-4.22 (1H, m, H^3), 3.85 (3H, s, H^8), 2.18 – 2.05 (1H, m, H^5), 2.03 – 1.96 (1H, m, H^5), 0.88 (9H, s, H^{13}), 0.13 (3H, s, $H^{11\text{ or }12}$), 0.10 (3H, s, $H^{11\text{ or }12}$).

^{13}C NMR (75 MHz, $CDCl_3$) δ_C 189.3 (C^9), 174.2 (C^7), 84.1 (C^3), 81.4 (C^1), 75.1 (C^2), 68.7 (C^6), 66.3 (C^4), 55.4 (C^8), 37.8 (C^{10}), 25.7 (C^{13}), 17.9 (C^5) -4.7 ($C^{11\text{ or }12}$), -4.9 ($C^{11\text{ or }12}$).

IR (neat): ν_{max}cm^{-1} 3443 (OH), 2954 (CH), 2929 (CH), 2857 (CH), 1797 (C=O), 1737 (C=O), 1251 (C=S), 1114 (C-O);

MS (ES+): 401.1 $[M+Na]^+$ (100%), 385.1 (12%), 779.2 $[2M+Na]^+$ (5%).

HRMS (TOF ES+): calcd for $C_{15}H_{26}O_7SSiNa$ $[M+Na]^+$ 401.1066, found 401.1022.

6.5 Experimental – Chapter 5

Ethyl (3*R*,4*S*,5*R*)-3,4,5-trihydroxycyclohex-1-ene-1-carboxylate (**5.01**)

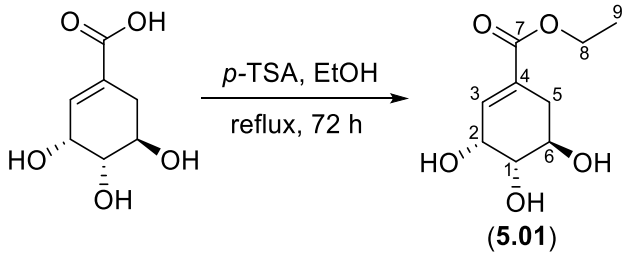

(**5.01**)

To a stirred round bottomed flask (250 mL) was added shikimic acid (5.00 g, 28.7 mmol), EtOH (125 mL) and *p*-toluenesulfonic acid monohydrate (0.50 g, 2.6 mmol). The resulting solution was put under a nitrogen atmosphere and heated at reflux. The reaction was monitored by TLC. After 72 h the reaction mixture was cooled to rt, filtered to remove insoluble impurities and the solvent removed under reduced pressure. The crude product was recrystallized from hot EtOAc (15 mL) to afford ethyl (3*R*,4*S*,5*R*)-3,4,5-trihydroxycyclohex-1-ene-1-carboxylate as off-white crystals (4.35 g, 22 mmol, 75%).

Mp = 85.6 - 86.7 ^{0}C;

$[\alpha]_D^{20}$ = -124 (*c* = 0.05, MeOH);

^{1}H NMR (300 MHz, Chloroform-*d*) δ 6.91 – 6.88 (1H, m, H^{3}), 4.47 (1H, t, *J* = 4.6 Hz, H^{2}), 4.22 (2H, q, *J* = 7.1 Hz, H^{8}), 3.98 (1H, td, *J* = 9.5, 5.5 Hz, H^{6}), 3.63 (1H, dd, *J* = 9.6, 4.6 Hz, H^{1}), 2.96 (1H, dd, *J* = 17.9, 5.5 Hz, H^{5}), 2.28 – 2.16 (1H, m, H^{5}), 1.30 (3H, t, *J* = 7.1 Hz, H^{9});

^{13}C NMR (75 MHz, Chloroform-*d*) δ_C 166.1 (C^{7}), 135.0 (C^{3}), 131.5 (C^{4}), 73.1(C^{2}), 67.0 (C^{1}), 66.0 (C^{6}), 61.1 (C^{8}), 32.1 (C^{5}), 14.1 (C^{9});

IR (neat): ν_{max}cm^{-1} 3330 (OH), 2984-2910 (CH), 1713 (C=O), 1655 (C=C).

n-Propyl (3*R*,4*S*,5*R*)-3,4,5-trihydroxycyclohex-1-ene-1-carboxylate (**5.02**)

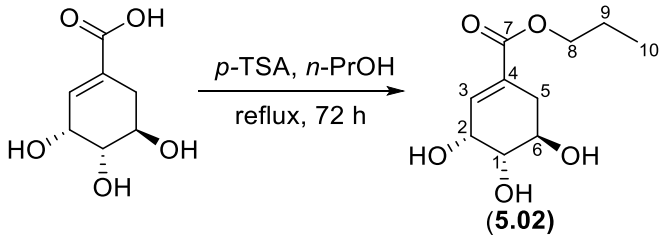

(**5.02**)

To a stirred round bottomed flask (250 mL) was added shikimic acid (2.00 g, 11.48 mmol), *n*-PrOH (100 mL) and *p*-toluenesulfonic acid monohydrate (0.21 g, 1.14 mmol). The resulting solution was put under a nitrogen atmosphere and heated at reflux. The reaction was monitored by TLC. After 72 h the reaction mixture was cooled, filtered and the solvent removed under reduced pressure. The crude product was recrystallized from hot EtOAc to afford propyl (3*R*,4*S*,5*R*)-3,4,5-trihydroxycyclohex-1-ene-1-carboxylate as an off-white crystal (1.51 g, 6.9 mmol, 61%).

Mp = 84.1- 85.2 ^{o}C;

^{1}H NMR (300 MHz, Chloroform-*d*) δ 6.77 (1H, d, *J* = 4.3 Hz, H^{3}), 4.36 (1H, t, *J* = 4.3 Hz, H^{2}), 4.03 (3H, t, *J* = 6.6 Hz, H^{8}), 3.97 – 3.89 (1H, m, H^{6}), 3.57 (1H, dd, *J* = 9.4, 4.2 Hz, H^{1}), 2.80 (1H, dd, *J* = 17.9, 5.1 Hz, H^{5}), 2.12 (1H, dd, *J* = 18.1, 7.7 Hz, H^{5}), 1.62 (2H, s, *J* = 7.2 Hz, H^{9}), 0.90 (3H, t, *J* = 7.4 Hz, H^{10});

^{13}C NMR (75 MHz, Chloroform-*d*) δ 166.7 (C^{7}), 135.9 (C3), 130.9 (C^{4}), 73.1 (C^{2}), 66.7 (C^{1}), 66.6 (C^{6}), 66.3 (C^{8}), 32.1 (C^{5}), 21.9 (C^{9}), 10.4 (C^{10});

IR (neat): v_{max}cm^{-1} 3344 (OH), 2968-2915 (CH), 1712 (C=O), 1656 (C=C)

Observed data (^{1}H, ^{13}C, IR) are consistent with that previously reported by Shoji[16].

Isopropyl (3*R*,4*S*,5*R*)-3,4,5-trihydroxycyclohex-1-ene-1-carboxylate (**5.03**)

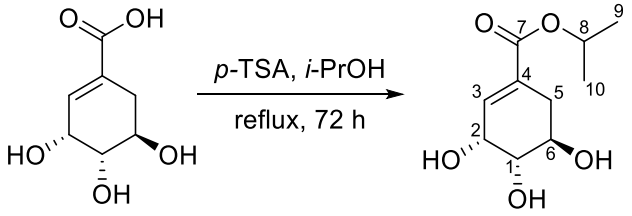

(**5.03**)

To a stirred round bottomed flask (250 mL) was added shikimic acid (5.00 g, 28.7 mmol), followed by *i*-PrOH (125 mL) and then *p*-TSA (0.50 g, 2.6 mmol). The resulting solution was put under a nitrogen atmosphere and heated at reflux. The reaction was monitored by TLC. After 72 h. The reaction mixture was cooled, filtered and the solvent removed under reduced pressure. The crude product was purified by column chromatography (DCM: MeOH, 9: 1) to afford isopropyl (3*R*,4*S*,5*R*)-3,4,5-trihydroxycyclohex-1-ene-1-carboxylate as white crystals (4.59 g, 21 mmol, 74 %).

R_f = 0.28 (DCM:MeOH, 9:1; UV light);

Mp = 116.7 – 118.1 ^{0}C;

$[\alpha]_D^{20}$ = -134 (*c* = 0.1, MeOH);

^{1}H NMR (300 MHz, Chloroform-*d*) δ 6.89 – 6.84 (1H, m, H^3), 5.06 (1H, h, *J* = 6.3 Hz, H^8), 4.46 (1H, t, *J* = 4.5 Hz, H^2), 3.97 (1H, td, *J* = 9.4, 4.5 Hz, H^6), 3.62 (1H, dd, *J* = 9.5, 4.5 Hz, H^1), 2.94 (1H, dd, *J* = 17.9, 5.5 Hz, H^5), 2.26 – 2.15 (1H, m, H^5), 1.27 (6H, dd, *J* = 6.2, 1.0 Hz, H$^{9 \text{ and } 10}$);
^{13}C NMR (75 MHz, Chloroform-*d*) δ_C 165.7 (C^7), 134.8 (C^3), 132.0 (C^4), 73.3 (C^2), 68.7 (C^1), 67.2 (C^6), 66.1 (C^8), 32.3 (C^5), 21.9 (C$^{9 \text{ and } 10}$);
IR (neat): v_{max}cm^{-1} 3313 (OH), 2984-2877 (CH), 1714 (C=O), 1652 (C=C).

Benzyl (3*R*,4*S*,5*R*)-3,4,5-trihydroxycyclohex-1-ene-1-carboxylate (**5.04**)

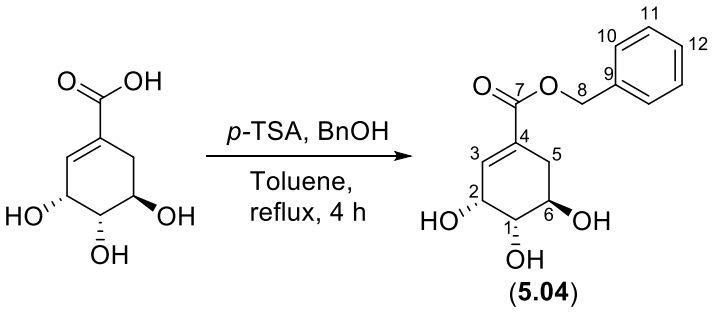

(**5.04**)

To a stirred round bottomed flask (250 mL) was added shikimic acid (1.00 g, 5.7 mmol), followed by *p*-TSA (1.2 g, 6.3 mmol) then toluene (20 mL) and BnOH (5 mL). The resulting solution was put under a nitrogen atmosphere and heated at reflux. After 4 h. The reaction mixture was cooled, filtered and the solvent removed under reduced pressure. The crude product was purified by column chromatography (DCM/MeOH, 9: 1) to give benzyl (3*R*,4*S*,5*R*)-3,4,5-trihydroxycyclohex-1-ene-1-carboxylate as a light brown oil in (0.56 g, 2.1 mmol, 37 %)

R_f = 0.36 (DCM:MeOH, 9:1; UV light);

$[\alpha]_D^{20}$ = -168 (*c* = 0.025, MeOH);

^{1}H NMR (300 MHz, $CDCl_3$) δ 7.28 – 7.23 (5H, m, H^9), 6.80 (1H, d, *J* = 4.7, Hz, H^3), 5.08 (2H, s, H^8), 4.31 (1H, t, *J* = 4.4 Hz, H^2), 3.92 (1H, m, H^6), 3.54 (1H, dd, *J* = 8.8, 4.4 Hz, H^1), 3.30 (s, 1H), 2.82 (1H, dd, *J* = 17.9, 5.4 Hz, H^5), 2.19 – 2.07 (1H, m, H^5).

^{13}C NMR (75 MHz, $CDCl_3$) δ 166.5 (C^7), 136.7 (C^3), 135.6 (C^4), 130.4 (C^9), 128.6 (C^{11}), 128.3 (C^{10}), 128.1 (C^{12}), 72.8 (C^2), 66.8 (C^1), 66.5 (C^6), 66.2 (C^8), 32.0 (C^5)

IR (neat): $v_{max}cm^{-1}$ 3307 (OH), 1638 (C=O).

(3*R*,4*S*,5*R*)-3,4,5-trihydroxy-*N*,*N*-dimethylcyclohex-1-ene-1-carboxamide (**5.05**)

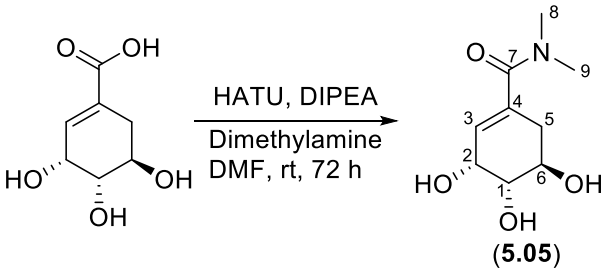

(**5.05**)

To a stirred round bottomed flask (250 mL) was added shikimic acid (1.00 g, 5.7 mmol), followed by HATU (2.6 g, 6.9 mmol) The round bottom flask was then put under a nitrogen atmosphere. Dry DMF (25 mL) was then added by syringe and the mixture stirred for 5 min. DIPEA (1.5 mL, 8.6 mmol) was then added by syringe followed by dimethyl amine (0.97 mL, 8.6 mmol) and the resultant reaction mixture was left stirring at rt. After 72 h, the solvent was removed under reduced pressure and the crude reaction material was purified by column chromatography (DCM/MeOH, 4: 1) to give (3*R*,4*S*,5*R*)-3,4,5-trihydroxy-*N*,*N*-dimethylcyclohex-1-ene-1-carboxamide as a clear oil (0.39 g, 1.9 mmol, 34 %).

R_f = 0.42 (DCM:MeOH, 4:1; UV light);

^{1}H NMR (300 MHz, $CDCl_3$) δ 6.88 (1H, d, *J* = 3.6 Hz, H^3), 5.43 (1H, dd, *J* = 7.5, 3.7 Hz H^2), 4.81 (1H, dd, *J* = 7.5, 6.7 Hz, H^1), 4.19 – 4.13 (1H, m, H^6), 3.81 (6H, s, $H^{8 \text{ and } 9}$), 2.77 – 2.70 (1H, m, H^5), 2.45 – 2.34 (1H, m, H^5),

^{13}C NMR (75 MHz, $CDCl_3$) δ 171.7 (C^7), 149.7 (C^4), 134.8 (C^3), 72.8 (C^2), 66.5 (C^1), 66.4 (C^6), 38.9 ($C^{8 \text{ and } 9}$), 33.6.(C^5).

IR (neat): $v_{max}cm^{-1}$ 3303 (OH), 2930 (CH), (1603 (C=O).

(3*R*,4*S*,5*R*)-*N*,*N*-diethyl-3,4,5-trihydroxycyclohex-1-ene-1-carboxamide (**5.06**)

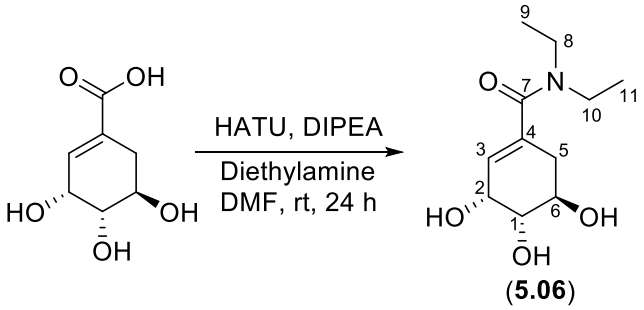

(**5.06**)

To a stirred round bottomed flask (250 mL) was added shikimic acid (1.00 g, 5.7 mmol), followed by HATU (2.6 g, 6.9 mmol) The round bottom flask was then put under a nitrogen atmosphere. Dry DMF (25 mL) was then added by syringe and the mixture stirred for 5 min. DIPEA (1.5 mL, 8.6 mmol) was then added by syringe followed by diethyl amine (0.89 mL, 8.6 mmol) and the resultant reaction mixture was left stirring at rt. After 24 h, the solvent was removed under reduced pressure and the crude reaction material was purified by column chromatography (DCM/MeOH, 4: 1) to give (3*R*,4*S*,5*R*)-*N*,*N*-diethyl-3,4,5-trihydroxycyclohex-1-ene-1-carboxamide as a clear oil (0.70 g, 3.0 mmol, 53 %).

R_f = 0.6 (DCM:MeOH, 4:1; UV light);

^{1}H NMR (300 MHz, $CDCl_3$) δ 5.81 – 5.74 (1H, m, H^3), 4.37 (1H, t, *J* = 4.4 Hz, H^2), 4.05 (td, *J* = 8.5, 5.4 Hz, H^6), 3.66 (1H, dd, *J* = 9.2, 5.3 Hz, H^1), 3.36 (4H, q, *J* = 6.8 Hz, $H^{8 \text{ and } 10}$), 2.68 (1H, dd, *J* = 17.6, 5.4 Hz, H^5), 2.25 (1H, dd, *J* = 18.0, 8.2 Hz, H^5), 1.14 (6H, t, *J* = 7.0 Hz, $H^{9 \text{ and } 11}$).

^{13}C NMR (75 MHz, $CDCl_3$) δ 171.8 (C^7), 150.1 (C^4), 134.8 (C^3), 72.9 (C^2), 66.6 (C^1), 66.4 (C^6), 43.8 ($C^{8 \text{ and } 10}$), 33.6.(C^5), 12.9 ($C^{9 \text{ and } 11}$).

IR (neat): ν_{max}cm^{-1} 3351 (OH), 2976 (CH), 1586 (C=O).

6.6 X-Ray Crystallography Data

The following crystal structure data were collected on a Xcalibur, Atlas, Gemini ultra diffractometer equipped with a fine-focus sealed X-ray tube (λ CuKα = 1.54184 Å) and an Oxford Cryosystems CryostreamPlus open-flow N2 cooling device. All crystals were grown by slow solvent evaporation. A list of solvents used to successfully grow single crystal structures is provided in chapter 5.The analysis of the X-ray diffraction data of all the following compounds were performed by Dr Paul Waddell.

Crystal structure determination of: **2.17**

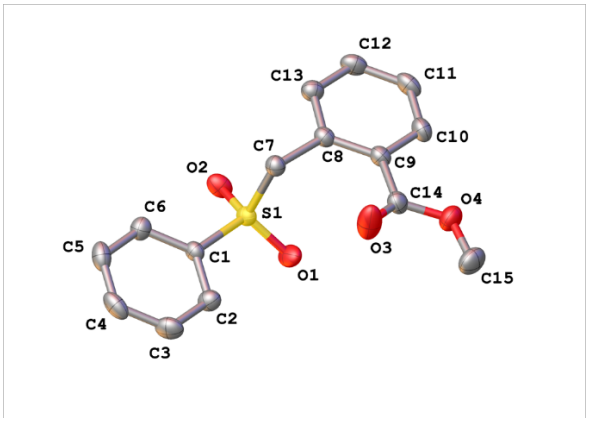

Crystal data and structure refinement for **2.17**

Identification code	mjh200001_fa
Empirical formula	$C_{15}H_{14}O_4S$
Formula weight	290.32
Temperature/K	150.0(2)
Crystal system	Monoclinic
Space group	I2/a
a/Å	15.2893(4)
b/Å	5.43113(14)
c/Å	32.7743(10)
α/°	90
β/°	94.253(3)
γ/°	90

Volume/Å^3	2714.04(13)
Z	8
ρ_{calc}g/cm^3	1.421
μ/mm^{-1}	2.224
F(000)	1216.0
Crystal size/mm^3	0.39 × 0.12 × 0.02
Radiation	CuKα (λ = 1.54184)
2Θ range for data collection/°	10.828 to 133.696
Index ranges	-18 ≤ h ≤ 18, -6 ≤ k ≤ 6, -38 ≤ l ≤ 39
Reflections collected	10173
Independent reflections	2416 [R_{int} = 0.0316, R_{sigma} = 0.0233]
Data/restraints/parameters	2416/0/182
Goodness-of-fit on F^2	1.028
Final R indexes [I>=2σ (I)]	R_1 = 0.0352, wR_2 = 0.0871
Final R indexes [all data]	R_1 = 0.0405, wR_2 = 0.0914
Largest diff. peak/hole / e Å^{-3}	0.41/-0.34

Crystal structure determination of: **2.22**

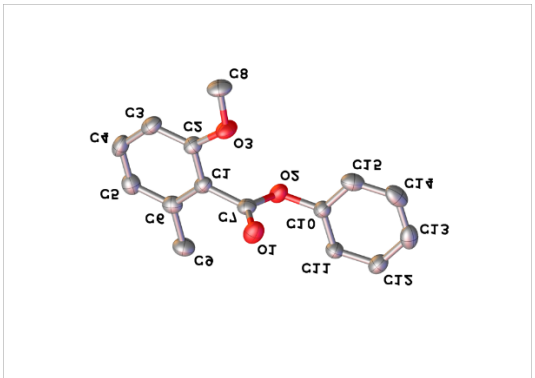

Crystal data and structure refinement for **2.22**

Identification code	mjh200026_fa
Empirical formula	$C_{15}H_{14}O_3$
Formula weight	242.26
Temperature/K	150.0(2)
Crystal system	monoclinic
Space group	$P2_1$
a/Å	5.62115(18)
b/Å	11.1341(4)
c/Å	20.3666(7)
α/°	90
β/°	96.952(3)
γ/°	90
Volume/Å^3	1265.30(8)
Z	4
ρ_{calc}g/cm^3	1.272
μ/mm^{-1}	0.718
F(000)	512.0
Crystal size/mm^3	0.37 × 0.12 × 0.06
Radiation	CuKα (λ = 1.54184)
2Θ range for data collection/°	8.748 to 133.664

Index ranges	$-5 \leq h \leq 6, -13 \leq k \leq 13, -23 \leq l \leq 24$
Reflections collected	9578
Independent reflections	3969 [R_{int} = 0.0455, R_{sigma} = 0.0502]
Data/restraints/parameters	3969/1/330
Goodness-of-fit on F^2	1.073
Final R indexes [I>=2σ (I)]	R_1 = 0.0386, wR_2 = 0.0799
Final R indexes [all data]	R_1 = 0.0512, wR_2 = 0.0879
Largest diff. peak/hole / e $Å^{-3}$	0.14/-0.14
Flack parameter	-0.32(17)

Crystal structure determination of: **3.12**

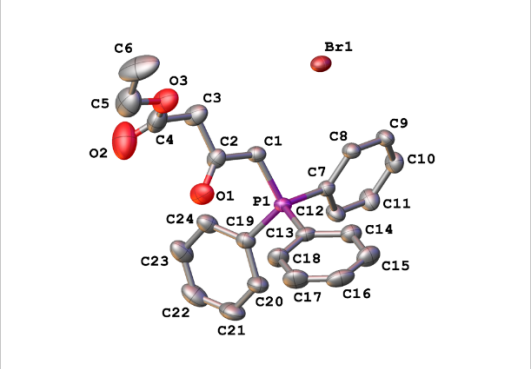

Crystal data and structure refinement for **3.12**

Identification code	mjh180011
Empirical formula	$C_{24}H_{24}BrO_3P$
Formula weight	471.31
Temperature/K	150.0(2)
Crystal system	orthorhombic
Space group	$P2_12_12_1$
a/Å	14.8743(3)
b/Å	17.0841(4)
c/Å	17.5529(3)
α/°	90
β/°	90
γ/°	90
Volume/Å^3	4460.43(16)
Z	8
ρ_{calc}g/cm^3	1.404
μ/mm^{-1}	3.366
F(000)	1936.0
Crystal size/mm^3	0.2 × 0.12 × 0.06
Radiation	CuKα (λ = 1.54184)
2Θ range for data collection/°	7.22 to 133.944

Index ranges	$-17 \leq h \leq 11$, $-19 \leq k \leq 20$, $-20 \leq l \leq 19$
Reflections collected	31741
Independent reflections	7879 [R_{int} = 0.0470, R_{sigma} = 0.0369]
Data/restraints/parameters	7879/0/525
Goodness-of-fit on F^2	1.026
Final R indexes [I>=2σ (I)]	R_1 = 0.0343, wR_2 = 0.0855
Final R indexes [all data]	R_1 = 0.0389, wR_2 = 0.0887
Largest diff. peak/hole / e $Å^{-3}$	0.50/-0.36
Flack parameter	-0.098(14)

Crystal structure determination of: **3.13**

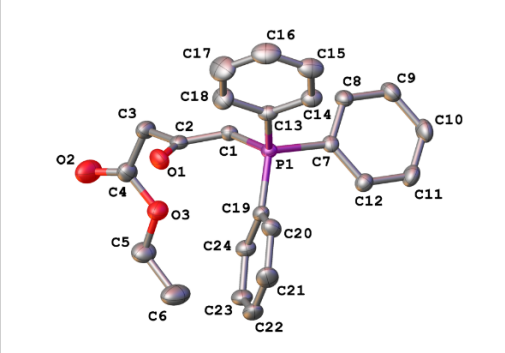

Crystal data and structure refinement for **3.13**.

Identification code	mjh180019
Empirical formula	$C_{25}H_{24}Cl_3O_3P$
Formula weight	509.76
Temperature/K	150.0(2)
Crystal system	triclinic
Space group	P-1
a/Å	8.7100(2)
b/Å	10.6752(3)
c/Å	13.7410(4)
α/°	96.188(2)
β/°	96.443(2)
γ/°	100.155(2)
Volume/Å^3	1239.03(6)
Z	2
ρ_{calc}g/cm^3	1.366
μ/mm^{-1}	4.161
F(000)	528.0
Crystal size/mm^3	0.41 × 0.23 × 0.05
Radiation	CuKα (λ = 1.54184)
2Θ range for data collection/°	8.488 to 133.702
Index ranges	-10 ≤ h ≤ 10, -12 ≤ k ≤ 12, -16 ≤ l ≤ 16

Reflections collected	33931
Independent reflections	4388 [R_{int} = 0.0359, R_{sigma} = 0.0172]
Data/restraints/parameters	4388/0/290
Goodness-of-fit on F^2	1.044
Final R indexes [I>=2σ (I)]	R_1 = 0.0402, wR_2 = 0.1063
Final R indexes [all data]	R_1 = 0.0448, wR_2 = 0.1103
Largest diff. peak/hole / e $Å^{-3}$	0.65/-0.63

Crystal structure determination of: **3.16**

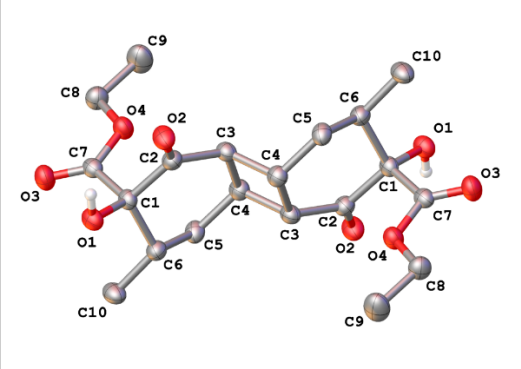

Crystal data and structure refinement for **3.16**

Identification code	mjh190018_fa_twin1_hklf4
Empirical formula	$C_{20}H_{28}O_8$
Formula weight	396.42
Temperature/K	150.0(2)
Crystal system	triclinic
Space group	P-1
a/Å	6.3257(2)
b/Å	7.2100(4)
c/Å	10.9771(9)
α/°	76.430(5)
β/°	79.641(5)
γ/°	87.367(4)
Volume/Å^3	478.73(5)
Z	1
ρ_{calc}g/cm^3	1.375
μ/mm^{-1}	0.887
F(000)	212.0
Crystal size/mm^3	0.15 × 0.1 × 0.02
Radiation	CuKα (λ = 1.54184)
2Θ range for data collection/°	8.414 to 134.018

Index ranges	$-7 \leq h \leq 7, -8 \leq k \leq 8, -13 \leq l \leq 13$
Reflections collected	3232
Independent reflections	3232 [R_{int} = ?, R_{sigma} = 0.0196]
Data/restraints/parameters	3232/0/133
Goodness-of-fit on F^2	1.062
Final R indexes [I>=2σ (I)]	R_1 = 0.0373, wR_2 = 0.0923
Final R indexes [all data]	R_1 = 0.0482, wR_2 = 0.0971
Largest diff. peak/hole / e $Å^{-3}$	0.28/-0.18

Crystal structure determination of: **4.06**

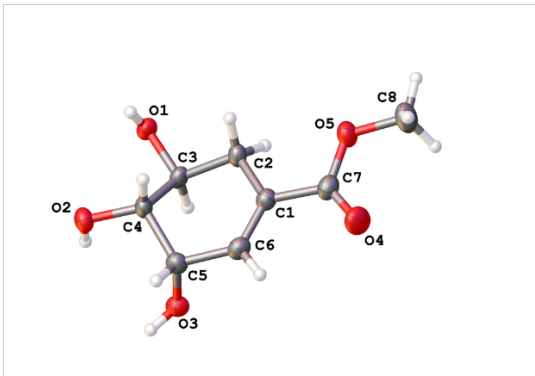

Crystal data and structure refinement for **4.06.**

Identification code	mjh170029
Empirical formula	$C_8H_{12}O_5$
Formula weight	188.18
Temperature/K	100.0(2)
Crystal system	monoclinic
Space group	$P2_1$
a/Å	25.5964(6)
b/Å	6.38050(10)
c/Å	33.7807(7)
α/°	90
β/°	108.702(2)
γ/°	90
Volume/Å^3	5225.69(19)
Z	24
ρ_{calc}g/cm^3	1.435
μ/mm^{-1}	0.113
F(000)	2400.0
Crystal size/mm^3	0.331 × 0.022 × 0.01
Radiation	? (λ = 0.6889)
2Θ range for data collection/°	1.628 to 53.146

Index ranges	$-33 \leq h \leq 33, -8 \leq k \leq 8, -43 \leq l \leq 43$
Reflections collected	73705
Independent reflections	23672 [R_{int} = 0.0887, R_{sigma} = 0.0870]
Data/restraints/parameters	23672/37/1528
Goodness-of-fit on F^2	0.925
Final R indexes [I>=2σ (I)]	R_1 = 0.0498, wR_2 = 0.1198
Final R indexes [all data]	R_1 = 0.0865, wR_2 = 0.1339
Largest diff. peak/hole / e $Å^{-3}$	0.33/-0.27
Flack parameter	1.9(4)

Crystal structure determination of: **4.07**

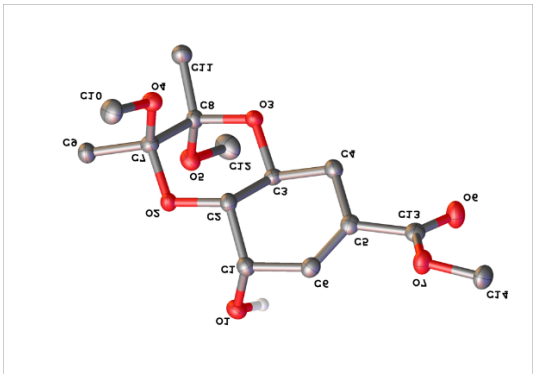

Crystal data and structure refinement for **4.07**

Identification code	mjh170002_fa
Empirical formula	$C_{14}H_{22}O_7$
Formula weight	302.31
Temperature/K	150.0(2)
Crystal system	monoclinic
Space group	$P2_1$
a/Å	6.87750(10)
b/Å	9.42550(10)
c/Å	11.24460(10)
α/°	90
β/°	97.0130(10)
γ/°	90
Volume/Å^3	723.465(15)
Z	2
ρ_{calc}g/cm^3	1.388
μ/mm^{-1}	0.940
F(000)	324.0
Crystal size/mm^3	0.2 × 0.1 × 0.04
Radiation	CuKα (λ = 1.54184)
2Θ range for data collection/°	7.922 to 133.648

Index ranges	$-8 \leq h \leq 8, -11 \leq k \leq 11, -13 \leq l \leq 13$
Reflections collected	19670
Independent reflections	2555 [R_{int} = 0.0345, R_{sigma} = 0.0166]
Data/restraints/parameters	2555/1/198
Goodness-of-fit on F^2	1.050
Final R indexes [I>=2σ (I)]	R_1 = 0.0245, wR_2 = 0.0606
Final R indexes [all data]	R_1 = 0.0265, wR_2 = 0.0624
Largest diff. peak/hole / e $Å^{-3}$	0.15/-0.14
Flack parameter	0.06(6)

Crystal structure determination of: **4.08**

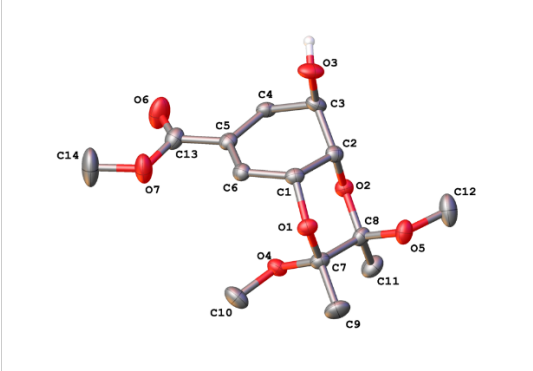

Crystal data and structure refinement for **4.08.**

Identification code	mjh170001_fa
Empirical formula	$C_{14}H_{22}O_7$
Formula weight	302.31
Temperature/K	150.0(2)
Crystal system	monoclinic
Space group	$P2_1$
a/Å	7.98700(10)
b/Å	10.81063(17)
c/Å	8.98516(11)
α/°	90
β/°	95.2572(11)
γ/°	90
Volume/Å^3	772.555(18)
Z	2
ρ_{calc}g/cm^3	1.300
μ/mm^{-1}	0.880
F(000)	324.0
Crystal size/mm^3	0.26 × 0.04 × 0.04
Radiation	CuKα (λ = 1.54184)
2Θ range for data collection/°	9.886 to 133.734

Index ranges	$-9 \leq h \leq 9, -12 \leq k \leq 11, -10 \leq l \leq 10$
Reflections collected	21032
Independent reflections	2677 [R_{int} = 0.0347, R_{sigma} = 0.0176]
Data/restraints/parameters	2677/1/198
Goodness-of-fit on F^2	1.030
Final R indexes [I>=2σ (I)]	R_1 = 0.0273, wR_2 = 0.0657
Final R indexes [all data]	R_1 = 0.0299, wR_2 = 0.0678
Largest diff. peak/hole / e $Å^{-3}$	0.12/-0.19
Flack parameter	0.00(6)

Crystal structure determination of: **4.12**

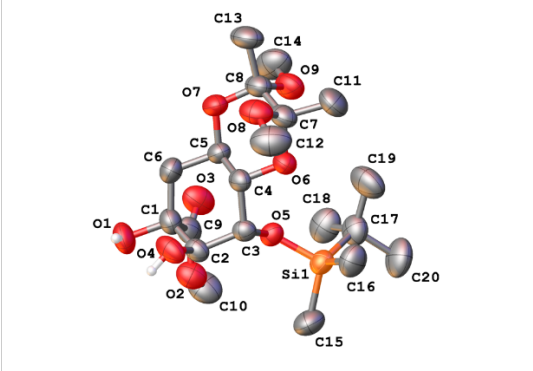

Crystal data and structure refinement for **4.12**

Identification code	mjh170021_fa
Empirical formula	$C_{20}H_{38}O_9Si$
Formula weight	450.59
Temperature/K	240.0(2)
Crystal system	Monoclinic
Space group	$P2_1$
a/Å	14.4321(2)
b/Å	9.84692(16)
c/Å	18.7141(3)
α/°	90
β/°	108.7387(17)
γ/°	90
Volume/Å^3	2518.52(7)
Z	4
ρ_{calc}g/cm^3	1.188
μ/mm^{-1}	1.196
F(000)	976.0
Crystal size/mm^3	0.4 × 0.11 × 0.06
Radiation	CuKα (λ = 1.54184)
2Θ range for data collection/°	9.356 to 133.996

Index ranges	$-17 \leq h \leq 17, -11 \leq k \leq 10, -22 \leq l \leq 22$
Reflections collected	69592
Independent reflections	8754 [R_{int} = 0.0463, R_{sigma} = 0.0211]
Data/restraints/parameters	8754/740/631
Goodness-of-fit on F^2	1.032
Final R indexes [I>=2σ (I)]	R_1 = 0.0408, wR_2 = 0.1085
Final R indexes [all data]	R_1 = 0.0481, wR_2 = 0.1160
Largest diff. peak/hole / e $Å^{-3}$	0.34/-0.23
Flack parameter	-0.029(13)

Crystal structure determination of: **5.01**

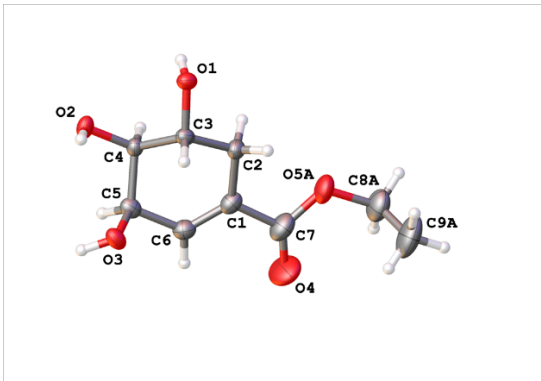

Crystal data and structure refinement for **5.01.**

Identification code	mjh180028_fa
Empirical formula	$C_9H_{14}O_5$
Formula weight	202.20
Temperature/K	150.0(2)
Crystal system	Monoclinic
Space group	C2
a/Å	16.7981(6)
b/Å	6.43158(19)
c/Å	19.1864(8)
α/°	90
β/°	106.640(4)
γ/°	90
Volume/Å^3	1986.06(13)
Z	8
ρ_{calc}g/cm^3	1.352
μ/mm^{-1}	0.942
F(000)	864.0
Crystal size/mm^3	0.29 × 0.05 × 0.02
Radiation	CuKα (λ = 1.54184)
2Θ range for data collection/°	9.622 to 133.824

Index ranges	$-20 \leq h \leq 19$, $-6 \leq k \leq 7$, $-22 \leq l \leq 22$
Reflections collected	7668
Independent reflections	3104 [R_{int} = 0.0412, R_{sigma} = 0.0467]
Data/restraints/parameters	3104/462/347
Goodness-of-fit on F^2	1.045
Final R indexes [I>=2σ (I)]	R_1 = 0.0386, wR_2 = 0.0880
Final R indexes [all data]	R_1 = 0.0499, wR_2 = 0.0954
Largest diff. peak/hole / e $Å^{-3}$	0.18/-0.16
Flack parameter	-0.01(16)

Crystal structure determination of: **5.03**

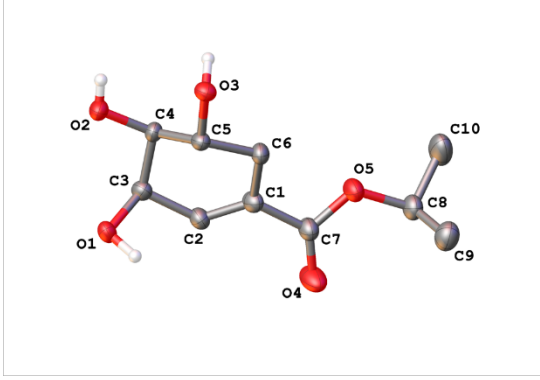

Crystal data and structure refinement for **5.03.**

Identification code	mjh180041_fa
Empirical formula	$C_{10}H_{16}O_5$
Formula weight	216.23
Temperature/K	150.0(2)
Crystal system	Monoclinic
Space group	$P2_1$
a/Å	5.8032(4)
b/Å	7.5952(5)
c/Å	12.0400(11)
α/°	90
β/°	90.067(7)
γ/°	90
Volume/Å^3	530.68(7)
Z	2
ρ_{calc}g/cm^3	1.353
μ/mm^{-1}	0.916
F(000)	232.0
Crystal size/mm^3	0.33 × 0.04 × 0.02
Radiation	CuKα (λ = 1.54184)
2Θ range for data collection/°	7.342 to 133.748

Index ranges	$-6 \leq h \leq 6, -9 \leq k \leq 8, -14 \leq l \leq 14$
Reflections collected	7597
Independent reflections	1692 [R_{int} = 0.0541, R_{sigma} = 0.0416]
Data/restraints/parameters	1692/112/149
Goodness-of-fit on F^2	1.059
Final R indexes [I>=2σ (I)]	R_1 = 0.0361, wR_2 = 0.0853
Final R indexes [all data]	R_1 = 0.0392, wR_2 = 0.0882
Largest diff. peak/hole / e $Å^{-3}$	0.18/-0.17
Flack parameter	-0.03(18)

Crystal structure determination of: **5.05**

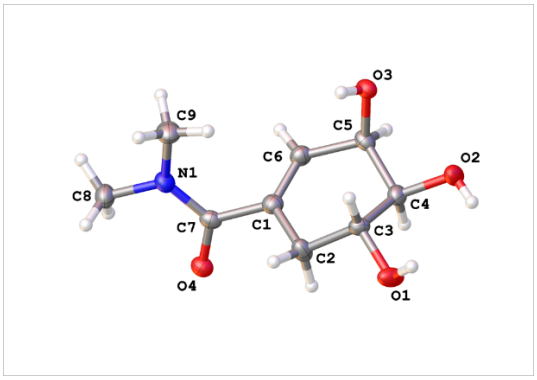

Crystal data and structure refinement for **5.05**

Identification code	mjh190016_fa
Empirical formula	$C_{10}H_{16}Cl_3NO_4$
Formula weight	320.59
Temperature/K	150.0(2)
Crystal system	Triclinic
Space group	P1
a/Å	6.0239(2)
b/Å	7.3958(2)
c/Å	16.0305(6)
α/°	97.738(3)
β/°	93.627(3)
γ/°	93.971(3)
Volume/Å^3	704.07(4)
Z	2
ρ_{calc}g/cm^3	1.512
μ/mm^{-1}	5.971
F(000)	332.0
Crystal size/mm^3	0.33 × 0.13 × 0.02
Radiation	CuKα (λ = 1.54184)
2Θ range for data collection/°	11.17 to 133.652

Index ranges	$-7 \leq h \leq 6, -8 \leq k \leq 8, -19 \leq l \leq 19$
Reflections collected	19148
Independent reflections	4816 [R_{int} = 0.0383, R_{sigma} = 0.0320]
Data/restraints/parameters	4816/3/347
Goodness-of-fit on F^2	1.046
Final R indexes [I>=2σ (I)]	R_1 = 0.0293, wR_2 = 0.0694
Final R indexes [all data]	R_1 = 0.0345, wR_2 = 0.0727
Largest diff. peak/hole / e $Å^{-3}$	0.21/-0.19
Flack parameter	-0.010(11)

Crystal structure determination of: 2:1 co-crystal of **4.01** and **5.03**

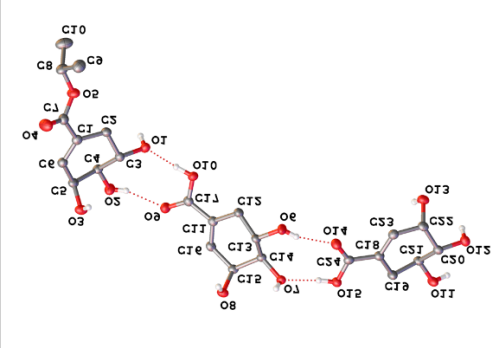

Crystal data and structure refinement for 2: 1 co-crystal of **4.01** and **5.03**

Identification code	mjh180038
Empirical formula	$C_{24}H_{36}O_{15}$
Formula weight	564.53
Temperature/K	150.0(2)
Crystal system	Monoclinic
Space group	$P2_1$
a/Å	5.86051(13)
b/Å	7.83710(18)
c/Å	27.3953(8)
α/°	90
β/°	89.357(2)
γ/°	90
Volume/Å^3	1258.17(6)
Z	2
ρ_{calc}g/cm^3	1.490
μ/mm^{-1}	1.072
F(000)	600.0
Crystal size/mm^3	0.25 × 0.18 × 0.02
Radiation	CuKα (λ = 1.54184)
2Θ range for data collection/°	9.686 to 133.866
Index ranges	-6 ≤ h ≤ 6, -9 ≤ k ≤ 9, -32 ≤ l ≤ 31

Reflections collected	17478
Independent reflections	4438 [R_{int} = 0.0484, R_{sigma} = 0.0411]
Data/restraints/parameters	4438/1/387
Goodness-of-fit on F^2	1.050
Final R indexes [I>=2σ (I)]	R_1 = 0.0347, wR_2 = 0.0800
Final R indexes [all data]	R_1 = 0.0411, wR_2 = 0.0837
Largest diff. peak/hole / e $Å^{-3}$	0.18/-0.17
Flack parameter	-0.03(11)

Appendix

Chem

CellPress

Article

Encapsulated Nanodroplet Crystallization of Organic-Soluble Small Molecules

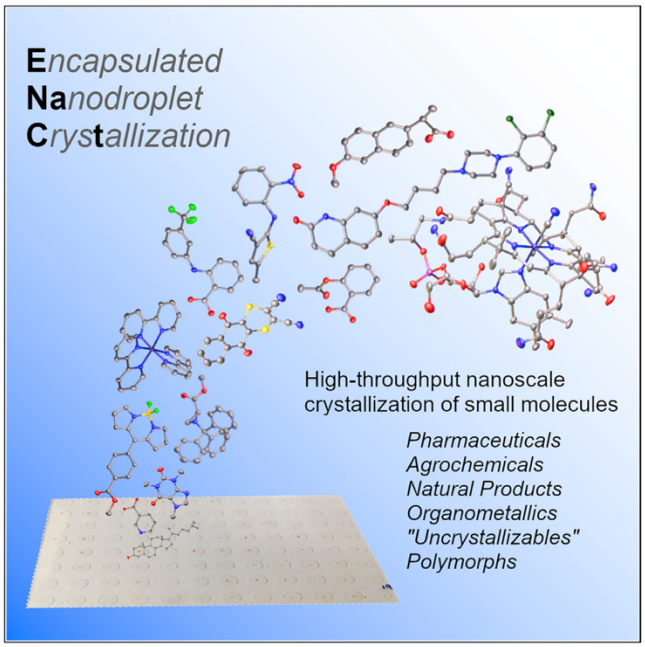

The routine crystallization of small molecules for single-crystal X-ray analysis remains a considerable experimental challenge. We report a general method for the high-throughput nanoscale crystallization of organic-soluble small molecules: encapsulated nanodroplet crystallization (ENaCt). ENaCt provides crystals suitable for X-ray analysis, allowing structural and *de novo* absolute stereochemical assignment for a diverse and challenging range of small molecules (bioactives, natural products, organometallics, etc.), as well as acting as a tool for new polymorph discovery.

Andrew R. Tyler, Ronnie Ragbirsingh, Charles J. McMonagle, ..., Paul Thaw, Michael J. Hall, Michael R. Probert

michael.hall@ncl.ac.uk (M.J.H.)
michael.probert@ncl.ac.uk (M.R.P.)

HIGHLIGHTS

Single crystals of small molecules are grown from nanoscale droplets of organic solvent

Discovery of the 13th polymorph (R18) of olanzapine precursor ROY

X-ray diffraction analysis of "uncrystallizable" agrochemical dithianon

Tyler et al., Chem 6, 1755–1765
July 9, 2020
https://doi.org/10.1016/j.chempr.2020.04.009

Chem

CellPress

Article

Encapsulated Nanodroplet Crystallization of Organic-Soluble Small Molecules

Andrew R. Tyler,[1] Ronnie Ragbirsingh,[1] Charles J. McMonagle,[1] Paul G. Waddell,[1] Sarah E. Heaps,[2] Jonathan W. Steed,[3] Paul Thaw,[4] Michael J. Hall,[1,5,*] and Michael R. Probert[1,*]

SUMMARY

Single-crystal X-ray diffraction analysis (SCXRD) constitutes a universal approach for the elucidation of molecular structure and the study of crystalline forms. However, the discovery of viable crystallization conditions remains both experimentally challenging and resource intensive in both time and the quantity of analyte(s). We report a robot-assisted, high-throughput method for the crystallization of organic-soluble small molecules in which we employ only micrograms of analyte per experiment. This allows hundreds of crystallization conditions to be screened in parallel with minimal overall sample requirements. Crystals suitable for SCXRD are grown from nanoliter droplets of a solution of analyte in organic solvent(s), each of which is encapsulated within an inert oil to control the rate of solvent loss. This encapsulated nanodroplet crystallization methodology can also be used to search for new crystal forms, as exemplified through both our discovery of a new (13th) polymorph of the olanzapine precursor ROY and SCXRD analysis of the "uncrystallizable" agrochemical dithianon.

INTRODUCTION

Single-crystal X-ray diffraction (SCXRD) allows for the direct analysis of crystalline small molecules, providing structural information with sub-Ångstrom resolution,[1] *de novo* absolute stereochemistry assignment (via anomalous dispersion),[2] and detailed information on intermolecular interactions and structural packing motifs. Modern in-house single-crystal diffraction instrumentation (e.g., microfocus X-ray tubes, multi-layer focusing optics, and very-low-noise area detectors) allows for the routine investigation of crystals, containing only light atoms, with dimensions ≈ 50 μm.[3] That, in combination with improved access to synchrotron radiation sources (e.g., remote-access beamlines),[4] has allowed SCXRD to become a ubiquitous research technique for molecular analysis, given a suitable crystalline sample; as of 2019, over one million crystal structures have been deposited in the Cambridge Crystallographic Data Centre (CCDC).[5]

Most small molecules are capable of existing as crystalline solids either as pure materials or in conjunction with other species (e.g., salts, hydrates, solvates, or co-crystals)[6] and thus are theoretically amenable to SCXRD analysis. However, the growth of suitably sized, high-quality single crystals remains experimentally challenging in that researchers still rely on time-consuming manual methods (i.e., solvent evaporation, exchange, or diffusion experiments),[7] which typically take many weeks to complete and require milligrams of analyte per experiment.

Recently, a number of approaches have attempted to circumnavigate the problems associated with traditional small-molecule crystal growth while retaining the

The Bigger Picture

Small molecules can form crystalline solids, in which individual molecules pack together into ordered three-dimensional arrays. Once a suitable crystal is grown, the packing and atomic connectivity of the constituent molecules can be studied by X-ray diffraction. However, the discovery of experimental conditions for successful crystal growth is often challenging. We have developed a nanoscale crystallization technique for organic-soluble small molecules by using high-throughput liquid-handling robotics to undertake multiple crystallization experiments simultaneously with minimal sample requirements and high success rates. We showcase our methodology through the crystallization of a diverse set of small molecules, including "uncrystallizables," combined with structural analysis by X-ray diffraction. We anticipate that this rapid and reliable method for small-molecule crystallization will have far-reaching impact, facilitating academic and industrial research in the molecular sciences.

analytical power provided by diffraction-based techniques. Fujita's "crystalline sponge" method relies on the long-range ordering of small organic "guest" molecules within a single crystal of a pre-prepared porous host, and subsequent SCXRD analysis of this host-guest complex provides structural information on the guest molecule.[8,9] However, as a result of weak host-guest interactions, the small-molecule guest must be carefully paired with an appropriate host, and the physical separation of guest molecules precludes analysis of any potential intermolecular interactions or other solid-state properties. Electron diffraction (e.g., MicroED) has subsequently emerged as a technique for the analysis of crystalline small molecules, where electron diffraction patterns are obtained from small single crystals (1–10 μm in each dimension).[10–12] However, the intensity of the electron beam causes rapid sample degradation via *in situ* radical generation; the crystals must be stable within the vacuum stage (precluding the study of hydrates and solvates), and the elucidation of absolute stereochemistry is far from routine (e.g., dynamical refinement).[13]

Thus, SCXRD remains the analytical technique of choice for the study of small molecules, although it is hampered by the practical constraints of crystal growth. Easy access to single crystals, suitable for SCXRD, would therefore be a significant enabling step across the molecular sciences. Solution-phase crystallization commences with nucleation from a supersaturated solution followed by crystal growth.[14] Nucleation is a stochastic process that, especially in the case of heterogeneous nucleation, is heavily influenced by the local environment (e.g., solvent[s], impurities, contact surfaces, and convection). Therefore, control is required over both the conditions of supersaturation and the number of nucleation sites present. The solid-state energy landscape of a molecule can be further complicated by the existence of multiple crystalline forms (e.g., salts, hydrates, solvates, co-crystals, or polymorphs). Hence, the discovery of successful crystallization conditions requires the exploration of large volumes of experimental space. Despite considerable research into the development of new small-molecule crystallization techniques, the current state of the art still requires the use of milligrams of analyte per experiment or is restricted to specific molecular classes, limiting the experimentally accessible envelope.[15–18]

Here, we discuss our use of high-throughput crystallization techniques as a general method for the growth of single crystals of organic-soluble small molecules on the nanoscale. Taking inspiration from "microbatch-under-oil" protein crystallization techniques,[19,20] our key enabling breakthrough involves the use of inert viscous oils to control the rate of solvent loss from nanoliter-scale droplets of organic solvent, each containing a few micrograms of small-molecule analyte. Oil encapsulation results in a slow increase in sample concentration up to and beyond the point of saturation, even for nanoliter-scale droplets of volatile organic solvents. When oil encapsulation is combined with the restricted number of nucleation sites available in such small droplets, we observe the growth of high-quality single crystals with dimensions $\geq$ 20 μm. These crystals are shown to provide excellent X-ray diffraction data sets on either in-house instrumentation or central facility beamlines.

We also show that encapsulated nanodroplet crystallization (ENaCt) experiments can be efficiently set up via a suitable liquid-handling robot, resulting in a semi-automated experimental approach in which hundreds of individual crystallization experiments can be initiated within a few minutes. This high-throughput parallel screening approach allows for rapid exploration of crystallization space and thus reliable access to suitable crystals. This is demonstrated here through the successful crystallization and SCXRD analysis of 14 structurally diverse molecules, including *de novo* absolute stereochemical analysis, polymorph discovery (including a hitherto

[1]Chemistry, School of Natural and Environmental Sciences, Newcastle University, Newcastle upon Tyne NE1 7RU, UK

[2]School of Mathematics, Statistics and Physics, Newcastle University, Newcastle upon Tyne NE1 7RU, UK

[3]Department of Chemistry, Durham University, Durham DH1 3LE, UK

[4]SPT Labtech, Melbourn Science Park, Melbourn, Hertfordshire SG8 6HB, UK

[5]Lead Contact

*Correspondence: michael.hall@ncl.ac.uk (M.J.H.), michael.probert@ncl.ac.uk (M.R.P.)

https://doi.org/10.1016/j.chempr.2020.04.009

unknown 13th polymorph of 5-methyl-2-[(2-nitrophenyl)amino]-3-thiophenecarbonitrile [ROY], R18), and the crystallization of "uncrystallizable" substrates (dithianon).

RESULTS AND DISCUSSION

Preliminary Oil-Encapsulated Nanodroplet Crystallizations

Nanoscale crystallizations are typically incompatible with the use of analyte solutions containing a high percentage of organic solvents because rapid solvent evaporation leads to deposition of the analyte as amorphous material. The rate of evaporative loss is proportional to the air-liquid interface surface area and is thus rapid in terms of percentage volume for a nanoliter-scale droplet.

We postulated that the evaporative loss from a nanodroplet of organic solvent could be slowed by reduction of the air-liquid interface surface area by encapsulation of said nanodroplet within a droplet of oil. This slower, more controlled concentration of the analyte would lead to improved crystal growth.

It should be noted that using oils to aid in the growth of single crystals for X-ray diffraction analysis from aqueous buffer solutions is known in protein crystallization[19,20] and has recently been applied to the crystallization of highly water-soluble salts of small organic molecules.[21] However, this "microbatch-under-oil" approach requires the use of aqueous solutions of water-soluble molecular analytes, typically in combination with low-density, mobile paraffin oils, to ensure phase separation while maintaining droplet mobility. These conditions are incompatible with most small organic molecular analytes because of their poor solubility in the aqueous buffers utilized, and the direct exchange of the aqueous buffer in such an experiment with an organic solvent would make the maintenance of phase separation challenging. Therefore, we chose to focus on using viscous oils with low miscibility in common organic solvents to encapsulate our organic nanodroplets, thus maintaining droplet integrity and encapsulation of the analyte solution.

Furthermore, the oils utilized would have to exhibit low vapor pressures to prevent evaporation and be chemically inert because of the anticipated long contact times with the organic solvent utilized. Thus, we undertook a series of preliminary oil-encapsulated nanodroplet crystallization experiments that involved using an SPT Labtech mosquito® liquid-handling robot to place 250 nL droplets of different test oils into a 96-well glass plate (Laminex or SWISSSCI LCP 100-micron), into which 50 nL of a solution of a small organic molecule (ROY) in an appropriate organic solvent was placed. ROY was chosen as a test substrate because of its propensity to form distinctively colored crystals, facilitating visual analysis of the crystallization process. The resulting 96-well plates were sealed (glass cover) and stored at room temperature (RT), and each well was examined periodically for crystal formation by polarizing light optical microscopy. After several days, we observed the formation of large numbers of crystals, many of which were single crystals of sufficient dimensions for SCXRD (Figure 1), providing the initial experimental support for our research postulate (see Methods Video S1).

Comparison of Encapsulated versus Non-encapsulated Nanodroplet Crystallizations

On the basis of these preliminary results, we attempted to further validate our experimental design through a comparison of organic-solvent-based nanodroplet crystallization conditions with and without oil encapsulation by employing a set of five representative small-molecule analytes: aspirin (**1**), caffeine (**2**), BODIPY (methyl 4-(5,5-difluoro-5*H*-4λ,^{4}5λ^4-dipyrrolo[1,2-c:2′,1′-*f*][1,3,2]diazaborinin-10-yl)benzoate) (**3**), (*R*)-BINOL (**4**), and

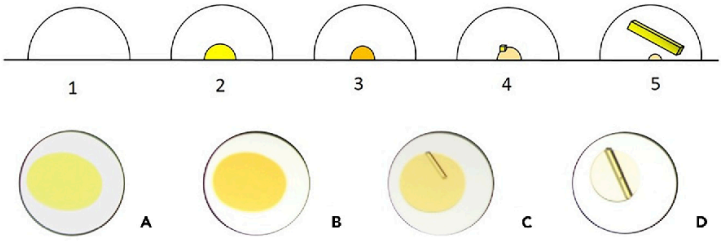

Figure 1. Cross-Section Schematic of an ENaCt Experiment (Top) and ENaCt Experiment with 200 nL Mineral Oil and 50 mg/mL ROY in DMSO (Bottom).

(1) Viscous inert oil dispensed onto a well of a 96-well glass plate, (2) solution of analyte in organic solvent injected into an oil droplet, (3) evaporative solvent loss to supersaturation, (4) nucleation, and (5) crystal growth. (A) solution of solvated analyte under oil, (B) evaporative solvent loss to supersaturation, (C) onset of crystal growth, and (D) complete crystallization.

(*S*)-naproxen (5). An SPT Labtech mosquito® liquid-handling robot was used to dispense the first two test oils (50–300 nL of Fluorinert FC-40 and polydimethyl siloxane [PDMSO]) on a 96-well glass plate (Laminex or SWISSCI LCP100-micron) and then dispense 50 nL of analyte solution in an organic solvent (40–50 mg/mL) either into the oil droplet or directly onto the plate. Six solvents were chosen—acetone, ethyl acetate, ethanol, 1,2-dichloroethane, *N*,*N*-dimethylformamide, and dimethyl sulfoxide—because they span a range of boiling points (bp = 56°C, 77°C, 79°C, 84°C, 153°C, and 189°C) and polarities (ε = 21, 6, 35, 11, 38, and 46). For control experiments employing no oil, we added additional solvent to give a total volume of 100–350 nL to maintain a comparable droplet size with oil-encapsulated experiments and thus a similar solvent-air interface area. After the experimental setup of the nanodroplets, the crystallization plates were partially sealed from atmospheric conditions with the use of a glass cover and stored at RT (see Supplemental Experimental Procedures). After 1, 3, 7, and 14 days, we photographed and assessed individual wells by optical, cross-polarizing light microscopy to establish the presence of single crystals. We chose 14 days as a common end point for the experiments to provide a balance between crystal formation and complete desolvation of the sample. Experimental outcomes were categorized on a 1–5 scale (1 = no solid [still solvated]; 2 = phase separation; 3 = solid [amorphous or microcrystalline]; 4 = small single crystals [<50 μm]; and 5 = large single crystals [>50 μm]) (Figure 2).

After 14 days, the majority of experiments had reached an end point (2–5). Visual inspection of the results showed that those crystallization conditions employing low-boiling-point solvents (acetone, ethyl acetate, and ethanol) without oil encapsulation had only given amorphous or microcrystalline solids resulting from the anticipated rapid evaporative solvent loss. Higher boiling solvents (1,2-dichloroethane, dimethylformamide [DMF], and dimethyl sulfoxide [DMSO]) without oil encapsulation did result in small numbers of single crystals (e.g., 4 in 1,2-dicholorethane), and some samples remained in solution (e.g., DMSO). However, as a consequence of more controlled solvent loss, oil encapsulation with both fluorous (FC-40) and non-fluorous (PDMSO) oils improved the experimental outcomes for all solvents examined such that many more small (4) and large (5) single crystals were observed. Interestingly, the oil encapsulation of nanodroplets of DMSO analyte solutions improved experimental outcomes, whereas non-encapsulated samples remained in solution. This suggests that in the case of oil-encapsulated DMSO nanodroplets, an additional route to crystal formation might be occurring (e.g., diffusional loss of solvent into the oil or nucleation at the solvent-oil interface).

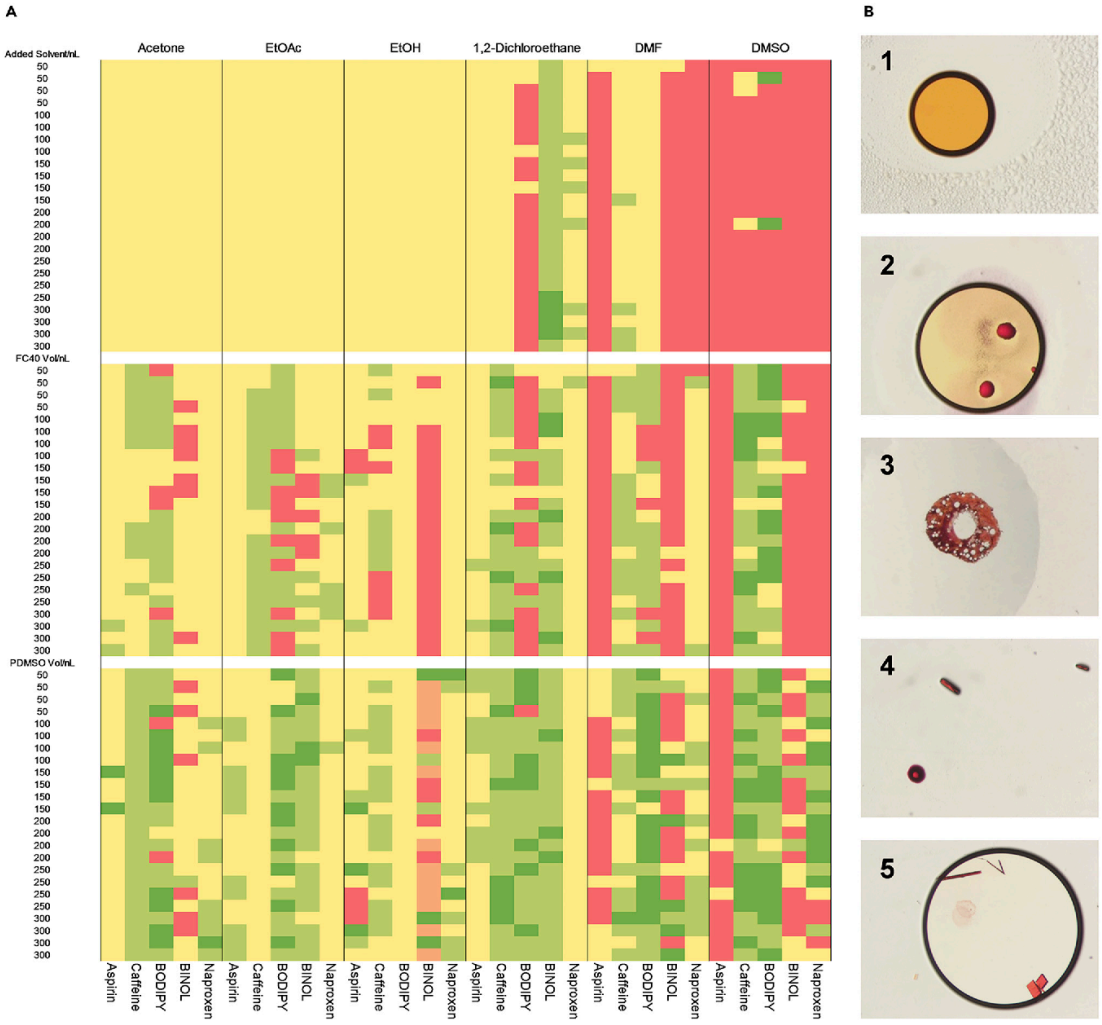

Figure 2. Encapsulated versus Non-encapsulated Nanodroplet Crystallizations

(A) Crystallization conditions for analytes 1–5 dissolved in organic solvents (acetone, ethyl acetate, ethanol, 1,2-dichoroethane, dimethylformamide, or dimethyl sulfoxide) with and without oil encapsulation (FC-40 or PDMSO). (1) Red: sample remains in solution; (2) orange: phase separation from solution and no solid; (3) yellow: amorphous or micro-crystalline solids; (4) light green: small single crystal(s); (5) dark green: large single crystal(s). (B) Representative experimental outcomes (1–5) shown with BODIPY (3) for ease of visualization.

To gain further insight into the impact of oil encapsulation on small-molecule crystallization, we performed a statistical analysis of the experimental outcomes. We fitted a proportional odds model for ordinal logistic regression in the Bayesian framework to access the relationship between the response variable (experimental outcomes 1–5) and the covariates (volume of solvent, volume of oil, type of solvent, type of oil, and molecule).[22] The use of oils, both FC-40 and PDMSO, showed a clear positive relationship with the outcome of the crystallization experiments such that more suitable single crystals were formed under oil-encapsulation conditions (see Supplemental Experimental Procedures).

Finally, suitable single crystals of each of the five compounds (**1**–**5**) were retrieved from their corresponding 96-well plates, mounted, and analyzed by SCXRD. In all cases, high-quality data were recorded to a minimum completeness of 99% at a minimum resolution of 0.84 Å on standard in-house diffractometers using Cu Kα X-radiation (λ = 1.54184 Å). Molecular structures were then obtained through structure solution and refinement using the OLEX2[23] interface to the SHELX[24] suite of programs. Furthermore, the absolute stereochemical assignments were confirmed by successful refinement of the Flack parameter derived from anomalous dispersion measurements for both **4** and **5** (Figure 3).

To further validate the capability of the ENaCt protocol, we subsequently applied it to a broader set of chemical compounds (**S1**–**S7**). These experiments were further refined through the addition of small volumes (up to 100 nL) of a secondary solvent to the solution of analyte within the inert oil droplet and the use of a wider range of inert oils, allowing an expansion of the protocol's experimental space-sampling capability through the fine-tuning of crystallization conditions. In all cases, suitable single crystals were successfully grown and subsequently analyzed by SCXRD, resulting in full structure solution and refinement coupled with absolute stereochemical assignments where appropriate (Figures S1 and S2).

Polymorph Screening of ROY

After the success of our previous crystallization experiments, we applied our ENaCt protocol to a well-known problem in solid-state chemistry, namely polymorphism. This is the phenomenon where a given compound crystallizes into different solid phases—differing only by the three-dimensional arrangement of molecules in space—that return to indistinguishable solution or liquid states.[25] The discovery of polymorphic forms is particularly suited to our ENaCt protocol because large numbers of crystallization experiments can be undertaken in parallel (reducing the total number of person hours required) with well-defined yet different crystallization conditions.

Polymorphism is particularly relevant to the pharmaceutical industry because different polymorphs of a compound can have significantly different physical properties (e.g., solubility and stability). This is a particular concern for the preparation of active pharmaceutical ingredients (APIs), where such physical properties directly affect the bioavailability of a compound. Thus, the early identification of accessible polymorphs of an API is of significant economic importance because an unexpected appearance of a previously unknown stable polymorphic phase can result in temporary market withdrawal pending reformulation.[26]

We chose 5-methyl-2-[(2-nitrophenyl)amino]-3-thiophenecarbonitrile (**6**), also known as ROY because of the different colors (red, orange, and yellow) exhibited by its various crystalline states. A synthetic precursor of the antipsychotic olanzapine, we envisaged this as an ideal test substrate for polymorph screening using our high-throughput platform. Since the discovery of the first polymorphs of ROY in 1998, it has been the target of numerous experimental and computational studies focusing on new polymorph discovery and prediction. This has resulted in 12 published polymorphs, nine of which have been characterized by X-ray diffraction.[27–30]

In order to screen for new and existing polymorphs of ROY, we undertook a large number of parallel experiments in which nanodroplets of ROY solutions were encapsulated in a selection of inert oils. Individual experiments were checked for crystal growth periodically, and the first single crystals appeared after 12 h.

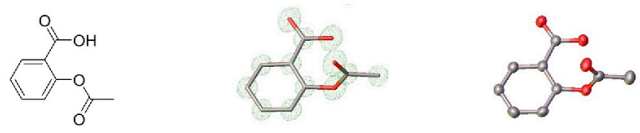

Aspirin (**1**): R_1 = 0.0659, $_wR_2$ = 0.1615, Residual e$^-$ density (e$^-$Å^3) min = -0.204 and max = 0.314

Caffeine (**2**): R_1 = 0.0610, $_wR_2$ = 0.1574, Residual e$^-$ density (e$^-$Å^3) min = -0.203 and max = 0.395

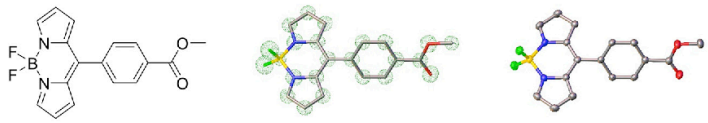

BODIPY (**3**): R_1 = 0.0377, $_wR_2$ = 0.0786, Residual e$^-$ density (e$^-$Å^3) min = -0.184 and max = 0.175

(*R*)-BINOL (**4**): R_1 = 0.0413, $_wR_2$ = 0.0839, Residual e$^-$ density (e$^-$Å^3) min = -0.135 and max = 0.143, Flack = 0.08(18)

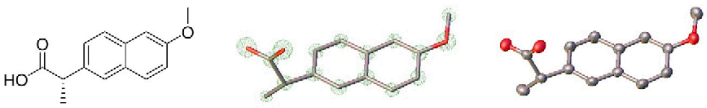

(*S*)-Naproxen (**5**): R_1 = 0.0299, $_wR_2$ = 0.0646, Residual e$^-$ density (e$^-$Å^3) min = -0.173 and max = 0.135, Flack = -0.015(7)

Figure 3. Molecular Structures, Electron Density Maps, and Refined Crystallographic Molecular Models Derived from SCXRD Analysis of Single Crystals of Compounds 1–5 Formed via the ENaCt Protocol

Each structure is provided with selected crystallographic information.

Suitable single crystals of ROY were obtained from a range of different experimental conditions.

Four of the known ROY polymorphs (Y, R, ON, and ORP) can be accessed through solution-phase crystal growth; the others arise directly or indirectly only via melt experiments. By using our ENaCt protocol, we were able to grow single crystals suitable for SCXRD analysis for all four of the solution-phase accessible polymorphs, where Y was the most commonly observed (Figure 4).

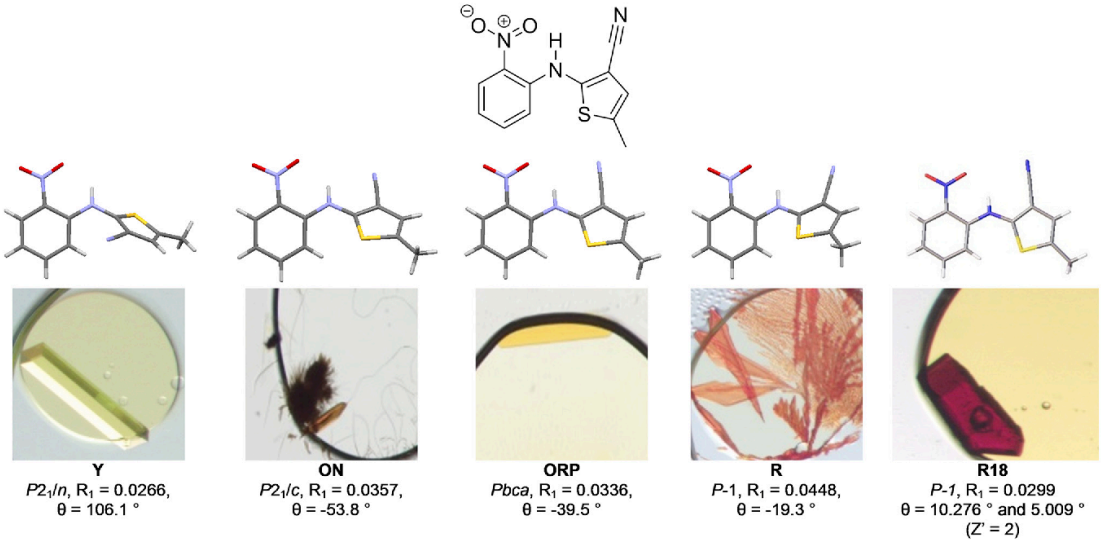

Figure 4. Molecular Structures, Crystal Growth Images, and SCXRD Data for Existing (Y, ON, ORP, and R) and New (R18) Polymorphs of ROY (6)

Additionally, deep-red block-shaped crystals of ROY were observed, and they did not match the color, morphology profile, or unit cell of any of the known ROY polymorphs (Figure 5). Full structural investigation by SCXRD (150 K, in-house X-ray diffractometer) confirmed this as a new ROY polymorph (R18) that had not previously been reported experimentally and as only the second ROY polymorph to have a Z′ value > 1. R18 is the 13th polymorph of ROY to be discovered and the tenth to be fully characterized through SCXRD, returning ROY to the status of world record holder for the most polymorphic organic molecule.

Thus, the discovery of R18 further validates the power of the ENaCt protocol not just as a crystallization method for X-ray analysis but also as a potential polymorph screening tool.

Crystallization of an "Uncrystallizable" Molecule: Dithianon (7)

Finally, we wished to apply our ENaCt methodology to the crystallization of a crystallographically challenging or previously deemed "uncrystallizable" sample. We envisaged that the high-throughput capability of ENaCt would allow for the rapid screening of the diverse crystallization conditions required to ensure the growth of a single crystal suitable for X-ray diffraction analysis of such a material. To this end, we selected the functionalized naphthoquinone dithianon (5,10-dioxo-5,10-dihydronaphtho[2,3-*b*][1,4]dithiine-2,3-dicarbonitrile) (7). Dithianon was first introduced in 1963 as a broad-spectrum foliar fungicide and is still used for controlling fungal infections in commercial agriculture.[31] Dinnebier and co-workers have previously shown the existence of four different polymorphs of dithianon (forms 1–4) via refinement against high-resolution X-ray powder diffraction data sets. However, they did not report a SCXRD data set because of "… the lack of single crystals of sufficient size and quality" as a result of the lack of strong intermolecular interactions in the solid state.[32]

Thus, following our ENaCt methodology, we undertook 384 individual crystallization experiments. We dispensed 200 nL of oils (FC 40, Fomblin YR, PDMSO, or mineral

Dithianon (7): R_1 = 0.048, $_wR_2$ = 0.1262, Residual e^- density ($e^-Å^3$) min = -0.2 and max = 0.4

200 nL PDMSO, 50 nL of 12.5 mg/mL of dithianon in DMF, 25 nL 2-methyl-2,4-pentanediol.

Figure 5. Molecular Structure, Crystal Growth Image, and SCXRD Data for Dithianon (7), Polymorph 1, Including Selected Crystallographic Information and ENaCt Crystal Growth Conditions

oil), followed by 50 nL of dithianon solution (2–50 mg/mL of DMSO or DMF) and 25 or 50 nL of a secondary solvent (toluene, chlorobenzene, 2-methyl-2,4-pentanediol, or water), into 96-well glass plates. After 14 days at RT, experiments were examined by polarizing optical microscopy. 72 crystalline samples (19% of the total number) exhibiting block-, plate-, and needle-like morphologies were identified, and a suitable block-like crystal was analyzed by SCXRD (Figure 5).

The structural model, derived from the SCRXD data, confirmed that we had successfully obtained a single crystal of dithianon (polymorph 1). The structure suffers from minor disorder components, ascribed to stacking faults within the crystal. Further analysis of the structure within the software package CrystalExplorer[33] indicated the presence of only a small number of weak intermolecular interactions within the structure and no interlayer component of the total energy framework exceeding 15 kJmol ^{1} (Figure S3). We propose that the presence of only weak interactions is the cause of the previously failed dithianon crystallization attempts using traditional methodologies. Thus, these experiments further demonstrate the capability of the ENaCt protocol to address even the most challenging of crystallization problems.

Conclusion

There is a requirement across the molecular sciences for a widely applicable, high-throughput crystallization method that operates on the microgram scale. The ENaCt protocol described here fulfills these requirements as a tailor-made solution to the crystallization problem. Our results—both the successful crystallization of a diverse set of small molecules (including the "uncrystallizable" dithianon) and the exploration of the polymorphs of ROY—provide strong evidence for the potential of ENaCt as a general tool for the crystallization of organic-soluble small molecules. We anticipate that such facile access to high-quality single crystals through the rapid sampling of large areas of the solid-state energy landscape will provide significant future benefits to the molecular science community.

EXPERIMENTAL PROCEDURES

Resource Availability

Lead Contact

Request for further information should be directed to and will be fulfilled by the Lead Contact, Michael J. Hall (michael.hall@newcastle.ac.uk).

Materials Availability

This study did not generate new unique materials.

Data and Code Availability

The accession numbers for the crystallographic data reported in this paper are CCDC: 1944195–1944211 and 1968245. These data can be obtained free of charge from the Cambridge Crystallographic Data Centre at https://www.ccdc.cam.ac.uk/structures.

SUPPLEMENTAL INFORMATION

Supplemental Information can be found online at https://doi.org/10.1016/j.chempr.2020.04.009.

ACKNOWLEDGMENTS

The authors acknowledge support from the Biotechnology and Biological Sciences Research Council and Natural Products Discovery and Bioengineering Network (BB/L013754/1), the N8 Research Partnership, and the Higher Education Innovation Fund for funding; the Engineering and Physical Sciences Research Council for access to X-ray crystallography facilities (EP/F03637X/1); and Diamond Light Source (beamline I19).

AUTHOR CONTRIBUTIONS

M.J.H. and M.R.P. directed and conceived this project; A.R.T., R.R., C.J.M., and P.G.W. conducted the experimental work; S.E.H. contributed statistical analysis; J.W.S. provided ROY and contributed to ROY-related experimental design; and P.T. contributed to robotic experimental design. All authors discussed the results and wrote the manuscript.

DECLARATION OF INTERESTS

A.R.T., M.J.H., and M.R.P. have filed a patent application based on this work: GB1908349.2.

Received: December 2, 2019
Revised: February 5, 2020
Accepted: April 15, 2020
Published: May 7, 2020

REFERENCES

1. Koritsanszky, T.S., and Coppens, P. (2001). Chemical applications of X-ray charge-density analysis. Chem. Rev. *101*, 1583–1627.

2. Flack, H.D., and Bernardinelli, G. (2008). The use of X-ray crystallography to determine absolute configuration. Chirality *20*, 681–690.

3. Howard, J.A.K., and Probert, M.R. (2014). Cutting-edge techniques used for the structural investigation of single crystals. Science *343*, 1098–1102.

4. Johnson, N.T., Waddell, P.G., Clegg, W., and Probert, M.R. (2017). Remote access revolution: chemical crystallographers enter a new era at diamond light source beamline. I9. Crystals *7*, 360.

5. Taylor, R., and Wood, P.A. (2019). A million crystal structures: the whole is greater than the sum of its parts. Chem. Rev. *119*, 9427–9477.

6. Grothe, E., Meekes, H., Vlieg, E., ter Horst, J.H., and de Gelder, R. (2016). Solvates, salts, and cocrystals: a proposal for a feasible classification system. Cryst. Growth Des. *16*, 3237–3243.

7. Spingler, B., Schnidrig, S., Todorova, T., and Wild, F. (2012). Some thoughts about the single crystal growth of small molecules. CrystEngComm *14*, 751–757.

8. Inokuma, Y., Yoshioka, S., Ariyoshi, J., Arai, T., Hitora, Y., Takada, K., Matsunaga, S., Rissanen, K., and Fujita, M. (2013). X-ray analysis on the nanogram to microgram scale using porous complexes. Nature *495*, 461–466.

9. Hoshino, M., Khutia, A., Xing, H., Inokuma, Y., and Fujita, M. (2016). The crystalline sponge method updated. IUCrJ *3*, 139–151.

10. Jones, C.G., Martynowycz, M.W., Hattne, J., Fulton, T.J., Stoltz, B.M., Rodriguez, J.A., Nelson, H.M., and Gonen, T. (2018). The CryoEM method MicroED as a powerful tool for small molecule structure determination. ACS Cent. Sci. *4*, 1587–1592.

11. Gruene, T., Wennmacher, J.T.C., Zaubitzer, C., Holstein, J.J., Heidler, J., Fecteau-Lefebvre, A., De Carlo, S., Müller, E., Goldie, K.N., Regeni, I., et al. (2018). Rapid structure determination of microcrystalline molecular compounds using electron diffraction. Angew. Chem. Int. Ed. *57*, 16313–16317.

12. Jones, C.G., Asay, M., Kim, L.J., Kleinsasser, J.F., Saha, A., Fulton, T.J., Berkley, K.R., Cascio, D., Malyutin, A.G., Conley, M.P., et al. (2019). Characterization of reactive organometallic species *via* MicroED. ACS Cent. Sci. *5*, 1507–1513.

13. Brázda, P., Palatinus, L., and Babor, M. (2019). Electron diffraction determines molecular absolute configuration in a pharmaceutical nanocrystal. Science *364*, 667–669.

14. Nývlt, J. (1995). The Ostwald rule of stages. Cryst. Res. Technol. *30*, 443–449.

15. Alvarez, A.J., and Myerson, A.S. (2010). Continuous plug flow crystallization of

pharmaceutical compounds. Cryst. Growth Des. *10*, 2219–2228.

16. Foster, J.A., Damodaran, K.K., Maurin, A., Day, G.M., Thompson, H.P.G., Cameron, G.J., Bernal, J.C., and Steed, J.W. (2017). Pharmaceutical polymorph control in a drug-mimetic supramolecular gel. Chem. Sci. *8*, 78–84.

17. Chen, C., Cook, O., Nicholson, C.E., and Cooper, S.J. (2011). Leapfrogging ostwald's Rule of Stages: crystallization of stable γ-glycine directly from microemulsions. Cryst. Growth Des. *11*, 2228–2237.

18. Nievergelt, P.P., Babor, M., Čejka, J., and Spingler, B. (2018). A high throughput screening method for the nano-crystallization of salts of organic cations. Chem. Sci. *9*, 3716–3722.

19. Chayen, N.E., Shaw Stewart, P.D., and Blow, D.M. (1992). Microbatch crystallization under oil – a new technique allowing many small-volume crystallization trials. J. Cryst. Growth *122*, 176–180.

20. Chayen, N.E. (1997). The role of oil in macromolecular crystallization. Structure *5*, 1269–1274.

21. Babor, M., Nievergelt, P.P., Čejka, J., Zvoníček, V., and Spingler, B. (2019). Microbatch under-oil salt screening of organic cations: single-crystal growth of active pharmaceutical ingredients. IUCrJ *6*, 145–151.

22. McCullagh, P. (1980). Regression models for ordinal data. J. R. Stat. Soc. B *42*, 109–127.

23. Dolomanov, O.V., Bourhis, L.J., Gildea, R.J., Howard, J.A.K., and Puschmann, H. (2009). OLEX2: a complete structure solution, refinement and analysis program. J. Appl. Crystallogr. *42*, 339–341.

24. Sheldrick, G.M. (2015). Structure determination revisited. Acta Crystallogr. A Found. Adv. *71*, s9.

25. Cruz-Cabeza, A.J., and Bernstein, J. (2014). Conformational polymorphism. Chem. Rev. *114*, 2170–2191.

26. Chemburkar, S.R., Bauer, J., Deming, K., Spiwek, H., Patel, K., Morris, J., Henry, R., Spanton, S., Dziki, W., Porter, W., et al. (2000). Dealing with the impact of ritonavir polymorphs on the late stages of bulk drug process development. Org. Process Res. Dev. *4*, 413–417.

27. Chen, S., Guzei, I.A., and Yu, L. (2005). New polymorphs of ROY and new record for coexisting polymorphs of solved structures. J. Am. Chem. Soc. *127*, 9881–9885.

28. Tan, M., Shtukenberg, A.G., Zhu, S., Xu, W., Dooryhee, E., Nichols, S.M., Ward, M.D., Kahr, B., and Zhu, Q. (2018). ROY revisited, again: the eighth solved structure. Faraday Discuss. *211*, 477–491.

29. Gushurst, K.S., Nyman, J., and Boerrigter, S.X.M. (2019). The P013 crystal structure of ROY. CrystEngComm *21*, 1363–1368.

30. Nyman, J., Yu, L., and Reutzel-Edens, S.M. (2019). Accuracy and reproducibility in crystal structure prediction: the curious case of ROY. CrystEngComm *21*, 2080–2088.

31. Vidhyasekaran, P. (2004). Concise Encyclopedia of Plant Pathology (Food Products Press).

32. Halasz, I., Dinnebier, R., Chiodo, T., and Saxell, H. (2012). Structures of four polymorphs of the pesticide dithianon solved from X-ray powder diffraction data. Acta Crystallogr. B *68*, 661–666.

33. Mackenzie, C.F., Spackman, P.R., Jayatilaka, D., and Spackman, M.A. (2017). CrystalExplorer model energies and energy frameworks: extension to metal coordination compounds, organic salts, solvates and open-shell systems. IUCrJ *4*, 575–587.